Conditions for the emergence of corticostriatal synaptic plasticity

Silvana Valtcheva

Université Pierre et Marie Curie (UPMC-Paris VI)

École Doctorale Cerveau-Cognition-Comportement (ED3C n°138)

Dynamics and Physiopathology of Neuronal Networks

Center for Interdisciplinary Research in Biology (CIRB)

Collège de France, Paris

Conditions for the emergence of corticostriatal synaptic plasticity

Thèse de doctorat de neuroscience par

Silvana VALTCHEVA

Dirigée par

Dr. Laurent VENANCE

Présentée et soutenue publiquement le 26 septembre 2016

Devant un jury composé de :

Dr. Alban DE KERCHOVE D'EXAERDE	Rapporteur
Dr. Gilad SILBERBERG	Rapporteur
Dr. Etienne AUDINAT	Examinateur
Pr. Stéphane CHARPIER	Examinateur
Dr. Stéphane OLIET	Examinateur
Dr. Laurent VENANCE	Examinateur

Acknowledgements

Thanks to Laurent Venance for guiding me through the 5 years I spent in this lab, for pushing me to the edge of the possible, for trusting me. Thanks for the encouragement, for letting me fight by myself, for being present when even I was absent. Thanks for accepting me, for correcting me, for continuously making me progress.

Thanks to Marie Vandecasteele for being extremely critical and sharp, challenging my logic, teaching me to first question myself before defending my position.

Thanks to Giuseppe Gangarossa for showing me that science extends beyond the lab, for teaching me how to be convincing and bright, how to spread my knowledge.

Thanks to Elodie Fino who taught me to be serious and ambitious and how to fight in order to survive in science.

Thanks to Sylvie Perez who taught me about the no-limits of what we can achieve and that giving up is not an option.

Thanks to Bertrand Degos for his strong sense of curiosity and general enthusiasm about science that was highly inspiring for me.

Thanks to Yves Gioanni for making me discover the music of the neurons and introducing me to the in vivo recordings I will later do by myself.

Thanks to Hao Xu who taught me to be consistent in my work and to take care about the details; at the same time keeping my internal peace.

Thanks to Asier Aristieta-Arbelaiz who was the best office buddy, who taught me to be patient but relentless about my experiments.

Thanks to Yihui Cui who taught me how to do science in a customized way and that the lab is our fortress.

Thanks to Gaëtan Vignoud for his fresh passion about science, for his desire to learn, for the discussions that brought me many knew questions.

Thanks to Willy Derousseaux for all the precious talks and chill-out sessions without which I wouldn't survive the most stressful months of my PhD.

Many thanks to Yulia Dembitskaya who was there for me in the lab and outside the lab; who was so delicate and caring in tough times; who was there to share any emotion and was seeing the word with the same evil sense of humor as I do.

Finally, I am exceptionally thankful to Alexander Mendes who was during all these years extremely tolerant to my absurdity, was reacting with patience to my high frequency mood oscillations and was truly my loyal friend.

Silvana VALTCHEVA

RESUME

According to Hebbian theory, neural networks refine their connectivity by patterned firing of action potentials in pre- and postsynaptic neurons. Spike-timing-dependent plasticity (STDP) is a synaptic Hebbian learning rule relying on the precise order and the millisecond timing of the paired activities on either side of the synapse. Temporal coding *via* STDP may be essential for the role of the striatum in learning of motor sequences in which sensory and motor events are associated in a precise time sequence. Corticostriatal long-term plasticity provides a fundamental mechanism for the function of the basal ganglia in procedural learning. Striatal output neurons act as detectors of distributed patterns of cortical and thalamic activity. Thus, corticostriatal STDP should play a major role in information processing in the basal ganglia, which is based on a precise time-coding process. Here, we explored the conditions required for the emergence of corticostriatal STDP.

I. GABAergic signaling drives the polarity of corticostriatal STDP along development.

We previously showed that GABAergic circuits control the polarity of corticostriatal STDP and thus operate as a Hebbian/anti-Hebbian switch. GABAergic circuits are subject to important developmental maturation. Here, we explored the implication for GABAergic signaling in shaping corticostriatal STDP along development.

(1) Corticostriatal STDP exhibited unidirectional asymmetric Hebbian STDP in young animals while anti-Hebbian STDP was observed at later developmental stages (juvenile and adult animals).

(2) Promoting tonic inhibition in the immature brain allowed the emergence of anti-Hebbian STDP.

(3) Blockade of tonic GABAergic signaling at juvenile stage reversed the anti-Hebbian STDP back to unidirectional asymmetric Hebbian STDP.

We showed that developmental maturation of GABAergic signaling drives the polarity of corticostriatal plasticity.

II. Astrocytic glutamate uptake *via* EAAT2 allows the expression of corticostriatal STDP.

Astrocytes, *via* excitatory amino-acid transporter type-2 (EAAT2), are the major sink for released glutamate and contribute to set the strength and timing of synaptic inputs. EAAT2 is highly expressed in the striatum and it controls corticostriatal transmission and short-term plasticity. EAAT2 increases the strength of cortical input filtering by the striatum. We questioned the role of astrocytes (*via* EAAT2) in the control of corticostriatal STDP.

(1) Transient EAAT2 blockade converted Hebbian plasticity (STDP) into aberrant non-Hebbian plasticity, which occurred for uncorrelated events or even unpaired activity.

(2) Distinct signaling pathways were selected in STDP and aberrant plasticity.

(3) EAAT2 overexpression (with ceftriaxone) impaired the detection of correlated activity resulting in a lack of STDP.

We showed that astrocytic glutamate uptake allows the emergence of bidirectional STDP and prevents aberrant plasticity. Thus, EAAT2 sets the proper glutamate dynamics allowing for optimal temporal contingency between pre- and postsynaptic activity necessary for STDP expression and places astrocytes as a gatekeeper of Hebbian synaptic plasticity.

In summary, the results presented in this thesis further extend our knowledge about the different conditions allowing the emergence of corticostriatal STDP.

RESUME (FR)

D'après le postulat de Hebb, les réseaux neuronaux adaptent leur connectivité sous l'influence des activités pré- et post-synaptiques. La « spike-timing-dependent plasticity » (STDP) est une règle d'apprentissage synaptique de type Hebbien, qui repose sur la structure temporelle précise des patrons d'activités appariées de part et d'autre de la synapse. La plasticité cortico-striatale serait le substrat biologique de l'apprentissage procédural effectué par les ganglions de la base. Les neurones de sortie du striatum agissent comme des détecteurs de coïncidence des activités corticales et thalamiques. La STDP cortico-striatale pourrait donc jouer un rôle crucial dans les processus d'encodage de l'apprentissage et la mémoire procédurale. Nous avons exploré les conditions d'émergence et d'expression de la STDP cortico-striatale.

I. La transmission GABAergique contrôle la polarité de la STDP cortico-striatale au cours du développement.

Nous avions précédemment montré que les circuits GABAergiques contrôlent la polarité de la STDP corticostratale : le GABA agit comme un commutateur Hebbien/anti-Hebbien. Les réseaux GABAergiques sont sujets à une maturation importante au cours du développement. Dans cette étude, nous avons exploré l'implication de la transmission GABAergique dans la modulation de la STDP corticostriatale au cours du développement. Nous avons observé que :
(1) La STDP est unidirectionnelle et asymétrique Hebbienne chez les animaux (rats) jeunes comparé aux juvéniles et adultes où la STDP est bidirectionnelle et anti-Hebbienne.
(2) Une STDP bidirectionnelle anti-Hebbienne peut être observée chez les animaux jeunes quand on crée (pharmacologiquement) une composante inhibitrice tonique.
(3) La STDP, anti-Hebbienne chez les juvéniles, est remplacée par une STDP unidirectionnelle Hebbienne comme chez les animaux jeunes, si on bloque la transmission GABAergique tonique.
Nous avons donc démontré que la maturation de la transmission GABAergique (et plus précisément de la composante tonique) contrôle la polarité de la STDP corticostriatale.

II. Les astrocytes, via la recapture de glutamate, permettent l'expression de la STDP
Les astrocytes, via le transporteur du glutamate de type-2 (EAAT2), constitue le principal système de capture du glutamate libéré et à ce titre contribuent au contrôle du poids et de la temporalité synaptique. EAAT2 est fortement exprimé dans le striatum où il régule la transmission cortico-striatale. Nous avons évalué le rôle des astrocytes (via EAAT2) dans l'expression de la STDP et ses conditions d'émergence. Nous avons observé que :
(1) Le blocage transitoire d'EAAT2 convertit une plasticité Hebbienne (STDP) en une forme aberrante de plasticité non-Hebbienne.
(2) des voies de signalisations différentes sous-tendent ces différentes plasticités.
(3) La surexpression d'EAAT2 (par le ceftriaxone) entraîne une disparition de l'expression de la STDP.
Nous avons donc démontré que le transport astrocytaire de glutamate (via EAAT2) permet l'émergence d'une STDP bidirectionnelle et prévient l'expression de plasticités aberrantes. EAAT2 permet donc d'établir les conditions optimales, en terme de dynamique spatio-temporelle du glutamate, permettant l'expression de la STDP. Les astrocytes sont donc les garants de l'expression d'une plasticité Hebbienne de type STDP.

En conclusion, les résultats présentés dans ce manuscrit de thèse permettent de mieux comprendre les conditions nécessaires à l'émergence et l'expression de la plasticité Hebbienne et en particulier de la STDP cortico-striatale.

TABLE OF CONTENTS

LITTERATURE REVIEW

METHODS

RESULTS

GENERAL DISCUSSION

ANNEX

ABBREVIATIONS

Δt - Temporal interval

2-AG - 2-arachidonoylglycerol

ACSF - Artificial cerebrospinal fluid

ACh - Acetylcholine

AChR - Acetylcholine receptor

AMPAR - α-amino-3-hydroxy-5-methyl-4-isoxazolepropionic acid receptor

AQP - Aquaporin channel

bAP - Backpropagating action potential

BDNF - Brain-derived neurotrophic factor

CB_1R - Type-1 endocannabinoid receptor

CNS - Central nervous system

D1R, D2R - Dopamine receptor Type-1/2

eCBs - Endocannabinoids

EPSC - Excitatory postsynaptic current

$GABA_AR$ - gamma-Aminobutyric acid receptor

GluR - Glutamate receptor

GPi and GPe - Internal and external segments of globus pallidus

HFS - High frequency stimulation

iGluR - Ionotropic glutamate receptor

KAR - Kainate receptor

L - Cortical layer

LTP - Long-term potentiation

LTD - Long-term depression

mGluR - Metabotropic glutamate receptor

NMDAR - N-methyl-D-aspartate receptor

PFC - Prefrontal cortex

PLC - Phospholipase C

PNS - Peripheral nervous system

STN - Subthalamic nucleus

TBS - Theta-burst stimulation

TCA cycle - Tricarboxylic acid cycle (or the Krebs cycle)

TRPV1 - Transient receptor potential vanilloid-type-1

VSCC - Voltage-sensitive calcium channels

LITERATURE REVIEW

PART I

Glutamate dynamics
(In and out of the cleft)

INTRODUCTION

Outside the biomedical scientific field, glutamic acid or glutamate is best known as monosodium glutamate, or food additive E620, which is used as a flavor or taste enhancer in food. However, the main motivation for the enormous scientific research is that apart from being one of the proteinogenic amino acids, glutamate also serves as the main excitatory neurotransmitter in the mammalian brain (Herring et al., 2015; Zhou and Danbolt, 2014). The closely related amino acid aspartate has been proposed to play a role as an excitatory neurotransmitter along with glutamate, given the fact that it is a selective NMDAR agonist (Patneau and Mayer, 1990). Nevertheless, recent evidence states that glutamate alone fully accounts for neurotransmission at excitatory synapses (at least in the hippocampus), thus excluding a role for aspartate as an excitatory neurotransmitter (Herring et al., 2015). Therefore, any aspartate released from synaptic vesicles would be at a concentration too low to be physiologically relevant.

The possible evolutionary origins of glutamate neurotransmission have been hypothesized to come with the emergence of protosynaptic (=without synapses) glutamatergic transmission as early as in the Metazoa clade (~1.2 millions of years ago) with the appearance of mGluRs which ancestral function remains unresolved. However, it has been proposed that protosynaptic mGluR activity modulates Ca^{2+} influx in sponge (Ryan and Grant, 2009). More recently, it has been hypothesized that glycine together with glutamate is a candidate neurotransmitter and also a ligand for iGluRs found in early Metazoa (Alberstein et al., 2015).

The fact that glutamate acts as a neurotransmitter in the CNS has taken a long time to demonstrate due to its abundance in brain tissue and that it has an important metabolic role in the brain (for review see (Zhou and Danbolt, 2014).

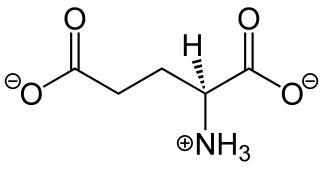

Figure 1. Chemical structure of glutamic acid (glutamate).

Glutamate is the most abundant free amino acid in the brain and there is 5–15 mmol glutamate per kg brain tissue, depending on the region (Zhou and Danbolt, 2014). The concentration of extracellular glutamate varies dramatically depending upon the biological compartment being measured. For non-brain tissue, serum and plasma glutamate levels are estimated in the range of 30-200 μM, whereas red blood cell cytoplasmic glutamate is ~0.5 mM, muscle cell cytoplasmic glutamate is ~5 mM and 10 μM in the cerebrospinal fluid (Featherstone and Shippy, 2008; Zhou and Danbolt, 2014).

INTRACELLULAR GLUTAMATE

Intracellular glutamate in the cytoplasm of neurons is significantly higher than in astrocytes (5 mM from Ottersen et al., 1990) and it has been estimated to be in the low mM range: 10-15 mM (Featherstone and Shippy, 2008; Zhou and Danbolt, 2014) and 2-30 mM (from (Bramham et al., 1990) and Storm-Mathisen et al. 1992) depending on cell type. In synaptic vesicles, around 2,000-4,000 molecules of glutamate per vesicle have been estimated, which is approximately 0.03-0.2 M of glutamate in a vesicle (Burger et al., 1989; Riveros et al., 1986; Shupliakov et al., 1992; Takamori et al., 2006); for review see (Marx et al., 2015).

EXTRACELLULAR GLUTAMATE

I. AMBIENT GLUTAMATE

1 - *In vivo* extracellular ambient glutamate

In contrast to the relative agreement concerning intracellular glutamate concentration in different biological compartments, estimates of the tonic basal concentration of glutamate within the extracellular space varies drastically (Cavelier and Attwell, 2005; Herman and Jahr, 2007; for review see (Moussawi et al., 2011). Assessment of the correct level of extracellular glutamate is critical for understanding the dynamics of receptor stimulation, the operation of transporters and thus the information processing at the level of the synapse. Extracellular glutamate has also a role in metabolic processes such as cellular redox potential and neurometabolic coupling between synaptic activity, glial metabolism, and blood flow (Magistretti, 2009).

In vivo studies using microdialysis or voltammetry with biosensors measure similar levels of extracellular glutamate in the range of 1–30 μM in different brain regions between different mammalian species (Moussawi et al., 2011). Due to the poor time resolution of these techniques, the pool of glutamate being sampled is mainly derived from non-synaptic origin (not from action potential mediated release) and thus represents a tonic pool of extracellular glutamate. As suggested, another issue is that a large portion of the glutamate sampled by microdialysis is of non-neuronal origin. Indeed, reverse transporter activity or glutamate release from glial cells could participate in the samples (Westerink, 1995). However, evidence from rapid microelectrode measurements suggests that it is possible to sample glutamate mainly of neuronal origin (Hascup et al., 2010).

Various concerns could be raised regarding the fidelity of the measurements by the different techniques mainly because of an over-estimation of the levels of extracellular glutamate. Reported values from *in vivo* measurements (1–5 μM) are in the range of the Kd for glutamate binding to NMDARs and thus a portion of these receptors would be desensitized (Fig.2). Non-physiological elevations of glutamate do not seem to be caused directly from acute damage to neuropil induced by inserting the dialysis probe. However, the possibility of glial infiltration, associated with oxidative stress, and the creation of an artificial extracellular compartment (a trauma layer) where glutamate can accumulate should be considered.

2 - *In vitro* extracellular ambient glutamate

In contrast to the reported low micromolar concentrations from *in vivo* studies, two studies using hippocampal slices find extracellular glutamate levels in the nanomolar range between 25 and 80 nM (Cavelier and Attwell, 2005; Herman and Jahr, 2007). In these studies, extracellular glutamate levels are assessed using NMDARs as 'glutamate sensors' by monitoring tonic NMDAR-currents mediated by non-synaptic extracellular glutamate. However, this current represents the activity of all NMDARs expressed by the neuron and does not differentiate between synaptic and extrasynaptic receptors. Therefore, the fraction of ambient glutamate detected by extrasynaptic NMDARs is difficult to assess.

Using the distribution of transporters (Lehre and Danbolt, 1998), models of the extracellular space predict that the glutamate concentration is in the range of 30–50 nM throughout the neuropil of hippocampus (Zheng et al., 2008), similar to the *in vitro* experimental estimates (Cavelier and Attwell, 2005; Herman and Jahr, 2007). However, this estimation differs from earlier work predicting a minimum maintainable concentration of extracellular glutamate of 0.6 µM (Bouvier et al., 1992) and 0.2 µM (Attwell et al., 1993).

Possible technical caveats concerning *in vitro* brain slice preparations that could influence the concentration of extracellular glutamate are the following: the age of the animals (juvenile for *in vitro* vs. adults for *in vivo* studies), the partial depletion of extracellular constituents (like cystine or ascorbic acid) or the tissue slicing procedure. All these factors could affect the extracellular levels of glutamate in tissue slices in a certain extend and thus bias its estimation.

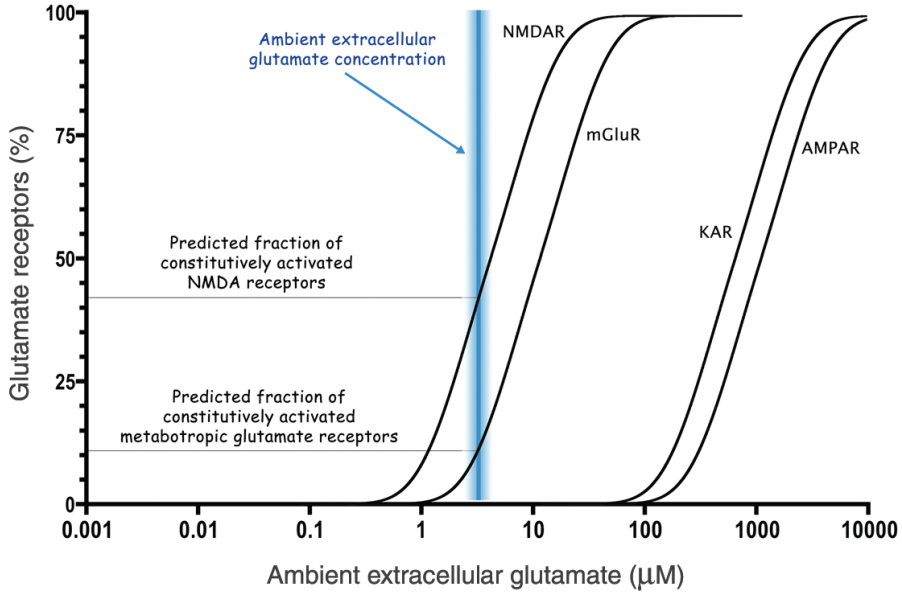

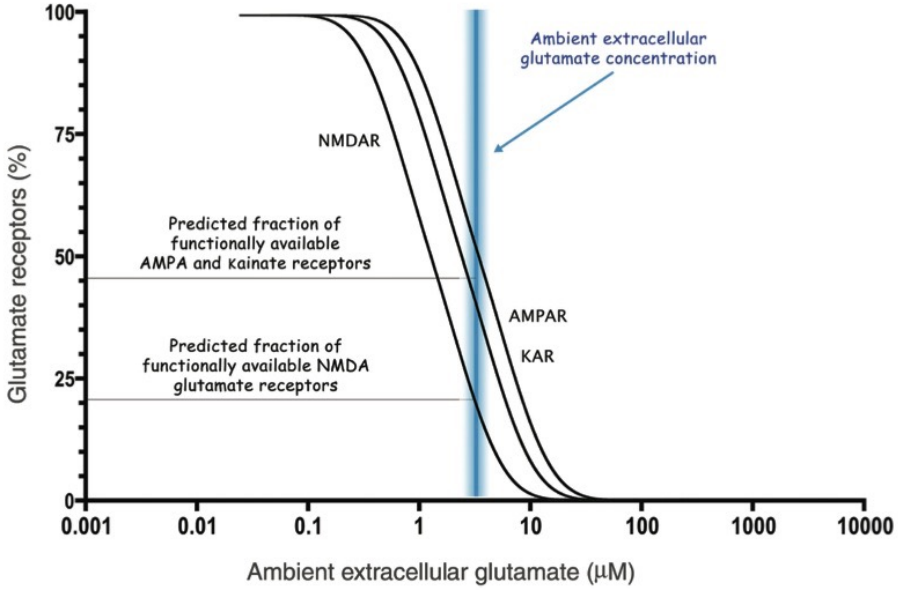

Figure 2. Glutamate dependence of activation (top) and desensitization (bottom) for different iGluRs, compared to the concentration of ambient extracellular glutamate. (Top) NMDARs and mGluRs are activated by relatively low concentrations of glutamate (1 to 20 μM), and thus have typically sigmoidal dose-response curves that are left-shifted compared to those from AMPARs and KARs, which are activated only by glutamate concentrations of 100 to 2000 μM. If ambient extracellular glutamate is ~2 μM, then about 40% of NMDARs and 10% of mGluRs could be constitutively activated *in vivo*. **(Bottom)** Steady-state desensitization of iGluRs receptor occurs at much lower glutamate concentrations (0.1 to 10 μM). If ambient extracellular glutamate is ~2 μM, then one-half to three-quarters of glutamate receptors might be constitutively desensitized, and thus functionally silent, *in vivo*. However, slight changes in ambient extracellular glutamate concentration or dose-dependence of steady-state desensitization could have dramatic effects on glutamate receptor availability and synaptic strength. (From (Featherstone and Shippy, 2008)).

3 - Compartmentalization of different glutamate concentrations - proposal

It has been proposed that part of the variability of the measurements may result from the sampling of glutamate in different extracellular compartments (synaptic versus extrasynaptic volumes). One explanation for the marked difference between different studies may be the existence of subcompartments of extracellular glutamate. Indeed, patterned expression of release and uptake sites around synapses could lead to different extracellular glutamate concentrations thus forming subcompartments (Bridges et al., 2012; Moussawi et al., 2011).

In contrast to this proposal, it has been reported that there is not a steep concentration gradient of glutamate between the synaptic and extrasynaptic space and, consequently, that the synaptic compartment is not preferentially shielded by glutamate transporters (Herman et al., 2011). Using patch-clamp combined with 2-photon calcium imaging on hippocampal brain slices Herman and colleagues conclude that ambient glutamate is not significantly compartmentalized but rather is universally low throughout the neuropil of the hippocampus. Nevertheless, this question is open to a debate as extrasynaptic glutamate could be low compared to synaptic glutamate because glutamate is highly concentrated during brief synaptic release events. This will transiently raise synaptic glutamate to 1000 to 3000 µM (Bergles et al., 1999; Clements et al., 1992). Alternatively, extracellular glutamate might be higher compared to synaptic glutamate because of localized glutamate uptake near perisynaptic sites.

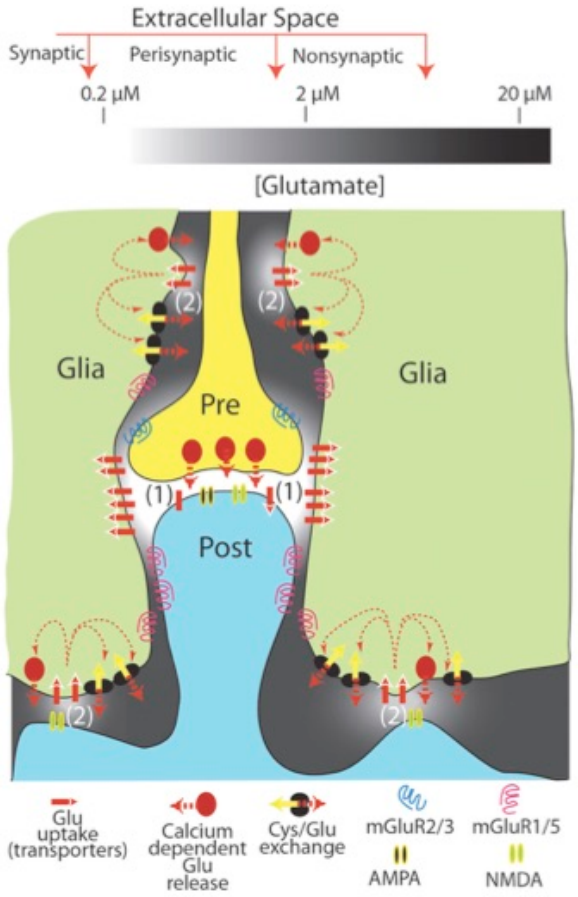

Figure 3. Proposed working model where the extracellular space is divided into three subcompartments. (1) In the synaptic cleft the glutamate concentration is in the low nanomolar range because glutamate levels are tightly regulated by both neuronal and glial glutamate uptake systems to prevent desensitization of iGluR. (2) The transitional perisynaptic zone and (3) the nonsynaptic compartment containing low micromolar glutamate maintained by glial release. (From (Moussawi et al., 2011)).

4 - Sources of extracellular glutamate - tonic glutamate release

In the absence of phasic glutamate release, the ionic stoichiometry of glutamate transporters provides sufficient accumulative power to lower the extracellular glutamate concentration to ~2nm (Levy et al., 1998; Zerangue and Kavanaugh, 1996), but microdialysis experiments *in vivo* report much higher values (~2µm) (Moussawi et al., 2011). Moreover, neuronal tonic excitatory currents, mediated by ambient glutamate, were detected in several brain structures, suggesting a constant release of glutamate (Cavelier and Attwell, 2005; Fleming et al., 2011; Jabaudon et al., 1999; Kőszeghy et al., 2014; Le Meur et al., 2007; Nie et al., 2010; Sah et al., 1988; Sasaki et al., 2012). This has raised questions concerning the origins of extracellular glutamate and several mechanisms have been proposed.

Neuronal release

Glutamate release of neuronal origin had been one of the primary hypothesis of the constant glutamate leak. However, tonic glutamate release does not reflect either action potential evoked or spontaneous exocytotic transmitter release (Cavelier and Attwell, 2005; Jabaudon et al., 1999). Indeed, tonic glutamate release is not *via* Ca^{2+}-dependent exocytosis, nor *via* Ca^{2+}-independent spontaneous vesicular release (Cavelier and Attwell, 2005; Jabaudon et al., 1999; Le Meur et al., 2007; Yang and Xu-Friedman, 2015).

There are several other modes of transmitter release that are candidates for mediating the tonic release of glutamate. In contrast, it is important to note that transmembrane diffusion would have a negligible effect on the tonic glutamate levels (Jabaudon et al., 1999).

Release via system xc-

Baker et al. have suggested, from microdialysis experiments, that most (60%) of the tonic glutamate release in the ventral striatum is generated by the cystine–glutamate exchanger (or system xc-), in which glutamate is released in exchange for cystine taken up to make glutathione (Baker et al., 2002; Lewerenz et al., 2013). However, patch-clamp experiments in hippocampal slices showed that cystine–glutamate exchange does not generate tonic glutamate release in the presence of physiological cystine (Cavelier and Attwell, 2005).

Glial origin of extracellular glutamate

Transient release of glutamate from glia, probably by exocytosis, can activate NMDARs in different regions, thus mediating slow inward currents (SICs) (Angulo et al., 2004; Fellin et al., 2004); for review see (Pál, 2015). A major concern about these observations comes from the fact that recordings are obtained in 0 Mg extracellular solution and in the presence of high concentration of $GABA_AR$ blocker (picrotoxin 100 μM). Anyway, Ca^{2+}-evoked glial glutamate release seems to not contribute significantly to tonic activation of glutamate receptors. Indeed, blocking prostaglandin- and Ca^{2+}-dependent glutamate release from astrocytes does not reduce the neuronal response to tonic glutamate (Cavelier and Attwell, 2005).

In addition, astrocytes can release glutamate by other mechanisms, and it has been demonstrated that at least a part of the tonic glutamate results from astrocytic release (Cavelier and Attwell, 2005; Jabaudon et al., 1999; Le Meur et al., 2007). Indeed, a rise of $[Ca^{2+}]i$ in astrocytes can release glutamate by a prostaglandin-dependent mechanism (Bezzi et al., 1998); and three distinct ion channels have been shown to release glutamate: (1) swelling-activated anion channels (Rutledge et al., 1998), (2) gap junctional hemichannels (Ye et al., 2003), and (3) P2X7 receptors gated by ATP (Sperlágh et al., 2002) but all of these mechanisms do not seem to significantly participate in the tonic glutamate release since blocking them does not preclude the tonic glutamate currents in neurons (Cavelier and Attwell, 2005).

Finally, tonic glutamate release has been showed to rely on astrocytes and to be mediated by a 4,4'-Diisothiocyanatostilbene-2,2'-disulphonic acid (DIDS) -sensitive mechanism (Cavelier and Attwell, 2005). DIDS has been found to block numerous anion transporters and channels *via* which glutamate might exit the cell and was found to decrease the neuronal response to tonic glutamate, implying that DIDS decreases the release of glutamate. However, it still remains unclear how DIDS might modulate glutamate efflux (Cavelier and Attwell, 2005).

5 - Role of tonic glutamate - biological meaning

Regardless of different estimations of the exact concentration of ambient glutamate, numerous studies have shown that both pre- and postsynaptic receptors situated peri- and/or extrasynaptically could be tonically activated by extracellular glutamate (Cavelier and Attwell, 2005; Jabaudon et al., 1999; Le Meur et al., 2007); for review see Featherstone and Shippy 2008). Thus, as a function of the level of extracellular glutamate in the hippocampus, tonic activation of NMDARs determines excitability of pyramidal neurons (Sah et al., 1988) and presynaptic group III mGluRs can modulate

GABAergic transmission between interneurons (Semyanov and Kullmann, 2000). Moreover, group III mGluRs sensing ambient glutamate are also responsible for the modulation of both evoked and spontaneous GABA release in the supraoptic nucleus (Piet et al., 2003); and group I mGluRs modulate excitation in the cochlear nucleus (Chanda and Xu-Friedman, 2011). This suggests that mGluRs can detect variations of ambient glutamate leading to disinhibition of interneurons and increase in inhibitory drive, therefore counteracting hippocampal excitability.

Astrocytes play a cardinal role in the regulation of ambient glutamate levels by the process of uptake (*see Part II - Glutamate uptake*). Moreover, astrocytic enwrapment of synapses is subject to experience-dependent remodeling. Thus, physiological reduction in synaptic glial coverage increases activation of mGluRs (Boudaba et al., 2003; Oliet et al., 2001; Piet et al., 2003) and NMDARs (Fleming et al., 2011) in the supraoptic nucleus. This shows that the tonic activation of receptors by ambient glutamate is itself a plastic process dynamically regulated by astocytes.

II. PHASIC GLUTAMATE

1 - Fate of glutamate following synaptic release

Estimations of the timecourse of phasic glutamate, following each release event, in and beyond the synaptic cleft have been assessed combining modeling and electrophysiological studies. The dynamics of the glutamate transient are determined by the rate of release, its peak concentration (glutamate 'spike'), the presence of GluRs and glutamate binding sites and the diffusive properties of the extracellular medium together with active uptake by glutamate transporters.

The average glutamate concentration in a single vesicle has been estimated to be 2 000 - 4 000 molecules of glutamate (Marx et al., 2015) with a concentration of 60-210 mM (Nicholls and Attwell, 1990). Following synaptic release, glutamate concentration in the cleft raises up to 1 µM (Barbour, 2001; Bergles et al., 1999; Zheng et al., 2008).

After release, glutamate molecules are subject to passive diffusion with estimated diffusion time of <1 ms out of the synaptic cleft (Attwell and Gibb, 2005). The tortuosity of the extracellular tissue has a direct effect on the spatiotemporal profile of glutamate diffusion following presynaptic exocytosis. Calculations of the diffusion coefficient of glutamate can slightly vary with structures: 0.45 µm2.ms-1 (Nielsen et al., 2004); 0.32 µm2.ms-1 (Zheng et al., 2008) because the synaptic cleft is packed with macromolecular obstacles (Zuber et al., 2005). The volume fraction (relative amount) of the extracellular space is estimated to be ~0.2 (Nicholson and Sykova, 1998). In a porous medium the diffusion coefficient for glutamate is ~0.3 µm.ms-1 (Min et al., 1998). However, the porous medium does not take into account spatial inhomogeneities and interactions with transporters and other binding sites, which could further slow diffusion. Using ion-sensitive microelectrodes, the tortuosity factor of the neuropil in baseline conditions has been estimated experimentally to be ~1.6 (Nicholson and Sykova, 1998); and an estimation by a modelling study is 1.34 (Rusakov and Kullmann, 1998). The tortuosity of the extracellular space has a crucial role in determining the degree of receptor activation following glutamate release. Thus, increasing extracellular viscosity, and so decreasing the glutamate diffusion coefficient to ~0.15 µm2.ms-1, potentiates synaptic receptors activation by 20-30% (Min et al., 1998).

2 - Sample the signal - role of glutamate receptors

The glutamate transient is a signal, which could be sampled at different degrees by GluRs (Attwell and Gibb, 2005). The timing of activation of GluRs is proportional to their distance from the pre-synaptic release site (Attwell and Gibb, 2005; Barbour and Häusser, 1997; Takumi et al., 1999). Distinct subtypes of GluRs are activated in response to different patterns of activity at excitatory synapses due to their relative affinity for glutamate which suggests the existence of glutamate receptor bandwidth (Attwell and Gibb, 2005; Karakossian and Otis, 2004). The kinetics of GluRs determines how the receptors respond to increases in glutamate concentration of different durations. GluRs decompose the incoming glutamate signal into different temporal components so this could enhance the spatial and temporal spread of neuronal signaling.

AMPARs have fast glutamate unbinding and a low glutamate affinity to allow fast information processing. To ensure high frequency synaptic transmission, AMPARs have high rate constant for the unbinding of glutamate. In addition, AMPARs transmit information on a millisecond timescale and this is made possible because released glutamate is cleared from the synaptic cleft on the same timescale (Diamond and Jahr, 2000, 1997). Under different conditions, AMPARs would be desensitized instead of deactivated. Glutamate clearance depends mainly on the rate and density of glutamate transporters which kinetics are matched with the properties of AMPARs (Diamond and Jahr, 2000, 1997). In contrast, diffusion rate (<1 ms) out of the synaptic cleft is too slow to account for a rapid removal of glutamate and thus avoiding AMPARs desensitization. In addition, electrophoretic interactions between AMPAR–mediated excitatory currents and negatively charged glutamate molecules accelerate the clearance of glutamate from the synaptic cleft, speeding up synaptic responses (Sylantyev et al., 2008). Therefore, low-affinity AMPARs mediate fast excitatory transmission.

In the contrary, NMDARs has a slow unbinding and so a high affinity for glutamate. NMDARs unbinding rate constant is 400 times lower than that for AMPARs. This property of NMDARs is crucial for their role in temporal coincidence detection of synaptic inputs (Attwell and Gibb, 2005; Sjöström et al., 2010) (*see Part III - STDP*). In this manner, back-propagating action potentials will activate NMDARs that were bound to glutamate within the preceding ~50-100 ms. Glutamate binding to NMDARs lasts for a sufficiently long time for the detection of other input occurring. Thus, NMDARs are able to temporally integrate incoming information and extend the duration of glutamate elevations.

Like NMDARs, mGluRs need longer elevations of glutamate to be activated but desensitize faster. Therefore, the kinetics of mGluR responses are in the midrange between AMPARs and NMDARs.

The sampling of glutamate transients by GluRs reflects the fact that synapses operate in different frequency ranges and activity regimes. Thus, the activity of GluRs could determine the speed of information processing at excitatory synapses.

3 - Terminating the signal - role of glutamate transporters

Synaptically released glutamate diffuses out of the synaptic cleft and binds to several receptor subtypes in the peri- or extrasynaptic membrane or at neighboring synapses (Barbour and Häusser, 1997; Kullmann and Asztely, 1998; Kullmann et al., 1996; M et al., 1997; Szapiro and Barbour, 2007). The extent of such extrasynaptic actions is regulated by the high affinity glutamate uptake (Asztely et al., 1997; Bergles and Jahr, 1997; Bergles et al., 1997; Lehre and Rusakov, 2002; Min et al., 1998; Rusakov and Kullmann, 1998; Zheng et al., 2008). mGluRs are preferentially localized perisynaptically (Baude et al., 1993) and NMDARs can be found at both peri- and extrasynaptic locations (Paoletti et al., 2013), implying that glutamate should escape from the synaptic cleft in order to activate these receptors. Glutamate transporters rapidly reduce the free concentration of glutamate but part of the content of the exocytosis of a single vesicle binds to receptors situated in the immediate perisynaptic space (Rusakov and Kullmann, 1998; Zheng et al., 2008). There is a critical role of glutamate diffusion in determining the balance of receptor activation and glial glutamate transporters control the degree to which receptors located outside the cleft are activated following each release event (Bergles et al., 1997; Min et al., 1998; Zheng et al., 2008). It is thus assumed that synaptic isolation is never reached and synapses do not operate as private communication channels.

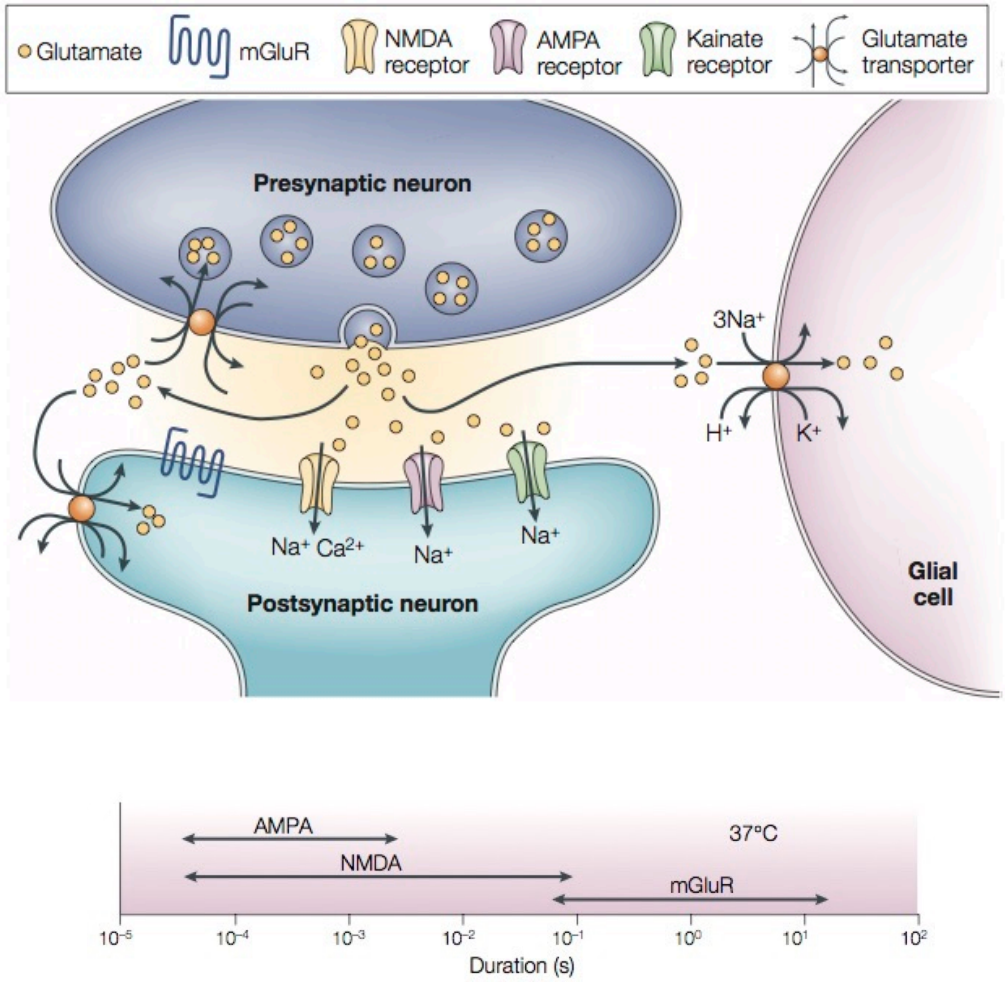

Figure 4. Glutamatergic transmission at central synapses. (Top) Schematic diagram of a glutamatergic synapse. Glutamate released from the presynaptic terminal acts on postsynaptic AMPARs, NMDARs, KARs and mGluRs. The synaptic actions of glutamate are terminated when its concentration in the synaptic cleft is reduced by diffusion, and by uptake by glutamate transporters into surrounding glial cells and into the pre- and postsynaptic neurons. **(Bottom)** Duration ranges of increases in glutamate concentration to which AMPARs, NMDARs and mGluRs can respond at 37°C (From (Attwell and Gibb, 2005)).

4 - Physiological relevance of glutamate spillover

Spillover of glutamate following physiological synaptic activity levels is a controversial issue (Barbour, 2001; Rusakov and Kullmann, 1998). The effect of glutamate spillover would be disadvantageous by reducing synaptic independence and thus reducing the storage capacity of the brain. However, a number of specialized synapses exist in the brain at which spillover has an important functional role. Indeed, glutamate spillover has been reported as the main mode of synaptic transmission in the hippocampus, cerebellum, olfactory bulb and the vestibular system (Carter and Regehr, 2000; DiGregorio et al., 2002; Dubois et al., 2016; Isaacson, 1999; Marcaggi et al., 2003;

Nielsen et al., 2004; Szapiro and Barbour, 2007). Most of these synapses also mediate conventional synaptic transmission and the role of spillover is essentially one of amplification by increasing the postsynaptic response to a given amount of transmitter (high-pass filtering). However, cerebellar climbing fiber-molecular layer interneuron connection is mediated exclusively by glutamate spillover (Szapiro and Barbour, 2007). Therefore, glutamate spillover plays a prominent role in information processing at central synapses together with point-to-point excitatory transmission.

III. QUANTIFYING GLUTAMATE

The concentration and timecourse of glutamate in and outside the synaptic cleft is of crucial importance for shaping excitatory transmission. Glutamate dynamics in the extracellular fluid can occur on a different timescale: from millisecond variations following release events, to slower changes directed by plastic remodeling of the network. Temporal and spatial resolutions are thus critical for monitoring glutamate dynamics in the brain. In an attempt to answer these requirements, various techniques for quantifying extracellular glutamate have been developed.

1- Microdialysis

Historically, glutamate concentration has been determined primarily by *in situ* microdialysis of cerebrospinal fluid (Benveniste et al., 1984; Zhang et al., 2005), but this technique is invasive and is limited by poor spatial and temporal resolution. Indeed, it provides only single-point sampling of bulk tissue with low temporal resolution (in order of tens of seconds). However, to fully understand the characteristics of glutamate dynamics, tools that are capable of assessing real time changes in glutamate transients are needed.

2 - Enzymes

Enzymes such as glutamate dehydrogenase or glutamate oxidase can be coupled to (1) NADH fluorescence in enzyme-linked fluorescence assays (Innocenti et al., 2000; Nicholls and Sihra, 1986); or (2) current through a microelectrode in enzymatic glutamate-selective electrodes (Oldenziel et al., 2007; Pomerleau et al., 2003). Nevertheless, these methods lack cellular resolution, have response times on the order of a second and are confounded by other potential sources of signal.

3 - Electrophysiology

Extracellular glutamate levels can be assessed using NMDARs as ‘glutamate sensors’ by displacement of a rapidly dissociating competitive antagonists (D-AA or D-CCP) from NMDARs during synaptic transmission (Clements et al., 1992); or by monitoring tonic NMDAR-currents mediated by non-synaptic extracellular glutamate (Arnth-Jensen et al., 2002; Herman and Jahr, 2007).

4 - Imaging

In vitro

Biosensors composed of glutamate-binding proteins coupled to a fluorescent probe have much greater spatial and temporal resolutions and signal can be unambiguously assigned in presence of glutamate. (1) Glutamate optical sensor (EOS) is a hybrid-type fluorescent indicator consisting of the glutamate-binding domain of the AMPAR subunit GluR2 and a fluorescent dye conjugated near the glutamate-binding pocket. EOS changes its fluorescence intensity upon binding of glutamate (Namiki et al., 2007; Okubo and Iino, 2011; Okubo et al., 2010). (2) The ligand-dependent conformational change in the *E. coli* glutamate transporter GltI has been used to create glutamate sensors from Förster resonance energy transfer (FRET) between two fluorescent proteins fused to the two protein termini (Dulla et al., 2009; Hires et al., 2008; Okumoto, 2010). Optical detection of glutamate using FRET-based sensor proteins offers the potential to greatly enhance the temporal and spatial resolution at which glutamate transients can be measured.

More recently, the development of real-time measurements of glutamate clearance *in vitro* or *in vivo* using optogenetic reporting allowed visualizing the spatio-temporal dynamics of extracellular glutamate under endogenous release conditions. Quantifying real-time glutamate dynamics has become possible by the use of a high-speed imaging of an intensity-based glutamate-sensing fluorescent reporter (iGluSnFR) (Marvin et al., 2013; Parsons et al., 2016). Important advance of optical methods compared to biochemical assays is that the timecourse of evoked iGluSnFR responses reflects not only transporter-mediated uptake but also diffusion, permitting an overall measure of glutamate clearance. Another crucial factor is that as a genetically encoded sensor, iGluSnFR expression can be driven under the control of a specific promoter allowing measurements of glutamate sensed at the neuronal extracellular surface (versus astrocytic surface as measured by STCs; *see Part II - Glutamate uptake*).

In vivo

Development of an imaging method to probe glutamate levels *in vivo* is of great interest because it would allow studying extracellular glutamate in various pathologies and brain states. The feasibility of this approach has been addressed using positron emission tomography (PET) imaging and the radiotracer 3-(6-methylpyri- din-2-ylethynyl)-cyclohex-2-enone-O-carbon-11-methyl-oxime ([11C]

ABP688), which binds to the allosteric site of the mGluR5 (Ametamey et al., 2006), in both in monkeys (Miyake et al., 2011; Sandiego et al., 2013) and human subjects (Martinez et al., 2014).

PART II

Glutamate uptake

INTRODUCTION

1 - Blood-brain barrier (BBB)

The BBB shields the brain from glutamate in the blood, which is much higher than concentrations that are toxic to neurons (50-200 µM in blood vs 2-5 µM for toxic levels for neurons). Although, brain barrier endothelial cells do not express significant levels of glutamate transporters (Berger and Hediger, 2000; Holmseth et al., 2012, 2009; Lehre et al., 1995), membrane glutamate transporters are heavily expressed in the astrocytic endfeet surrounding the blood vessels. It exists as well an efflux mechanism for glutamate reducing glutamate in the cerebrospinal fluid (Zhou and Danbolt, 2014). Therefore, the BBB prevents glutamate entering from outside the extracellular fluid.

2 - Membrane glutamate transporters

Because there are no enzymes extracellularly that can degrade glutamate (Logan and Snyder, 1971), low extracellular concentrations require efficient cellular uptake systems. Thus, the primary mechanism through which the action of extracellular glutamate is terminated is the active transport *via* excitatory amino acid transporters (EAATs). Another reason to keep the extracellular glutamate levels low is that glutamate is toxic in high concentrations, due to excessive activation of GluRs (Danbolt, 2001; Marcaggi and Attwell, 2004). Therefore, powerful uptake systems like EAATs prevent excessive activation of GluRs and excitotoxicity by continuously removing glutamate from the extracellular fluid in the brain. This uptake is catalyzed by a family of transporter proteins located at the cell surface of both astrocytes and neurons (Beart and O'Shea, 2007; Danbolt et al., 2016; Gegelashvili et al., 2000; Grewer and Rauen, 2005; Tzingounis and Wadiche, 2007; Vandenberg and Ryan, 2013).

3 - Intracellular glutamate carriers

Although it will not be discussed here, it is important to mention that glutamate, once entered the cell, is subject to an intracellular transport (for review see (El Mestikawy et al., 2011; Palmieri, 2013)). When glutamate enters the cytoplasm, it may undergo further redistribution to mitochondria or synaptic vesicles. Mitochondrial mechanisms for glutamate translocation rely on four enzyme carriers located in mitochondria: AGC1, AGC2, GC1 and GC2. Glutamate transporters in synaptic vesicles or vesicular glutamate transporters (VGLUTs) are three different isoforms: VGLUT1, VGLUT2 and VGLUT3. These intracellular glutamate carriers are very different from the glutamate transporters in the plasma membranes.

MEMBRANE GLUTAMATE TRANSPORTERS

I. MECHANISM & STOICHIOMETRY

The glutamate uptake process is electrogenic and is driven by the ion gradients of K^+ and Na^+ (Levy et al., 1998; Owe et al., 2006; Zerangue and Kavanaugh, 1996). Stoichiometry: glutamate influx is driven by the cotransport of 3 Na^+ and 1 H^+ ions, and the counter-transport of 1 K^+ ion (Fig.1). The dependency of the transport process on the electrochemical gradients across the plasma membranes implies that the uptake can reverse if the gradients are sufficiently weakened. The transporters can also operate as exchangers inducing release of internal endogenous glutamate by heteroexchange (Danbolt, 2001). All the EAATs catalyze Na^+- and K^+-coupled transport of L-glutamate as well as L- and D-aspartate, but not D-glutamate. EAATs also function as chloride channels (Machtens et al., 2015) (*see below Cl- conductance*).

The 3:1 ratio of Na^+ to glutamate molecules transported causes a significant Na^+ influx into glial cells during glutamate uptake. The majority of the $[Na^+]_i$ is then removed from the cell by the action of the Na^+/K^+-ATPase (Chatton et al., 2000; Cholet et al., 2002). Such large and long-lasting elevations of $[Na^+]_i$ can strongly affect all Na^+-dependent processes in astrocytes (Kirischuk et al., 2015). Once extracellular glutamate is transported into astrocytes, it is transformed into glutamine by the enzyme glutamine synthetase (*see below Restoring glutamate*).

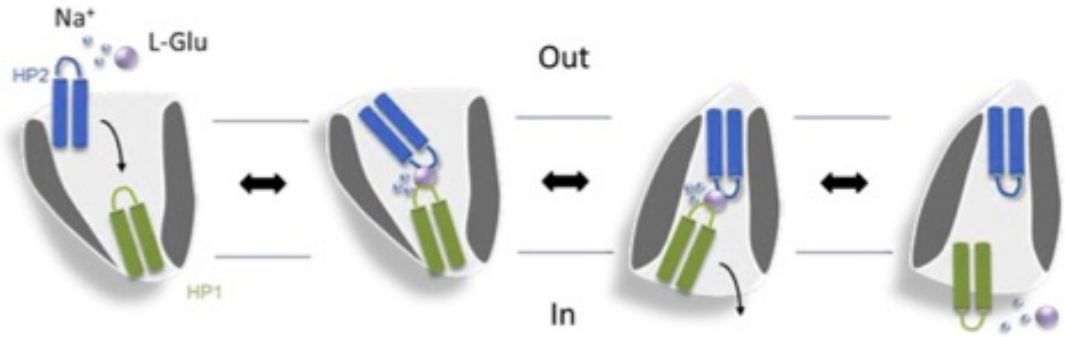

Figure 1. Hypothetical model of glutamate transport mechanism across the plasma membrane from the extracellular space (Out) to the cytosol (In). For the sake of clarity, only the protomer shapes with its hairpins are drawn. L-glutamate (L-Glu) and sodium ions (Na^+) are represented as purple and blue balls, respectively. In the ‘‘open’’ conformation that is closed from the cytosol side, L-glutamate is trapped by HP2 and HP1 in the cavity. After an intermediate state, where the cavity is closed on both sides, the repositioned HP2 finally releases L-glutamate. This mechanism is coupled to the transport of 3 Na+ ions. (Adapted from (Reyes et al., 2009))

II. TYPES / DISTRIBUTION / LOCALIZATION

1 - Regional distribution

To date, five subtypes of EAATs (EAAT1-5) are found in the mammalian brain. Western blot analysis of total brain homogenates completed by immunohistochemistry, immunogold and in situ mRNA studies revealed distinct regional distribution for each glutamate transporter subtype (Chaudhry et al., 1995; Furuta et al., 1997; Kanai and Hediger, 1992; Lehre et al., 1995; Rothstein et al., 1994).

EAAT1 (*Slc1a3* gene) is most abundant in the cerebellar molecular layer, expressed by Bergmann glia cells, but is also found in cortex, hippocampus, superior colliculus and deep cerebellar nuclei (Arriza et al., 1994; Lehre et al., 1995; Rothstein et al., 1994; Wadiche and Kavanaugh, 1998). EAAT2 (*Slc1a2* gene) is present in cortex, hippocampus and striatum (Furuta et al., 1997; Lehre et al., 1995; Rothstein et al., 1994). Higher levels of EAAT3 (*SLC1A1* gene) are found in the cortex, the hippocampus, striatum and cerebellum, and lower levels in the spinal cord (Fairman et al., 1995; Furuta et al., 1997; Lehre et al., 1995; Rothstein et al., 1994; Wadiche et al., 1995b). EAAT3 could be found also in non-neuronal peripheral tissues, including small intestine, kidney, and liver (Arriza et al., 1994; Grewer et al., 2000; Holmseth et al., 2012; Kanai and Hediger, 1992; Rothstein et al., 1994). EAAT4 (*SLC1A6* gene) is expressed in the cerebellum (Dehnes et al., 1998; Fairman et al., 1995; Furuta et al., 1997; Massie et al., 2008) and EAAT5 (*SLC1A7* gene) - in the retina (Arriza et al., 1997).

2 - Cellular/ultrastructural localization

EAAT1 is selectively expressed in astrocytes (somata and processes) (Lehre et al., 1995) with plasma membrane facing neuropil having higher densities than those facing cell bodies (Chaudhry et al., 1995). EAAT2 is specifically expressed in astrocytic processes ensheathing synaptic complexes, but not in astocytic cell bodies (Danbolt et al., 1992; Furuta et al., 1997; Holmseth et al., 2009; Lehre et al., 1995; Levy et al., 1998; Minelli et al., 2001; Rothstein et al., 1994). Particularly in the striatum, EAAT2-immunoreactive astrocytic processes were found to ensheath virtually all striatal neuron somata and envelop synaptic complexes (Rothstein et al., 1994). EAAT2 is also found on neurons but at much lower level than in astrocytes (~10% of astrocytic EAAT2). The physiological role of neuronal EAAT2 remains uncertain based on their very low level of expression but also on their distribution in most of the axon-terminal membranes and not being concentrated in the synapses (Danbolt et al., 2016; Furness et al., 2008; Petr et al., 2015; Rimmele and

Rosenberg, 2016). EAAT3 is found in neurons (Conti et al., 1998; Rothstein et al., 1994) in pre- and postsynaptic elements. EAAT4 is expressed by cerebellar Purkinje cells in particular on extra-synaptic sites (Dehnes et al., 1998; Tanaka et al., 1997). EAAT5 is expressed in the photoreceptors, bipolar and amacrine cells of the retina and has been suggested to mainly act as glutamate-activated chloride channel to control the excitability of retinal neurons (Arriza et al., 1997; Eliasof and Jahr, 1996; Schneider et al., 2014).

3 - Subcellular localization

Both amino and carboxyl terminals of EAAT1 and EAAT2 are located intracellularly (Lehre et al., 1995). The EAAT2b isoform has been found to have a basolateral membrane expression; in contrast, EAAT2a isoform displays a predominant distribution within intracellular vesicle compartments, constitutively cycling to and from the membrane (Underhill et al., 2015). In the retina, it exists a different splice variant of EAAT2, named GLT1c (Rauen et al., 2004), which is expressed by neurons. Alternate splicing might modify the targeting of EAAT2 to distinct membrane domains but does not necessarily confer novel functional properties (Rauen et al., 2004; Schneider et al., 2014; Takahashi et al., 2015).

III. ROLE OF EAATS

1 - Buffering and transport of glutamate

As there are no extracellular enzymes to degrade glutamate, after release, glutamate molecules are subject to passive diffusion combined with active transport. It is hypothesized that thousands of EAATs should be present around synapses to efficiently remove glutamate on a rapid timescale (Diamond and Jahr, 1997; Lehre and Danbolt, 1998). EAATs have similar affinities for glutamate as GluRs (Arriza et al., 1994) and so they compete for the extracellular glutamate. The transport cycle of EAATs is slow (12-70 ms per cycle), relative to the time course of glutamate in the synaptic cleft (Bergles and Jahr, 1998; Clements et al., 1992; Wadiche et al., 1995b). High expression of which is essential to compensate for EAATs slow transport cycle. Thus, the main role of EAATs is to terminate the glutamate transient by primary acting as glutamate buffers followed by active transport. In addition, diffusion in the plasma membrane contributes to the buffering capacity of glial EAATs. EAATs control the degree to which receptors located in the perisynaptic space or outside the cleft are activated following each release event (Bergles et al., 1997; Min et al., 1998; Zheng et al., 2008) (*see Part I - Glutamate dynamics*). Therefore, EAATs efficiently follow the time course of synaptic activation in a temperature-dependent manner (Asztely et al., 1997; Bergles and Jahr, 1998, 1997; Diamond and Jahr, 2000, 1997).

2 - Glutamate metabolism

Glutamate released from the presynaptic terminal is cleared from the cleft through diffusion followed by active transport *via* EAATs that are primarily expressed on astrocytes. Replenishing neuronal stores of glutamate is thus of crucial importance for the normal functioning of the synapses and for maintaining adequate levels of excitatory neurotransmission (Marx et al., 2015). Furthermore, glutamate is also redistributed from synaptic to extrasynaptic sites following uptake by astrocytes.

Glutamate to glutamine

Astrocytic metabolism plays a key role in the process of replenishment of neuronal stores of glutamate vesicular pool. This process is known as the glutamate-glutamine cycle (McKenna, 2007; Robinson and Jackson, 2016; Stobart and Anderson, 2013). Glutamate is mainly amidated to form

glutamine by the enzyme glutamine synthetase. However, during periods of high neuronal activity up to 50% of the intracellular glutamate in astrocytes following uptake may alternatively be deaminated to form a-ketoglutarate and enter the TCA cycle (McKenna, 2007; Robinson and Jackson, 2016; Stobart and Anderson, 2013). Astrocytic glutamine is subsequently transported out of astrocytes and into neurons, where it is used as a precursor for glutamate synthesis, forming a glutamate-glutamine cycle (Hertz et al., 1999; Kirischuk et al., 2012; Marx et al., 2015; Stobart and Anderson, 2013). The astrocytic glutamine transporters LAT2 (Na^+-independent) and SNAT3 (Na-dependent) are capable of mediating glutamine release (Kirischuk et al., 2015). The $[Na^+]i$ rise that occurs as a consequence of astrocytic glutamate influx has the potential to directly stimulate the release of glutamine from this pool *via* SNAT3 transport (Kirischuk et al., 2015). Because glutamate influx by EAATs is coupled to the influx of three Na^+ ions (Zerangue and Kavanaugh, 1996) whereas glutamine efflux *via* SNAT3 is coupled to the efflux of only one Na^+ (Chaudhry et al., 1995), there is potential for 3:1 amplification in the coupling of glutamate uptake to glutamine. Glutamine released from astrocytes is subsequently transported directly into presynaptic terminals where it is converted back to glutamate by glutaminases to support further glutamatergic neurotransmission (Billups et al., 2013). Thus, the astrocytic glutamine release mechanism is therefore a central process in the synapse ability to maintain a sustained level of neurotransmission. Glutamate can be also synthesized *de novo* from glucose in astrocytes *via* the Krebs cycle, followed by transamination or reductive amination of α-oxoglutarate (Erecińska and Silver, 1990).

System xc-

In parallel of being metabolized and converted into glutamine, glutamate following uptake could be also released from astrocytes at distinct extrasynaptic domains. System xc- is located on astrocytic process and functions as a cystine-glutamate antiporter or exchanger that couples the uptake of cystine and glutamate on a 1:1 stoichiometry. The direction of the exchange is determined by the relative substrate concentration gradients. Glutamate release from system xc- has been shown to regulate synaptic neurotransmitter release by stimulating extrasynaptic glutamate receptors and to regulate synaptic plasticity (Bridges et al., 2012; Lewerenz et al., 2013; Moussawi et al., 2011).

GABA synthesis

There is some evidence that the glutamate used for GABA synthesis comes, in part, from glutamate *via* EAATs, and thus alterations of EAATs activity alters also the strength of synaptic inhibition as demonstrated in the hippocampus (Mathews and Diamond, 2003; Sepkuty et al., 2002).

3 – EAATs and chloride conductance

EAATs also function as chloride channels (Fahlke et al., 2016). In addition to the ion-coupled glutamate translocation, EAATs mediate a thermodynamically uncoupled chloride flux activated by the transport of sodium and glutamate molecules, which behaves as an independent process from the coupled flux. In addition to this substrate-activated anion conductance, the EAATs also possess a 'leak' anion conductance (Eliasof and Jahr, 1996; Fairman et al., 1995; Kanner and Borre, 2002; Ryan and Mindell, 2007; Takayasu et al., 2009; Wadiche et al., 1995a; Zerangue and Kavanaugh, 1996). The fraction of the transporter-mediated anionic current varies among EAAT proteins. Single channel amplitudes for Cl- conductance are similar across the different EAAT isoforms but the EAAT4 and EAAT5 channels have a higher probability of opening. Thus, EAAT4 and EAAT5 have the largest chloride conductance (Gameiro et al., 2011; Mim et al., 2005), and may function more as inhibitory glutamate receptors than as transporters (Dehnes et al., 1998; Veruki et al., 2006; Wersinger et al., 2006). Function of EAAT5 transporters on bipolar cells in the retina, for example, lies in their ion channel properties rather than their conventional glutamate transporter activity (Veruki et al., 2006; Wersinger et al., 2006). Similar example also in the retina is a feedback mechanism from horizontal cells to cones where glutamate spillover activates GluT-associated chloride conductance (Vroman and Kamermans, 2015).

4 - H2O/urea cotransport

In addition, a general feature of sodium coupled transport is the transport of water (MacAulay and Zeuthen, 2010; MacAulay et al., 2004). EAATs are cotransport proteins shown to possess the ability to transport fixed amount of water molecules against and independently of external osmotic gradients (along with KCC, NKCC1, GluT, GAT-1, etc …), a feature, not found in AQPs but physiologically important when water transport against on osmotic gradient is needed (MacAulay and Zeuthen, 2010; MacAulay et al., 2004). EAATs are expressed in astrocytic membranes facing the synaptic cleft, an expression pattern opposite to that of AQPs found on perivascular membranes. Besides the secondary active water transport, EAATs have in addition a passive water transport driven entirely by the osmotic gradient like in AQPs. The unit water permeability of EAAT1 is around 20-fold smaller than that of AQP1 (but higher than AQP0) but due to its abundant expression in astocytic membranes facing the neuropil, they would be important for water permeability of those specific membrane areas. Moreover, EAAT1 is also able to cotransport urea (MacAulay and Zeuthen, 2010; MacAulay et al., 2004).

IV. PHYSIOLOGY & PATHOLOGY

A. Development

During embryonic stages, EAAT2 mRNA is expressed at high levels in the ventricular zone and expression continues postnatally in the subventricular zone and persists in this proliferative zone in the adult brain. Transcript levels steadily increase postnatally to reach maximal levels around 14-20 days of age (Furuta et al., 1997; Sutherland et al., 1996; Ullensvang et al., 1997). In addition, the postnatal maturation of EAAT2 expression could differ among regions as for instance astrocyte glutamate transporter currents mature later in the neocortex compared with hippocampus (Hanson et al., 2015). Similar to what is observed in the rodent brain, a study using human tissue suggest that EAAT2 expression appears to be low in mid-gestation, whereas its expression increases later in development (Bar-Peled et al., 1997). These dynamic developmental regulations suggest that EAAT2 not only regulates the excitatory synaptic transmission at mature stages, but also could be involved in the brain development.

B. Regulation

1 - Endogenous regulation

Regulation of transcription, mRNA processing, and translation

The expression and trafficking of EAAT2 is tightly regulated by several factors (Danbolt, 2001; Fontana, 2015; Seal and Amara, 1999; Takahashi et al., 2015).

Neuronal activity can dynamically modulate EAAT2 expression (Benediktsson et al., 2012; Poitry-Yamate et al., 2002). Neurons cultured in the absence of astrocytes express EAAT2 dependent on the presence of neuronal soluble factors (Gegelashvili et al., 2001, 2000, 1997; Plachez et al., 2004; Zhou, 2004). Ablation results in downregulation of glial EAAT2 after glutamatergic differentiation (Ginsberg et al., 1995; Liévens et al., 2000a, 2000b) and sensory experience can increase the envelopment of synapses and EAAT2 expression in sensory cortex (Genoud et al., 2006). Moreover, electrical coupling through gap junctions in astrocytes has also been shown to control EAAT2 expression (Figiel et al., 2007). Indeed, reduced astrocytic coupling by blockade of gap junctions suppress transcriptional activity of EAAT2 promoter resulting in downregulation of EAAT2.

The EAAT2 promoter contains several transcription factor-binding sequences, including NF-kB, Sp1, N-myc, CREB, EGR, and NFAT (Ghosh et al., 2011; Su et al., 2003). NF-kB can be both

positive and negative regulator of EAAT2 function. EGF induces transcriptional activation of EAAT2, whereas TNF-alpha can repress EAAT2 expression, both *via* NF-kB (Sitcheran et al., 2005). Dexamethasone (a glucocorticoid) increases EAAT2 mRNA levels and upregulates EAAT2 protein expression and activity (Wen et al., 2005; Zschocke et al., 2005). Akt (protein kinase B) induces the expression of EAAT2 through increased transcription (Li et al., 2006). Delta opioid receptor activation upregulates EAAT2 in cell culture (Liang et al., 2014). Corticosterone and retinol are both able to increase the translation of EAAT2 transcripts (Tian et al., 2007). EphA4/ephrin-A3 signaling controls EAAT2 expression (Filosa et al., 2009).

Regulation via post-translational modifications

There are two main types of post-translational modifications of EAAT2: phosphorylation and glycosylation. Studies performed using in *Xenopus* oocytes and cell cultures showed that phosphorylation by kinases SPAK and OSR1, and protein kinase C are powerful negative regulators of EAAT2 (Abousaab et al., 2015; Kalandadze et al., 2002), but that kinase GSK3β and proteine kinase C stimulate the activity of EAAT2 (Casado et al., 1993; Jiménez et al., 2014).

Discs large homolog 1 (DLG1; SAP97) scaffolding protein stabilizes EAAT2b isoform at the surface and activation of CaMKII decreases EAAT2b surface expression but does not alter the distribution of EAAT2a (Underhill et al., 2015). Other factors found to stimulate EAAT2 expression are epidermal growth factor (EGF) (Zelenaia et al., 2000) and pituitary adenylate cyclase-activating peptide (PACAP) (Figiel and Engele, 2000). Furthermore, EAATs possess redox-sensing properties, and their oxidation can result in reduced uptake capacity (Trotti et al., 1997) and so nitric oxide through selective nNOS-dependent S-nitrosylation modulates glutamate uptake, metabolism, conversion to glutamine, and glutamatergic transmission (Raju et al., 2015).

Trafficking

There are several molecular mechanisms regulating intracellular trafficking, endocytosis and exocytosis, and surface expression of EAAT2. Intracellular compartmentalization of EAAT2 is regulated by sumoylation (Foran et al., 2014). cAMP modulates VAMP3 vesicle traffic in astrocytes regulating the recycling of EAATs (Li et al., 2015). EAATs are integral membrane proteins and they depend on the lipid environment, and are influenced by fatty acids such as arachidonic acid (Barbour et al., 1989; Trotti et al., 1995; Zerangue et al., 1995) and by oxidation (Trotti et al., 1998). Surface diffusion of EAAT2 is regulated in activity-dependent manner and it varies according to its surface

location (Murphy-Royal et al., 2015). Thus, EAAT2 mobility is strongly reduced in the vicinity of glutamatergic synapses, favoring transporter retention.

2 - EAAT Plasticity

EAATs can undergo plastic changes in both their activity and their level of expression. There are few reports (from the same team) indicating that the regulation of glutamate uptake itself may be important for maintaining the synaptic strength during long-term changes in synaptic efficacy. Indeed, hippocampal LTP is associated with increase in EAAT3- and EAAT2-dependent glutamate uptake during the early and late phase of LTP, respectively; and translocation of EAAT3 from the cytosol to the plasma membrane (Levenson et al., 2002; Pita-Almenar et al., 2006; Pita-almenar et al., 2005). Furthermore, contextual fear conditioning increases the rate of glutamate uptake and EAAT3 membrane expression (Levenson et al., 2002). However, whether the increase in glutamate uptake simply reflects changes in synaptically released glutamate following plasticity-induction protocols or it is indeed a genuine long-term potentiation of the uptake itself remains underexplored.

In addition, astrocytic group I mGluR-dependent potentiation of EAAT2 glutamate uptake as well as membrane insertion of EAAT1 has been reported (Devaraju et al., 2013; Shen and Linden, 2005) suggesting an important contribution of astrocytic calcium signaling in the regulation of glutamate uptake (Bazargani and Attwell, 2016).

Moreover, EAAT2 function can vary with experience. Astroglial wrapping of neurons controlling glutamate clearance is plastic and can be modulated by different physiological processes such as lactation or dehydration (Bernardinelli et al., 2014; Boudaba et al., 2003; Oliet et al., 2001). Furthermore, sensory experience can increase the envelopment of synapses and EAAT2 expression in sensory cortex (Genoud et al., 2006).

3 - Pharmacological regulation

There are numerous synthetic and natural compounds modulating EAATs function and expression (Beart and O'Shea, 2007; Fontana, 2015; Jensen et al., 2015; Soni et al., 2014) (Fig.2).

Inhibitors

Synthetic inhibitors of glutamate transport can be: (1) competitive non-transportable inhibitors: TBOA (all EAATs), DHK (EAAT2) and analogs; or (2) noncompetitive inhibitors: HIP-8 and WAY-213,613 (EAAT2). Several endogenous nutrients and exogenous compounds have been found to be allosteric modulators of EAATs: (1) inhibitors are Zn^{2+} and arachidonic acid (Vandenberg and Ryan, 2013); and negative allosteric mudulators are UCPH-101 and UCPH-102 (EAAT1). Activators of EAATs are MS-153, riluzole and spider toxin, which is a transporter activity enhancer *via* a non-competitive mechanism.

Transcriptional/translational modulators

This type of modulators targets a wide range of transcriptional and translational processes, and consequently they are structurally very diverse. They exhibit pronounced subtype-selectivity since they may act through targets involved in the expression of a specific EAAT gene. A potential drawback is that many of the mechanisms targeted underlie the expression of numerous other genes, and thus transcriptional/translational modulators could potentially exert off-target effects outside the glutamatergic system (Fig.2). Activators of EAAT2 are beta-lactams (Lee et al., 2008; Rothstein et al., 2005), neuroimmunophilin ligand GPI-1046, LDN/OSU-0212320 and harmine. Acids like clavulanic acid, valproic acid and retinoic acid are also found to be EAAT2 activators.

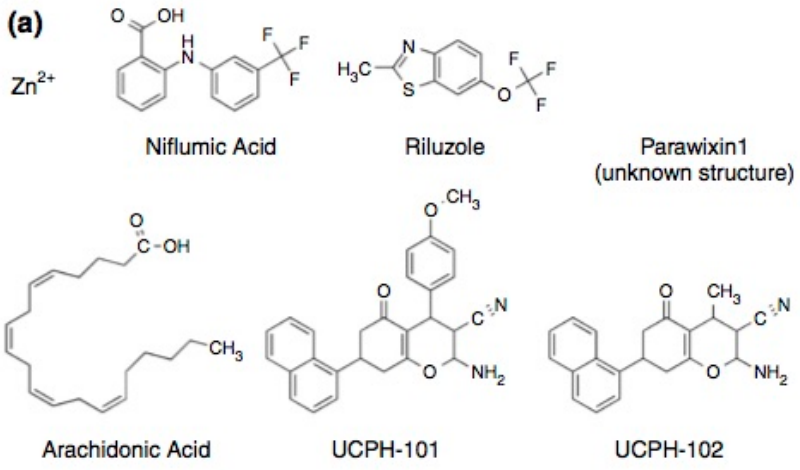

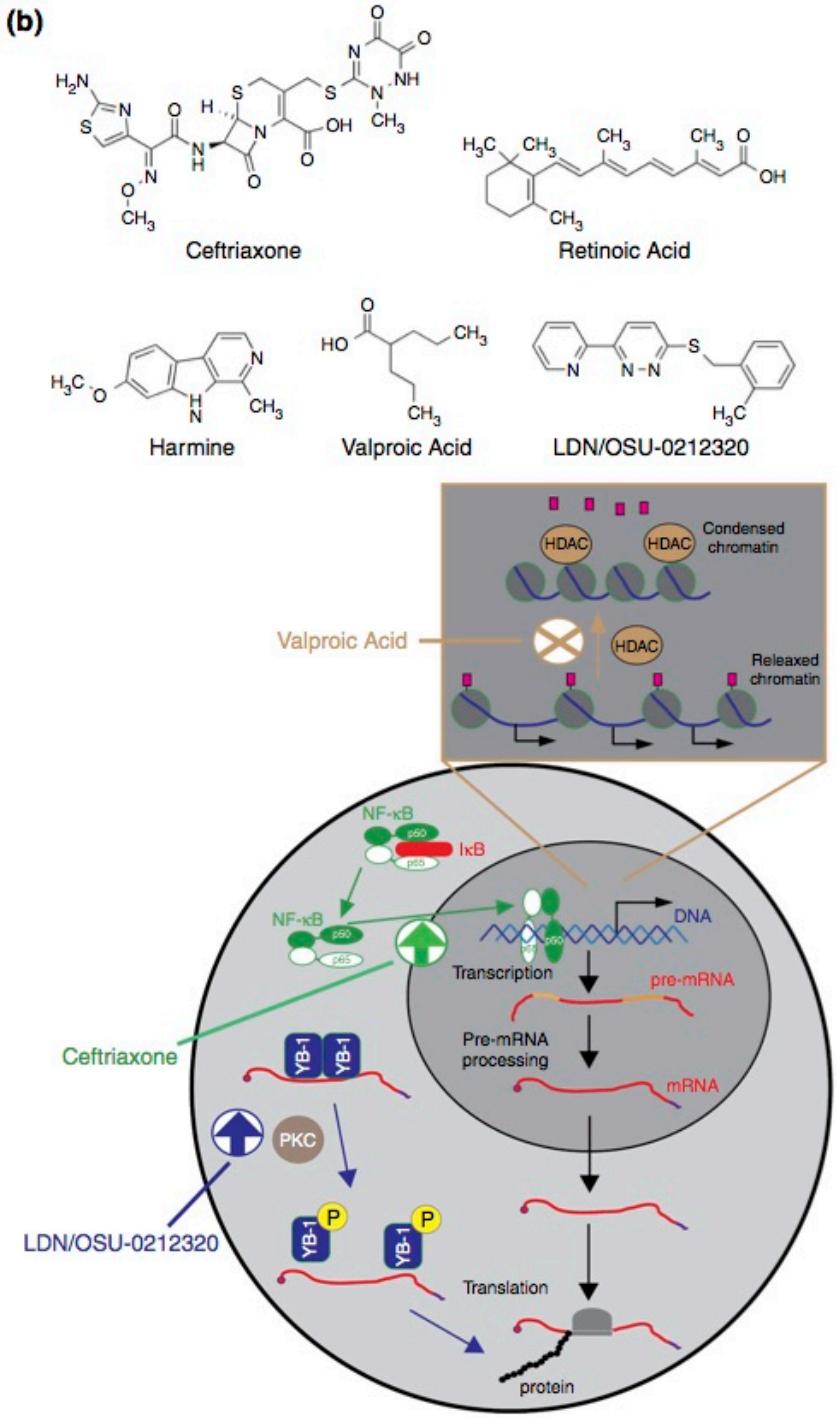

Figure 2. Novel approaches to EAAT modulation. (a) Chemical structures of allosteric EAAT ligands. **(b)** Transcriptional/translational modulators of EAATs. Top: Chemical structures of transcriptional/translational EAAT modulators. Bottom: The proposed mechanisms of action underlying the induction of higher EAAT expression levels by valproic acid, cefriaxone and LDN/OSU-0212320. Valproic acid is a transcriptional EAAT3 activator acting through inhibition of histone deacetylases (HDACs). These enzymes catalyze the deacetylation of specific lysine residues in histones enabling these to wrap DNA tightly hereby disabling gene transcription. Ceftriaxone has been proposed to augment EAAT2 expression level by promoting nuclear translocation of the transcription factor nuclear factor-kB (nF-kB) through proteasomal degradation of IkB. nF-kB subsequently binds to the EAAT2 promoter and increases the transcription of the gene. LDN/OSU- 0212320 is a translational EAAT2 activator acting in part through protein kinase C-mediated stimulation of Y-box-binding protein 1 (YB-1), an intracellular protein among other functions regulates the translation by binding to mRNA. (From (Jensen et al., 2015))

C. Role in physiology

1 - Physiological importance

Generation of specific KO mice for EAAT subtypes has revealed their physiological importance. EAAT2 is the only one of the EAAT-type of glutamate transporters that is required for survival under non-challenging conditions (Petr et al., 2015; Tanaka et al., 1997). Deletion of the astrocytic EAAT2 leads to dramatic effects such as excess mortality, lower body weight, and spontaneous seizures (Holmseth et al., 2012; Matsugami et al., 2006; Petr et al., 2015; Tanaka et al., 1997; Voutsinos-Porche et al., 2003), whereas no detectable neurological abnormalities could be observed with neuronal EAAT2 deletion (Petr et al., 2015). EAAT1 KO mice exhibit altered motor coordination but develop normally (Watase et al., 1998). Mice lacking EAAT3 (Peghini et al., 1997) develop dicarboxylic aminoaciduria, but do not show signs of neurodegeneration at young age and do not display epilepsy (Aoyama et al., 2006; Peghini et al., 1997). EAAT4 knockout mice are viable and appear normal (Huang, 2004) albeit with some alteration of receptor activation (Nikkuni et al., 2007). At present, no EAAT5 KO mice are available.

2 - Transmission

Synaptic transmission

EAATs are efficiently activated by synaptic activation (Bergles and Jahr, 1998, 1997; Bergles et al., 1997; Diamond and Jahr, 2000, 1997) and glutamate uptake affects both the fast and slower components of the synaptic glutamate transient (Asztely et al., 1997; Bergles and Jahr, 1998, 1997; Carter and Regehr, 2000; Clark and Cull-Candy, 2002; Diamond, 2001; Goubard et al., 2011; Kullmann and Asztely, 1998; Marcaggi et al., 2003; Nielsen et al., 2004; Otis et al., 1997, 1996; Overstreet et al., 1999; Sadeghi et al., 2014; Takayasu, 2005; Takayasu et al., 2006; Tong and Jahr, 1994; Turecek and Trussell, 2000); for review see (Coddington et al., 2014; Tzingounis and Wadiche, 2007). EAATs also shape synaptic transmission through surface diffusion (Murphy-Royal et al., 2015). Interestingly, in the retina, regulation of glutamate release by presynaptic EAATs have been found to be regulated by the transporter-associated anion current that hyperpolarizes the presynaptic terminal and thereby inhibits synaptic transmission as a result of shunting inhibition (Veruki et al., 2006; Vroman and Kamermans, 2015). In the same line, Purkinje cell EAAT4 controls AMPAR activation of Bergman glia (Tsai et al., 2012). Thus, fast removal of glutamate by

transporters contributes to set the strength and timing of synaptic inputs by controlling receptor activation during neuronal activity.

Spillover

Glutamate transport is crucial for limiting the spill-out to extrasynaptic receptors and the spillover to neighboring synapses, thus tightly controlling both cooperation and synaptic independence. High-affinity extrasynaptic NMDARs and mGluRs, located on peri- or extrasynaptically (Baude et al., 1993; Paoletti et al., 2013), or on neighboring neurons, mediate most of the spillover responses and their activation is limited by active glutamate uptake (Coddington et al., 2013; Huang and Bergles, 2004; Kullmann and Asztely, 1998). Control of NMDARs on glutamatergic neurons, by glutamate transporters, has been shown in the olfactory bulb (Isaacson, 1999); hippocampus (Arnth-Jensen et al., 2002; Diamond, 2001); retina (Chen and Diamond, 2002); spinal cord (Nie and Weng, 2009) and prefrontal cortex (Chalifoux and Carter, 2011). Glutamate uptake also controls activation of NMDARs on GABAergic neurons mainly at cerebellar synapses: parallel fiber (PF)-stellate cell (Carter and Regehr, 2000); PF-molecular layer interneurons (Clark and Cull-Candy, 2002); climbing fiber (CF)-molecular layer interneurons (Szapiro and Barbour, 2007); GABAergic terminals to Purkinje cells (Huang and Bergles, 2004). In addition, glutamate transport regulates mGluR activation on GABAergic terminals in cerebellum at both PF-Purkinje cell and CF-Purkinje cell synapses (Brasnjo and Otis, 2001; Dzubay and Otis, 2002; Reichelt and Knöpfel, 2002). In a similar manner, astrocytic glutamate uptake controls activation of mGluRs located on hippocampal interneurons (Huang et al., 2004).

Tonic activation of receptors

Both pre- and postsynaptic receptors situated peri- and/or extrasynaptically could be tonically activated by extracellular glutamate and EAATs are crucial for the regulation of ambient glutamate levels (Cavelier and Attwell, 2005; Jabaudon et al., 1999; Le Meur et al., 2007); for review see (Featherstone and Shippy, 2008) (*see Part I - Glutamate dynamics*). Tonic activation of NMDARs determines excitability of pyramidal neurons (Sah et al., 1988) and mGluRs sensing ambient glutamate modulate GABAergic transmission (Chanda and Xu-Friedman, 2011; Piet et al., 2003; Semyanov and Kullmann, 2000). Moreover, physiological reduction in synaptic glial coverage, and thus, in glutamate uptake, increases activation of mGluRs (Boudaba et al., 2003; Oliet et al., 2001; Piet et al., 2003) and NMDARs (Fleming et al., 2011) in the supraoptic nucleus. Therefore, besides

modulating receptor activation after phasic glutamate release, EAATs are important in shaping the degree of tonic activation of receptors by ambient glutamate.

3 – Synaptic plasticity

Genetic and pharmacological manipulations of EAATs have brought important insights in EAAT role in synaptic plasticity, investigated using rate-coding protocols such as low- and high-frequency stimulation (LFS and HFS) or theta-burst stimulation (TBS). Pharmacological inhibition of EAATs enhances HFS-LTD (Pinard et al., 2003), has a permissive role for the expression of LFS-LTD (Massey et al., 2004) or induces heterosynaptic LTP in amygdala (Tsvetkov et al., 2004). Previous studies showed that astrocytic EAAT2 is mandatory for HFS-LTP expression by using either EAAT2 knockout mice (Katagiri et al., 2001) or by pharmacological inhibition (Wang et al., 2006). EAAT2 upregulation by chronic treatment with ceftriaxone, impairs LFS-LTD and reduces HFS-LTP magnitude (Omrani et al., 2009). As exemplified by the use of EAAT3 knockout mice, neuronal transporters have also been demonstrated to control synaptic plasticity by regulating the balance between potentiation and depression elicited by TBS and LFS, respectively (Scimemi et al., 2009). Finally, cerebellar LTD depends on the patterned expression of neuronal EAAT4 on Purkinje cells (Wadiche and Jahr, 2005) and is enhanced by EAAT4 blockade (Brasnjo and Otis, 2001).

4 - Brain energy

A mechanism known as the astrocyte-neuron lactate shuttle (ANLS) accounts for the coupling between synaptic activity and energy delivery. Indeed, glutamate stimulates glucose uptake and lactate production in astrocytes (Magistretti and Allaman, 2015; Pellerin and Magistretti, 2012; Robinson and Jackson, 2016). This glutamate-stimulated aerobic glycolysis is triggered by the uptake of glutamate, which is cotransported with sodium with a stoichiometry of one glutamate to three Na^+, resulting in the disruption of the sodium gradient. This triggers the activity of the energy-consuming Na^+/K^+ ATPase at the expense of one ATP per cycle of the pump to extrude three Na^+. Glutamate is mainly converted to glutamine by glutamine synthetase at the expense of another ATP. Thus, glutamate uptake and recycling in astrocytes result in a decrease in ATP content (Magistretti and Chatton, 2005). This decrease in the energy charge of the cell promotes glucose uptake and metabolism (Fig.3). The ANLS mechanism thus suggests that the uptake of synaptically released glutamate *via* EAATs into astrocytes and the ensuing increase in intracellular sodium represent a key signal for activated neurons to import glucose into astrocytes and produce lactate as an energy substrate (Magistretti and Allaman, 2015; Pellerin and Magistretti, 2012; Robinson and Jackson, 2016).

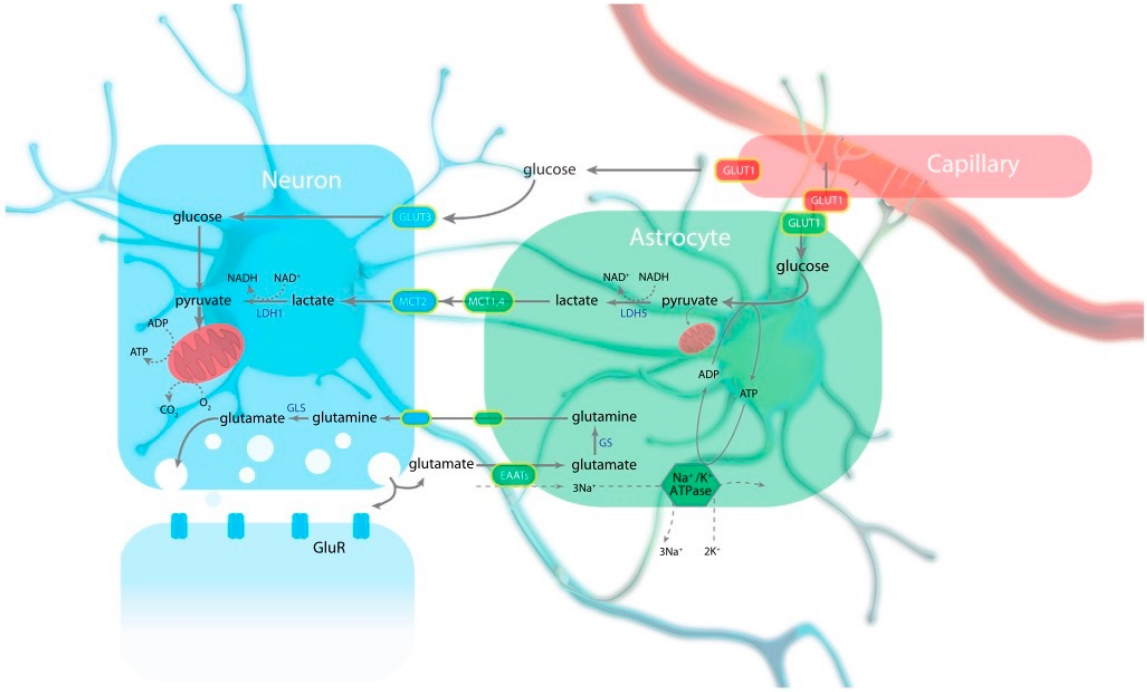

Figure 3. Schematic representation of the astrocyte-neuron lactate shuttle. Glutamate released at the synapse activates glutamatergic receptors (GluRs), a process associated with energy expenditure in neuronal compartments. A large proportion of the glutamate released at the synapse is taken up by astrocytes *via* EAATs (more specifically, EAAT1 and EAAT2). The disrupted Na^+ homeostasis is reestablished by the action of the Na^+/K^+, an ATP-consuming process. Following its uptake by astrocytes, glutamate is converted to glutamine by the action of glutamine synthetase (GS), also an ATP-consuming process, and shuttled to neurons, where it is converted back to glutamate by glutaminases (GLSs). The metabolic burden created by glutamate uptake triggers nonoxidative glucose utilization in astrocytes and glucose uptake from the circulation through the glucose transporter GLUT1 expressed by both capillary endothelial cells and astrocytes. Glycolytically derived pyruvate is converted to lactate by lactate dehydrogenase 5 (mainly expressed in astrocytes) and shuttled to neurons through monocarboxylate transporters (mainly MCT1 and MCT4 in astrocytes and MCT2 in neurons). In neurons, lactate can be used as an energy substrate following its conversion to pyruvate by LDH1 (mainly expressed in neurons). Under basal conditions, neurons can also take up glucose *via* the neuronal GLUT3. Concomitantly, astrocytes participate in the recycling of synaptic glutamate *via* the glutamate-glutamine cycle. (Fom Magistretti and Allaman, 2015)

D. Role in pathology

Alterations in the proper uptake of glutamate by astrocytes can lead to glutamate excitotoxicity, which is a pathological process. This results in sustained elevation of extracellular glutamate levels and excessive activation of post-synaptic GluRs resulting in increased Ca^{2+} influx (Nilsson et al., 1990) and activation of a cascade of phospholipases, endonucleases, and proteases that can lead to apoptotic or necrotic cell death (Raghupathi, 2004). In excitotoxic states, the extracellular concentrations of glutamate reaches a millimolar range, causing degeneration of neurons through excessive stimulation of glutamate receptors (Clements et al., 1992; Meldrum and Garthwaite, n.d.; Rosenberg et al., 1992; Zhou and Danbolt, 2014). Therefore, the tight regulation of the glutamate signal by EAAT2 is of crucial importance for normal glutamate neurotransmission and, when altered, it can lead to pathological states.

EAAT2 function has been extensively studied in the case of different neurological conditions including neurodegenerative diseases and addiction but the discerning between cause and effect in terms of EAAT2 dysfunction remains difficult to access (Beart and O'Shea, 2007; Fontana, 2015; Oliveira et al., 2015). Nevertheless, these pathological conditions are linked to profound impairment of cognitive functions, which further strengthens the fact that normal EAAT2 function is crucial for learning and memory.

1 - Mechanisms of EAAT2 deregulation

Reversal of the EAAT2 transporter is mechanism shown to mediate glutamate excitotoxicity in ischemia (Rossi et al., 2000). Different mechanisms leading to EAAT2 dysfunction are altered splicing of EAATs and/or altered expression of splice variants found in ALS, epilepsy, hypoxia, human glioma and astrocytoma (Beart and O'Shea, 2007; Fontana, 2015).

Another possibility of EAAT2 dysfunction is the altered protein and mRNA expression levels (both up- or downregulation). EAAT2 downregulation is observed in various neurodegenerative diseases including Parkinson's, Huntington's and Alzheimer's. In this context, ceftriaxone appears as a new drug strategy for treatment (Beart and O'Shea, 2007; Medina et al., 2013; Soni et al., 2014; Takahashi et al., 2015). On the contrary, EAAT2 is upregulated in the prefrontal cortex of schizophrenics (Matute et al., 2005) but downregulated in thalamus (McCullumsmith et al., 2015).

Negative experience also regulates EAAT2 expression. EAAT2 downregulation in striatum and habenula is found in a rat model of depression (Almeida et al., 2010; Cui et al., 2014). Moreover, ceftriaxone has been reported to display antidepressent-like effects (Mineur et al., 2007); for review

see (Medina et al., 2013; Sanacora et al., 2008). Glucocorticoids or chronic stress could affect EAAT2 expression (Popoli et al., 2012; Reagan et al., 2004) and acute stress has been shown to result in EAAT2 downregulation (Yang et al., 2005).

Chronic exposure to drugs of abuse such as nicotine, ethanol, cocaine or heroin has also been shown to induce a down-regulation of EAAT2 in the nucleus accumbens leading to enhance extracellular glutamate levels and aberrant potentiation of glutamate transmission (Scofield and Kalivas, 2014). EAAT2 up-regulation following chronic ceftriaxone treatment (Rothstein et al., 2005) constitutes a promising tool to restore glutamate homeostasis, to attenuate some of the motor and/or cognitive symptoms of Huntington's, Parkinson's or Alzheimer's diseases (Soni et al., 2014), to reverse drug-induced plasticity and to inhibit drug seeking (Scofield and Kalivas, 2014). Thus, EAAT2 appears to be a major target for the treatment of neurological as well as psychiatric diseases and addiction and the development of novel therapeutical targets (Jensen et al., 2015; Kim et al., 2011; Sanacora et al., 2008; Scofield and Kalivas, 2014; Soni et al., 2014).

2 - Effect of EAAT2 alterations on behavior

On the contrary, few studies reported the effect of altering EAAT2 expression on pathological behavior (Oliveira et al., 2015). Blockade of EAAT2 induces depressive-like effects and anhedonia (Bechtholt-Gompf et al., 2010; John et al., 2012) and blockade of EAAT2 in amygdala alters social behavior (Lee et al., 2007). EAAT2 KO mice exhibit seizures and premature death (Petr et al., 2015; Tanaka et al., 1997). Recently, an inducible astrocyte-specific EAAT2 KO in dorsal striatum showed pathological repetitive behaviors and an increased corticostriatal excitatory transmission (Aida et al., 2015). Moreover, this phenotype was reversed by blockade of extrasynaptic NMDARs by memantine treatment, confirming that excessive glutamate spillover due to EAAT2 dysfunction underlies these repetitive behaviors emerging from deregulation of the corticostriatal pathway. On the other hand, EAAT2 overexpression has been reported to impair hippocampal learning (Matos-Ocasio et al., 2014).

	Human tissue	*Experimental models*
ALS	[Glu] ↑ in CSF.[1] ↓ Uptake in CNS tissue.[2] ↓ GLT-1 in CNS tissue.[3]	ALS mutant SOD1 inactivates EAAT2.[4] Extracellular [Glu] ↑ in the cortex of ALS-SOD1 transgenic mice.[5] Focal EAAT2 loss in ALS-SOD1 transgenic mice.[6]
Epilepsy	↑Plasma [Glu] in epileptic patients.[7] ↑Hippocampal [Glu] in seizures.[8] Temporal lobe epilepsy: EAAT3 ↑ in hippocampal granule cells, EAAT2 ↓ in hilus and CA1, EAAT1 ↑ in CA2/3.[9] ↑Incidence of aberrant EAAT2 splicing in temporal lobe epilepsy patients.[10]	Fatal seizures in EAAT2 knockout mice.[11] ↓ EAAT1, 2 and 3 protein in GLAST, GLT-1 and EAAC1 protein in the brain of genetically epileptic rats.[12]
Huntington's disease	EAAT2 mRNA ↓ in neostriatum, but the number of cells expressing EAAT2 mRNA ↑.[13] Uptake ↓ in the caudate and putamen.[14]	EAAT2 mRNA and uptake down in the striatum and cortex of R6 transgenic mice.[15] Impaired Glu metabolism in R6/2 mouse brains.[16]
Alzheimer's disease	Uptake ↓ in the cortex[17] and astrocytes[18] and EAAT2 protein ↓[19] in AD patients. Aberrant neuronal expression of EAAT1[20] and EAAT2[21] associated with tau accumulation.	Glu uptake and EAAT1, EAAT2 protein ↓ in APP transgenic mice.[22] ↓ EAAT2 and Glu uptake in GFAP-tau transgenic mice.[23] β-amyloid ↓ Glu uptake.[24]
Ischaemic stroke injury	EAAT2 promoter polymorphism associated with ↑ [Glu] and frequency of stroke.[25] Neonatal hypoxic–ischaemic encephalopathy: EAAT1 ↓ in molecular layer, ↑ in Purkinje and inner granule cell layer; EAAT4 ↓ in Purkinje cells.[26]	EAAT reversal in severe ischaemia *in vitro*.[27] EAAT2/3 ↓ in piglet brain and neuronal expression of EAAT2 after hypoxia–ischaemia.[28] EAAT2 ↑ in the cortex, ↓ in the striatum after hypoxia–ischaemia in rats.[29]
White matter injury	↑ Serum [Glu] in relapsing MS patients.[30] ↑ [Glu] in white matter and acute lesions of MS brains.[31] ↓ EAAT1 and EAAT2 in oligodendrocytes in MS lesions.[32] ↓ EAAT1/2/3 in CNS tissue from MS patients.[33] ↑ EAAT1 and EAAT2 mRNA, protein and uptake in MS optic nerve.[34]	TNF-α ↓ EAAT-1 expression and Glu uptake in cultured oligodendrocytes.[32] Depolarization causes EAAT reversal in spinal white matter.[35]
Infection	↑ Plasma [Glu] in HIV patients.[36] Strong expression of EAAT1 in activated macrophages/ microglia of HIV-infected brains.[37] Uptake ↓ by >50% in AIDS dementia brains.[38]	TNF-α ↓ uptake in primary human astrocytes.[39] TNF-α, interferon-γ and interleukin-1β ↓ uptake in cultures of rat hippocampus.[40] HIV-1 or gp120 ↓ EAAT2 and uptake in astrocytes.[41] Microglia and macrophages express EAAT2 in SIV-infected primates.[42] LPS ↑ EAAT2 in cultured astrocytes and microglia.[43]
Retinal disease/ Glaucoma	↑ [Glu] in vitreous body of glaucoma[44] and diabetic retinopathy patients.[45] ↑ [Glu] in aqueous humor in retinal artery occlusion.[46] ↓ EAAT1 in glaucomatous eyes.[47]	↑ Intraocular [Glu] after optic nerve lesion.[48] ↓ EAAT1 activity after retinal ischaemia.[49]
Neuropsychiatric disorders	↑ EAAT1 and EAAT2 mRNA in the thalamus of schizophrenia.[50] ↓ Striatal EAAT3/4 mRNA in bipolar disorder,[51] ↓ striatal EAAT3 mRNA in schizophrenia,[51] ↓ striatal EAAT4 mRNA in major depression.[51] ↑ mRNA for EAAT3- and EAAT4-interacting proteins in the thalamus in schizophrenia.[52] ↑ mRNA for EAAT2 in prefrontal cortex of untreated schizophrenics, reduced by antipsychotic treatment.[53]	Altered expression of mRNA for EAAT-interacting proteins in clozapine-treated rats.[52] Clozapine and haloperidol ↓ EAAT2/3 mRNA in regions of rat brain.[54] Clozapine ↓ EAAT2 and uptake in cultured astrocytes.[55]

Abbreviations: AD, Alzheimer's disease; ALS, amyotrophic lateral sclerosis; CSF, cerebrospinal fluid; EAAT, excitatory amino-acid transporter; GFAP, glial fibrillary acidic protein; MS, multiple sclerosis; SOD, superoxide dismutase; TNF-α, tumour necrosis factor-α.

[1] Rothstein *et al.* (1990); [2] Rothstein *et al.* (1992); [3] Rothstein *et al.* (1995); [4] Trotti *et al.* (1999); [5] Alexander *et al.* (2000); [6] Howland *et al.* (2002); [7] Janjua *et al.* (1992); [8] During and Spencer (1993); [9] Mathern *et al.* (1999); [10] Hoogland *et al.* (2004); [11] Tanaka *et al.* (1997); [12] Dutuit *et al.* (2002); [13] Arzberger *et al.* (1997); [14] Cross *et al.* (1986); [15] Liévens *et al.* (2001); [16] Behrens *et al.* (2002); [17] Masliah *et al.* (1996); [18] Liang *et al.* (2002); [19] Li *et al.* (1997); [20] Scott *et al.* (2002); [21] Thai (2002); [22] Masliah *et al.* (2000); [23] Dabir *et al.* (2006); [24] Keller *et al.* (1997); Lauderback *et al.* (1999); [25] Mallolas *et al.* (2006); [26] Inage *et al.* (1998); [27] Rossi *et al.* (2000); [28] Martin *et al.* (1997); Pow *et al.* (2004); [29] Cimarosti *et al.* (2005); [30] Westall *et al.* (1980); [31] Srinivasan *et al.* (2005); [32] Pitt *et al.* (2003); [33] Werner *et al.* (2001); [34] Vallejo-Illarramendi *et al.* (2006); [35] Li *et al.* (1999); Li and Stys (2001); [36] Droge *et al.* (1993); [37] Vallat-Decouvelaere *et al.* (2003); [38] Sardar *et al.* (1999); [39] Fine *et al.* (1996); [40] Ye and Sontheimer (1996); [41] Wang *et al.* (2003); [42] Chretien *et al.* (2002); [43] O'Shea *et al.* (2006); Persson *et al.* (2005); [44] Dreyer *et al.* (1996); [45] Ambati *et al.* (1997); [46] Wakabayashi *et al.* (2006); [47] Naskar *et al.* (2000); [48] Yoles and Schwartz (1998); [49] Barnett *et al.* (2001); [50] Smith *et al.* (2001); [51] McCullumsmith and Meador-Woodruff (2002); [52] Huerta *et al.* (2006); [53] Matute *et al.* (2005); [54] Schmitt *et al.* (2003); [55] Vallejo-Illarramendi *et al.* (2005b).

Figure 4. Alterations in glutamate uptake in various pathological conditions: parallel between human and animal studies. (Fom Beart and O'Shea, 2007)

V. PROBING GLUTAMATE UPTAKE

1 - Biochemical uptake assays

The most common approach to quantify glutamate transport is by biochemical uptake assays in brain tissue by liquid scintillation counting of radio-labeled exogenous glutamate or aspartate that is taken up by a synaptosomal preparation on a timescale of minutes. However, an important caveat of this technique is that the rapid release from presynaptic terminals and reuptake by nearby transporters that characterize synaptic transmission, are both lost with biochemical uptake assays. Furthermore, the uptake of exogenous substrates in the brains slices and synaptosomal preparations mostly occurs in the nerve terminals rather than in astrocytes (Danbolt et al., 2016; Furness et al., 2008; Petr et al., 2015). This favors the use of real-time measurements of glutamate clearance *in situ* using electrophysiology or optogenetic reporting.

2 - Electrophysiology

Endogenous glutamate clearance in brain slices could be monitored online by electrophysiological measures of synaptically evoked transporter-mediated currents (STCs) recorded from astrocytes in various brain regions (Barakat and Bordey, 2002; Bergles and Jahr, 1997; Cammack and Schwartz, 1993; Clark and Barbour, 1997; Diamond and Jahr, 2000; Diamond et al., 1998; Goubard et al., 2011; Otis et al., 1997; Wadiche and Jahr, 2005). STCs are generated by the Na^+ influx into glial cells during glutamate uptake and allow a direct measurement of the transport of glutamate from synaptic origin upon electrical stimulation of afferents. The specific properties of STCs are that they present a rectifying inward current at peak, have a large amplitude at negative potentials that is reduced with depolarization of the recorded astrocyte, and have no reversal of current (contrary to ion fluxes through channels).

PART III

Spike timing-dependent plasticity (STDP)

INTRODUCTION

1 - Information processing

Information processing at central synapses is governed by two main neural coding strategies: integration and coincidence detection, which rely on spike-rate (=spike count) and spike-time coding, respectively (DeCharms and Zador, 2000); Dayan & Abbott 2001; Gerstner et al., 2014). Whether neurons use rate coding or temporal coding is a topic of intense debate. Truth stands in the middle.

Action potentials convey information through their timing and can be characterized simply by their time of occurrence. (1) An independent-spike code is based solely on the time-dependent firing rate of a neuron when a stimulus is present. In this case, individual action potentials encode independently of each other and the generation of each spike is independent of all the other spikes in the train. (2) A correlation code is the case when correlations between spike times (=interspike intervals) may carry additional information and individual spikes do not encode independently of each other. In reality, information is likely to be carried both by individual spikes and through spike correlations.

2 - Temporal code

When precise spike timing or high-frequency firing rate fluctuations carry information, the neural code is identified as a temporal code. In the case of an independent-spike code, if the time-dependent firing rate varies slowly, the code is identified as a rate code, and if it varies rapidly, the code is considered as a temporal code. Thus, both inter-spike intervals (in the case of correlation code) and variations in the time-dependent firing rate (in the case of independent-spike code) could underlie temporal coding.

3 - Operation modes

Accordingly, depending on the type of code used, neurons are considered to operate as integrators or as coincidence detectors based on how they process input (Ratté et al., 2013). Integrators can summate temporally dispersed (asynchronous) inputs, whereas coincidence detectors respond only to temporally coincident (synchronous) inputs. In other words, integrators and coincidence detectors are both sensitive to synchronous input, but coincidence detectors are selective for it (Ratté et al., 2013).

Rate coding

The use of rate coding implies good temporal integration of synaptic inputs, a feature that is usually limited by membrane conductances that allow synaptically delivered charge to leak out of the cell over time. Rate coding is associated with long (=infinite) membrane time constant, allowing neurons to perform accurate temporal integration of synaptic inputs.

Coincidence detection

In contrast, coincidence detection depends on short membrane time constant permitting otherwise quiescent neurons to fire only during coincident input, but also on the spiking threshold and the statistics of the input, which should be synchronous. Coincidence detectors can sum their inputs using a narrow time window, whereas integrators use a broad window (Ratté et al., 2013).

The question of whether individual neurons encode and process information by using precise spike timings, thus, working as coincidence detectors, or spike rates, thus, working as temporal integrators, has been highly debated (DeCharms and Zador, 2000). Both mechanisms generally coexist in the same neuron. In the PFC, depending on the inputs to L5 pyramidal neurons, dendrites behave either as temporal integrators or as coincident detectors by responding to spatially distributed signals within a narrow time window (Dembrow et al., 2015). Furthermore, STN neurons operate by combining integration and coincidence detection and the use of one or the other function is dependent on the ongoing activity that the neurons receive (Farries et al., 2010). Theoretical work has shown that cortical pyramidal neurons are capable of operating in a continuum between coincidence detection and temporal integration, depending on the characteristics of the synaptic inputs (synchronous *vs* dispersed) (Rudolph and Destexhe, 2003).

ASSOCIATIVE LEARNING

Activity-dependent modifications in synaptic strength are widely believed to be the basic phenomenon underlying learning and memory, and are also thought to play a crucial role in the development of neural circuits. Experience and training modify synapses and these modifications lead to network remodeling and changes in patterns of neuronal firing to affect behavior.

1 - Hebb

In 1949, Canadian psychologist Donald Hebb speculated that if input from neuron A often contributes to the firing of neuron B, then the synapse from A to B should be strengthened. Hebb suggested that such synaptic modification could produce neuronal assemblies that reflect the relationships experienced during training Hebb 1949; (Sejnowski, 1999).

"When an axon of cell A is near enough to excite B and repeatedly or persistently takes part in firing it, some growth process or metabolic change takes place in one or both cells such that A's efficiency, as one of the cells firing B, is increased." (Hebb 1949)

The Hebbian theory was later summarized by the American neurobiologist Carla J. Shatz in the famous *"Cells that fire together, wire together"*.

"Segregation to form the columns in the visual cortex [...] proceeds when the two nerves are stimulated asynchronously. In a sense, then, cells that fire together wire together. The timing of action-potential activity is critical in determining which synaptic connections are strengthened and retained and which are weakened and eliminated" (Shatz 1992)

The Hebb postulate forms the basis of much of the research done on the role of associative synaptic plasticity in learning and memory. For example, this rule can be applied to neurons that fire together during training due to an associating between a stimulus and a response. As a consequence, these neurons would develop strong interconnections, and subsequent activation of some of them by the stimulus could produce the synaptic drive needed to activate the remaining neurons and generate the associated response.

2 - Coincidence detection

Hebb's words have been interpreted to mean that synaptic plasticity should be based on coincidence detection. Strengthening of the synapse should, thus, occur when the release of neurotransmitters from a presynaptic terminal coincides with the depolarization of the postsynaptic neuron. Hebb's original suggestion concerned increase in synaptic strength, but it has been generalized to include a decrease in synaptic strength due to repeated failure of neuron B to be activated by neuron A. Gunther Stent suggested a supplementary hypothesis to Hebb's postulate:

"When the presynaptic axon of cell A repeatedly and persistently fails to excite the postsynaptic cell B while cell B is firing under the influence of other presynaptic axons, metabolic changes take place in one or both cells such that A's efficiency, as one of the cells firing B, is decreased." (Stent, 1973)

Evidence for a coincidence detection mechanism has first been found in the dentate gyrus of the rabbit hippocampus, where long-term potentiation (LTP) elicited by repeated tetanic stimulation, was shown to be Hebbian (Bliss and Lømo, 1973; Kelso et al., 1986). Later, long-term depression was found in Purkinje cells in the cerebellum (Ito et al., 1982).

SPIKE TIMING-DEPENDENT PLASTICITY

I. STDP FEATURES

Studies in different brain regions and under varying experimental conditions have revealed a large spectrum of different types of STDP (Abbott and Nelson, 2000; Caporale and Dan, 2008; Feldman, 2012; Fino and Venance, 2011). Although the majority of the experimental and theoretical work consists in investigating the timing dependence of suprathreshold activities in pre- and postsynaptic neurons, it is important to note that subthreshold activities can also act as Hebbian signals for plasticity induction (Brandalise and Gerber, 2014; Dudman et al., 2007; Fino et al., 2009a; Sjöström et al., 2004).

While the plasticity of excitatory synaptic connections in the brain has been widely studied, the plasticity of inhibitory connections is much less understood. Therefore, the focus here will be on excitatory STDP; for a review on inhibitory STDP see (Vogels et al., 2013).

1 - Pairing and order-dependence

A cardinal feature of STDP is that it relies on the concomitant activation of both pre- and postsynaptic elements whose activities are temporally "paired", meaning that there is a temporal correlation between them. In contrast, non-Hebbian forms of synaptic plasticity modify synaptic strength solely on the basis of pre- or postsynaptic firing and thus, do not require paired synaptic activity.

In classical forms of bidirectional STDP (named Hebbian STDP), pre- leading postsynaptic temporal order (pre-post pairing) induces timing-dependent LTP (t-LTP), whereas post-pre pairings leads to t-LTD (Bi and Poo, 1998; Debanne et al., 1998; Markram, 1997). Hebbian STDP polarity was found mainly at excitatory synapses in neocortex (D'amour and Froemke, 2015; Feldman, 2000; Froemke et al., 2005; Nevian and Sakmann, 2006; Sjöström et al., 2001), hippocampus (Debanne et al., 1998; Nishiyama et al., 2000; Wittenberg and Wang, 2006) and striatum (Fino et al., 2009b, 2008) (Fig.1). Human hippocampal synapses also show Hebbian STDP (Testa-Silva et al., 2010).

The inverse requirement in the order of pre- and postsynaptic activities, is named anti-Hebbian STDP. In this case, pre-post pairings lead to t-LTD, whereas post-pre pairings induce t-LTP. Anti-Hebbian STDP polarity was first observed in the electric fish (Bell et al., 1997; Han et al., 2000). Later, anti-Hebbian STDP was found in the dorsal cochlear nucleus (Tzounopoulos et al., 2007,

2004) and striatum (Cui et al., 2015; Fino et al., 2008, 2005) of rodents and in the neocortex of humans (Verhoog et al., 2013) (Fig.1). In some of these cases, pairing-dependent STDP could not be dependent on the order of pre- and postsynaptic activation, thus resulting in unidirectional STDP (*see below Polarity and direction*).

GABA has been shown to control the polarity of STDP in striatum (Fino et al., 2010; Paillé et al., 2013) and that Hebbian (Pawlak and Kerr, 2008; Shen et al., 2008) or anti-Hebbian (Cui et al., 2015; Fino et al., 2005; Schulz et al., 2010) STDP were observed, depending on whether $GABA_A$ receptor antagonists are used.

Similarly, Hebbian t-LTP or anti-Hebbian t-LTD at corticostriatal synapses can be triggered depending on the level of CB1R activation (strong *vs* moderate, respectively) (Cui et al., 2016), or on whether D2R is endogenously activated (Cui et al., 2015). Dopaminergic modulation can also alter the sign of STDP in the hippocampus (Brzosko et al., 2015).

Finally, flipping Hebbian STDP into anti-Hebbian STDP could occur through development (*see Results*).

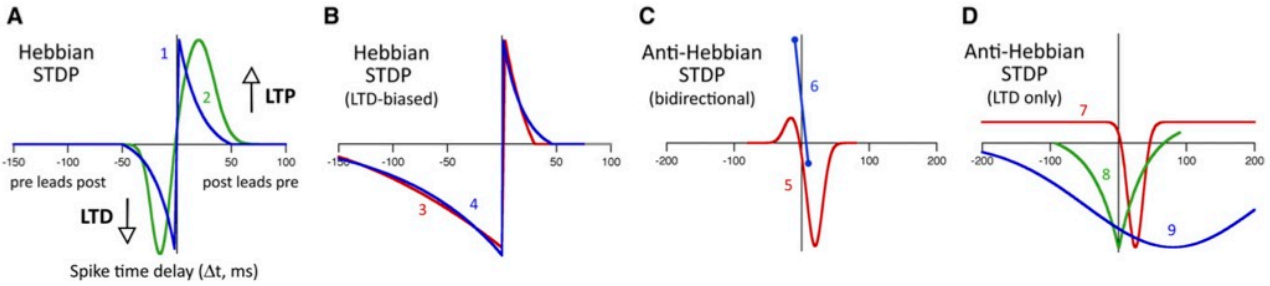

Figure 1. STDP exists in different forms. Selected examples illustrating each form are shown schematically. **(A)** Hebbian STDP that is equally balanced between LTP and LTD. 1, Froemke et al. (2005). 2, Fino et al. (2008). **(B)** Hebbian STDP that is biased toward LTD. 3, Celikel et al. (2004). 4, Froemke et al. (2005). **(C)** Anti-Hebbian STDP that contains both LTP and LTD. 5, Fino et al. (2005). 6, Letzkus et al. (2006). **(D)** Anti-Hebbian STDP that contains only LTD (anti-Hebbian LTD). 7, Han et al. (2000). 8, Lu et al. (2007). 9, Safo and Regehr (2008). (from Feldman 2012)

2 - Timing-dependence and symmetry

A key requirement for STDP is translating precise pre- and postsynaptic activity into a salient time-coded message. Thus, the main characteristic of STDP is a high degree of sensitivity to spike times. This implies that pre- and postsynaptic activities can lead to changes in the synaptic strength, following STDP paradigm, only within a sharp temporal window in the order of few milliseconds. Uncorrelated events (occurring with more than 30-100 ms interval in most cases) therefore fail to trigger plasticity and are not considered as pertinent events for an engram.

Depending on the synaptic inputs onto the same neuron, the width of the temporal window of STDP could be different. Thus, vertical inputs onto layer 2/3 postsynaptic neurons in mouse barrel cortex have larger window than horizontal inputs (Banerjee et al., 2014). Neuromodulation can also modulate the STDP window and activation of beta-adrenergic receptors can enhance the width of the induction window for t-LTP in hippocampus (Lin et al., 2003). In addition, experience can also modulate the temporal window of STDP since tissue damage (incision of the hindpaw muscle) during a critical period of early life widens the temporal window for t-LTP (Li and Baccei, 2016).

Depending on the width of the temporal window, STDP rules could be symmetric or asymmetric. In most cases, the post-pre window (t-LTD) is larger than the pre-post window (t-LTP), leading to the term of asymmetric STDP.

3 - Polarity and direction (uni-/bidirectional)

In most cases, anti-Hebbian STDP is unidirectional, thus exhibiting only t-LTD and is often referred to simply as anti-Hebbian t-LTD. Unidirectional asymmetric STDP (t-LTD only), which is order-dependent, occurs at GABAergic cartwheel neurons in the dorsal cochlear nucleus (Tzounopoulos et al., 2007, 2004). It also occurs at parallel fiber synapses onto Purkinje-like neurons in the electrosensory lobe of the electric fish, where it co-occurs with timing-independent LTP (Bell et al., 1997; Han et al., 2000).

Unidirectional asymmetric Hebbian STDP (t-LTP only) for pre-post pairings exists at cortical and thalamic inputs to the lateral amygdala (Shin et al., 2006). Conversely, unidirectional asymmetric anti-Hebbian STDP (t-LTP only), with exclusively post-pre pairings, has been found at corticostriatal synapses (Cui et al., 2016, 2015). This t-LTP is induced by low number of pairings (5-10 pairing) in contrast to the bidirectional anti-Hebbian STDP at corticostriatal synapses observed with 100 pairings. Recently, asymmetric anti-Hebbian t-LTP has also been described at sensory synapses onto spinal projection neurons (Li and Baccei, 2016).

In some cases, STDP is dependent on the timing of pre- and postsynaptic activation since it occurs in a fixed temporal window, but the direction of the change in synaptic weight is independent on the temporal order of pre- and postsynaptic activities. This means that both pre-post and post-pre pairings induce either t-LTP, or t-LTD, resulting in a unidirectional symmetric STDP.

Unidirectional symmetric STDP (t-LTD only), independent of temporal order, occurs at excitatory inputs onto fast-spiking interneurons in neocortex (Lu et al., 2007); onto spiny stellate cells in somatosensory cortex (Egger et al., 1999); at temporal association cortex synapses (Verhoog et al.,

2013); at thalamocortical synapses onto L2/3 pyramidal neurons (Itami et al., 2016); as well as on parallel fiber-Purkinje cell synapse (Safo and Regehr, 2005; Wang et al., 2000).

Unidirectional symmetric STDP (t-LTP only), independent of temporal order, has been found in CA3-CA3 recurrent synapses in the hippocampus (Mishra et al., 2016), L4–L2/3 cortical synapses early in development (Itami and Kimura, 2012) and at corticostriatal synapses when frequency of pairings is increased (Cui et al., 2016).

However, transition from lack of plasticity to unidirectional STDP, or from uni- to bidirectional STDP is possible notably when neuromodulation is involved. In visual cortex, activation of adrenergic receptors promotes bidirectional order-dependent Hebbian STDP in fast-spiking interneurons (Huang et al., 2013) and activation of adrenergic together with cholinergic receptors induces bidirectional order-dependent Hebbian STDP in cortical pyramidal cells (Seol et al., 2007). Dopamine has a permissive role in Hebbian and anti-Hebbian t-LTP expression in the prefrontal cortex (Ruan et al., 2014; Xu and Yao, 2010) and lateral amygdala (Bissière et al., 2003), and can switch t-LTD into t-LTP in hippocampus (Brzosko et al., 2015). Conversely, D1R activation can promote unidirectional symmetric STDP in hippocampus (Yang and Dani, 2014); and the neuromodulator octopamine found in insects can switch bidirectional Hebbian STDP in to unidirectional symmetric STDP (t-LTD only) in the locust olfactory system (Cassenaer and Laurent, 2012). Acetylcholine also modulates STDP polarity since activation of mAChRs mediates input-specific conversion of Hebbian t-LTP to anti-Hebbian t-LTD in the dorsal cochlear nucleus (Zhao and Tzounopoulos, 2011). BDNF appears as a key player in STDP induction (Edelmann et al., 2015); for review see (Edelmann et al., 2014). Finally, astrocytes mediate cortical t-LTD, *via* the release of glutamate (Min and Nevian, 2012), and hippocampal t-LTD *via* the release of D-serine (Andrade-Talavera et al., 2016).

The bidirectionality of STDP is a key parameter because it solves the problem of balancing t-LTP and t-LTD at a single synapse, thus enabling adaptive changes of the synaptic weight.

4 - Input-dependence

Paired stimulation of thalamic and cortical auditory inputs to the lateral amygdala during auditory fear conditioning results in persistent potentiation of synaptic transmission in both cortical and thalamic inputs (Cho et al., 2011). This ITDP curve is similar to unidirectional symmetric STDP with t-LTP only.

In cortical pyramidal cells, Hebbian and anti-Hebbian STDP can co-occur in the same neuron, depending on the dendritic location of the inputs (Letzkus et al., 2006; Sjöström and Häusser, 2006). Therefore, anti-Hebbian STDP is observed at distal L2/3 synapses onto L5 pyramidal cells. Anti-Hebbian t-LTD on cortical pyramidal cells can be converted into Hebbian STDP by depolarization of the dendrites or promoting the spread of back-propagating action potentials (bAPs) (Letzkus et al., 2006; Sjöström and Häusser, 2006; Zilberter et al., 2009). The efficiency of the bAP could be also influenced by the morphology of the dendritic tree (Fig.2).

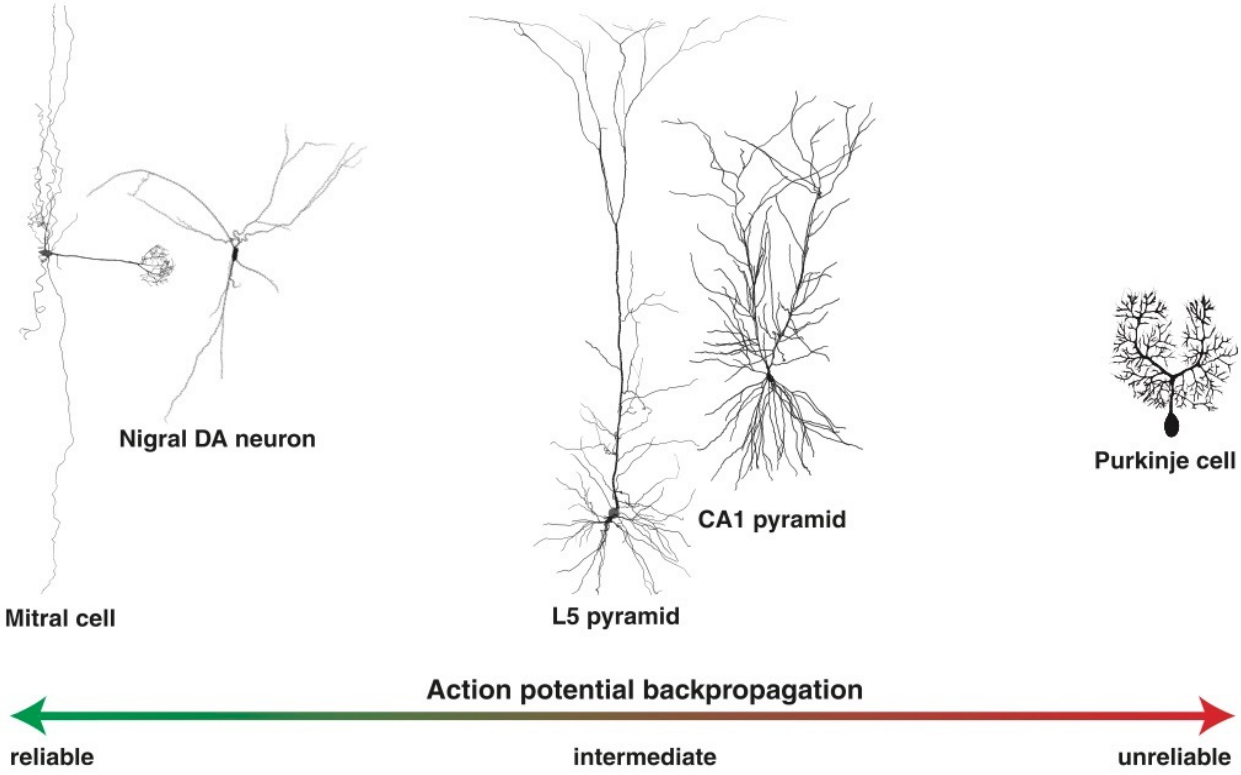

Figure 2. Action potential propagation depends on dendritic morphology. The reliability of AP back-propagation spans a wide range in different cell types. In mitral cell apical dendrites as well as in the axon-bearing dendrite of substantia nigra dopaminergic neurons (left), APs backpropagate at nearly full amplitude. At the other end of the range are cerebellar Purkinje cells (right), whose dendrites do not support propagation well. The apical dendrites of neocortical L5 and hippocampal CA1 pyramidal neurons actively support AP backpropagation (middle). (from Sjöström et al., 2010)

II. STDP MECHANISMS

1 - Calcium dependence and calcium hypothesis

According to the so-called calcium hypothesis, the magnitude and time course of calcium flux into spines can determine the polarity of plasticity outcome. Thus, t-LTP is induced with brief, high calcium influxes; and prolonged moderate calcium influxes generates t-LTD. Low calcium induces no plasticity (Koester and Sakmann, 1998; Lisman, 1989; Magee and Johnston, 1997; Markram, 1997; Schiller et al., 1998); for review see (Feldman, 2012; Sjöström et al., 2010). However, calcium transients cannot always account for the direction of changes in synaptic efficacy (Nevian and Sakmann, 2006).

2 - Single coincidence detector

Classical Hebbian STDP at glutamatergic synapses requires NMDARs as a unique coincident detector. This occurs at CA3-CA1 hippocampal synapses, some synapses on neocortical L2/3 pyramidal cells (Froemke et al., 2005; Nishiyama et al., 2000), al well as at corticostriatal synapses onto fast-spiking interneurons (Fino et al., 2008). In that case both t-LTP and t-LTD are NMDAR-mediated and thus share the same calcium pool. The order of correlated presynaptic release and postsynaptic depolarization trigger calcium influx through post-synaptic NMDARs and VSCCs. In cases where both t-LTP and t-LTD rely on a single coincidence detector (Nishiyama et al., 2000; Froemke et al., 2005), the magnitude of the NMDAR and VSCCs calcium signal determines the sign of plasticity (Fig.4).

Pre-post pairings produce a strong supralinear calcium signal. Presynaptic activity leads to postsynaptic EPSP that activate voltage-gated sodium channels and/or inactivate A-type K^+ channels. This leads to a brief temporal window in which bAPs (induced by somatic current injection) are boosted in active dendrites (Hoffman et al., 1997; Stuart and Häusser, 2001). NMDARs have non-instantaneous kinetics of Mg^{2+} unblock induced by bAP. This causes maximal NMDAR current when glutamate binds to NMDARs before the incoming bAP by a short time interval (Kampa et al., 2004; Sjöström et al., 2010) (Fig.3). In addition, of crucial importance is the AMPAR-mediated local depolarization that boosts the supralinear interaction between NMDAR current and the bAP (Fuenzalida et al., 2010; Holbro et al., 2010).

Post-pre pairings triggers a weaker, sublinear calcium signal. In this case, the EPSP coincides not with the bAP itself, but with the modest afterdepolarization following the bAP, generating small NMDAR currents (Karmarkar and Buonomano, 2002; Shouval et al., 2002).

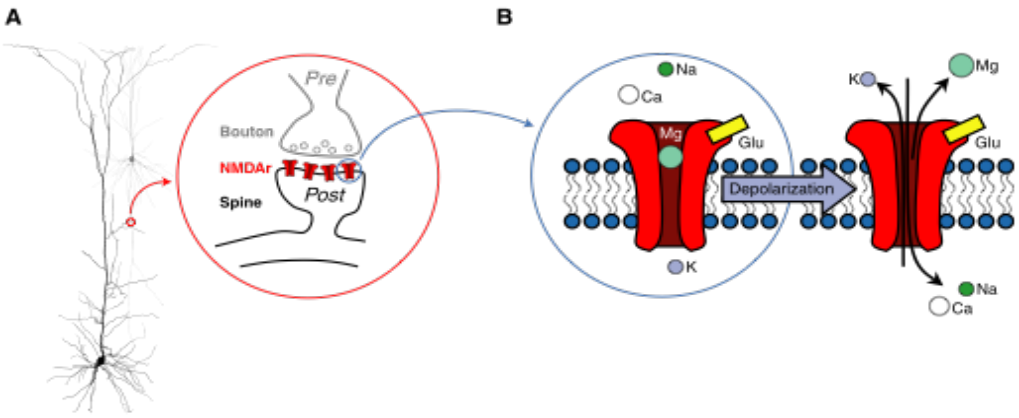

Figure 3. Relieve of the Mg^{2+} block from NMDARs through depolarization. (A) Illustration of a connected pair of neocortical neurons (L2/3 gray, L5 black). The synapse (red circle) is relatively far from the soma, which means that the somatically initiated AP will be attenuated considerably before it reaches the NMDA receptors residing in the spine. **(B)** bAP of insufficient amplitude cannot expel the Mg^{2+} from the pore of a glutamate-bound NMDA receptor (left). With adequate degree of depolarization, however, the NMDA receptor will be unblocked (right), resulting in ion flux and dramatically increased spine levels of Ca^{2+}. The reliability of bAP thus has a critical impact on the induction of synaptic plasticity. (from Sjöström et al., 2010)

3 - Distinct coincidence detectors

Hebbian or anti-Hebbian STDP could also require two distinct coincident detectors and so, separate calcium pools, for t-LTP and t-LTD. The level of intracellular calcium acts differentially by two opposing calcium-triggered pathways. Thus, NMDARs are required for t-LTP induction, but t-LTD depends on postsynaptic group I mGluRs and/or CB1Rs, VSCCs and calcium release from IP3 receptor-gated internal stores (for review see: Feldman, 2012). In this case, PLCbeta is the coincident detector for t-LTD induction since coincident activation of mGluRs and VSCCs synergistically activates PLCbeta. This leads to 2-AG synthesis and release from the postsynaptic terminal and retrograde eCB signaling to presynaptic CB1R. This subsequently leads to decrease in release probability (Feldman 2012) (Fig.4).

Similarly, anti-Hebbian t-LTD is often mGluR- or CB1-dependent and can be expressed both pre- or postsynaptically (Feldman 2012). Recently, anti-Hebbian t-LTP has been described which depends on mGluR and CB1R and is expressed presynaptically (Cui et al., 2015; Cui et al., 2016). In addition to presynaptic CB1R activation, this form of t-LTP also requires postsynaptic TRPV1 activation.

Finally, anti-Hebbian STDP outcome can be also controlled by eCB levels and dynamics. Prolonged and moderate levels of eCB lead to eCB-mediated t-LTD, while short and large eCB

transients produce eCB-mediated t-LTP (Cui et al., 2016). In contrast to the NMDAR-dependent Hebbian STDP where a single molecular coincident detector can trigger both t-LTP and t-LTD depending on the order of pairings, eCB levels vary with the number of pairings. Thus, low number of pairings (5-10) induces eCB-dependent t-LTP, whereas eCB-dependent t-LTD is induced with high number of pairings (75-100) (Cui et al., 2015; Cui et al., 2016).

Thus, synaptic efficacy changes are driven by intracellular calcium transients evoked by the order of pre- and postsynaptic spikes, or their number, through potentiation and depression thresholds.

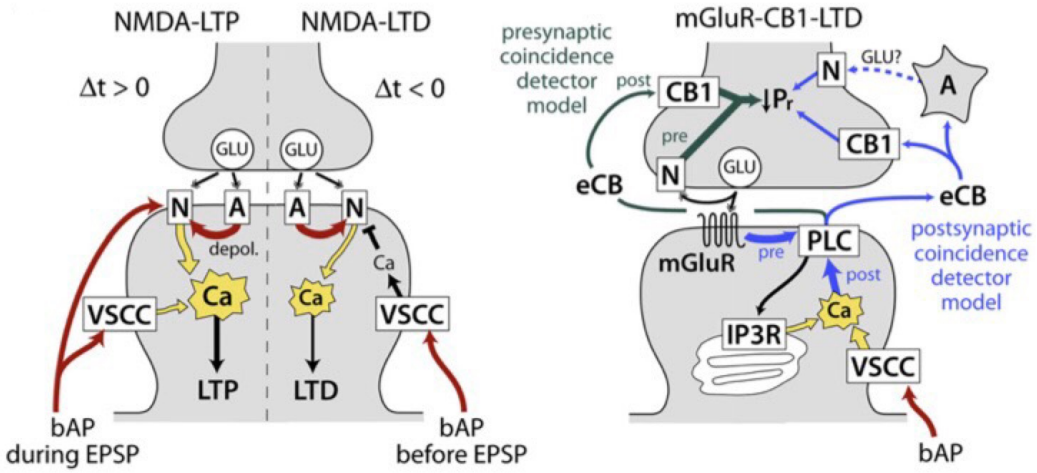

Figure 4. Cellular Mechanisms for Timing Dependence of Plasticity. Biochemical signaling pathways for major forms of STDP. N and A, NMDA and AMPA receptors. Red, depolarization. For mGluR-CB1-LTD, the proposed presynaptic coincidence detector is in green, and the postsynaptic coincidence detector is in blue. A, astrocyte. Signals conveying pre- and postsynaptic spike timing in each model are labeled. (from Feldman 2012)

III. MODULATION

1 - Development

STDP is itself a plastic process and Hebbian or anti-Hebbian, uni- or bidirectional STDP can exist at different developmental stages. Indeed, developmental switch in STDP occurs at the end of the second postnatal week in somatosensory cortex, when unidirectional order-independent STDP (t-LTP only) at L4–L2/3 cortical synapses is transformed to bidirectional Hebbian STDP (Itami and Kimura, 2012). In addition, thalamocortical terminals to L2/3 pyramidal cells display unidirectional order-independent STDP (t-LTP only) that is transformed to t-LTD only between the first and the second postnatal week (Itami et al. 2016). Conversely, corticostriatal asymmetric Hebbian t-LTD early in development is flipped to bidirectional anti-Hebbian STDP at later stages (*see Results*). The induction threshold for STDP can also be modulated. Indeed, tonic GABAergic inhibition at regulates dendritic bAP in juvenile, but not in younger animals, leading for higher threshold for STDP induction in juvenile animals (Groen et al., 2014).

2 - Experience

Moreover, experience can also shape STDP expression. In the case of visual deprivation when animals are dark-reared, t-LTD in visual cortex can be maintained at later developmental stages (Larsen et al., 2014).

3 - Astrocytic coverage

Astrocytes actively control various synaptic functions and, therefore, play a key role in the modulation of neuronal activity (Chung et al., 2015; Fields et al., 2014; Oliveira et al., 2015). The glial synaptic coverage may differ considerably between brain structures and can undergo experience-dependent remodeling (Bernardinelli et al., 2014).

Control of neuronal computation by astrocytes is *via* the release and uptake of transmitters, such as glutamate or D-serine. Glutamate release by astrocytes plays an important role in STDP at L4-L2/3 neocortical synapses, by controlling t-LTD through the activation of astrocytic CB_1R (Min & Nevian 2012) and hippocampal t-LTD is dependent on the release of D-serine by astrocytes (Andrade-Talavera et al., 2016). Furthermore, astrocytes play a key role in the establishment of corticostriatal STDP, through EAAT2-mediated glutamate uptake (*see Results*). Indeed, EAAT2 allows translating precise pre- and postsynaptic activity into a salient time-coded message.

4 - Neuromodulation

The fact that different neuromodulators can promote bidirectional STDP, or switch Hebbian to anti-Hebbian STDP, indicates that the emergence of STDP is a dynamic process, associated with the behavioral state and the level of arousal, which ensures the gating of Hebbian synaptic plasticity (Frémaux and Gerstner, 2016) (Fig.5).

		Interaction type	Quantitative neuromodulation	Neuromodulator timing	Details
Dopamine	Bissière et al., 2003	Inhibition-mediated gating	Baseline vs. bath application	5–10 min around stimulation	Lateral amygdala, mouse slice
	Pawlak and Kerr, 2008	Gating	Baseline vs. bath application	Always in bath	Corticostriatal, rat slice
	Shen et al., 2008	Gating	Baseline vs. bath application	Always in bath	Corticostriatal, mouse slice
	Zhang et al., 2009	Window shape alteration	Baseline vs. bath application	10 min around stimulation	Hippocampal culture, rat
	Xu and Yao, 2010	Inhibition-mediated gating	Baseline vs. bath application	5–10 min around stimulation	Prefrontal cortex, mouse slice
	Schulz et al., 2010	Unclear, gating of anti-Hebbian STDP?	Physiological via visual input and disinhibition of SC	100–250 ms after pairing	Corticostriatal, mouse Anesthesized
Non-dopamine	Lin et al., 2003	Window shape alteration	Baseline vs. bath application	Always in bath	Noradrenaline, hippocampus, rat
	Seol et al., 2007	Window shape alteration	Baseline vs. varying concentrations of two neuromodulators	10 min application, 10–60 min prior to stimulation	Acetylcholine and noradrenaline, visual cortex, rat
	Couey et al., 2007	Window shape alteration	Baseline vs. bath application	5–10 min around stimulation	Acetylcholine, prefrontal cortex, mouse

Figure 5. Selection of experimental results addressing the interaction of neuromodulation and STDP. (from Frémaux & Gerstner 2016)

IV. STDP *IN VIVO*

There are several ways to test STDP occurrence *in vivo*. In sensory-spike pairing, STDP is induced by presenting a sensory stimulus at a specific time delay relative to spikes in a single neuron, evoked by direct current injection. In stimulus-timing-dependent plasticity, presentation of two precisely timed sensory stimuli alters sensory tuning with time and order dependence consistent with STDP. In psychophysical experiments, paired-associative stimulation (PAS) alters sensory perception with STDP-like time and order dependence; for review see (Carson and Kennedy, 2013; Feldman, 2012; Shulz and Jacob, 2010) (Fig.6). Lastly, *in vivo* STDP could also be induced by stimulation of afferent pathways (Schulz et al., 2010).

1 - Sensory-spike pairing

In visual cortex, receptive fields can be modified by pairing a visual input with spiking response in a single pyramidal neuron induced by intracellular current injection (Meliza and Dan, 2006) in contrast to earlier studies using direct electrical stimulation in the cortex (Schuett et al., 2001). Similar paradigm leads to unidirectional depression in the somatosensory cortex (Jacob et al., 2007). In addition, in the locust olfactory system, a bidirectional Hebbian STDP can be induced *in vivo* (Cassenaer and Laurent, 2012).

2 - Stimulus timing-dependent plasticity

In the cat visual cortex, change in receptive fields depends on the temporal order and interval between visual stimuli in a manner consistent with STDP (Fu et al., 2002). Thus, during visual conditioning, random spatial patterns are flashed asynchronously in two adjacent retinal regions to manipulate the relative spike timing of two groups of cortical neurons. Similarly, repetitive pairing of visual stimuli at two orientations induce a shift in orientation tuning of cat visual cortical neurons, with the direction of the shift depending on the temporal order of the pair (Yao and Dan, 2001; Yao et al., 2004).

Bimodal stimulation of auditory and somatosensory inputs to the guinea pig dorsal cochlear nucleus modulates spontaneous and sound-driven activity in a manner consistent with STDP (Koehler and Shore, 2013a). The degree of inhibition influences whether neurons displays Hebbian or anti-Hebbian stimulus timing-dependent plasticity (Koehler and Shore, 2013a). Furthermore, it shifts

from Hebbian to anti-Hebbian orientation when animals are exposed to noise (Koehler and Shore, 2013b). The stimulus timing-dependent plasticity in the guinea pig dorsal cochlear nucleus can also be induced by transcutaneous induction of stimulus-timing-dependent plasticity (Wu et al., 2015). In this way, auditory and transcutaneous electrical stimulation of the face and neck are paired to activate trigeminal and dorsal column pathways to the cochlear nucleus.

Repeated, asynchronous pairing of tones of different frequencies can alter sound frequency selectivity in auditory cortex in a manner consistent with the STDP (Dahmen et al., 2008). Pairing sounds with locus coeruleus activation, and thus increasing the noradrenergic tone, enhances auditory responses on a long-term scale (days or weeks) on a single-cell level in the auditory cortex (Martins and Froemke, 2015). Similarly, nucleus basalis activation paired with pure tones improves auditory perception in the auditory cortex (Froemke et al., 2013). Pairing natural auditory stimuli (pup calls) with oxytocin receptor activation potentiates auditory excitatory synaptic responses in the left auditory cortex of virgin mice (Marlin et al., 2015). Similarly, pairing oxytocin application with pure tones, increases tone-evoked synaptic responses (Mitre et al., 2016). Thus, neuromodulators facilitate the detection of previously imperceptible auditory stimuli at the level of the cortex.

Species	Age	Structure	Protocol	Measured variable	Number of pairings	Pairing frequency (Hz)	Change (LTP) (% baseline)	Change (LTD) (% baseline)	Temporal window for LTP (ms)	Temporal window for LTD (ms)	Effect duration (min)	Reference
Cat	Juvenile	V1	V + ES	Intrinsic signal	>25,000	7	28	–24	ns	ns	840	Schuett et al. (2001)
Cat	Adult	V1	V + V	TC shift*	1600–4800	8	**	**	20	–20	10	Yao and Dan (2001)
Cat	Adult	V1	V + V	RF shift*	800	10	1.9	–1.7	10	–10	8	Fu et al. (2002)
Electric fish	Adult	Electrosensory lobe	sCD + IC	EPSPs	270–700	3–4	***	***	<–10	>+100	6	Bell et al. (1993)
Ferret	Adult	A1	A + A	BF shift*	600	7–9	1.7	–2.2	12	–12	6	Dahmen et al. (2008)
Rat	Adult	Hippocampus	ES + ES	EPSPs	600	5	12	–13.4	>15	<–15	>60	Dong et al. (2008)
Rat	Adult	S1	T + sAP	AP	400	3	ns	–33.6	ns	–17	5	Jacob et al. (2007)
Human	Adult	S1	ES + TMS	EP	180	0.1	12.5	–10	5	–20	>90	Wolters et al. (2005)
Xenopus	Embryo	Tectum	V + IC	CSC	100	0.33	30.4	–28.9	30	–40	>30	Mu and Poo (2006)
Rat	Juvenile	S1	T + IC	EPSPs	100	0.5	38.9	–16	>15	–33	12	Jacob et al. (2007)
Xenopus	Embryo	Tectum	ES + ES	EPSCs	100	1	42	–33	20	–30	>30	Zhang et al. (1998)
Xenopus	Embryo	Tectum	V + IC	CSC	90	0.3	24.8	–20.3	20	–25	>35	Vislay-Meltzer et al. (2006)
Human	Adult	M1	ES + TMS	EP	90	0.05	51	–25	10	–20	30	Wolters et al. (2003)
Xenopus	Embryo	Tectum	Moving V	CSC	60	0.2	48	ns	ns	ns	60	Engert et al. (2002)
Rat	Juvenile	V1	V + IC	EPSCs	30–40	0.33	16	–23.8	>30	<–50	60	Meliza and Dan (2006)
Locust	Adult	Mushroom body	O + IC	EPSPs	5–25	0.1	29.6	–33.9	30	–30	>4	Cassenaer and Laurent (2007)
Rat	Adult	Hippocampus	ES + ES****	LFP	8	0.1	47	–17	20	<–20	>5	Levy and Steward (1983)

A, auditory stimulus; AP, action potentials; BF, best frequency; CSC, Compound synaptic current; EP, Evoked potentials; EPSC, Excitatory postsynaptic currents; EPSP, Excitatory postsynaptic potentials; ES, Electrical afferent stimulation; IC, Intracellular current; LFP, Local field potential; Moving V, Moving oriented light bar; ns, not studied; O, Olfactory stimulus; RF, Receptive field; sAP, Spontaneous action potential; sCD, spontaneous corollary discharge; T, Tactile stimulus; TC, Tuning curve; TMS, Transcranial magnetic stimulation; V, Visual stimulus. Cumulated effect = LTP – LTD.
**No significant modifications of response amplitudes were observed. Thus, we considered here the percentage shift of the RF or BF. **The percentage change compared to baseline is not provided for the shift of the TC, ***the percentage change compared to baseline is not provided. ****Trains of 8 pulses at 400 Hz repeated eight times at 0.1 Hz.*

Figure 6. STDP experiments conducted in intact nervous systems (sorted by the number of pairings). (from Shulz and Jacob 2010)

3 - STDP in humans

In awake humans, PAS protocols are designed by pairing a single electrical stimulus of a peripheral nerve to transcranial magnetic stimulation (TMS) delivered to the somatosensory afferents and transcranial magnetic stimulation (TMS) of cerebral cortex (Carson and Kennedy, 2013).

For example, repeated application of TMS to somatosensory cortex prior to the median nerve-evoked potential results in a long-lasting decrease in median nerve-evoked potentials. Conversely, while TMS quasi concomitant with the evoked potential peak causes a long-lasting increase in evoked potential. These results are interpreted to reflect Hebbian STDP in cortical circuits by pairing of median nerve-evoked EPSPs with TMS-evoked postsynaptic spiking (Litvak et al., 2007; Wolters et al., 2005). In motor cortex, similar pairing bidirectionally alters the amplitude of motor-evoked potentials (Wolters et al., 2003).

The polarity of the induced effects by PAS appears to depend on the order of the stimulus-generated cortical events, and the effective inter-stimulus intervals are within a restricted (milliseconds) temporal window. Thus, it has been proposed that it resembles STDP paradigm for plasticity induction (Carson and Kennedy, 2013). However, while these phenomena exhibit timing-

dependence similar to STDP, whether they represent STDP induced at cortical synapses is unknown.

Another paradigm used in humans is the stimulus timing-dependent plasticity similar in that used in mammals (Fu et al., 2002; Yao and Dan, 2001). In a face perception experiment involving high-level vision, rapid serial presentation of two faces biases face perception toward the second face presented, but only for positive pairing delays (McMahon and Leopold, 2012). These findings argue that STDP-like plasticity occurs in the intact, attentive brain, and influences human visual perception, but again direct evidence that STDP is the causal cellular process is lacking.

PART IV

Striatum

I. STRUCTURE

1 - Anatomy

Dorsal and ventral striatum

The striatum is divided into dorsal and ventral subregions. The dorsal striatum is composed of caudate nucleus and putamen in humans, and dorsomedial striatum (DMS) and dorsolateral striatum (DLS) in rodents (Voorn et al., 2004). The distinction of these two main regions is mainly based on their specific physiological function and afferent/efferent circuitry. However, clear anatomical boundary between the two regions does not exist. The ventral striatum, also called nucleus accumbens (NAc) is further divided into shell and core (Fig.1).

Because this PhD focused on the synaptic plasticity of neuronal circuits between the somatosensory cortex and the dorsolateral striatum, the following introduction will be concentrated on the dorsal region of the striatum.

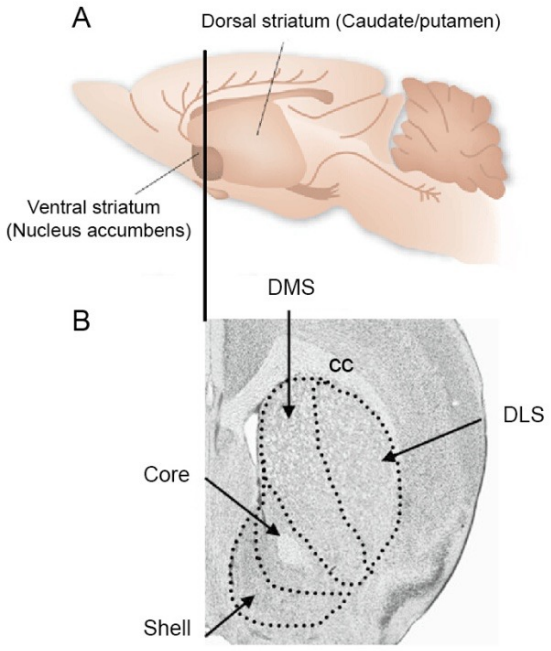

Figure 1. Anatomy of the striatum.
(A) The schematic sagittal view of a rat brain with the striatum. **(B)** The major functional domains of the striatum. An illustration of the striatum from a coronal brain hemisphere section. Note that these four functional subdivisions are anatomically continuous, including nucleus accumbens shell and core (limbic striatum), dorsomedial (DMS, association) striatum, and dorsolateral (DLS, sensorimotor) striatum. cc: corpus callosum. Note: The ventral striatal regions (e.g. areas posterior to the nucleus accumbens) are not included here. (Modified from (Lerchner et al., 2007; Yin et al., 2008))

2 - Compartments

The striatum lacks a laminar organization and exhibits no stereotyped organization or segregation of synaptic inputs. However, the dorsal striatum exhibit mosaic organization and can be differentiated based into two compartments on immunochemical characteristics and difference in the input/output: matrix (10%) and striosomes (or patch) (90%) (Gerfen, 1992; Graybiel and Ragsdale, 1978; Pert et al., 1976) (Fig.2).

Matrix

The matrix compartment is enriched in acetylcholinesterase, somatostatin, calbindin, CB1R, TH and other proteins (Crittenden and Graybiel, 2011). MSNs belonging to the both direct and indirect trans-striatal pathways (*see below Modulation and connectivity*) are equally presented in this compartment. The matrix is innervated preferentially from associative and sensorimotor cortices and the intralaminar thalamic nuclei (Crittenden and Graybiel, 2011; Fujiyama et al., 2015; Graybiel and Ragsdale, 1978).

Striosomes (patch)

Different proteins can be segregated into these two compartments. Patch compartment is enriched in mu-opioid receptor, D1R and AChRs among others (Crittenden and Graybiel, 2011). The striosomes receive afferents preferentially from the limbic cortex and the paraventricular thalamic nucleus (Crittenden and Graybiel, 2011; Fujiyama et al., 2015; Graybiel and Ragsdale, 1978). Most of the striosomal MSNs belong to the indirect pathway (Lévesque and Parent, 2005) and target directly the dopaminergic neurons in the SNc (Fujiyama et al., 2011). Recently, the involvement of striosomes in decision-making has been demonstrated (Friedman et al., 2015).However, it remains unknown how these striatal compartments contribute to a specific behavior. It has been hypothesized that the matrix would perform action selection through the basal ganglia output nuclei (GPe and SNr), whereas the striosome compartment would mediate reward prediction error through dopaminergic and limbic control (Amemori et al., 2011; Houk and Wise, 1995).

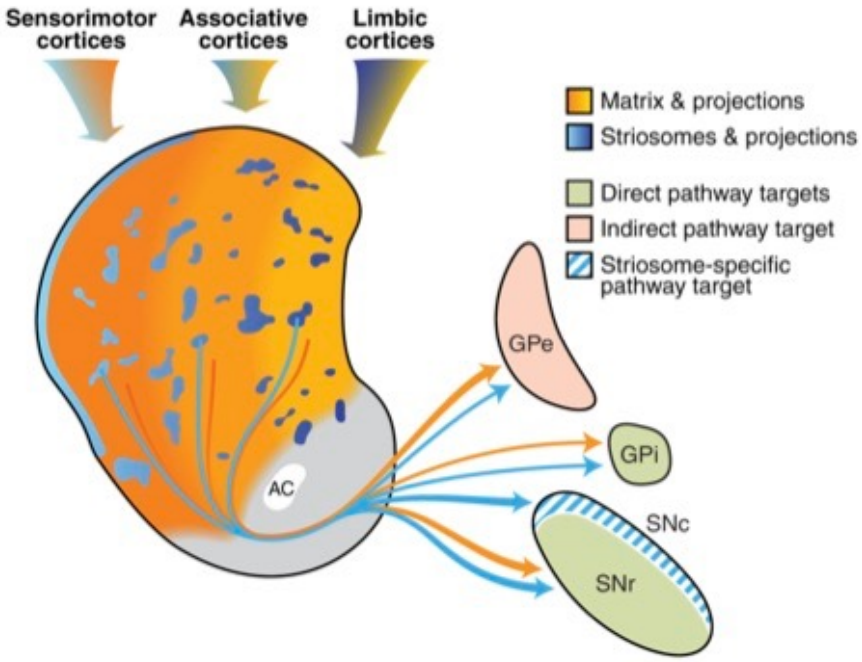

Figure 2. A simplified diagram of striosome and matrix compartmental organization of corticostriatal, striatonigral and striatopallido pathways. Model of the direct, indirect, and striosome-specific striatal projection pathways from the dorsal striatum. Striosomes are shown in blue, and the extra-striosomal matrix in orange. Shading of the striatum from medial (right) to lateral (left) schematically indicates limbic, associative, and sensorimotor striatal domains. Arrows flowing into the striatum are colored to represent the relative abundance of inputs from limbic cortical regions to striosomes and from sensorimotor and associative regions to the matrix. Arrows exiting the striatum represent GABAergic efferent connections from the MSNs in the striosome and matrix compartments to their respective downstream target nuclei. The nucleus accumbens is shown in gray. GPe, external segment of the globus pallidus; GPi, internal segment of the globus pallidus (entopeduncular nucleus, in rodents); SNr, substantia nigra pars reticulata; SNc, dopamine-containing substantia nigra, pars compacta; AC, anterior commissure. (From Crittenden and Graybiel, 2011)

3 - Cell types

The striatum is a heterogeneous structure and comprises almost entirely different GABAergic neurons. The majority of the striatal neurons, at least 95%, in species ranging from rodent to primate are medium-sized spiny projection neurons (MSNs or SPNs) that are the only source of output from the striatum (Wilson, 2007). The remaining cell types comprise large aspiny cholinergic interneurons, and distinct types of GABAergic interneurons (Tepper and Bolam, 2004; Tepper et al., 2010, 2004).

Principal neurons - MSNs

GABAergic MSNs constitute the principal neurons in the striatum and the only output neurons. They represent around 75-80% of the striatal neurons in primates and 90-95% in rodents (Rymar et al., 2004). They are characterized by a medium-sized cell body (~10-15 μm) and a heavy investment of dendritic spines (Wilson and Groves, 1981). The MSNs dendritic trees spread out spherically ~300-400 micrometers around the cell bodies. The axons of the MSNs arising from the soma or from a large dendritic trunk near the soma mainly project downstream toward the basal ganglia output structures. It also exists some electrical and chemical (GABAergic) transmission between MSNs within the striatum through the distal dentrites and the axon collateral plexus, respectively (Venance et al., 2004). Interestingly, electrical and chemical synapses are mutually exclusive. In addition, MSNs display several specific electrophysiological properties, such as a very hyperpolarized resting membrane potential (~-90mV *in vivo* and ~-80mV *in vitro*, a low input resistance, a marked inward rectification of the I/V curve, and a long delay to initial spike (Charpier and Deniau, 1997; Nisenbaum and Wilson, 1995). Such intrinsic membrane features are mainly shaped by inwardly rectifying potassium channels (Kirs) (Mahon, 2000; Mermelstein et al., 1998).

MSNs are divided into two main sub-populations based on the segregated expression of dopamine receptors and neuropeptides, and as a function to their distinct projection targets (Fig.3). The D1R-expressing MSNs (D1R-MSNs), or striatonigral MSNs, are enriched in the neuropeptides substance P and dynorphin, and M4. The D2R-expressing MSNs (D2R-MSNs), or striatopallidal MSNs, express the neuropeptide enkephalin and A2AR (Calabresi et al., 2014; Gerfen, 1992; Surmeier et al., 1996; Valjent et al., 2009). The two MSN populations exhibit similar passive and active electrophyological properties. However, D2R-MSNs are characterized with a lower rheobase and thus, are more excitable than D1R-MSNs (Gertler et al., 2008; Planert et al., 2013) (Fig.3). Moreover, D1R- and D2R-MSNs differ in their somatodendritic morphology. The total length of the dendrites of the D1R-MSNs is significantly greater than that of the D2R-MSNs due to more primary dendrites, branch points and tips. However, the two types of MSNs have similar mean dendritic length (Gertler et al., 2008) (Fig.3).

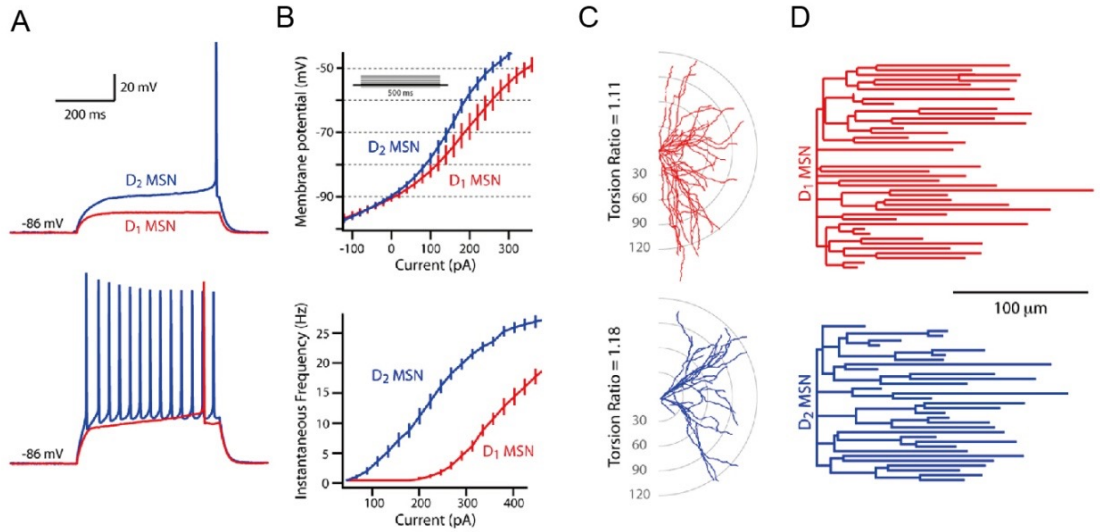

Figure 3. Electrophysiological and morphological characterizations of D1R- and D2R-MSNs.
(A) Sample responses to intrasomatic current injection revealed that rheobase is significantly higher in D1R-MSNs. **(B)** Up: membrane responses to intrasomatic current injection revealed a significant subthreshold divergence. Down: firing rate of D1R- and D2R-MSNs to intrasomatic current steps demonstrated increased excitability in the D2R-MSNs. **(C)** Fan-in diagrams displayed no apparent preferred orientation in either the D1R- or D2R-MSNs. **(D)** Dendrograms displaying in two dimensions the length, number, and connectivity of dendritic segments in sample neurons. (From Gertler et al., 2008)

GABAergic interneurons

Aspiny fast-spiking (FS) interneurons expressing parvalbumin (PV) account for about 1% of striatal neurons (Tepper and Bolam, 2004; Tepper et al., 2008, 2004) (Fig.4). PV+ interneurons receive a powerful excitatory input from the cortex with multiple serial contacts from single corticostriatal axons within short distance (Ramanathan et al., 2002). Thus, they participate in powerful feedforward inhibition of MSNs by contacting them perisomaticaly and making repeated contacts along proximal dendrites (Kreitzer, 2009; Tepper and Bolam, 2004; Tepper et al., 2010, 2004). Reciprocal connections (MSN-FS) have not been observed (Koós and Tepper, 1999; Taverna et al., 2007). FS are connected with gap junctions that could help synchronize firing (Koós and Tepper, 1999; Tepper et al., 2004). FS exhibit a hyperpolarized resting membrane potential *in vitro* (~ -70 - -75 mV) and low input resistance similar to MSNs (50-150 MΩ).

Aspiny GABAergic interneurons positive for somatosatin (nNOS) comprise about ~1% of the striatal neurons (Kawaguchi, 1993; Kawaguchi et al., 1995; Rymar et al., 2004). *In vitro*, nNOS interneurons have relatively depolarized resting membrane potential (-60 - -55 mV), high input resistance (>500 MΩ) and low action potential threshold (Tepper et al., 2010). They exhibit a doublet of action potential at rheobase followed by a persistent discharge. They are also named "persistent

and low-threshold spike (PLTS)" interneurons (Fino and Venance, 2011; Kawaguchi, 1993). Compared to fast-spiking interneurons, nNOS interneurons contact MSN dendrites mainly on the neck of the spines, form weaker inhibitory synapses (Gittis et al., 2010; Kubota and Kawaguchi, 2000). It has been shown that a burst of spikes in nNOS interneuron induces large inhibitory postsynaptic currents (IPSCs) which delays the depolarization-induced firing at the level of MSNs (Tepper and Bolam, 2004).

Another type is the aspiny GABAergic interneurons immunoreactive for calretinin (Kawaguchi et al., 1995), that express tyrosine hydroxylase (Ibáñez-Sandoval et al., 2015; Unal et al., 2011) but lack the ability to release dopamine (Tritsch et al., 2016; Xenias et al., 2015). They exert inhibitory control of MSN excitability (West, 2004). Neuropeptide-Y neurogliaform neurons (NPY-NGF) interneurons are found to translate synchronous activity of cholinergic interneurons into inhibition of MSNs (Ibáñez-Sandoval et al., 2011). Lastly, the fast-adapting interneurons (FAIs) receive a powerful nicotinic cholinergic input and are densely connected to MSNs (Faust et al., 2015).

Cholinergic interneurons

Cholinergic interneurons (or tonically active neurons, TANs) are the only non-GABAergic cells within the dorsal striatum and constitute 0.3~2% of the striatal neurons in rodents (Kreitzer, 2009; Rymar et al., 2004) (Fig.4). They are also known as giant aspiny neurons because of their large cell bodies (50 μm) and their widespread axonal fields (up to 1 mm). In vitro, they have depolarized resting potential (-60mV), prominent afterhyperpolarization and high input resistance (~ 300MΩ) (Kawaguchi, 1993). Driven by the combined action of the persistent Na^+ currents and hyperpolarization-activated cation currents (Ih), cholinergic interneurons spontaneously fire at 2-10 Hz *in vivo* (Bennett et al., 2000). Cholinergic interneurons respond to salient environmental stimuli with stereotyped responses, through pause in their firing, that are temporally aligned with the responses of dopaminergic neurons of the SNc (Apicella, 2007; Morris et al., 2004)

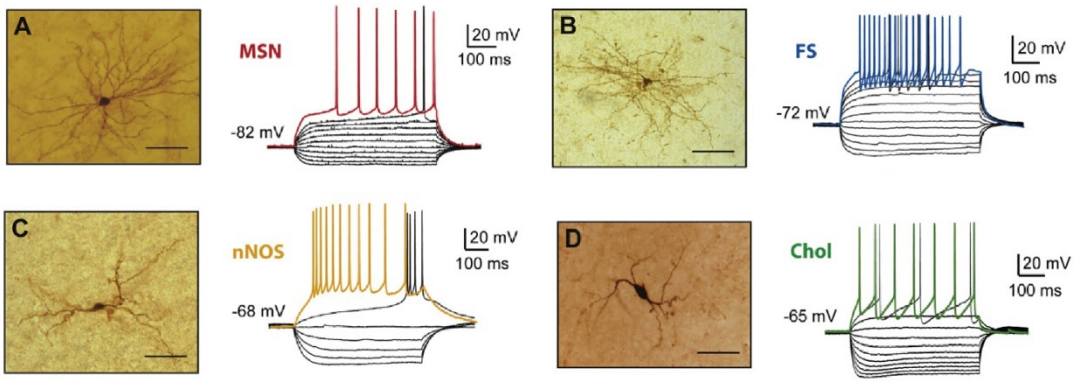

Figure 4. Anatomical and electrophysiological characteristics of the different striatal interneurons compared to MSNs. Biocytin injections and current-clamp recordings in rat brain slices: **(A)** the medium-sized spiny neurons (MSNs), **(B)** the fast-spiking GABAergic interneurons (FS), **(C)** the neuronal nitric oxide synthase interneurons (nNOS) and **(D)** the cholinergic interneurons (Chol). (From Fino and Venance, 2011)

II. MODULATION AND CONNECTIVITY

1 - Inhibitory control

There are two major potential sources of the fast GABAergic inhibition of striatal output: feedforward inhibition from the GABAergic interneurons and feedback inhibition from the axon collaterals of the MSNs themselves. Furthermore, GABAergic inputs from the globus pallidus provide an additional source of inhibitory control onto MSNs. The existence of different GABAergic pathways is crucial for the differential sculpting of striatal output under a variety of conditions and brain states (Wilson, 2007).

Feedforward inhibition

MSNs receive independent streams of feedforward inhibition. The robust and widespread connectivity from FS interneurons to MSNs exerts unidirectional feedforward inhibition (Gittis et al., 2014; Koós and Tepper, 1999; Koos et al., 2004; Mallet and Moine, 2005; Planert et al., 2010; Szydlowski et al., 2013). Inhibition by FS interneurons is reliable, homogenous, and exerted by the same FS cells onto both striatonigral and striato-pallidal projection neurons (Planert et al., 2010) at perisomatic level (Tepper et al., 2008). Feedforward inhibition by FS interneurons is highly selective in terms of postsynaptic targets. FS interneurons contact neighboring MSNs with high probability providing strong and reliable inhibition, while cholinergic interneurons are avoided (but see(Gonzales et al., 2013) for macaque monkey putamen) and LTS interneurons are contacted only with low probability (Szydlowski et al., 2013). GABAergic interneurons produce strong feedforward inhibitory effect on MSNs, and control the precise timing and the pattern of firing of MSNs (Wilson, 2007). They can delay or even prevent the discharge in MSNs (Koós and Tepper, 1999; Planert et al., 2010; Plenz and Kitai, 1998). This strong inhibitory effect is mediated by $GABA_A$Rs expressed on MSNs (Koós and Tepper, 1999; Koos et al., 2004).

Finally, cholinergic interneurons can also provide a source of feedforward inhibition (English et al., 2012). They modulate the sub- and supra-threshold responses of MSNs to cortical and/or thalamic afferents, particularly in reward-related behaviors (Calabresi et al., 2000; Ding et al., 2010).

Therefore, the function of striatal interneurons may not be limited to feed-forward gating of cortical and thalamic input onto MSNs. Instead, the interconnected cholinergic and GABAergic interneurons may transmit afferent signals that are not directly received by projection neurons and integrate them with other striatal inputs through the emergent dynamics of their circuitry.

Collateral feedback inhibition between MSNs

In addition to their extrastriatal projections, MSNs give rise to a relatively dense local axon collateral arborization. Most of these axons form synapses with dendrites or spine shafts in the more distal regions of MSNs, with only a small percentage forming axosomatic contacts (Tepper et al., 2008). MSNs are sparsely and weakly interconnected with a minority of neighboring neurons forming synaptic connections (Czubayko and Plenz, 2002; Guzmán et al., 2003; Koos et al., 2004; Planert et al., 2010; Plenz, 2003; Taverna et al., 2004; Tunstall et al., 2002; Venance et al., 2004). Striatopallidal collateral connections are differentially modulated by dopamine (Tecuapetla et al., 2009). Thus, although individual presynaptic MSNs are not very effective at affecting action potential generation in their postsynaptic MSN targets, a single MSN-MSN synapse could exert powerful effects on local dendritic processing. This could include strong influences on spike back-propagation, dendritic calcium entry and other events that could play a significant role in long-term corticostriatal and/or thalamostriatal plasticity (Carter and Sabatini, 2004; Kerr and Plenz, 2002; Kerr, 2004; Plenz, 2003).

Globus pallidus input

In addition to the intrastriatal GABAergic inhibitory control, PV+ neurons from globus pallidus (comprising about 40% of globus pallidus neurons) also enervate the striatum (Bevan et al., 1998; Mallet et al., 2012; Saunders et al., 2016). Pallidostriatal axons make potent inhibitory synapses on PLTS and FS interneurons in the striatum, but rarely on MSNs (Saunders et al., 2016).

2 - Neuromodulatory control

Dopaminergic control

Striatal circuitry is strongly modulated by the dopamine afferences from midbrain nuclei (Gerfen and Surmeier, 2011; Tritsch and Sabatini, 2012). Up and down states in MSNs are bidirectionally regulated by DR signaling. The somatic up state is increased by the activation of D1Rs in D1R-MSNs, whereas it is shortened by activation of D2Rs in D2R-MSNs (Plotkin et al., 2011). In addition, recent evidences suggest that dopamine-containing neurons in the VTA and SNc monosynaptically inhibit MSNs through Ca2+-dependent release of a $GABA_AR$ agonist (Tritsch and Sabatini, 2012; Tritsch et al., 2014).

GABAergic interneurons express both D1R and D2Rs (Centonze et al., 2003) and D2Rs are highly expressed by cholinergic cells, whose activation slows down the autonomous pacemaking and reduces neurotransmitter acetylcholine (ACh) release (Bergson et al., 1995; Morris et al., 2004; Yan and Surmeier, 1997; Yan et al., 1997).

Cholinergic control

In turn, cholinergic interneurons modulate MSNs activity through muscarinic receptors positioned at corticostriatal synapses (Calabresi et al., 2000). Two families of muscarinic receptors (M1 and M4) are broadly distributed on both classes of MSNs. Striatonigral MSNs express both M1R (excitatory) and M4R (inhibitory) while striatopallidal MSNs only express M1R. However, muscarinic agonists (acetylcholine or muscarine) exert mainly an excitatory effect on MSNs by increasing their evoked discharge (Perez-Rosello et al., 2005) due to postsynaptic M1R activation. Cholinergic interneurons also modulate GABAergic interneurons since acetylcholine potently depolarizes and excites fast-spiking interneurons *via* the activation of ionotropic nicotinic ACh receptor (Koos and Tepper, 2002). They are thought to modulate nNOS interneurons since their expression of M1R and M2R (Bernard et al., 1998). Furthermore, the pedunculopontine nucleus (PPN) and the laterodorsal tegmentum (LDT) nuclei in the brain stem send prominent cholinergic afferents to DLS and DMS, respectively (Dautan et al., 2014). These cholinergic terminals target both MSNs and interneurons.

III. INPUT AND TARGETS

1 - Activity of MSNs

The striatum is the largest nucleus and also the major input of the basal ganglia. Although most of the neurons in the striatum are GABAergic, most of the synapses are not. 80% of the synapses in the striatum consist of asymmetric glutamatergic synapses originating from the principal excitatory afferents to MSNs - cortex and thalamus (Wilson, 2007).

MSNs have low discharge rate *in vivo* (for review see Wilson, 2007) and exhibit mainly subthreshold responses (Reig and Silberberg, 2014); but see (Pidoux et al., 2011). They require significant excitatory synaptic drive to spike (Wickens and Wilson, 1998). The subthreshold transitions between hyperpolarized potentials (-90 to -70 mV) to more depolarized potentials (-60 to -40 mV) in MSNs correspond to Down and Up states (Mahon et al., 2001; Plenz and Kitai, 1998; Stern et al., 1998, 1997; Wickens and Wilson, 1998; Wilson and Kawaguchi, 1996; Wilson and Groves, 1981) (Fig.5). Spiking activity is usually triggered by noisy fluctuations in the Up state (Stern et al., 1997; Wickens and Wilson, 1998). The Down state of MSNs is attributable to the high expression of inwardly rectifying K^+ channels which allow keeping MSNs quiescent near the K^+ equilibrium potential and limit the membrane depolarization in response to excitatory synaptic inputs for cerebral cortex or thalamus (Nisenbaum and Wilson, 1995). The Up state near the spike threshold depends on a temporally convergent excitatory synaptic inputs from cortex and thalamus, interacting with voltage-gated intrinsic membrane conductances (Blackwell et al., 2003; Wilson and Kawaguchi, 1996). Transitions from Down to Up state are mainly due to the activation of NMDA receptors and voltage-dependent Ca^{2+} channels (Plotkin et al., 2011).

Importantly, Up and Down states are found to be much less prominent in awake animals than under different anesthetics and during slow-wave sleep (Mahon et al., 2006, 2001). During the awaking state, MSNs display continuous and irregular membrane potential fluctuations together with random action potential discharges (Mahon et al., 2006). Contrasting with the conventional bistable activities in the anesthetic conditions, the spontaneous synaptic activities in the awake head-restrained animal indicate that the membrane potential fluctuations and firing patterns of MSNs are much more versatile than expected, and strongly depend on the state of vigilance. Although the neural function of this complex cellular behavior remains unclear and the neural activities could differ from that occurring during natural behaviors (particularly in sensorimotor specific tasks), these findings in the awake animal provide the natural intracellular activities of MSNs during wakefulness and suggest multiple capabilities of information processing in the basal ganglia.

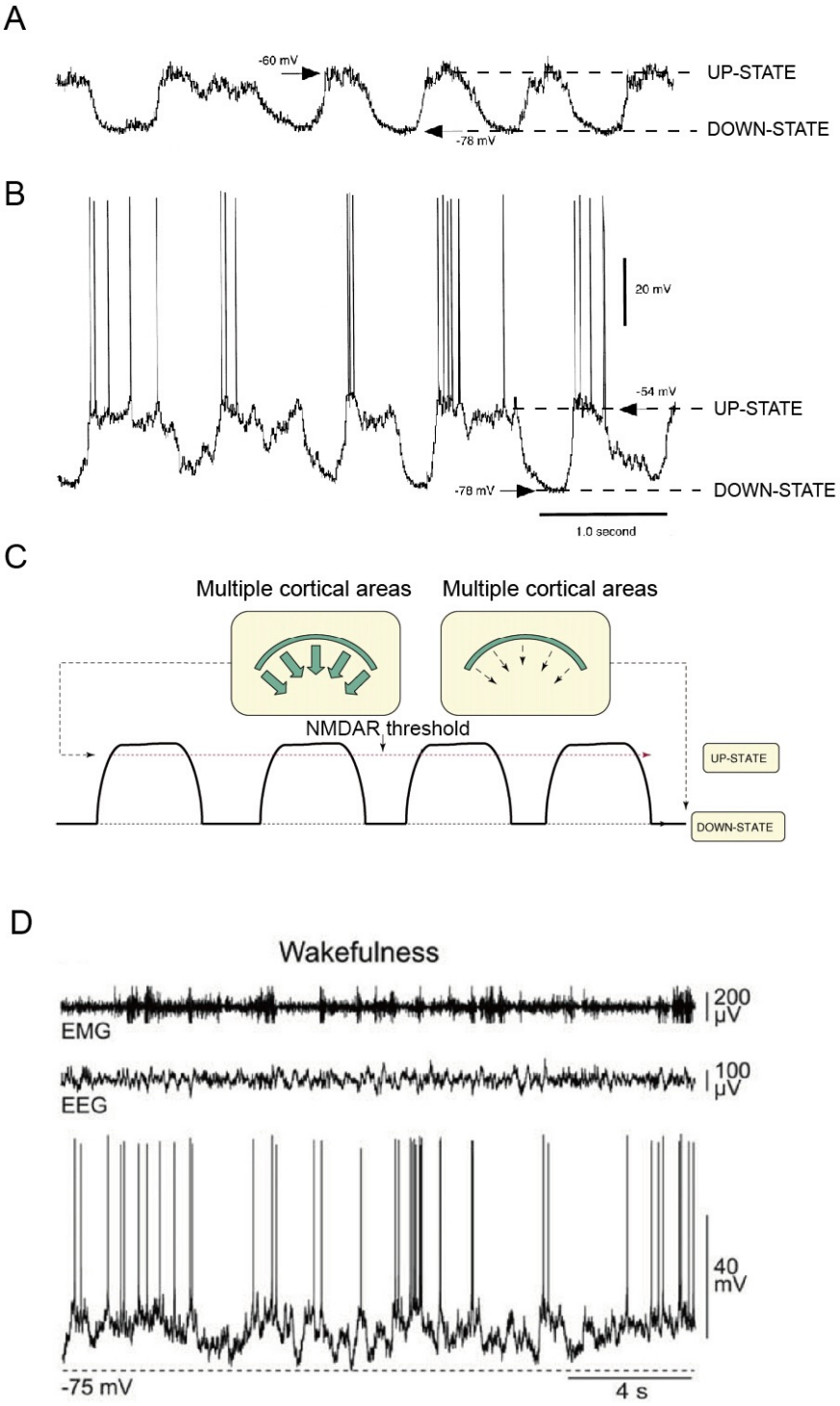

Figure 5. Up and Down states in MSNs. (A) Intracellular recordings from a silent MSN displaying up and down subthreshold membrane potential fluctuations. **(B)** Intracellular recordings from a spontaneously firing MSN. Both neurons (A and B) displayed subthreshold membrane potential fluctuations between a depolarized Up state and a hyperpolarized Down states, but only one fired action potentials while being in the Up state. **(C)** The membrane potential values of MSNs oscillate between Up state and Down state, depending on the degree of cortical activity. **(D)** MSNs intracellular recordings (bottom trace) together with the corresponding electromyographic (EMG) and electroencephalographic (EEG) activity during wakefulness. Note that Up and Down states were absent. (Modified from Wickens and Wilson, 1998; Mahon et al., 2006; Calabresi et al., 2007).

2 - Targets

The classical model of striatal output connectivity relies on the suggestion that D1R- and D2R-expressing MSNs project to different output structures *via* the two trans-striatal pathways. Thus, D1R-MSNs belong to the so-called direct pathway projecting to the GPi and SNr. The indirect pathway D2R-MSNs project to the two intermediate relay nuclei of the basal ganglia - the GPe and STN. Downstream connectivity connects the two pathways since the output structures of the indirect pathway are also GPi and SNr (Gerfen and Surmeier, 2011; Gerfen, 1992; Surmeier et al., 1996; Valjent et al., 2009) (Fig.6).

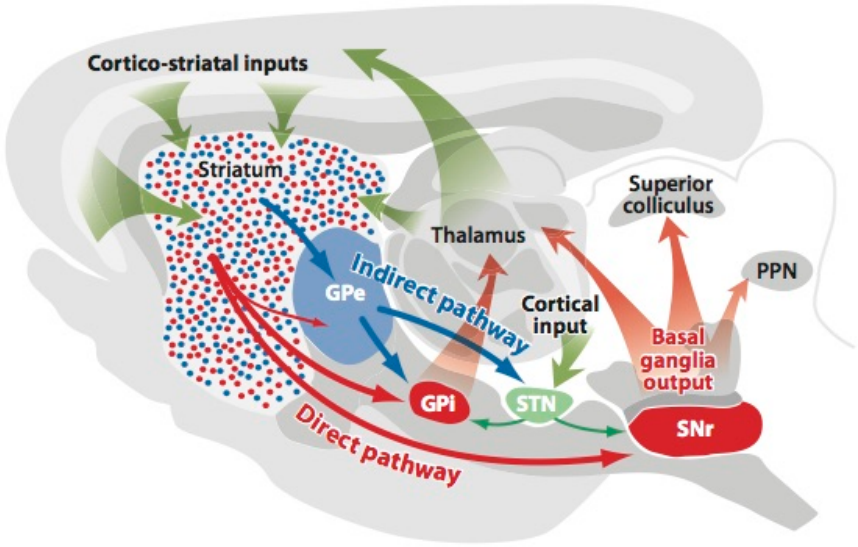

Figure 6. Diagram of basal ganglia circuits. The striatum receives excitatory corticostriatal and thalamic inputs. Outputs of the basal ganglia arise from the internal segment of the globus pallidus (GPi) and substantia nigra pars reticulata (SNr), which are directed to the thalamus, superior colliculus, and pendunculopontine nucleus (PPN). The direct pathway originates from D1R-MSNs that project to the GPi and SNr output nuclei. The indirect pathway originates from D2R-MSNs that project only to the external segment of the globus pallidus (GPe), which together with the subthalamic nucleus (STN) contain transsynaptic circuits connecting to the basal output. (Modified from Gerfen and Surmeier, 2011).

IV. FUNCTION

1 - Involvement of the striatum in different valuation systems

Different corticostriatal circuits are thought to control competing behavioral strategies during choice situations. Striatum is involved in both flexible (planning or goal-directed) and stimulus–response (habit) decision-making: DLS (or sensorimotor striatum) is involved in stimulus–response strategies and ventral striatum and DMS (or associative striatum) are involved in goal-directed strategies (Lavoie and Mizumori, 1994; O'Doherty et al., 2004); for review see (Johnson et al., 2007) (Fig.7,8).

DLS plays a crucial part in the control of habits and is an important component of incremental (procedural, route-based) stimulus–response learning (Graybiel, 1998; Yin and Knowlton, 2006, 2004; Yin et al., 2004). This evidence has gain support from lesion (Packard and McGaugh, 1996), pharmacological (Gold, 2004) and recording studies (Barnes et al., 2005; Jog et al., 1999; Samejima et al., 2005; Schmitzer-Torbert and Redish, 2004).

In contrast to the involvement of DLS in outcome-independent control and habit formation, DMS is involved in flexible goal-directed actions, including the map-based components of navigation (place learning) tasks (Devan and White, 1999; Yin and Knowlton, 2004) and the learning and performance of goal-directed actions of instrumental conditioning tasks (Ragozzino et al., 2002; Yin et al., 2005a, 2005b). Rats with DMS lesions (Adams et al., 2001; Yin et al., 2004) or with NMDA-receptor antagonist infusions into DMS (Yin et al., 2005a) are insensitive to contingency degradation of outcome, suggesting that DMS is a key component in the processing of action–outcome relationships.

Important difference between habitual and goal-directed systems is how they respond to changes in the environment. Goal-directed system updates the value of an action as soon as the value of its outcome changes, whereas the habit system does not (Rangel et al., 2008).

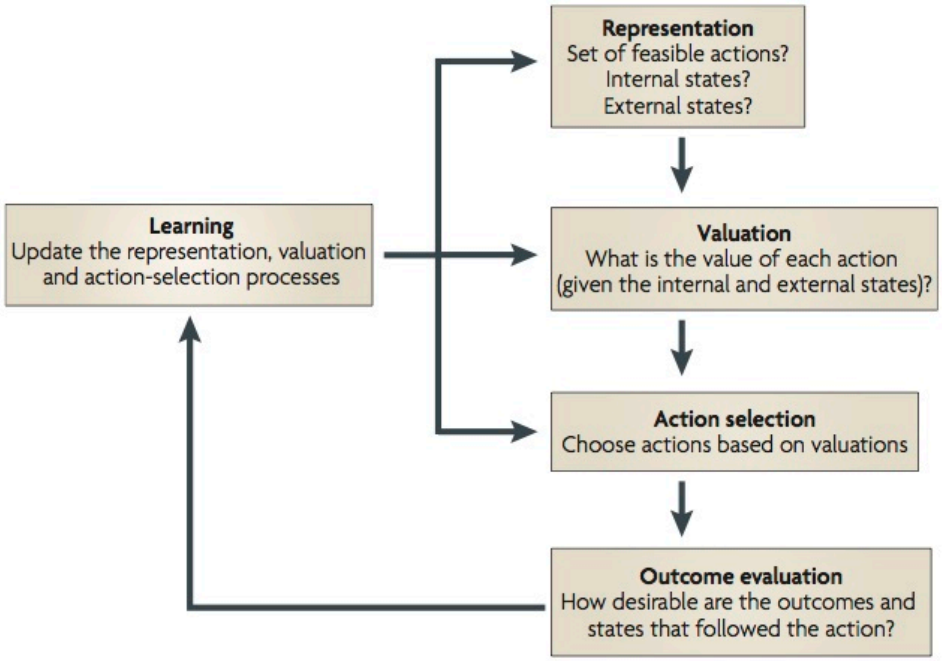

Figure 7. Basic computations involved in making a choice. Value-based decision making can be broken down into five basic processes: first, the construction of a representation of the decision problem, which entails identifying internal and external states as well as potential courses of action; second, the valuation of the different actions under consideration; third, the selection of one of the actions on the basis of their valuations; fourth, after implementing the decision the brain needs to measure the desirability of the outcomes that follow; and finally, the outcome evaluation is used to update the other processes to improve the quality of future decisions. (From Rangel et al., 2008).

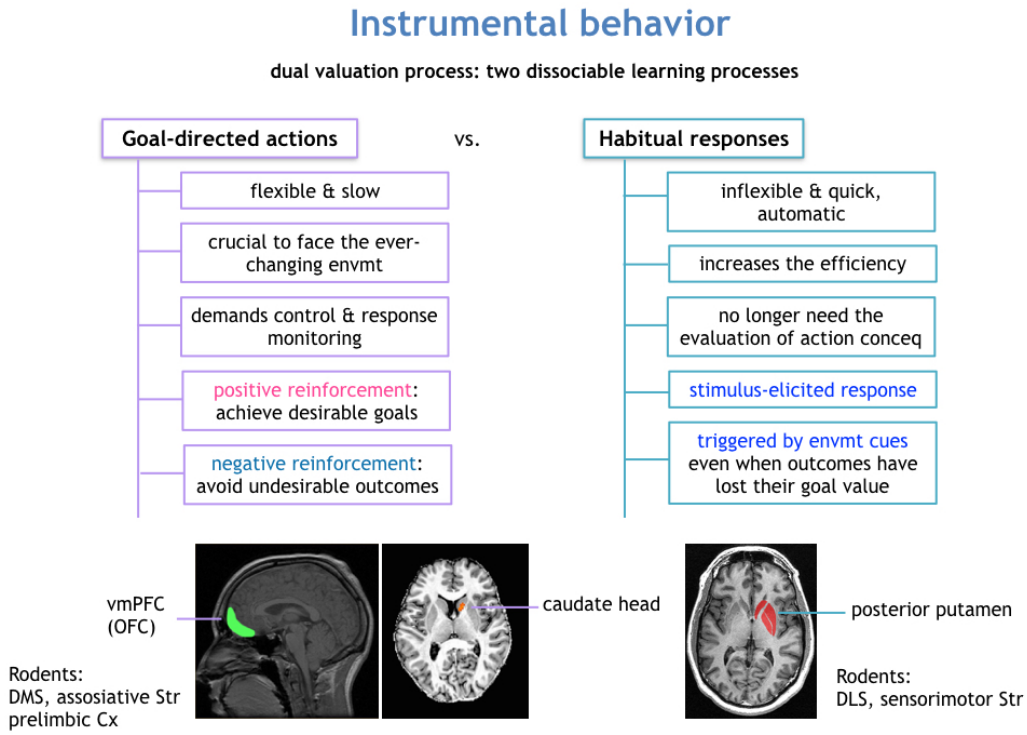

Figure 8. Valuation systems. Action-outcome and stimulus-response systems are dependent on different brain regions (bottom) and have different characteristics: (left) goal-directed actions; (right) habitual reponses. Abbreviations: mPFC – medial prefrontal cortex; OFC – orbitofrontal cortex; Cx - cortex; Str - striatum.

2 - Habit formation and learning procedures

With practice, neuronal activity shifts from more ventral and anterior striatal regions to more caudal zones in the striatum (Doyon and Benali, 2005; Graybiel, 2008, 2005; Isoda and Hikosaka, 2007; Poldrack et al., 2005).

Chuncking

Habits could be viewed as complex action sequences that are grouped together into units, or "chunked", that allows them to be rapidly executable, fluid, and robust to changes in outcome contingency (Barnes et al., 2011; Graybiel and Grafton, 2015; Graybiel, 2008, 1998; Jin and Costa, 2010; Jog et al., 1999; Pennartz et al., 2009; Smith and Graybiel, 2014; Tang et al., 2009; Thorn et al., 2010).

DLS and related pathways are thought to be necessary for the transition of instrumental behavior into habits. During habit acquisition, neuronal activity patterns change dynamically and at the end remain stabilized into specific 'chunked' patterns. Thus, neuronal activity changes from variable to repetitive. Parallel to that, there is a transition in behavioral output from a testing, exploratory mode to a focused, exploitive mode during the crystallization of habitual behaviors (Graybiel 2008; Pennartz et al., 2009).

On the contrary, a nearly inverse pattern of spike activity has been shown to gradually develop in the DMS, which is critical for goal-directed behavior, translated by increased firing during a task, especially around the decision period of the task. Much less activity is observed at the beginning and end of the task. Moreover, this decision-period activity becomes less intense during late learning, opposing to the beginning and end activity in the DLS (Graybiel and Grafton, 2015; Smith and Graybiel, 2014; Thorn et al., 2010).

Task bracketing

Chunks represent activity patterns emphasizing the beginning and end of entire behavioral sequences. Thus, it has been hypothesized that such acquired task-bracketing patterns might reflect behavioral chunking of the procedure as successful learning occurred. These representations may be a neural signature of learning-related behavioral chunking (Barnes et al., 2011, 2005). The task-bracketing pattern in the DLS is extremely resistant to degradation. It could be suppressed but not erased by removal of rewards. This suggests that the task-bracketing pattern cannot be fully blocked

but it rather stays latent and could be rapidly retrievable (Graybiel and Grafton, 2015; Smith and Graybiel, 2014). These patterns reflect entire behavioral sequences from beginning to end, which initially are goal directed, but after long training can become nearly autonomous. Thus, the bracketing could be a neural sign of the chunking of behaviors.

3 - Shift from goal-directed to habitual behavior

Goal-directed behavior is essential to face the ever-changing environment, but demands an effortful control and monitoring of the response. The continuous control and attention that this process demands could result in an unnecessary expenditure of resources and could be inefficient in some situations. Therefore, automatization of recurring decision processes as a habit could increase the efficiency and balances the need for flexibility. Habits are performed automatically allowing attention to be focused elsewhere. A broad spectrum of behavioral routines and rituals can become habitual and stereotyped through learning (acquired *via* experience-dependent plasticity), although others have a strong innate basis (Graybiel 2008). Habitual responses no longer need the evaluation of their consequences and can be elicited by particular situations or stimuli (Balleine et al., 2007; Yin and Knowlton, 2006). Habits could be advantageous when behavior is repeated regularly for extensive periods without major changes in outcome value or contingency, or under uncertain situations where the probability of obtaining an outcome could not be manipulated (Dickinson, 1985).

The ability to shift between these two types of strategies is necessary for appropriate decision-making. Thus, in some situations, the ability to inhibit a habit and use a goal-directed strategy may be crucial. Decision-making refers to the act or process of choosing a preferred option or course of action from a set of alternatives; and guides the selection of actions. In this case, the outcome is part of the resources that are available for action-selection. Action selection is the process of selecting what to do next in dynamic and unpredictable environments in real time. Therefore, appropriate decision-making relies on the ability to shift between different behavioral strategies according to the context in which decisions are made.

This behavioral flexibility is impaired in various conditions including drug addiction, obsessive-compulsive spectrum disorders (OCDs) and response to chronic stress. There alterations result in strengthening of the behavior, making it more compulsive and difficult to disrupt, thus resulting in loss of flexibility and the ability to shift between goal-directed and habitual responses. Furthermore, repetitive behaviors can appear as cardinal symptoms in a broad range of neurological and neuropsychiatric diseases and addiction (Graybiel 2008). Various neuronal and circuit adaptations in drug addiction, for example, result in the compulsive focusing of behavior on drug-associated stimuli and

reduced responding to non-drug stimuli (Everitt and Robbins, 2005; Kalivas and Volkow, 2005). Repetitive behaviors and thoughts are major presenting features in disorders such as Tourette syndrome and OCDs. Stereotypies and repetitive behaviors appear in a range of other clinical disorders including schizophrenia and Huntington's disease (Burguière et al., 2015; Graybiel and Rauch, 2000; Graybiel, 2008).

Chronic unpredictable stress also alters the flexibility in shifting between the two types of strategies. Indeed, rats subjected to chronic unpredictable stress become insensitive to reinforcer devaluation and resistant to changes in action-outcome contingency (Dias-Ferreira et al., 2009). Similar insensitivity to changes in outcome devaluation is found in humans subjected to prolonged stress (Soares et al., 2012). Thus, stress induces a bias in decision-making strategies and promotes a shift to habitual behavior.

METHODS

METHODS

I. ANIMALS AND HOUSING

All experiments were performed in accordance with the local animal welfare committee (Center for Interdisciplinary Research in Biology Ethical Committee) and EU guidelines (directive 2010/63/EU). Every precaution was taken to minimize stress and the number of animals used in each series of experiments. OFA rats P7-80 of both sexes (Charles River, L'Arbresle, France) were used for brain slice electrophysiology.

A. Standard housing

Young rats

Pregnant OFA female rat was ordered from Charles River, L'Arbresle, France and housed until and after delivery with its litter (usually 6-8 pups of both sexes) in standard 12 hours light/dark cycles and food and water were available *ad libitum*. Shelter and paper for nesting material were available in the cage as a part of standard environment housing. Cages were located in a common housing room with other cages housing exclusively female rats or female rats and litter of pups.

Juvenile rats before weaning

OFA female rat with a litter of 10-12 juvenile rats, mainly males (P18-P28) were housed in standard 12 hours light/dark cycles and food and water were available *ad libitum*. Shelter and paper for nesting material were available in the cage. Juvenile rats were housed with the female rat until use for electrophysiology. Cages were located in a common housing room with other cages housing exclusively female rats or female rats and litter of pups.

Adult rats

After weaning, three-four OFA male littermates (P30—P80) were group housed in standard 12 hours light/dark cycles and food and water were available *ad libitum*. Shelter and paper for nesting material were available in the cage. Cages were located in a common housing room with other cages housing exclusively male rats.

B. Saline and ceftriaxone injections

After weaning, four OFA male littermates (P20—P42) were group housed in standard 12 hours light/dark cycles and food and water were available *ad libitum*. Shelter and paper for nesting material were available in the cage. The cage usually consisted of mixed littermates receiving either daily injections of physiological saline or ceftriaxone (Rocepin, La Roche). Cages were located in a common housing room with other cages housing exclusively male rats.

II. CEFTRIAXONE CHRONIC TREATMENT

Male OFA rats (P30-P42) were housed as described above (see Special housing and chronic treatments section above) received a daily intraperitoneal (i.p.) injection of either ceftriaxone (Rocefin, Roche; 200mg/kg per day dissolved in saline) or equal volumes of physiological saline for 8 consecutive days. Electrophysiological and immunohistochemistry experiments were carried from Day 9 after the beginning of the treatment protocol (see Fig. 1 below). Validation of the protocol was done by immunohistochemistry to confirm overexpression of EAAT2 by ceftriaxone (see Immunohistochemistry section below).

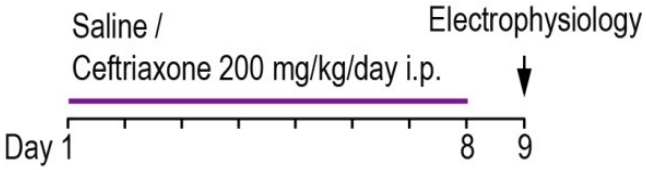

Figure 1. Ceftriaxone chronic treatment and electrophysiology experiments timeline.

III. ELECTROPHYSIOLOGY

A. Acute brain slice preparation

Rats from various ages and treatments (see Animals and housing section above) were used for *in vitro* acute slice preparation.

Dorsolateral striatal (DLS) slices

Horizontal brain slices containing the somatosensory cortical area and the corresponding corticostriatal projection field were prepared according to the methods previously described (Fino et al., 2005). Corticostriatal connections (between somatosensory cortex layer 5 and dorsal striatum) are preserved in a horizontal plane. DLS brain slices with a thickness of 300-330 μm were prepared.

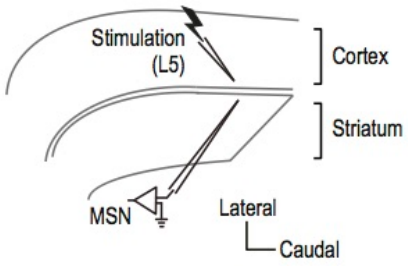

Figure 2. Corticostriatal brain slice with stimulation and recording sites. Electrical stimulation was placed in the L5 of the somatosensory cortex. Whole-cell recordings were made from MSNs in the

Surgery and acute brain slice preparation

Rats were anesthetised with isoflurane and brains removed. Slices were prepared using a vibrating blade microtome (VT1200S, Leica Micosystems, Nussloch, Germany). Brains were sliced in a 95% O2/5%CO2-bubbled, ice-cold cutting solution containing (in mM) 125 NaCl, 2.5 KCl, 25 glucose, 25 $NaHCO_3$, 1.25 NaH_2PO_4, 2 $CaCl_2$, 1 $MgCl_2$, 1 pyruvic acid, and transferred into the same solution at 34°C during cutting and then moved to room temperature.

B. Electrophysiology recordings

Solutions

Patch-clamp recordings were performed as previously described (Paillé et al. 2013; Cui et al. 2015; Cui et al. 2016). Briefly, borosilicate glass pipettes of 6-8 MΩ resistance used for whole-cell recordings were filled with either K-based or Cs-based intracellular solution. KOH-based intracellular solution was used for both CC and VC mode whole-cell recordings in $P_{7\text{-}10}$ rats and contained (in mM): 105 K-gluconate, 30 KCl, 10 HEPES, 10 phosphocreatine, 4 Mg-ATP, 0.3 Na-GTP, 0.3 EGTA (adjusted to pH 7.35 with KOH). For whole-cell recordings in $P_{17\text{-}25}$ rats, the KOH-based intracellular solution contained (in mM): 122 K-gluconate, 13 KCl, 10 HEPES, 10 phosphocreatine, 4 Mg-ATP, 0.3 Na-GTP, 0.3 EGTA (adjusted to pH 7.35 with KOH). Cs-based intracellular solution was used exclusively in VC mode for monitoring sIPSCs and contained (in mM): 135 CsCl, 10 HEPES, 10 phosphocreatine, 4 ATP-Mg, 0.3 GTP-Tris, 0.3 EGTA (adjusted to pH 7.35 with CsOH). The composition of the ACSF extracellular solution was (mM): 125 NaCl, 2.5 KCl, 25 glucose, 25 $NaHCO_3$, 1.25 NaH_2PO_4, 2 $CaCl_2$, 1 $MgCl_2$, 10 µM pyruvic acid bubbled with 95% O_2 and 5% CO_2.

Signal recording

Signals were amplified using EPC9-2, EPC10-3 and EPC10-4 amplifiers (HEKA Elektronik, Lambrecht, Germany). All recordings were performed at 34°C using a temperature control system (Bath-controller V, Luigs&Neumann, Ratingen, Germany) and slices were continuously superfused at 2 ml/min with the extracellular solution. Slices were visualized on an Olympus BX51WI microscope (Olympus, Rungis, France) using a 4x/0.13 objective for the placement of the stimulating electrode and a 40x/0.80 water-immersion objective for localizing cells for whole-cell recordings. Current-clamp (CC) recordings were filtered at 2.5 kHz and sampled at 5 kHz and voltage-clamp (VC) recordings were filtered at 5 kHz and sampled at 10 kHz using the Patchmaster v2x32 program (HEKA Elektronik).

Identification of neurons and basic properties

Medium-sized spiny neurons (MSNs) and fast-spiking interneurons (FS) were visualised on a microscope (see above for details) and identified based on their distinct electrophysiological properties as previously described (Fino et al. 2007; Fino & Venance 2011). Recordings were made in CC mode with 0 pA intracellular current injection allowing the recorded neuron to stay at its RMP. 500 ms long current steps with 10-20 pA step increase starting from -300 pA were applied. Current steps were applied until 200 pA after spiking threshold.

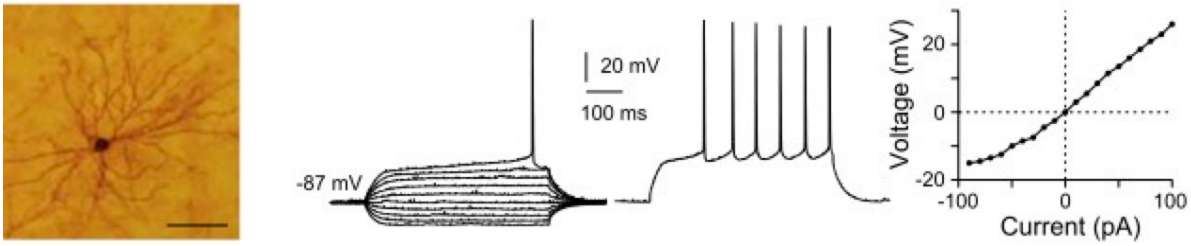

Figure 3. Identification of MSNs. **(Left)** MSN injected with biocytin (scale bar, 100 m). **(Right)** Characteristic membrane properties and spiking pattern of MSN: note the very hyperpolarized RMP (-87 mV), the inward rectification (illustrated in the steady-state I–V relationship), and the long depolarizing ramp to the AP threshold leading to a delayed spike discharge (the delay to first spike is 452 ms in this example). Raw traces show individual voltage responses to series of 500mscurrent pulses from -90 to 90 pA with 20pA increasing current steps and to 50 pA above AP threshold (spike frequency, 15 Hz) (adapted from (Fino et al. 2005)).

Protocols without afferent stimulation

a. Reversal potential of $GABA_AR$-mediated current in MSNs

RMP and E_{GABA} are required to determine the value of the driving force of chloride ions through $GABA_ARs$. Thus, E_{GABAA} and RMP were measured based on cell-attached recordings of single-channel i_{GABA} and i_{NMDA} (Dehorter et al. 2009). The value of RMP was estimated from i_{NMDA} which is known to reverse at a membrane potential close to 0 mV, and E_{GABA} was determined based on the relationship between i_{GABA} and the extracellular potential to the patch of the membrane. $E_{GABA(A)} = DF_{GABA(A)} + RMP$. For this purpose, two different intra-pipette solutions were used (mM): (1) for i_{NMDA} measurement, 140 NaCl, 3.5 KCl, 1.8 CaCl2, 10 HEPES pH 7.3, 10 µM NMDA, 10 µM Glycine and 1 µM strychnine, and (2) for i_{GABA} measurement, 120 NaCl, 20 TEA-Chloride, 5 KCl, 5 4-aminopyridine, 0.1 CaCl2, 10 MgCl2, 10 Glucose, 10 HEPES buffered to pH 7.3, GABA 5 µM, isoguvacine 5 µM and CsCl 3 µM.

b. Spontaneous inhibitory post-synaptic currents (sIPSCs)

Spontaneous phasic and tonic $GABA_AR$ currents were measured using a Cs^+-high-chloride based intracellular solution (see composition above). Phasic and tonic GABAergic components were estimated after inhibition of ionotropic glutamatergic receptors by adding D-AP5 (50 µM) and CNQX (10 µM) at the beginning of the experiment. Phasic and tonic components were analyzed during 50sec recording segments before and after pharmacological treatments. Concerning phasic current, spontaneous IPSCs (sIPSCs) were identified using a semi-automated amplitude threshold based detection software (Mini Analysis 6.0.7 Program, Synaptosoft, Fort Lee, NJ, USA) and were visually confirmed. Concerning tonic current, the holding current was sampled every 100 ms for a 50 sec period preceding drug application and discarded points landing on IPSCs. The corresponding distribution, not skewed by synaptic events, was fitted by a Gaussian and the peak indicated the mean holding current (I_{hold}) required maintaining the membrane potential at -80 mV. After pharmacological treatment, a new I_{hold} and ΔI_{hold} was determined corresponding to the tonic component affected by the drug. In some cases, bath-applied PTX was added at the end of the experiment to estimate the magnitude of the tonic GABAergic signaling.

c. Continuous membrane potential monitoring

Continuous recording in CC mode with 0 pA intracellular current injection was performed allowing the recorded neuron to stay at its RMP. Recordings were made either in the absence of drugs in standard ACSF solution (see composition above) or in the constant presence of (1) AP5 (50 μM); (2) CNQX (20 μM); or CNQX (20 μM) + MCPG (500 μM). Stable baseline for 5-10 min was established and DHK (300 μM) was applied for 5 min. The resulting depolarisation of the recorded neuron was estimated comparing the mean RMP during baseline with the membrane potential reached after 5 min of DHK. The return to baseline membrane potential was estimated comparing the baseline RMP and the membrane potential reached after 15 min of DHK washout.

d. Spontaneous activity

Continuous recording in CC mode with 0 pA intracellular current injection was performed allowing the recorded neuron to stay at its RMP. Recordings were made in the absence of drugs in standard ACSF solution (see composition above). Stable baseline for 5-10 min was established and DHK (300 μM) was applied for 5 min. The resulting spontaneous activity of the recorded neuron was estimated calculating the mean spontaneous spiking frequency (in Hz) reached after 5 min of DHK. The return to baseline state of spontaneous spiking activity was estimated after 15 min of DHK washout.

Stimulation protocols

Electrical stimulations were performed with a concentric bipolar electrode (Phymep, Paris, France) placed in the layer 5 of the somatosensory cortex (Fino et al. 2005). Electrical stimulations were monophasic at constant current (ISO-Flex stimulator, AMPI, Jerusalem, Israel). Currents were adjusted to evoke 100-300 pA EPSCs VC mode and 15-20 mV EPSPs in CC mode.

a. Paired-pulse ratio (PPR)

Repetitive control stimuli (x5) were applied at 0.1 Hz in VC mode. The inter-stimulus intervals (ISI) between all each two of the five stimuli were 50, 100, 250 and 500 ms, by which MSNs in the DLS display a bidirectional short-term plasticity (Goubard et al., 2012). For PPR estimation, the amplitude of 10-20 successive EPSCs were measured and PPR was calculated by the mean of EPSC2 amplitude/EPSC1 amplitude for each sweep.

b. Triggered spiking responses

Repetitive control stimuli were applied at 0.1 Hz in CC mode with 0 pA intracellular current injection allowing the recorded neuron to stay at its RMP. Stable baseline for 5-10 min was established and DHK (300 μM) was applied for 5 min. The resulting triggered spiking response of the recorded neuron was estimated calculating the probability of triggered spikes by the control stimuli reached after 5 min of DHK. The return to baseline state was estimated comparing the probability of triggered spiking response during baseline and the probability of triggered spiking response after 15 min of DHK washout.

c. Spike-timing dependent plasticity protocols and random Δt_{STDP} patterns

Repetitive control stimuli were applied at 0.1 Hz in VC mode. STDP protocols in DLS slices consisted in pairings of pre- and postsynaptic stimulations (at 1 Hz in CC mode) with the two events separated by a specific temporal interval (Δt_{STDP}). Presynaptic stimulations corresponded to cortical stimulations and the postsynaptic stimulation of an action potential evoked by a depolarizing current step (30 ms duration) in MSN. Δt_{STDP}<0 ms and Δt_{STDP}>0ms refer to post-pre and pre-post pairings, respectively. Δt_{STDP}=±500 ms refer to post-pre and pre-post pairings performed around Δt_{STDP}=-500 ms and Δt_{STDP}=+500 ms. Note that for Δt_{STDP}=-500 ms and Δt_{STDP}=+500 ms the order (post-pre *vs* pre-post) was determined only by the first pairing of the STDP protocol since for the remaining pairings the pre- and post-stimulations were separated by 500 ms and thus could be considered both as post-pre or pre-post pairings when performed at 1 Hz. For this reason, data for both Δt_{STDP}=-500 ms and Δt_{STDP}=+500 ms were pooled together (Δt_{STDP}=±500 ms) and represented in the figures as a single average. Neurons were recorded for 10 min during baseline and for at least 40-60 min after STDP protocol; long-term synaptic efficacy changes were measured from 40 to 60 min. 60 successive EPSCs were individually measured and then averaged, comparing the last 10min of the recording with the 10min of baseline. Neurons were recorded in VC mode during baseline and the 60 min of recording after STDP protocol, and in CC during STDP protocol. Variation of input resistance above 20% led to the rejection of the experiment.

For the random Δt_{STDP} patterns we used the following algorithm (programmed in Igor Pro 6.3 software, WaveMetrics): for each pairing, we first selected a temporal window with a length randomly chosen between 500 and 1500 ms (with uniform distribution) and located the presynaptic stimulation time in the middle of this window. The postsynaptic stimulation time was then randomly cho-

sen within this window (with uniform distribution). The Δt_{STDP} pattern was formed by the concatenation of 100 of those windows. This generated both a close-to-uniform distribution of the Δt_{STDP} and a variable interval between two successive presynaptic stimulations.

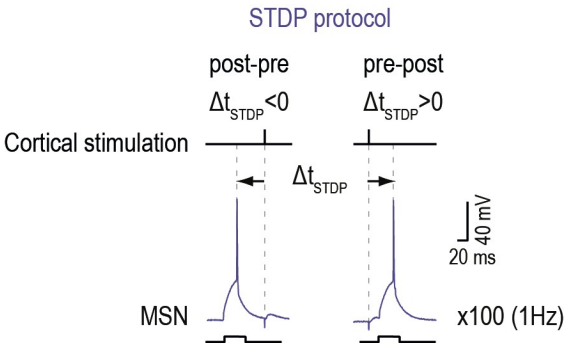

Figure 4. STDP protocol. Pairings of pre- and postsynaptic stimulations (at 1 Hz) were performed in CC mode with the two events separated by a specific temporal interval (Δt_{STDP}). Presynaptic stimulations corresponded to cortical stimulations and the postsynaptic stimulation of an action potential evoked by a depolarizing current step (30 ms duration) in MSN.

C. Chemicals

All chemicals were purchased from Tocris (Ellisville, MO, USA), except picrotoxin (Sigma). (2S,3S,4R)-2-Carboxy-4-isopropyl-3-pyrrolidineacetic acid (Dihydrokainic acid, DHK; 300 µM), DL-2-amino-5-phosphono-pentanoic acid (D-AP5; 50 µM), (1S,2S)-2-[2-[[3-(1H-Benzimidazol-2yl)propyl]methylamino]ethyl]-6-fluoro-1,2,3,4-tetrahydro-1-(1-methylethyl)-2-naphthalenyl methoxyacetoacetate dihydrochloride (Mibefradil; 20 µM), 6-Cyano-7-nitroquinoxaline-2,3-dione (CNQX; 20 µM), (αR,βS)-α-(4-Hydroxyphenyl)-β-methyl-4-(phenylmethyl)-1-piperidinepropanol maleate (Ro 25-6981; 10 µM), 3,5-Dimethyl-tricyclo[3.3.1.13,7]decan-1-amine hydrochloride (Memantine; 10 µM), SR 95531 hydrobromide (gabazine; 10 µM and 200 nM) (Tocris), L655,708 (10 µM) (Tocris), (*R*)-1-(1-Phenylethyl)-1*H*-imidazole-5-carboxylic acid ethyl ester (etomidate, 3 µM) (Tocris), (±)-3-Piperidine carboxylic acid (nipecotic acid, 500 µM) (Tocris), N-Methyl-D-aspartate (NMDA, 10mM) (Tocris), Glycine (10mM) (Tocris), Strychnine (1mM) (Tocris), isoguvacine (5mM) (Tocris), GABA (5mM) (Tocris), Tetraethylammonium chloride (TEA-Cl, 20mM) (Tocris) and 4-aminopyridine (4-AP, 5mM) (Tocris) were dissolved directly in the extracellular solution. N-(piperidin-1-yl)-5-(4-iodophenyl)-1-(2,4-dichlorophenyl)-4-methyl-1H-pyrazole-3-carboxamide (AM251; 3 µM) and picrotoxin (50 µM) were dissolved in ethanol and added in the external solution at a final concentration of ethanol of 0.01-0.1%. (S)-α-Methyl-4-carboxyphenylglycine (MCPG; 500 µM) was dissolved in 1.1 eq. NaOH, and added in the external solution. *N*-[4-(2-Bromo-4,5-difluorophenoxy)p henyl]-L-asparagine (WAY 213613; 50 µM) was

dissolved in DMSO and added in the external solution at a final concentration of DMSO of 0,5%. BAPTA (10 mM) and dizocilpine maleate (i-MK801; 1mM) were dissolved directly into the intracellular solution.

The contrasting activity patterns of synaptic and extrasynaptic NMDARs result in a differential degree of memantine blockade (Lipton 2006; Xia et al. 2010). Due to the agonist concentration-dependence of memantine blockade kinetics, slices were pre-incubated with low dose of memantine (10 μM) for at least one hour previous to recording to allow enough time to achieve equilibrium block.

D. EAAT2 transient blockade with DHK

DHK (300μM), a selective non-transportable inhibitor of EAAT2 (Arriza et al. 1994), was bath-applied during a time-lapse as brief as possible to keep its effect on Vm compatible with a proper analysis of the synaptic efficacy changes. Indeed, blocking EAAT2 results in a marked depolarization (Goubard et al. 2011)and present study), which may impair the estimation of the synaptic efficacy changes. After establishing a 10 min stable baseline, DHK was bath-applied for 5 min. We systematically ensured the efficiency of DHK application before applying the STDP protocol. This depolarization was used as an indication for the DHK efficiency. DHK was washed out at the STDP protocol offset. The full DHK washout took 15min and during this period a significant and transient decrease of EPSC magnitude (due to DHK-induced inward shift in $I_{holding}$ and AMPAR desensitization) (Goubard et al. 2011) was observed. Accordingly, in all figures the synaptic efficacy changes are illustrated from 15min after the DHK removal. Synaptic efficacy changes were evaluated at 60 min after the start of the DHK washout, i.e. at least 30 min after the full recovery of baseline $I_{holding}$.

E. Electrophysiological data analysis

Off-line analysis was performed using Fitmaster (Heka Elektronik). Statistical analysis was performed using Prism 5.02 software (San Diego, CA, USA). In all cases “n” refers to a single cell experiment from single slice. All results were expressed as mean±SEM in the text and as mean±SD in the figures (except when specified), and statistical significance was assessed using the unpaired t test or the one sample t test when appropriate at the significance level (p) indicated or one-way ANOVA with Bonferroni correction when specified.

IV. IMMUNOHISTOCHEMISTRY

Animals

Immunohistochemistry experiments were carried on male OFA rats (P30-P42) subjected to chronic ceftriaxone treatment and the corresponding saline controls. Rats were treated for 8 days with daily i.p. injection of either saline (n=4 rats) or ceftriaxone (n=4 rats) as described above. Immunohistochemistry experiments started 24 hours after the last injection (Fig. 5).

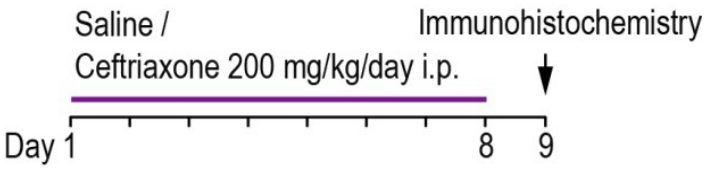

Figure 5. Ceftriaxone chronic treatment and immunohistochemistry experiments timeline.

Fixed brain slice preparation

Rats were anesthetized with pentobarbital and transcardiacally perfused with 4% paraformaldehyde. Brains were postfixed in 4% paraformaldehyde overnight, then transfered in 1X phosphate-buffered saline (PBS) the next day and sliced in 1X PBS into 30µm horizontal or coronal sections with a vibratome (Microm HM650V, ThermoScientific). Slices were conserved until use at -20°C in cryoprotectant solution containing (in %): 30 glycerol, 30 ethylene glycol, 10 10X PBS, 30 Milli-Q water.

Immunohistochemistry protocol

Immunostaining was performed on free-floating sections using guinea pig EAAT2 antibody (1:5000; AB1783, Merck Millipore) for 48 hours at 4°C and then with a secondary Cyanine Cy™3-conjugated antibody (1:1000; Jackson Laboratories) dissolved in PBS 1X for one hour. Detailed protocol is described in Table 2 below.

Day 1

5x wash PBS 1X (5x10min)
MeOH 500µL + H2O2 180µL + PBS 4.3mL (5min)
5x wash PBS 1X (5x10min)
Triton 10% 100µL + PBS 4.9mL (20min)

5x wash PBS 1X (5x10min)
BSA 3% in PBS (1h) [BSA 150mg in PBS 1X 5mL]
GLT1 AB (1:5000) in BSA 1% in PBS 1mL + Triton 10% 10µL
48h at 4°C

Day 3

5x wash PBS 1X (5x10min)
ABII (1:1000) in PBS 1X (1h) in dark
5x wash PBS 1X (5x10min) in dark
1x wash PB 0.1M (15min) in dark
mount slices on slides in PB 0.1M
dry at room T° (24h) in dark
put coverslip with DPX mounting medium
dry at room T° (overnight) in dark
store at 4°C in dark

Image acquisition and data analysis

Images were acquired using an SP5 confocal system (Leica, Germany) and optical density was analysed with ImageJ (NIH, USA).

RESULTS

RESULTS
INTRODUCTION

I. ARTICLE 1

Developmental control of spike-timing-dependent plasticity polarity by tonic GABAergic signaling in striatum

Valtcheva S*, Paillé V*, Gangarossa G, Perez S, Dembitskaya Y, Fino E and Venance L

(in preparation)

Rationale:

We previously showed that GABAergic signaling governs the corticostriatal STDP polarity and thus operates as a Hebbian/anti-Hebbian switch in striatum (Paillé et al. 2013). Although GABAergic microcircuits are subject to important developmental maturation, it remains unclear whether STDP is developmentally shaped by GABAergic maturation. Here, we explored the contribution of tonic and phasic GABAergic signaling in the expression of STDP, a major physiological relevant form of Hebbian learning.

Physiological relevance:

The striatum is constituted by a vast majority of GABAergic neurons providing an efficient feed-forward and feedback inhibition onto MSNs. Therefore, GABAergic networks have a crucial role in shaping MSN responses to incoming cortical inputs and in modulating striatal output. Corticostriatal long-term synaptic plasticity provides a fundamental mechanism for the function of the basal ganglia in procedural learning. How corticostriatal plasticity rules are modified during development remains unexplored. Tonic and phasic GABAergic signaling have differential developmental maturation and so, should be critically involved in driving corticostriatal STDP along development.

Novelty:

GABAergic circuits control the polarity of corticostriatal STDP and thus operate as a Hebbian/anti-Hebbian switch. Here, we explored the implication for GABAergic signaling in shaping corticostriatal STDP along development. We show that at the single-cell level:

(1) Corticostriatal STDP exhibits unidirectional asymmetric Hebbian STDP in $P_{7\text{-}10}$ young animals while bidirectional anti-Hebbian STDP is observed at later developmental stages ($P_{17\text{-}25}$ juvenile and $P_{60\text{-}80}$ adult animals).

(2) Promoting tonic inhibition in the immature brain (in $P_{7\text{-}10}$ rats) allows the emergence of bidirectional anti-Hebbian STDP.

(3) Blockade of tonic GABAergic signaling at juvenile stage reverses the bidirectional anti-Hebbian STDP back to unidirectional asymmetric Hebbian STDP.

Here, we show that developmental maturation of GABAergic signaling drives the polarity of corticostriatal plasticity. To our knowledge this is the first study exploring the contribution of tonic inhibition in the developmental switch of STDP timing rule. Therefore, GABAergic networks not only in orientate STDP polarity (Paillé et al. 2013) in juvenile and adult animals, but also play a key role in the establishment of bidirectional anti-Hebbian STDP in the mature brain.

II. ARTICLE 2

Astrocytes gate Hebbian synaptic plasticity in striatum

Valtcheva S and Venance L

(Nat Commun, in revision)

Rationale:

Astrocytes, via the excitatory amino acid transporter type-2 (EAAT2), are the major sink for released glutamate and contribute to set the strength and the timing of synaptic inputs. Glutamate dynamics is therefore expected to impact strongly on STDP expression. However, the proper conditions for the emergence of Hebbian plasticity out of distributed neuronal activity remain unknown. EAAT2 is known to be responsible for 95% of glutamate reuptake and thus tightly controls glutamate dynamics. Here, we questioned the role of astrocytes (via EAAT2) in the expression of STDP.

Physiological relevance:

It has been shown at various synapses (including the corticostriatal synapse) that glutamate spillover occurs in a different extent depending on glutamate transporters expression, astrocytic coverage and synaptic firing regimes. By investigating the role of EAAT2 in STDP expression, we determine the conditions required for the expression of Hebbian plasticity, which is critical for a better understanding of the mechanisms underlying learning and memory. STDP, as a canonical form of Hebbian plasticity, has attracted considerable interest in experimental as well as in computational neurosciences. In addition, dysfunction of EAAT2 has been observed in neurodegenerative diseases and drug of abuse exposure.

Novelty:

STDP is triggered by correlated activity on either side of the synapse and here we unravel a new role for astrocytes in the establishment of Hebbian synaptic plasticity. Indeed, we show that at the single-cell level in striatum:

(1) A transient blockade of EAAT2 converts Hebbian plasticity (STDP) into aberrant non-Hebbian plasticity, which occurs for uncorrelated or even unpaired activity; such activities are inefficient to trigger long-term changes in the synaptic weight in control conditions. We show that distinct signaling pathways are selected in STDP and aberrant plasticity.

(2) On the contrary, EAAT2 overexpression (with ceftriaxone) impairs the detection of correlated activity resulting in a lack of STDP.

(3) Astrocytic glutamate uptake allows the emergence of bidirectional STDP and prevents the occurrence of aberrant plasticity.

To our knowledge this is the first report showing the involvement of astrocytes (via EAAT2) in Hebbian synaptic learning rule (STDP) and in preventing the occurrence of aberrant non-Hebbian plasticity. Here, we thus demonstrate that astrocytes set the appropriate glutamate dynamics allowing for optimal temporal contingency between pre- and postsynaptic activity necessary for STDP emergence and places astrocytes as gatekeepers of Hebbian plasticity. In this aspect, EAAT2 gates the conversion from timing-dependent to timing-independent plasticity.

RESULTS

Article I

Developmental control of spike-timing-dependent plasticity polarity by tonic GABAergic signaling in striatum

Valtcheva S*, Paillé V*, Gangarossa G, Perez S, Dembitskaya Y, Fino E and Venance L

(in preparation)

Developmental control of spike-timing-dependent plasticity polarity by tonic GABAergic signaling in striatum

Silvana VALTCHEVA[#], Vincent PAILLE[#], Giuseppe GANGAROSSA, Sylvie PEREZ, Yulia DEMBITSKAYA, Elodie FINO and Laurent VENANCE[*]

Dynamics and Pathophysiology of Neuronal Networks Team, Center for Interdisciplinary Research in Biology, College de France, CNRS UMR7241/INSERM U1050, MemoLife Labex Paris, France

: co-first authors

[*]Correspondence: laurent.venance@college-de-france.fr

Conflict of interest: the authors have no competing financial interest to declare.

Running title: Developmental control of STDP by tonic GABA

Abstract

Activity-dependent long-term potentiation (LTP) and depression (LTD) of synaptic strength underlie multiple forms of learning and memory. Spike-timing dependent plasticity (STDP) is a synaptic Hebbian learning rule that could account for experience-dependent changes in neural networks. We previously showed that GABAergic signaling governs the STDP polarity and thus operates as a Hebbian/anti-Hebbian switch in striatum. Although GABAergic microcircuits are subject to important developmental maturation, it remains unclear whether STDP is developmentally shaped by GABAergic maturation. Here, we found that in immature rats ($P_{7\text{-}10}$), striatal STDP displays unidirectional Hebbian tLTD whereas in juvenile ($P_{17\text{-}25}$) and adult ($P_{60\text{-}80}$) animals STDP is bidirectional and anti-Hebbian. Both tonic (extrasynaptic) and phasic (synaptic) GABAergic signaling are differently implicated in controlling STDP. More specifically, we found that the tonic GABAergic signaling, which is developmentally regulated, is a crucial actor in the shaping of STDP rules along development and for the establishment of the striatal anti-Hebbian STDP. Thus, developmental maturation of GABAergic signaling tightly drives the polarity of striatal plasticity.

Introduction

Bidirectional long-term synaptic efficacy changes (LTD and LTP) are involved in multiple forms of learning and memory (Citri and Malenka, 2008; Nabavi et al, 2014). Experience-dependent plasticity requires a fine balance of excitation-inhibition as evidenced in the visual cortex (Takesian and Hensch, 2013) or hippocampus (Donato et al., 2013). Spike-timing dependent plasticity (STDP) has been proposed as candidate mechanism accounting for experience-dependent changes in the neural networks (Feldman, 2012). We previously showed that GABAergic signaling operates as a Hebbian/anti-Hebbian switch of striatal STDP, i.e. depending on the presence or absence of $GABA_AR$ transmission the polarity of the plasticity (LTP vs LTD) is reversed (Fino et al., 2010; Paillé et al., 2013). STDP is a major form of synaptic Hebbian learning rule, in which the occurrence of spike-timing long-term potentiation (tLTP) or depression (tLTD) relies on the precise order and relative millisecond timing of the paired activities on either side of the synapse (Sjöström et al., 2008; Feldman, 2012). GABAergic feedforward signaling modulates the spike timing (Higley and Contreras, 2006; Pouille and Scanziani, 2001; Wehr and Zador, 2003) and the electrotonic properties of the dendritic tree (Froemke et al., 2010), which are key parameters known to orientate STDP preferentially toward LTP or LTD (Sjöström et al., 2008).

The striatum is constituted by a vast majority of GABAergic neurons. Given the efficient feedforward (Koos and Tepper, 1999; Szydlowski et al., 2013) and feedback (Venance et al., 2004; Koos et al., 2004) inhibition onto the striatal medium-sized spiny neurons (MSNs) (Tepper et al., 2008; Gittis and Kreitzer, 2012; Silberberg and Bolam, 2015), we tested the effects of the GABAergic maturation in STDP-timing rules establishment along development. GABAergic signaling and circuits are subject to important developmental maturation (Ben-Ari et al., 2007; Farrant and Nusser, 2005; Glykys and Mody, 2007; Brickley and Mody, 2012). In striatum, it is known that at least two populations of GABAergic cells, the parvalbumin interneurons and the MSNs, mature considerably between P_8 and P_{19} (Chesselet et al., 2007; Santhakumar et al., 2010). In addition, tonic and phasic GABAergic signaling also have differential developmental maturation (Ade et al., 2008; Kirmse et

al., 2008; Santhakumar et al., 2010; Luo et al., 2013). We tested the hypothesis of developmentally-driven STDP-timing rules by GABAergic maturation investigating STDP at different developmental stages: young (P_{8-10}), juvenile (P_{20-25}) and adult (P_{60-90}) rats. Here, we found that in P_{7-10} rats, striatal STDP displays a unidirectional Hebbian tLTD whereas in older animals STDP acquires bi-directional and anti-Hebbian features. We found that tonic and phasic GABAergic signaling are differently engaged in shaping plasticity. Notably, tonic GABAergic signaling appears to play a key role in controlling STDP expression and polarity along development. Indeed, tonic GABAergic component, which arises from P_{16}, is mandatory for the establishment of bidirectional anti-Hebbian STDP in striatum. The emergence of bidirectional anti-Hebbian STDP is tightly linked to the developmental maturation of GABAergic signaling in striatum.

METHODS

Animals

All experiments were performed in accordance with the guidelines of the local animal welfare committee (Center for Interdisciplinary Research in Biology Ethics Committee) and the EU (directive 2010/63/EU). Every precaution was taken to minimize stress and the number of animals used in each series of experiments. OFA rats P7-80 (Charles River, L'Arbresle, France) were used for brain slice electrophysiology. Animals were housed in standard 12-hour light/dark cycles and food and water were available *ad libitum*.

Brain slice preparation and patch-clamp recordings

Horizontal brain slices containing the somatosensory cortical area and the corresponding corticostriatal projection field were prepared as previously described (Fino et al., 2005). Corticostriatal connections (between somatosensory cortex layer 5 and the dorsal striatum) are preserved in the horizontal plane. Horizontal brain slices (300-330 µm-thick) were prepared from rats with a vibrating blade microtome (VT1200S, Leica Microsystems, Nussloch, Germany). Brains were sliced in an ice-cold cutting solution (125 mM NaCl, 2.5 mM KCl, 25 mM glucose 25 mM $NaHCO_3$, 1.25 mM NaH_2PO_4, 2 mM $CaCl_2$, 1 mM $MgCl_2$, 1 mM pyruvic acid) through which 95% O_2/5% CO_2 was bubbled. The slices were transferred to the same solution at 34°C for one hour and then to room temperature. Patch-clamp recordings were performed as previously described (Fino et al., 2010; Paillé et al., 2013). Briefly, for whole-cell recordings in $P_{7\text{-}10}$ rats, borosilicate glass pipettes of 6-8MΩ resistance were filled with (in mM): 105 K-gluconate, 30 KCl, 10 HEPES, 10 phosphocreatine, 4 Mg-ATP, 0.3 Na-GTP, 0.3 EGTA (adjusted to pH 7.35 with KOH). For whole-cell recordings in $P_{17\text{-}25}$ rats, borosilicate glass pipettes of 6-8MΩ resistance were filled with (in mM): 122 K-gluconate, 13 KCl, 10 HEPES, 10 phosphocreatine, 4 Mg-ATP, 0.3 Na-GTP, 0.3 EGTA (adjusted to pH 7.35 with KOH). In a subset of experiments (for the analysis of the phasic

and tonic GABAergic inhibition), the chloride concentration was increased to obtain an $E_{(Cl-)rev} \approx 0$ mV and K^+ was replaced by Cs^+; the composition of the internal solution was (in mM): 135 CsCl, 10 HEPES, 10 phosphocreatine, 4 ATP-Mg, 0.3 GTP-Tris, 0.3 EGTA (adjusted to pH 7.35 with CsOH). The composition of the extracellular solution was (mM): 125 NaCl, 2.5 KCl, 25 glucose, 25 $NaHCO_3$, 1.25 NaH_2PO_4, 2 $CaCl_2$, 1 $MgCl_2$, 10 µM pyruvic acid bubbled with 95% O_2 and 5% CO_2. Signals were amplified using with EPC9-2 amplifiers (HEKA Elektronik, Lambrecht, Germany). All recordings were performed at 34°C, using a temperature control system (Bath-controller V, Luigs & Neumann, Ratingen, Germany) and slices were continuously superfused with extracellular solution, at a rate of 2 ml/min. Slices were visualized under an Olympus BX51WI microscope (Olympus, Rungis, France), with a 4x/0.13 objective for the placement of the stimulating electrode and a 40x/0.80 water-immersion objective for the localization of cells for whole-cell recordings. Current-clamp recordings were filtered at 2.5 kHz and sampled at 5 kHz and voltage-clamp recordings were filtered at 5 kHz and sampled at 10 kHz, with the Patchmaster v2x32 program (HEKA Elektronik).

Spike-timing-dependent plasticity protocols

Electrical stimulations were performed with a concentric bipolar electrode (Phymep, Paris, France) placed in layer 5 of the somatosensory cortex. Electrical stimulations were monophasic, at constant current (ISO-Flex stimulator, AMPI, Jerusalem, Israel). Currents were adjusted to evoke 50-200 pA EPSCs. Repetitive control stimuli were applied at 0.1 Hz. STDP protocols consisted of pairings of pre- and postsynaptic stimulations (at 1 Hz) separated by a specific time interval (Δt_{STDP}). Presynaptic stimulations corresponded to cortical stimulations and the postsynaptic stimulation of an action potential evoked by a depolarizing current step (30 ms duration) in MSNs. $\Delta t_{STDP}<0$ ms for post-pre pairings, and $\Delta t_{STDP}>0$ ms for pre-post pairings. Recordings on neurons were made over a period of 10 minutes at baseline, and for at least 60 minutes after the SDTP protocols; long-term changes in synaptic efficacy were measured from 45 to 60 minutes. We individually measured

and averaged 60 successive EPSCs, comparing the last 10 minutes of the recording with the 10-minute baseline recording. Neuron recordings were made in in voltage-clamp mode during baseline and for the 60 minutes of recording after the STDP protocol, and in current-clamp mode during STDP protocol. Experiments were excluded if input resistance (Ri) varied by more than 20%.

Chemicals

DL-2-amino-5-phosphono-pentanoic acid (D-AP5, 50 μM) (Tocris, Ellisville, MO, USA), 6-cyano-7-nitroquinoxaline-2,3-dione (CNQX, 10 μM) (Tocris), SR 95531 hydrobromide (gabazine, 10 μM and 200 nM) (Tocris), L655,708 (10 μM) (Tocris), N-Methyl-D-aspartate (NMDA, 10mM) (Tocris), Glycine (10mM) (Tocris), Strychnine (1mM) (Tocris), isoguvacine (5mM) (Tocris), GABA (5mM) (Tocris), Tetraethylammonium chloride (TEA-Cl, 20mM) (Tocris), 4-aminopyridine (4-AP, 5mM) (Tocris), (*R*)-1-(1-Phenylethyl)-1*H*-imidazole-5-carboxylic acid ethyl ester (etomidate, 3 μM) (Tocris) and (±)-3-Piperidine carboxylic acid (nipecotic acid, 500 μM) (Tocris) were dissolved directly in the extracellular solution and bath applied. Picrotoxin (50 μM) (Sigma) was dissolved in ethanol and then added in the external solution at a final concentration of ethanol of 0.01%.

Phasic and tonic $GABA_A$ currents measurement

Spontaneous phasic and tonic $GABA_A$ currents were measured using a Cs^+-high-chloride based intracellular solution (in mM): 135 CsCl, 10 HEPES, 10 phosphocreatine, 4 ATP-Mg, 0.3 GTP-Tris, 0.3 EGTA (adjusted to pH 7.35 with CsOH). Phasic and tonic GABAergic components were estimated after inhibition of ionotropic glutamatergic receptors by adding D-AP5 (50μM) and CNQX (10μM) at the beginning of the experiment. Phasic and tonic components were analyzed during 50sec recording segments before and after pharmacological treatments. Concerning phasic current, spontaneous IPSCs (sIPSCs) were identified using a semi-automated amplitude threshold based detection software (Mini Analysis 6.0.7 Program, Synaptosoft, Fort Lee, NJ, USA) and were

visually confirmed. Concerning tonic current, we sampled the holding current every 100 ms for a 50 sec period preceding drug application and discarded points landing on IPSCs. The corresponding distribution, not skewed by synaptic events, was fitted by a Gaussian and the peak indicated the mean holding current (I_{hold}) required maintaining the membrane potential at -80 mV. After pharmacological treatment, we determined a new I_{hold} and ΔI_{hold} corresponded to the tonic component affected by the drug. Bath-applied picrotoxin was systematically added at the end of the experiment to estimate the magnitude of the tonic GABAergic signaling.

Reversal potential of the $GABA_A$-mediated current

To determine the value of the driving force of chloride ions through $GABA_A$Rs, one needs to know RMP and $E_{GABA(A)}$. $E_{GABA(A)}$ and RMP were measured based on cell-attached recordings of single-channel i_{GABA} and i_{NMDA} (Paillé et al., 2013). Briefly, we estimated the value of RMP from i_{NMDA} which is known to reverse at a membrane potential close to 0 mV, and E_{GABA} was determined based on the relationship between i_{GABA} and the extracellular potential to the patch of the membrane. $E_{GABA(A)} = DF_{GABA(A)} + RMP$. For this purpose, two different intra-pipette solutions were used (mM): (1) for i_{NMDA} measurement, 140 NaCl, 3.5 KCl, 1.8 CaCl2, 10 HEPES pH 7.3, 10µM NMDA, 10µM Glycine and 1µM strychnine, and (2) for i_{GABA} measurement, 120 NaCl, 20 TEA-Chloride, 5 KCl, 5 4-aminopyridine, 0.1 CaCl2, 10 MgCl2, 10 Glucose, 10 HEPES buffered to pH 7.3, GABA 5µM, isoguvacine 5µM and CsCl 3µM.

Electrophysiological data analysis

Off-line analysis was performed with Fitmaster (Heka Elektronik), Igor-Pro 6.0.3 (Wavemetrics, Lake Oswego, OR, USA) and MiniAnalysis 6.0.7 software (Synaptosoft, Fort Lee, NJ, USA). Spontaneous post-synaptic currents (sPSCs) were identified using a semi-automated amplitude threshold based detection software (Mini Analysis 6.0.7 Program, Synaptosoft, Fort Lee, NJ, USA) and were visually confirmed. Statistical analysis was performed with Prism 5.02 software (San Die-

go, CA, USA). In all cases “n” refers to an experiment on a single cell from a single slice. All results are expressed as mean ± SEM in the text and as mean ± SD in the figures. Statistical significance was assessed in unpaired *t* tests or in one-sample *t* tests, as appropriate, using the indicated significance threshold (*p*).

RESULTS

We investigated the effect of $GABA_AR$ signaling on STDP along development, using whole-cell recordings from striatal medium-sized spiny neurons (MSNs) in horizontal corticostriatal brain slices (Fino et al., 2005) from young (P_{7-10}), juvenile (P_{17-25}) and adult (P_{60-80}) rats. Baseline excitatory postsynaptic currents (EPSCs) were recorded for 10 minutes in voltage-clamp mode and then recordings were switched to current-clamp mode to pair a single presynaptic stimulation with a single postsynaptic spike induced by a brief depolarization of the MSN. The STDP protocol involved pairing pre- and postsynaptic stimulation with a certain fixed timing interval, Δt_{STDP} ($\Delta t_{STDP}<0$ indicating that postsynaptic stimulation preceded presynaptic stimulation, i.e. post-pre pairings, and $\Delta t_{STDP}>0$ indicating that presynaptic stimulation preceded postsynaptic stimulation, i.e. pre-post pairings), repeated 100 times at 1 Hz. After the STDP pairings, recordings were obtained in voltage-clamp mode, and EPSCs were monitored at 0.1 Hz for one hour.

Developmental switch in STDP polarity and expression

In control conditions (i.e. without any pharmacological treatment), and consistent with previous results (Fino et al., 2005; Fino et al., 2010), we observed bidirectional STDP in MSNs for post- and presynaptic activities paired within $-30<\Delta t_{STDP}<+30$ ms in juvenile (P_{17-25}) rats: post-pre pairings induced spike-timing-dependent long-term potentiation (tLTP) whereas pre-post pairings induced spike-timing-dependent long-term depression (tLTD). An example of the tLTP induced by post-pre pairings (Δt_{STDP}=-19 ms) is illustrated in Figure 1a1; the mean baseline EPSC amplitude was 191±8 pA before pairings, and increased by 242% to 654±14 pA one hour after pairings. Ri remained stable over this period. Conversely, pre-post pairings (Δt_{STDP}=+13 ms) induced tLTD, as shown in the example in Figure 1b1: the mean baseline EPSC amplitude, 208±3 pA, had decreased by 35%, to 135±3 pA, one hour after pairing. To summarize, post-pre pairings ($-30<\Delta t_{STDP}<0$ms) induced tLTP (mean EPSC amplitude recorded 60 min after protocol induction: 181±30% of baseline, p=0.0429, n=6; 5 of 6 cells displayed tLTP) (Fig. 1a2), whereas pre-post pairings ($0<\Delta t_{STDP}<+30$

ms) induced tLTD (62±4%, p=0.0004, n=5; 5/5 cells displayed tLTD) (Fig. 1b2), resulting in anti-Hebbian STDP. In adult rats (P_{60-80}), we found similar results: anti-Hebbian STDP in control conditions. Indeed, post-pre pairings induced tLTP (as exemplified in Figure 1c1 with an increase of EPSCs by 117% for Δt_{STDP}= -17 ms; 133±14%, p=0.0380, n=12; 8/12 cells displayed tLTP; Fig. 1c2) whereas pre-post pairings induced tLTD (see example in Figure 1d1 with a decrease of EPSCs by 22% for Δt_{STDP}=+18 ms; 70±8%, p=0.0078, n=7; 6/7 cells displayed tLTD; Fig. 1d2).

Remarkably in P_{7-10} rats, we found a different picture than the anti-Hebbian STDP observed in juvenile and adult rats: post-pre pairings induced tLTD whereas pre-post pairing failed to trigger significant plasticity (Fig. 1e-f). An example of the tLTD induced by post-pre pairings (Δt_{STDP}=-15 ms) is shown in Figure 1e1; the mean baseline EPSC amplitude was 163±6 pA before pairings, and decreased by 69% to 51±3 pA one hour after pairings. Pre-post pairings (Δt_{STDP}=+18 ms) did not induce plasticity, as illustrated in the example in Figure 1f1: the mean baseline EPSC amplitude, 226±8 pA, did not significantly change (7% increase), one hour after pairing, 242±5pA. To summarize, post-pre pairings (-30<Δt_{STDP}<0ms) induced tLTD (59±10%, p=0.0036, n=8; 7/8 cells displayed tLTD) (Fig. 1e2), whereas pre-post pairings (0<Δt_{STDP}<+30 ms) failed inducing plasticity (89±10%, p=0.287, n=8; 5/8 cells displayed tLTD) (Fig. 1f2), resulting in an asymmetric unidirectional Hebbian STDP in P_{7-10} rats.

In conclusion, corticostriatal STDP expression and polarity is developmentally regulated and displays a transition from asymmetric unidirectional Hebbian STDP at P_{7-10} to bidirectional anti-Hebbian after P_{17}.

$GABA_AR$ transmission differentially controls STDP polarity depending on the developmental stage

We have previously shown that GABAergic signaling controls the polarity of corticostriatal STDP (Fino et al., 2010; Paillé et al., 2013). Indeed, Hebbian (Pawlak and Kerr, 2008; Shen et al., 2008)

or anti-Hebbian (Fino et al., 2005; Fino et al., 2010; Schultz et al., 2010) STDP were observed, depending on whether $GABA_A$ receptor ($GABA_ARs$) antagonists are applied (Paillé et al., 2013). Here, we confirmed our previous finding with bath-application of picrotoxin (50µM), an activity dependent blocker of $GABA_ARs$. The examples in Figure 2a1 and 2b1 show that with picrotoxin post-pre pairings at Δt_{STDP}=-15 ms induced tLTD (the mean baseline EPSC amplitude was 223±7 pA before pairings and had decreased by 24%, to 171±4 pA, one hour after pairings; Fig. 2a1) whereas pre-post pairings at Δt_{STDP}=+20 ms induced tLTP (the mean baseline EPSC amplitude was 219±X pA before pairings and had increased by 64%, to 358±6 pA, one hour after pairings; Fig. 2b1). In summary, in P_{17-25} rats blockade of $GABA_ARs$ reversed STDP polarity: post-pre pairings induced tLTD (79±5%, *p*=0.0142, *n*=5; 5/5 cells displayed tLTD; Fig. 2a2) and pre-post pairings triggered tLTP (179±32%, *p*=0.0405, *n*=8; 7/8 cells displayed tLTP; Fig. 2b2). In adult rats (P_{60-80}), we found similar results: anti-Hebbian STDP in control conditions and Hebbian STDP with blockade of $GABA_ARs$. Indeed, with blockade of $GABA_ARs$, post-pre pairings induced tLTD (as exemplified in Figure 2c1 with a decrease of EPSCs by 36% for Δt_{STDP}= -20 ms; 64±3%, *p*=0.0004, *n*=5; 5/5 cells displayed tLTP; Fig. 2c2) whereas pre-post pairings induced tLTP (as exemplified in Figure 2d1 with an increase of EPSCs by 72% for Δt_{STDP}=+18 ms; 132±12%, *p*=0.0405, *n*=7; 4/7 cells displayed tLTP; Fig. 2d2).

In P_{7-10} rats, we found an unidirectional Hebbian STDP in control conditions (Fig. 1e-f). Knowing that striatal GABAergic circuits are subject to marked developmental maturation (Chesselet et al., 2007; Ade et al., 2008; Kirmse et al., 2008; Santhakumar et al., 2010), we investigated the effect of a blockade of $GABA_A$ transmission for STDP expression in P_{7-10} rats. With blockade of $GABA_ARs$, we observed a bidirectional Hebbian STDP (Fig. 2e and 2f). The examples in Figures 2e1 and 2f1 show that with picrotoxin post-pre pairings at Δt_{STDP}=-12 ms induced tLTD (the mean baseline EPSC amplitude was 130±2 pA before pairings and had decreased by 33%, to 87±2 pA, one hour after pairings; Fig. 2e1) whereas pre-post pairings at Δt_{STDP}=+13 ms induced tLTP (the mean base-line EPSC amplitude was 118±4 pA before pairings and had increased by 59%, to 188±4 pA, one

hour after pairings; Fig. 2f1). In summary, in $P_{7\text{-}10}$ rats blockade of $GABA_A$Rs uncovered a Hebbian STDP: post-pre pairings induced tLTD (64±7%, *p*=0.0013, *n*=8; 8/8 cells displayed tLTD; Fig. 2e2) and pre-post pairings triggered tLTP (147±11%, *p*=0.0049, *n*=8; 8/8 cells displayed tLTP; Fig. 2f2). In conclusion, corticostriatal STDP is differentially controlled by $GABA_A$R signaling depending on the developmental stage. Indeed, with blockade of $GABA_A$Rs STDP shifted from a unidirectional asymmetric Hebbian STDP to a bidirectional Hebbian STDP in $P_{7\text{-}10}$ animals whereas it is switched from bidirectional anti-hebbian STDP into bidirectional Hebbian STDP in juvenile and adult rats (Fig. 2g). Remarkably, regardless of the developmental stage, blockade of $GABA_A$ transmission promotes tLTD with post-pre pairings (Fig. 2g1), whereas tLTP is induced with pre-post pairings (Fig. 2g2).

Tonic GABAergic component is developmentally regulated

There are two ionotropic GABAergic signaling depending on the location of $GABA_A$Rs: the tonic and the phasic signaling which rely, respectively, on extrasynaptic and synaptic $GABA_A$Rs (Farrant and Nusser, 2005; Glykys and Mody, 2007; Brickley and Mody, 2012). Phasic and tonic activation of $GABA_A$Rs display distinct roles in the control of neuronal excitability (Farrant and Nusser, 2005; Glykys and Mody, 2007). Using a high-chloride cesium-based intracellular solution (see Methods) associated with bath-applied D-AP5/CNQX and specific inhibition of $GABA_A$Rs, we first verified that both GABAergic components were present in MSNs in juvenile rats (Fig. 3a). Picrotoxin (50µM) treatment removed the phasic component (spontaneous IPSCs), and the tonic signaling was revealed by a significant change of the injected current (Δ_{Ihold}) necessary to hold the resting membrane potential (RMP) (Δ_{Ihold}=23.4±3.1pA, n=9, p<0.01) together with a decrease of the SD of the synaptic noise (before picrotoxin: 2.9±0.3pA, and after picrotoxin: 1.9±0.2pA, n=9, p<0.05) (Fig. 3a1-a3).

We then assessed the presence of the tonic and phasic GABAergic components in $P_{7\text{-}10}$ rats (Fig. 3b). sIPSCs recorded at $P_{7\text{-}10}$ had a similar frequency than those observed at $P_{17\text{-}25}$ (2.6±0.5Hz, n=6 versus 3.3±0.6Hz, n=9, respectively; $p>0.05$) while their amplitude was larger (46.7±5.4pA, n=6 versus 20.4±3.7pA, n=9, respectively; $p<0.05$) (Fig. 3b1). The tonic GABAergic component was absent in $P_{7\text{-}10}$ rats. Indeed, picrotoxin did not induce a significant variation of I_{hold} (-3.1±5.1pA, $p>0.05$, n=6) and synaptic noise (2.5±0.2pA, $p>0.05$, n=6) (Fig. 3b1-b3). This is consistent with previous observation reporting the apparition of tonic inhibition in striatum later in development (~P_{16}) (Ade et al., 2008; Kirmse et al., 2008; Santhakumar et al., 2010). Therefore, phasic GABAergic signaling appeared to be the sole $GABA_AR$ mediated-transmission in $P_{7\text{-}10}$ rats.

The reversal potential of $GABA_A$-mediated current ($E_{GABA(A)}$) is -35mV in MSNs from $P_{7\text{-}10}$ rats

It has been reported a decreased MSN excitability following blockage of GABA (Ade et al., 2008; Bracci and Panzeri, 2006). This could be attributed to a depolarizing effect of the GABA due to the positive difference between GABA reversal potential ($E_{GABA(A)}$) and the RMP of MSNs. We estimated E_{GABA} and RMP with cell-attached recordings of single-channel NMDAR and $GABA_A$ mediated-currents (i_{NMDA} and $i_{GABA(A)}$) (see Methods) (Fig. 3c). In $P_{17\text{-}25}$ MSNs, we previously reported a $E_{GABA(A)}$=-60.8 mV (with a driving force of chloride ions through $GABA_ARs$ of 17.2±7 mV and RMP=-78.1±1.1 mV; n=4) (Paillé et al., 2013). Interestingly, in $P_{7\text{-}10}$ MSNs we measured a driving force of chloride ions through $GABA_ARs$ of 33.0±1.8 mV from $E_{GABA(A)}$=-34.6 mV and RMP=-67.5±2.8 mV (n=5). This shows the depolarizing effect of GABA in MSNs from $P_{17\text{-}25}$ as well as in $P_{17\text{-}25}$ animals.

Promoting tonic GABAergic signaling induces anti-Hebbian t-LTD in P_{7-10} MSNs

We now asked whether the absence of the tonic GABAergic component in P_{7-10} rats could account for the unidirectional asymmetric Hebbian STDP observed at this stage. To answer this question we aimed at promoting tonic GABAergic component using two distinct strategies: (1) by pharmacological stimulation of the high-affinity extrasynaptic $GABA_A$Rs (Farrant and Nusser, 2005; Glykys and Mody, 2007) β2/β3-subunit containing $GABA_A$Rs (Janssen et al., 2009) and (2) by pharmacological blockade of the GABA transporters (GATs) which promotes the accumulation of GABA and activation of $GABA_A$Rs resulting in the subsequent induction of tonic GABAergic signaling (Nusser and Mody, 2002; Rossi et al., 2003; Semyanov et al., 2003; Kirmse et al., 2008; Goubard et al., 2012).

We first tested the efficiency of etomidate, a general anesthetic and selective agonist for β2/β3-subunit containing $GABA_A$Rs (Hill-Venning et al. 1997), to induce a tonic GABAergic component at P_{7-10}. Using a high-chloride cesium-based intracellular solution associated with bath-applied D-AP5/CNQX, we observed that etomidate (3 μM) did not affect the phasic signaling but created a potent tonic component (Fig. 4a). We observed a significant change of Δ_{Ihold} (Δ_{Ihold}=-22,29±4,69 pA, n=8, p<0.021) without significant increase of the SD of the synaptic noise (before etomidate: 6,42±1,03 pA, and after: 9,16±2,31 pA, p<0.113, n=8) (Fig. 4a1-a3). After validating the specificity and efficiency of etomidate in promoting tonic GABAergic signaling, we explored the effect of etomidate on STDP in P_{7-10} rats. With etomidate (3 μM), we observed tLTD for both post-pre and pre-post pairings. Indeed, both post-pre and pre-post pairings induced tLTD (88±6%, *p*=0.0491, *n*=11, 7/11 cells displayed tLTD, and 53±8%, *p*=0.0025, *n*=6, 6/6 cells displayed tLTD, respectively) (Fig. 4b and 4c).

We then blocked GABA uptake with nipecotic acid, a competitive inhibitor of GAT-1/2/3 subtypes (Shousboe et al., 1979; Liu et al., 1993). Nipecotic acid (500 μM) was able to induce a tonic GABAergic signaling at P_{7-10}. Using a high-chloride cesium-based intracellular solution with D-AP5/CNQX, nipecotic acid did not affect significantly the mean frequency (4,44±0,60 Hz before vs

4,55±0,58 Hz after nipecotic acid, p<0.278, n=10) or the mean amplitude of the remaining spontaneous IPSCs (28,46±2,63 pA before vs 29,31±2,63 pA after nipecotic acid, p<0.713, n=10) (Fig.4d). As previously reported (Kirmse et al. 2008; Goubard et al., 2012), nipecotic acid induced a significant increase of the SD of the synaptic noise (before nipecotic acid: 5.82±0.98 pA, and after: 8,76±1.00 pA, p<0.004, n=8; Fig.4d2) with a significant increase of the tonic $GABA_AR$-mediated conductances (Δ_{Ihold}=-73,18±26,69 pA, n=8, p<0.029; Fig. 4d3). Therefore, the blockade of GATs generated a tonic inhibition at high-affinity extrasynaptic $GABA_ARs$ and a decrease of corticostriatal transmission. Similarly to the plasticity observed with etomidate treatment, with nipecotic acid (500 µM), we observed a symmetric tLTD i. e. for both post-pre and pre-post pairings. Both post-pre and pre-post pairings induced tLTD (77±6%, *p*=0.0030, *n*=10, 8/10 cells displayed tLTD, and 86±5%, *p*=0.0332, *n*=8, 6/8 cells displayed tLTD, respectively) (Fig. 4e and 4f).

In conclusion, promoting tonic GABAergic signaling at $P_{7\text{-}10}$ was able to partially restore anti-Hebbian STDP by inducing tLTD for pre-post pairings.

Tonic and phasic GABAergic signaling differentially shape anti-Hebbian STDP at $P_{17\text{-}25}$

We then specifically inhibited the phasic or tonic GABAergic component in $P_{17\text{-}25}$ rats to estimate their contribution to STDP expression and polarity.

The phasic component was specifically precluded with low concentration of gabazine (200nM), a $GABA_ARs$ competitive antagonist, without affecting the tonic signaling (Fig. 5a). Indeed, using a high-chloride cesium-based intracellular solution with D-AP5/CNQX, frequency and amplitude of sIPSCs were significantly reduced after gabazine treatment (frequency: 6.0±1.8Hz before vs 1.2±0.2Hz after gabazine, p<0.05, n=5; amplitude: 30.9±2.2pA before vs 13.3±2.6pA after gabazine, p<0.01, n=5) without significant changes in the tonic component (ΔI_{hold}=2.3±2.5pA, p>0.05, n=5). We thus inhibited the phasic GABAergic component with the use of low concentration of gabazine (200nM) in $P_{17\text{-}25}$ rats (see Fig. 2b and 2c). For post-pre pairings, which

induced tLTP in control conditions (Fig. 1a), we still observed a robust tLTP with gabazine (147±16%, *p*=0.0236, *n*=7, 5/7 cells displayed tLTP) (Fig. 5b). For pre-post pairings with gabazine no significant plasticity could be observed (102±4%, *p*=0.6765, *n*=8, 2/8 cells displayed tLTD) (Fig. 5c). Therefore, anti-Hebbian tLTD, but not tLTP, at P_{17-25} is dependent on phasic GABAergic signaling.

Ambient GABA can generate tonic inhibition at high-affinity extrasynaptic $GABA_A$Rs (Farrant and Nusser, 2005; Glykys and Mody, 2007) composed by the α5-subunit in striatum (Ade et al., 2008). L655,708 (10μM), a α5-$GABA_A$R-selective inverse agonist, inhibited the tonic (ΔI_{hold}=29.0±7.7pA, $p<0.05$, n=4) without affecting the phasic component (sIPSC frequency: 4.4±1.0Hz before vs 4.6±1.1Hz after L655,708, $p>0.05$, n=5; sIPSC amplitude: 28.1±2.9pA before vs 24.6±2.9pA after L655,708, $p>0.05$, n=5) (Fig. 5d). Note that the corticostriatal transmission was not affected by L655,708 (EPSC mean amplitude: 127±9pA before vs 132±13pA after L655,708, $p>0.05$, n=11). We then inhibited the tonic GABAergic component by bath-applying L655,708 in P_{17-25} rats (see Fig. 5e and 5f) and we observed a dramatic change in STDP expression. For post-pre pairings, which induced tLTP in control conditions (Fig. 1b), we observed tLTD with L655,708 (10μM) (83±5%, *p*=0.0124, *n*=7, 5/7 cells displayed tLTD) (Fig. 5e). For pre-post pairings with L655,708, no significant plasticity could be detected (91±17%, *p*=0.6193, *n*=7, 4/7 cells displayed tLTD) (Fig. 5f). Therefore, blockade of the tonic GABAergic component in P_{17-25} rats induced a switch in STDP polarity thus promoting unidirectional asymmetric Hebbian STDP similar to our results in P_{7-10} rats (in which tonic signaling is lacking).

DISCUSSION

This study demonstrates that along development striatal STDP exhibits distinct polarity, which is mainly controlled by the tonic GABAergic component. Indeed, we found that in immature P_{7-10} rats, STDP displays asymmetric and unidirectional Hebbian tLTD whereas in older animals (P_{17-25} and P_{60-80} rats) STDP is bidirectional and anti-Hebbian. We uncovered that tonic and phasic GABAergic signaling are differently engaged in controlling STDP. Most importantly, the tonic GABAergic signaling is a key actor for the control of STDP polarity along development. Indeed, tonic GABAergic component, which arises from P_{16} in striatum (Ade et al., 2008; Kirmse et al., 2008; Santhakumar et al., 2010), is necessary to the shift from asymmetric and unidirectional Hebbian tLTD in immature animals to bidirectional anti-Hebbbian STDP observed at later developmental stages (Fino and Venance, 2010). Therefore, the tonic GABA appears to be a key actor in controlling STDP polarity because it is sufficient to explain the shift from STDP observed in P_{17-25} rats (bidirectional anti-Hebbian) to those observed in P_{7-10} rats (unidirectional Hebbian STDP). To our knowledge, our study is the first to explore corticostriatal STDP in the immature brain and to show its reshaping along development. Indeed, the contribution of tonic GABA was investigated in hippocampal STDP (Groen et al. 2014): tonic GABAergic inhibition regulates dendritic bAP in juvenile, but not in younger animals and blockade of the tonic GABAergic component leads to higher threshold for STDP induction in juvenile animals but without changing the polarity of STDP (Groen et al. 2014). Numerous studies in juvenile rodents investigated different forms of long-term plasticity using pharmacological blockade of the $GABA_AR$-mediated transmission. These conditions affect the physiological polarity of STDP. Indeed, Hebbian and anti-Hebbian polarity of the corticostriatal STDP have been observed depending on the use (Hebbian STDP) (Pawlak and Kerr, 2008; Shen et al., 2008) or not (anti-Hebbian STDP) (Fino et al., 2005; Fino et al., 2010) of $GABA_AR$ antagonists (Paillé et al., 2013); This is in accordance with *in vivo* experiments in adult rats showing that corticostriatal STDP without pharmacological treatment displays anti-Hebbian polarity (Schulz et al., 2010). Thus, in juvenile and adult animals, GABA operates as a

Hebbian/anti-Hebbian switch and this is most likely due to its depolarizing effect in striatum (Paillé et al., 2013). Developmental maturation of GABAergic signaling is tightly linked to the emergence of bidirectional anti-Hebbian STDP in striatum.

MSNs of the dorsal striatum can be divided into two main subpopulations based on their belonging to the direct (striato-nigral) or indirect (striato-subthalamo-nigral) output pathways (Calabresi et al., 2014). MSNs of the direct and indirect pathways express D1-like and D2-like dopamine receptors, respectively. Using D1-GFP mice, we have previously shown that GABA exerts similar control on STDP polarity regardless of the belonging of MSNs to the direct ($D1^+$ MSNs) or the indirect ($D2^+$ MSNs) pathway (Paillé et al., 2013). Although it has been reported that $D2^+$ MSNs express a slightly higher tonic component in young/juvenile mice (Ade et al., 2008; Santhakumar et al., 2010; Luo et al., 2013), we did not observe segregation of our STDP results when either blocking selectively tonic GABAergic signaling in juvenile rats or, conversely, promoting tonic GABAergic component in immature rats. Therefore, the occurrence of plasticity in our experimental conditions indicates a lack of segregation between the two trans-striatal pathways. It should be noted that in P>30 mice, tonic GABAergic signaling increases in $D1^+$ MSNs whereas it decreases in $D2^+$ MSNs (Santhakumar et al., 2010). Previous observations have reported that FS interneurons contact both subpopulations of MSNs and exert a strong inhibitory weight on both (Bennett and Bolam, 1994; Planert et al., 2010), indicating that the phasic GABA is similar in $D1^+$ and $D2^+$ MSNs (Ade et al., 2008). We observed similar effects of GABA in both $D1^+$ and $D2^+$ MSNs, highlighting that the control of STDP by GABA would not be specific to these MSN subpopulations. It remains to investigate the impact of dopamine (absence or presence, various activity patterns of nigrostriatal dopaminergic cells), which could unveil differential control of STDP by tonic GABAergic signaling along development.

The present results confirm the crucial role of GABAergic transmission in controlling plasticity depending on developmental stages. It implies that similar paired stimulations (post-pre pairings) should induce tLTD in pre-juvenile brain while a LTP will occur at a later stages, and conversely for

pre-post pairings (a lack of plasticity vs LTD). This means that GABA should have different effect on learning in young versus adult animals. Importantly, the difference between young and juvenile animals is not likely due to a different effect of GABA in term of polarization because in immature and juvenile animals $E_{GABA(A)}$ is more depolarized than RMP. Our results show that $E_{GABA(A)}$, although depolarizing in $P_{7\text{-}10}$ and juvenile animals, is different in both cases (-35 mV *vs* -60 mV) (Fig. 3c and Paillé et al. 2013). However, the RMP of MSNs in $P_{7\text{-}10}$ animals is also shifted towards more depolarized values. Therefore, the shunting inhibition operated by GABAergic signaling should increase the membrane conductance in an identical manner. This will result in a similar reduction in the membrane time constant and therefore less temporal integration of inputs in both in $P_{7\text{-}10}$ and older ($P_{17\text{-}25}$ and $P_{60\text{-}80}$) animals. This suggests that the information transfer regarding temporal coding at early developmental stages is expected to be similar in mature animals. Therefore, the sole change in $E_{GABA(A)}$ cannot account for the observed changes in the corticostriatal STDP rule. The establishment of the canonical form of anti-Hebbian STDP in the dorsolateral striatum appears to be due to the expression along development of the tonic GABAergic component. For earlier developmental stage than P_{16}, MSNs have the required equipment to sense tonic GABA since with either pharmacological activation of β2/β3-subunit containing $GABA_ARs$ (Janssen et al., 2011) or with inhibition of GATs, a tonic GABAergic component was observed in MSNs from immature rats. It has been reported that etomidate impairs hippocampal LTP (induced with theta burst stimulation) most likely via α5-subunit containing $GABA_ARs$ (Rogers et al., 2015). Tonic GABAergic signaling can be prevented in the immature striatum through various mechanisms which would limit the GABA spillover and/or its effects: a high expression of GAT-2/3 in the early phases of phases of postnatal development (Conti et al. 2004), a more complete astrocytic coverage of the corticostriatal synapses or extra-synaptic $GABA_ARs$ clustered in domains too far away from the GABA releasing sites. Thus, STDP-timing rule is tightly developmentally-driven by the maturation of GABAergic circuits and associated signaling.

The differential effect of GABA observed along development could rely on the maturation of the different subtypes of striatal interneurons (Tepper et al., 2008), as well as the functional maturation of synaptic and extra-synaptic $GABA_AR$s and associated signaling. The best candidates for the feedforward inhibition are the fast-spiking interneurons because they exert the strongest inhibition on MSNs (Koos and Tepper, 1999; Tepper et al., 2008). Nevertheless, at least two other types of GABAergic interneurons, NO-synthase and calretinin containing interneurons exerting feedforward inhibition on MSNs (Tepper et al., 2008; Gittis and Kreitzer, 2012; Silberberg and Bolam, 2015), and MSNs colaterals exerting feedback inhibition (Venance et al., 2004; Koos et al., 2004). It remains thus to analyze the impact of each interneuronal subpopulation and/or MSNs in the developmental shift of STDP.

Corticostriatal STDP shifts from Hebbian-LTD to anti-Hebbian STDP along development. Developmental regulation of STDP has been also investigated at L4–L2/3 cortical synapses (Itami & Kimura 2012). Developmental switch in STDP occurs at the end of the second postnatal week in somatosensory cortex, when unidirectional symmetric STDP (t-LTP) is flipped to bidirectional Hebbian STDP. In addition, thalamocortical terminals to L2/3 pyramidal cells display unidirectional order-independent STDP (t-LTP only) that is transformed to t-LTD only between the first and the second postnatal week (Itami et al. 2016).

The physiological relevance of anti-Hebbian STDP in striatal function is yet to be unraveled. The hypothesis is that anti-Hebbian tLTD, also observed in the cerebellum-like sensory structures in electric fish (Bell et al., 1997) or in the dorsal coclear nucleus (Tzounopoulos et al., 2007), would serve to cancel out predictable inputs and consequently allowed novel sensory inputs to be better represented (Roberts and Bell, 2000), or keep synapses weak (Sjöström and Häusser, 2006). This could be a crucial requirement for striatum, which is acting as a coincident detector of distributed patterns of cortical and thalamic activity (REFs). Thus, an overriding question is what would be the advantage of a bidirectional anti-Hebbian STDP at later developmental stages compared to unidirectional Hebbian tLTD? The use of neuronal network model would allow determining the

efficiency for information storage and recall of various forms of STDP (Mishra et al., 2016) and thus eventually answer the question of the developmental benefit of the shift in STDP polarity.

REFERENCES:

Ade, K.K., Janssen, M.J., Ortinski, P.I., and Vicini, S. (2008). Differential tonic GABA conductances in striatal medium spiny neurons. J Neurosci 28, 1185-1197.

Ben-Ari, Y., Gaiarsa, J.L., Tyzio, R., and Khazipov, R. (2007). GABA: a pioneer transmitter that excites immature neurons and generates primitive oscillations. Physiol Rev 87, 1215-1284.

Bell CC, Han VZ, Sugawara Y, Grant K. (1997). Synaptic plasticity in a cerebellum-like structure depends on temporal order. Nature 387(6630):278-81.

Bennett, B.D., and Bolam, J.P. (1994). Synaptic input and output of parvalbumin-immunoreactive neurons in the neostriatum of the rat. Neuroscience 62, 707-719.

Bracci, E., and Panzeri, S. (2006). Excitatory GABAergic effects in striatal projection neurons. J Neurophysiol 95, 1285-1290.

Brickley SG, Mody I. (2012) Extrasynaptic GABA(A) receptors: their function in the CNS and implications for disease. Neuron 73(1):23-34.

Calabresi, P., Picconi, B., Tozzi, A., Ghiglieri, V., Di Filippo, M., 2014. Direct and indirect pathways of basal ganglia: a critical reappraisal. Nat. Neurosci. 17, 1022–1030.

Chesselet, M.F., Plotkin, J.L., Wu, N., and Levine, M.S. (2007). Development of striatal fast-spiking GABAergic interneurons. Prog Brain Res 160, 261-272.

Citri A, Malenka RC. 2008. Synaptic plasticity: multiple forms, functions, and mechanisms. Neuropsychopharmacology. 33: 18-41.

Conti F1, Minelli A, Melone M. (2004) GABA transporters in the mammalian cerebral cortex: localization, development and pathological implications. Brain Res Brain Res Rev. 45(3):196-212.

Donato F, Rompani SB, Caroni P. (2013) Parvalbumin-expressing basket-cell network plasticity induced by experience regulates adult learning. Nature 504(7479):272-6.

Farrant, M., and Nusser, Z. (2005). Variations on an inhibitory theme: phasic and tonic activation of GABA(A) receptors. Nat Rev Neurosci 6, 215-229.

Feldman DE. 2012. The spike-timing dependence of plasticity. Neuron. 75:556-571.

Fino, E., Glowinski, J., and Venance, L. (2005). Bidirectional activity-dependent plasticity at corticostriatal synapses. J Neurosci 25, 11279-11287.

Fino, E., Paille, V., Cui, Y., Morera-Herreras, T., Deniau, J.M., and Venance, L. (2010). Distinct coincidence detectors govern the corticostriatal spike timing-dependent plasticity. J Physiol 588, 3045-3062.

Fino E, Venance L (2010). Spike-timing dependent plasticity in the striatum. Front Synaptic Neurosci 2, 6.

Froemke, R.C., Letzkus, J.J., Kampa, B.M., Hang, G.B., and Stuart, G.J. (2010). Dendritic synapse location and neocortical spike-timing-dependent plasticity. Front Synaptic Neurosci 2, 29.

Gittis AH, Kreitzer AC. (2012) Striatal microcircuitry and movement disorders. Trends Neurosci. 35(9):557-64.

Glykys, J., and Mody, I. (2007). Activation of GABAA receptors: views from outside the synaptic cleft. Neuron 56, 763-770.

Goubard V, Fino E, Venance L. (2011). Contribution of astrocytic glutamate and GABA uptake to corticostriatal information processing. The Journal of Physiology. 589:2301-2319.

Groen MR, Paulsen O, Pérez-Garci E, Nevian T, Wortel J, Dekker MP, Mansvelder HD, van Ooyen A, Meredith RM. (2014). Development of dendritic tonic GABAergic inhibition regulates excitability and plasticity in CA1 pyramidal neurons. J Neurophysiol. 112(2):287-99.

Higley, M.J., and Contreras, D. (2006). Balanced excitation and inhibition determine spike timing during frequency adaptation. J Neurosci 26, 448-457.

Hill-Venning C, Belelli D, Peters JA, Lambert JJ. (1997). Subunit-dependent interaction of the general anaesthetic etomidate with the gamma-aminobutyric acid type A receptor. Br J Pharmacol. 120(5):749-56.

Itami C, Kimura F. (2012). Developmental switch in spike-timing-dependent plasticity at layers 4-2/3 in the rodent barrel cortex. J Neurosci 32, 15000-15011.

Itami C, Huang JY, Yamasaki M, Watanabe M, Lu HC, Kimura F. (2016). Developmental Switch in Spike Timing-Dependent Plasticity and Cannabinoid-Dependent Reorganization of the Thalamocortical Projection in the Barrel Cortex. J Neurosci. 36(26):7039-54.

Janssen MJ, Yasuda RP, Vicini S. (2011). GABA(A) Receptor β3 Subunit Expression Regulates Tonic Current in Developing Striatopallidal Medium Spiny Neurons. Front Cell Neurosci. 5:15.

Janssen MJ, Ade KK, Fu Z, Vicini S. (2009). Dopamine modulation of GABA tonic conductance in striatal output neurons. J Neurosci. 29(16):5116-26.

Kirmse, K., Dvorzhak, A., Kirischuk, S., and Grantyn, R. (2008). GABA transporter 1 tunes GABAergic synaptic transmission at output neurons of the mouse neostriatum. J Physiol 586, 5665-5678.

Koos, T., and Tepper, J.M. (1999). Inhibitory control of neostriatal projection neurons by GABAergic interneurons. Nat Neurosci 2, 467-472.

Koos T, Tepper JM, Wilson CJ. (2004). Comparison of IPSCs evoked by spiny and fast-spiking neurons in the neostriatum. J Neurosci. 24(36):7916-22.

Luo R, Partridge JG, Vicini S. (2013). Distinct roles of synaptic and extrasynaptic GABAAreceptors in striatal inhibition dynamics. Front Neural Circuits. 7:186.

Mishra RK, Kim S, Guzman SJ, Jonas P.(2016). Symmetric spike timing-dependent plasticity at CA3-CA3 synapses optimizes storage and recall in autoassociative networks. Nat Commun. 7:11552.

Nabavi S, Fox R, Proulx CD, Lin JY, Tsien RY, Malinow R. 2014. Engineering a memory with LTD and LTP. Nature. 511:348-352. doi: 10.1038/nature13294.

Nusser Z, Mody I. (2002). Selective modulation of tonic and phasic inhibitions in dentate gyrus granule cells. J Neurophysiol. 87(5):2624-8.

Paillé V, Fino E, Du K, Morera Herreras T, Perez S, Hellgren Kotaleski J, Venance L. 2013. GABAergic circuits control spike-timing-dependent plasticity. The Journal of Neuroscience. 33: 9353-9363. doi: 10.1523/JNEUROSCI.5796-12.2013.

Pawlak, V., and Kerr, J.N. (2008). Dopamine receptor activation is required for corticostriatal spike-timing-dependent plasticity. J Neurosci 28, 2435-2446.

Planert, H., Szydlowski, S.N., Hjorth, J.J., Grillner, S., and Silberberg, G. (2010). Dynamics of synaptic transmission between fast-spiking interneurons and striatal projection neurons of the direct and indirect pathways. J Neurosci 30, 3499-3507.

Pouille, F., and Scanziani, M. (2001). Enforcement of temporal fidelity in pyramidal cells by somatic feed-forward inhibition. Science 293, 1159-1163.

Roberts PD, Bell CC. (2000). Computational consequences of temporally asymmetric learning rules: II. Sensory image cancellation. J Comput Neurosci. 9(1):67-83.

Rodgers FC, Zarnowska ED, Laha KT, Engin E, Zeller A, Keist R, Rudolph U, Pearce RA. (2015). Etomidate Impairs Long-Term Potentiation In Vitro by Targeting α5-Subunit Containing GABAA Receptors on Nonpyramidal Cells. J Neurosci. 35(26):9707-16.

Rossi DJ, Hamann M, Attwell D.(2003). Multiple modes of GABAergic inhibition of rat cerebellar granule cells. J Physiol. 548(Pt 1):97-110.

Santhakumar, V., Jones, R.T., and Mody, I. (2010). Developmental regulation and neuroprotective effects of striatal tonic GABAA currents. Neuroscience 167, 644-655.

Schulz, J.M., Redgrave, P., and Reynolds, J.N. (2010). Cortico-striatal spike-timing dependent plasticity after activation of subcortical pathways. Front Synaptic Neurosci 2, 23.

Semyanov A, Walker MC, Kullmann DM. (2003). GABA uptake regulates cortical excitability via cell type-specific tonic inhibition. Nat Neurosci. 6(5):484-90.

Shen, W., Flajolet, M., Greengard, P., and Surmeier, D.J. (2008). Dichotomous dopaminergic control of striatal synaptic plasticity. Science 321, 848-851.

Silberberg G1, Bolam JP2. (2015). Local and afferent synaptic pathways in the striatal microcircuitry. Curr Opin Neurobiol. 33:182-7.

Sjostrom, P.J., Rancz, E.A., Roth, A., and Hausser, M. (2008). Dendritic excitability and synaptic plasticity. Physiol Rev 88, 769-840.

Sjöström PJ, Häusser M. (2006). A cooperative switch determines the sign of synaptic plasticity in distal dendrites of neocortical pyramidal neurons. Neuron. 51(2):227-38.

Szydlowski SN, Pollak Dorocic I, Planert H, Carlén M, Meletis K, Silberberg G. (2013). Target selectivity of feedforward inhibition by striatal fast-spiking interneurons. J Neurosci. 33(4):1678-83.

Takesian AE1, Hensch TK. (2013). Balancing plasticity/stability across brain development. Prog Brain Res. 207:3-34.

Tepper, J.M., Wilson, C.J., and Koos, T. (2008). Feedforward and feedback inhibition in neostriatal GABAergic spiny neurons. Brain Res Rev 58, 272-28.

Tzounopoulos T1, Rubio ME, Keen JE, Trussell LO. (2007). Coactivation of pre- and postsynaptic signaling mechanisms determines cell-specific spike-timing-dependent plasticity. Neuron 54(2): 291-301.

Venance L, Glowinski J, Giaume C. (2004). Electrical and chemical transmission between striatal GABAergic output neurones in rat brain slices. J Physiol. 559(Pt 1):215-30.

Wehr, M., and Zador, A.M. (2003). Balanced inhibition underlies tuning and sharpens spike timing in auditory cortex. Nature 426, 442-446.

Author Contributions: SV, VP, GG, EF and LV conceived and designed the experiments; SV, VP, SP, GG, YD, EF performed experiments; SV, VP and YD analyzed data; LV wrote the manuscript and supervised the project and all authors have edited and corrected the manuscript.

Acknowledgments: We thank the members of the LV laboratory, Kim T Blackwell and Jeanette Hellgren Kotaleski for helpful suggestions and critical comments. SV is a Research Fellow of the MRT and the LabEx MemoLife; GG is a Research Fellow of Fondation Brou de Laurrière; YD is a Research Fellow of ANR Dopaciumcity. This work was supported by grants from INSERM, *Collège de France*, CNRS and ANR.

Competing Financial Interests statement: the authors have no competing financial interests to declare.

FIGURE LEGENDS:

Figure 1. Developmental switch in STDP polarity and expression.

(**a-b**) Corticostriatal STDP in P_{17-25} rats in control conditions for post-pre pairings. (**a1**) Example of tLTP induced by 100 post-pre pairings in control conditions. Top, EPSC strength before and after pairings. Bottom, time course of Ri (baseline: 77±0.5MΩ and 40-50 min after pairings: 91±0.5MΩ; change of 18%). (**a2**) Averaged time-courses of tLTP induced by 100 post-pre pairings in control conditions. Scatter plot of the STDP experiments; each point represents a single STDP experiment. Postsynaptic EPSC traces during 10 minutes of baseline (black trace) and 60 minutes after the STDP protocol (grey trace). (**b1**) Example of tLTD induced by 100 pre-post pairings in control conditions. Top, EPSC strength before and after pairings. Bottom, time course of Ri (baseline: 65±0.5MΩ and 40-50 min after pairings: 58±0.4MΩ; change of 11%). (**b2**) Averaged time-courses of tLTD induced by 100 pre-post pairings in control conditions. (**c-d**) Corticostriatal STDP in P_{60-80} rats. (**c1**) Example of tLTP induced by 100 post-pre pairings. Top, EPSC strength before and after pairings. Bottom, time course of Ri (baseline: 87±1MΩ and 40-50 min after pairings: 82±0.2MΩ; change of 7%). (**c2**) Averaged time-courses of tLTP induced by 100 post-pre pairings. (**d1**) Example of tLTD induced by 100 pre-post pairings. Top, EPSC strength before and after pairings. Bottom, time course of Ri (baseline: 39±0.4MΩ and 40-50 min after pairings: 44±0.2MΩ; change of 15%). (**d2**) Averaged time-courses of tLTD induced by 100 pre-post pairings. (**e-f**) Corticostriatal STDP in P_{7-10} rats. (**e1**) Example of tLTD induced by 100 post-pre pairings. Top, EPSC strength before and after pairings. Bottom, time course of Ri (baseline: 67±0.2MΩ and 50-60 min after pairings: 64±0.3MΩ; change of 5%). (**e2**) Averaged time-courses of tLTD induced by 100 post-pre pairings. (**f1**) Example of the lack of plasticity induced by 100 pre-post pairings. Top, EPSC strength before and after pairings. Bottom, time course of Ri (baseline: 438±5MΩ and 50-60 min after pairings: 511±8MΩ; change of 17%). (**f2**) Averaged time-courses of the lack of plasticity by 100 pre-post pairings.

Error bars represent the SD. *: $p<0.05$; **: $p<0.01$; ***: $p<0.001$; ns: not significant.

Figure 2. $GABA_AR$ transmission differentially controls STDP polarity depending on the developmental stage

(**a-b**) Corticostriatal STDP in P_{17-25} rats with bath-applied picrotoxin (50μM). (**a1**) Example of tLTD induced by 100 post-pre pairings with picrotoxin. Top, EPSC strength before and after pairings. Bottom, time course of Ri (baseline: 127±0.9MΩ and 40-50 min after pairings: 137±1MΩ; change of 8%). (**a2**) Averaged time-courses of tLTD induced by 100 post-pre pairings with picrotoxin. Scatter plot of the STDP experiments; each point represents a single STDP experiment. Postsynaptic EPSC traces during 10 minutes of baseline (black trace) and 60 minutes after the STDP protocol (gray trace). (**b1**) Example of tLTP induced by 100 pre-post pairings with picrotoxin. Top, EPSC strength before and after pairings. Bottom, time course of Ri (baseline: 163±2MΩ and 50-60 min after pairings: 160±2MΩ; change of 2%). (**b2**) Averaged time-courses of tLTP induced by 100 pre-post pairings with picrotoxin. (**c-d**) Corticostriatal STDP in P_{60-80} rats with picrotoxin. (**c1**) Example of tLTD induced by 100 post-pre pairings with picrotoxin. Top, EPSC strength before and after pairings. Bottom, time course of Ri (baseline: 104±0.4MΩ and 50-60 min after pairings: 92±0.6MΩ; change of 11%). (**c2**) Averaged time-courses of tLTD induced by 100 post-pre pairings with picrotoxin. (**d1**) Example of tLTP induced by 100 pre-post pairings with picrotoxin. Top, EPSC strength before and after pairings. Bottom, time course of Ri (baseline: 79±1MΩ and 40-50 min after pairings: 89±0.5MΩ; change of 14%). (**d2**) Averaged time-courses of tLTP induced by 100 pre-post pairings with picrotoxin. (**e-f**) Corticostriatal STDP in P_{7-10} rats with picrotoxin. (**e1**) Example of tLTD induced by 100 post-pre pairings with picrotoxin. Top, EPSC strength before and after pairings. Bottom, time course of Ri (baseline: 190±1MΩ and 50-60 min after pairings: 181±0.8MΩ; change of 5%). (**e2**) Averaged time-courses of tLTD induced by 100 post-pre pairings with picrotoxin. (**f1**) Example of tLTP induced by 100 pre-post pairings with picrotoxin. Top, EPSC strength before and after pairings. Bottom, time course of Ri (baseline: 194±2MΩ and 50-60 min after pairings: 176±2MΩ; change of 9%) (**f2**) Averaged time-courses of

tLTP induced by 100 pre-post pairings with picrotoxin. (**g**) Summary graphs illustrating the corticostriatal STDP expression and polarity along development in control conditions and with picrotoxin for post-pre (g1) and pre-post (g2) pairings. Regardless of the developmental stage, blockade of GABAA transmission promotes tLTD with post-pre pairings, whereas tLTP is favored with pre-post pairings.

Error bars represent the SD. *: $p<0.05$; **: $p<0.01$; ***: $p<0.001$.

Figure 3. Tonic GABAergic component and reversal potential of $GABA_A$-mediated current (E_{GABA}) are developmentally regulated

(**a**) Picrotoxin (50μM) inhibits both tonic and phasic GABAAR transmission in P_{17-25} rats. (**a1**) Raw traces with D-AP5/CNQX and then with picrotoxin (showing the phasic (IPSCs) and tonic (holding current, dashed line, and synaptic noise) GABAergic components. (**a2**) All point histograms are build on data from 50 sec recordings in the presence or absence of picrotoxin (with D-AP5/CNQX). (**a3**) Frequency and amplitude of IPSCs with and without picrotoxin (in D-AP5/CNQX). Both phasic and tonic GABAergic components were present in MSNs recorded from P_{17-25} rats. Bath-applied picrotoxin prevented the phasic component (IPSCs) and abolished the tonic signaling, which was revealed by a significant shift in ΔIhold and a decrease of the synaptic noise. (**b**) Picrotoxin (50μM) inhibits only the phasic GABAAR transmission in P_{7-10} rats (**b1**) Raw traces illustrate that in P_{7-10} rats the holding current (indicated by dashed line) and synaptic noise were not significantly affected by the application of picrotoxin, denoting an absence of tonic GABAergic signaling at this stage of development. (**b2**) All point histograms are build from 50 sec recordings with or without picrotoxin (in D-AP5/CNQX). (**b3**) Frequency and amplitude of sIPSCs with or without picrotoxin (in D-AP5/CNQX). Then in MSNs from P_{7-10} rats, it exists a phasic but not a tonic GABA component. (**c**) The reversal potential of $GABA_A$-mediated current (E_{GABA}) is -35mV in MSNs from P_{7-10} rats. (**c1**) Cell-attached recordings of unitary NMDA currents at various holding potentials (left traces) and i_{NMDA}-V relationship. RMP is determined at the value indicated by the

arrow on the graph. E_{GABA} = DF_{GABA} + RMP. (**c2**) Cell-attached recordings of unitary $GABA_A$ currents at various holding potentials (left traces) and i_{GABA}-V relationship. The driving force of chloride ions (DF_{GABA}) through $GABA_A$Rs is determined at the value indicated by the arrow. To extract E_{GABA}, we used the following relationship E_{GABA} = DF_{GABA} – RMP. (Data for P_{17-25} rat MSNs are adapted from Paillé et al., 2013).

Error bars represent the SD. *: p<0.05; ns: not significant.

Figure 4. Promoting tonic GABAergic signaling at P_{7-10} induces anti-Hebbian t-LTD

(**a**) Etomidate (3 μM) promotes tonic $GABA_A$R-current without affecting the phasic component in P_{7-10} rats. (**a1**) Sample traces illustrate that etomidate induces an increase of I_{hold} (dashed line) accounting for a tonic GABAergic signaling. (**a2**) All point histograms build from 50 sec recordings with etomidate (in D-AP5/CNQX) illustrate that etomidate promotes tonic $GABA_A$R-current. (**a3**) Etomidate promotes tonic (left panel) without affecting phasic (right panels) $GABA_A$R-current. (**b**) Averaged time-courses of tLTD induced by 100 post-pre pairings with etomidate in P_{7-10} rats. (**c**) Averaged time-courses of tLTD induced by 100 pre-post pairings with etomidate in P_{7-10} rats. (**d**) Nipecotic acid (500μM) promotes tonic $GABA_A$R-current without affecting the phasic component in P_{7-10} rats. (**d1**) Sample traces illustrate that nipecotic acid induces an increase of I_{hold} (dashed line) accounting for a tonic GABAergic signaling. (**d2**) All point histograms build from 50 sec recordings with nipecotic acid (in D-AP5/CNQX) illustrate that nipecotic acid promotes tonic $GABA_A$R-current. (**d3**) Nipecotic acid promotes tonic (left panel) without affecting phasic (right panels) $GABA_A$R-current. (**e**) Averaged time-courses of tLTD induced by 100 post-pre pairings with nipecotic acid in P_{7-10} rats. (**f**) Averaged time-courses of tLTD induced by 100 pre-post pairings with nipecotic acid in P_{7-10} rats.

Error bars represent the SD. *: p<0.05; ; **: p<0.01; ***: p<0.001.

Figure 5. Tonic and phasic GABAergic signalling differentially shape anti-Hebbian STDP at P_{17-25}

(**a**) Low concentration of gabazine (200nM) specifically precluded the phasic without affecting the tonic $GABA_AR$-current in P_{17-25} rats. Sample traces (**a1**) and all point histograms (build from 50 sec recordings) (**a2**) illustrate that I_{hold} was not affected by gabazine (200nM); gabazine at 10µM inhibits both phasic and tonic components. (**a3**) Gabazine at 200nM inhibited phasic (right panels) without affecting tonic (left panels) $GABA_AR$-current, whereas at 10µM gabazine inhibited both phasic and tonic GABAergic signaling. (**b**) Averaged time-courses of tLTP induced by 100 post-pre pairings with gabazine (200nM) in P_{17-25} rats. (**c**) Averaged time-course of the lack of plasticity observed with 100 pre-post pairings with gabazine (200nM) in P_{17-25} rats. (**d**) L655,708 inhibited the tonic GABAergic signaling without affecting the phasic component in P_{17-25} rats. (**d1**) Sample traces illustrate that I_{hold} (dashed line) was affected by L655,708 (10µM). Accordingly, picrotoxin applied after L655,708 did not affect I_{hold}. (**d2**) All point histograms build from 50 sec recordings with L655,708 and with L655,708/picrotoxin (in D-AP5/CNQX) illustrate that L655,708 inhibited the tonic component. (**d3**) L655,708 (10µM) inhibited tonic (left panel) without affecting phasic (right panels) $GABA_AR$-current. (**e**) Averaged time-courses of tLTD induced by 100 post-pre pairings with L655,708 in P_{17-25} rats. (**f**) Averaged time-course of the lack of plasticity observed with 100 pre-post pairings with L655,708 in P_{17-25} rats.

Error bars represent the SD. *: $p<0.05$; ns: not significant.

Figure 6. Schematic representation of the control operated by tonic GABAergic component on STDP expression and polarity in the striatum

The tonic GABAergic component in striatum arises from P_{14} and would switch the Hebbian tLTD occurring at earlier developmental stages to a bidirectional anti-Hebbian STDP at later stages. Therefore, selective inhibition of the tonic GABAergic component in P_{17-25} rats shifts the bidirectional anti-Hebbian STDP into Hebbian tLTD. Conversely, promoting tonic GABAergic

component in $P_{7\text{-}10}$ rats partially restores the anti-Hebbian STDP observed at later developmental stages.

Figure 1

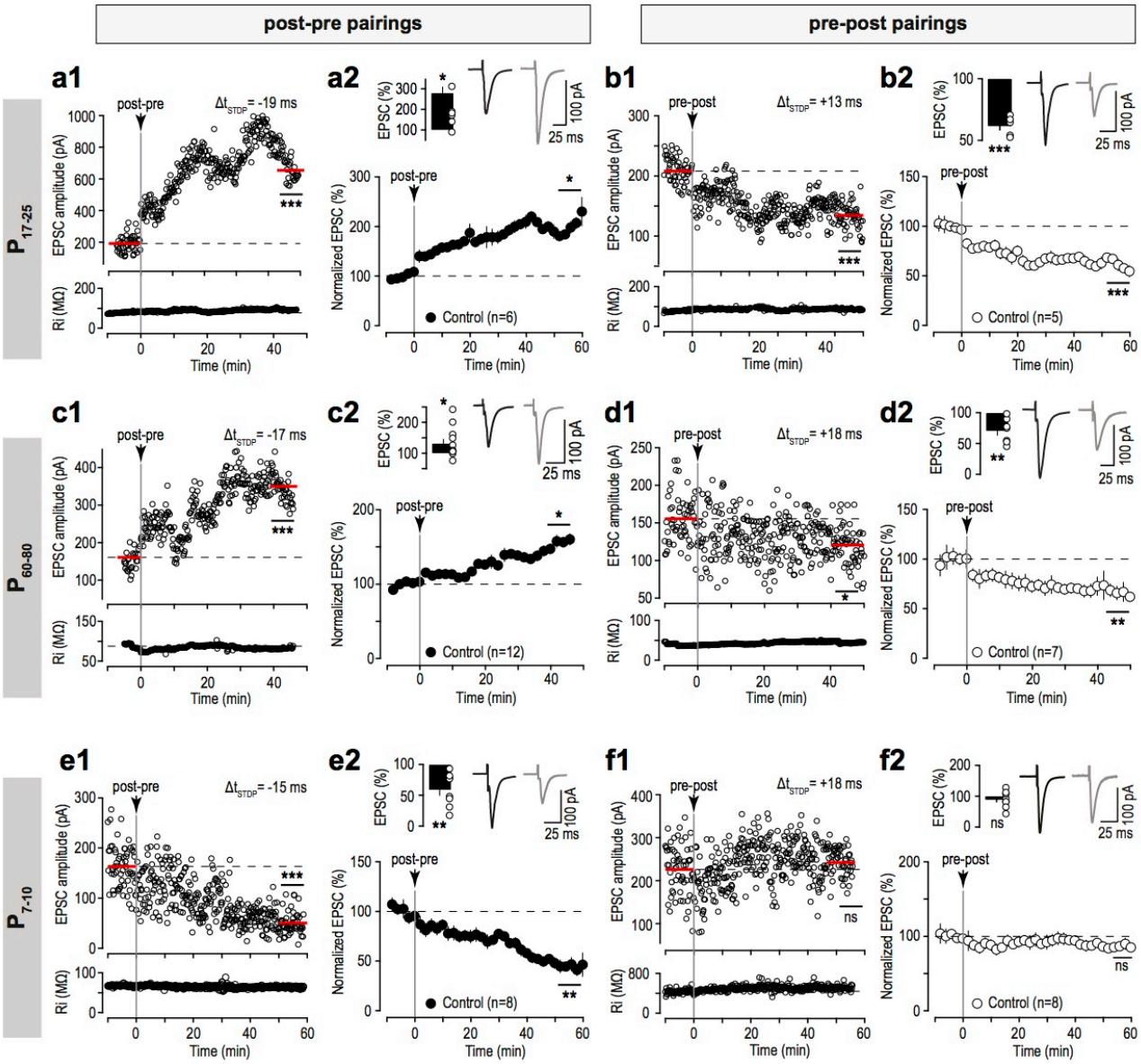
post-pre pairings
pre-post pairings
a1
a2
b1
b2
c1
c2
d1
d2
e1
e2
f1
f2
P17-25
P60-80
P7-10
post-pre
pre-post
Δt_STDP = -19 ms
Δt_STDP = +13 ms
Δt_STDP = -17 ms
Δt_STDP = +18 ms
Δt_STDP = -15 ms
Δt_STDP = +18 ms
EPSC amplitude (pA)
Ri (MΩ)
Normalized EPSC (%)
EPSC (%)
Time (min)
100 pA
25 ms
Control (n=6)
Control (n=5)
Control (n=12)
Control (n=7)
Control (n=8)
Control (n=8)
ns

Figure 2

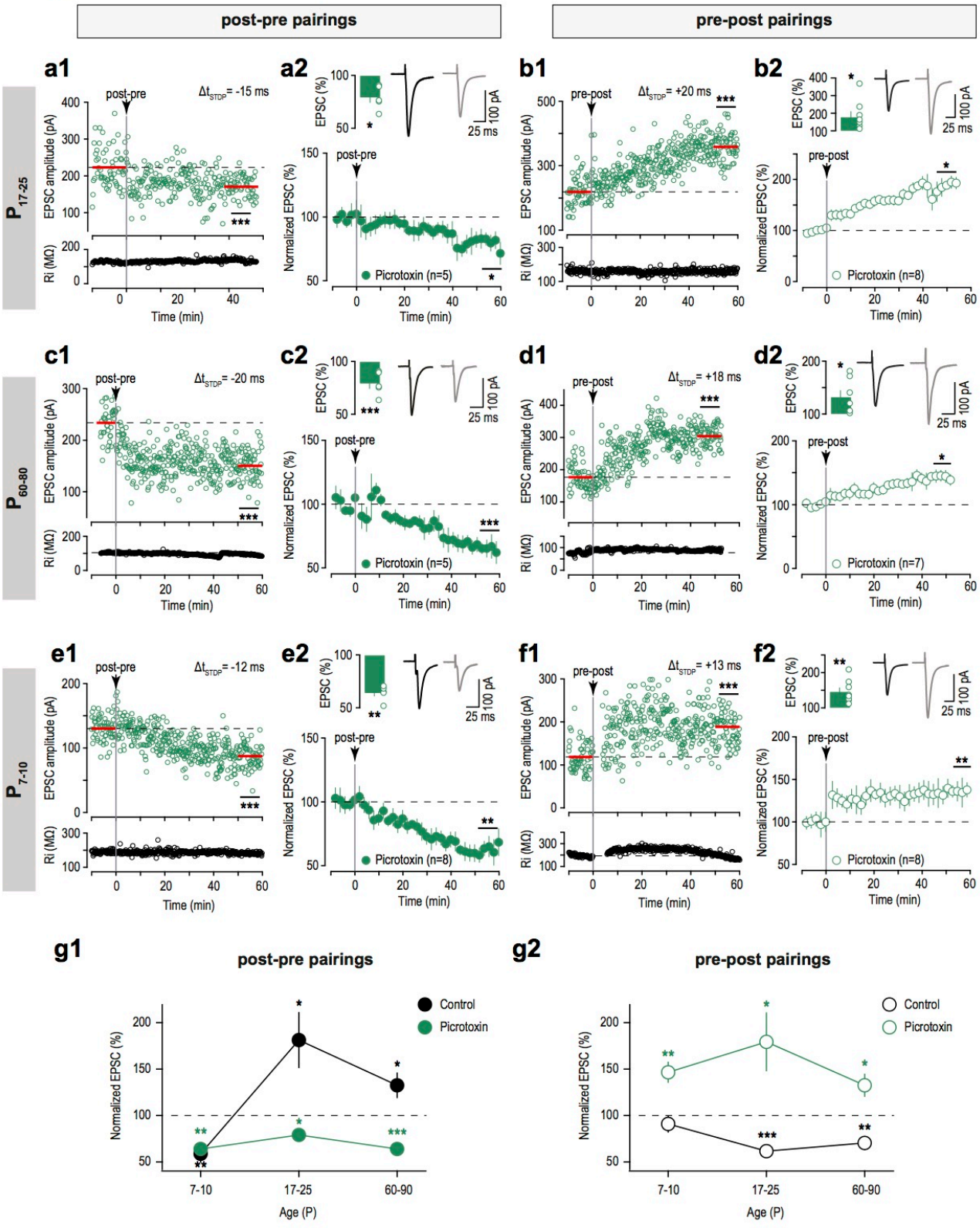
post-pre pairings
pre-post pairings
a1
a2
b1
b2
c1
c2
d1
d2
e1
e2
f1
f2
P17-25
P60-80
P7-10
post-pre
pre-post
Δt_STDP = -15 ms
Δt_STDP = +20 ms
Δt_STDP = -20 ms
Δt_STDP = +18 ms
Δt_STDP = -12 ms
Δt_STDP = +13 ms
EPSC amplitude (pA)
Ri (MΩ)
Normalized EPSC (%)
EPSC (%)
Time (min)
100 pA
25 ms
Picrotoxin (n=5)
Picrotoxin (n=8)
Picrotoxin (n=7)
g1
g2
post-pre pairings
pre-post pairings
Control
Picrotoxin
Normalized EPSC (%)
Age (P)
7-10
17-25
60-90

Figure 3

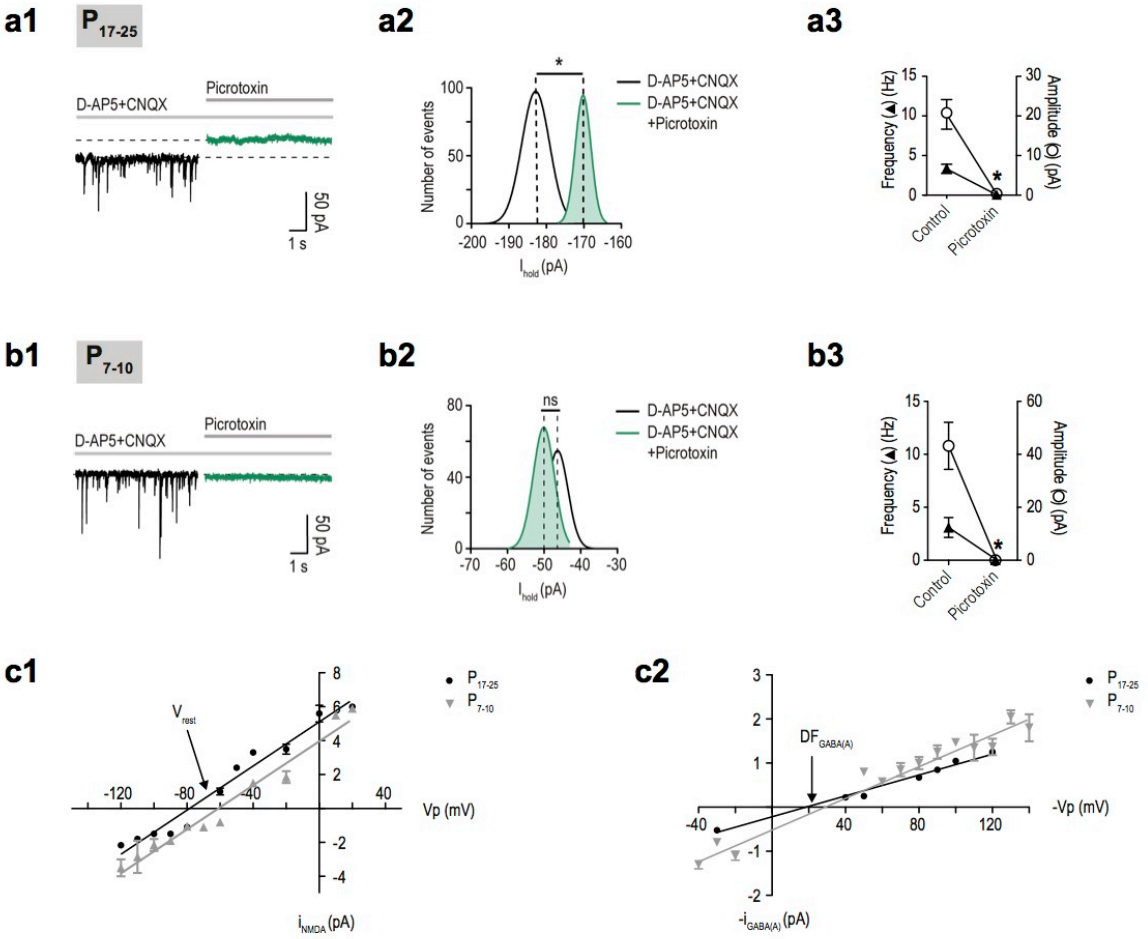
a1
P17-25
D-AP5+CNQX
Picrotoxin
50 pA
1 s
a2
Number of events
D-AP5+CNQX
D-AP5+CNQX
+Picrotoxin
Ihold (pA)
a3
Frequency (▲) (Hz)
Amplitude (○) (pA)
Control
Picrotoxin
b1
P7-10
b2
ns
b3
c1
Vrest
P17-25
P7-10
Vp (mV)
iNMDA (pA)
c2
DFGABA(A)
-Vp (mV)
-iGABA(A) (pA)

Figure 4

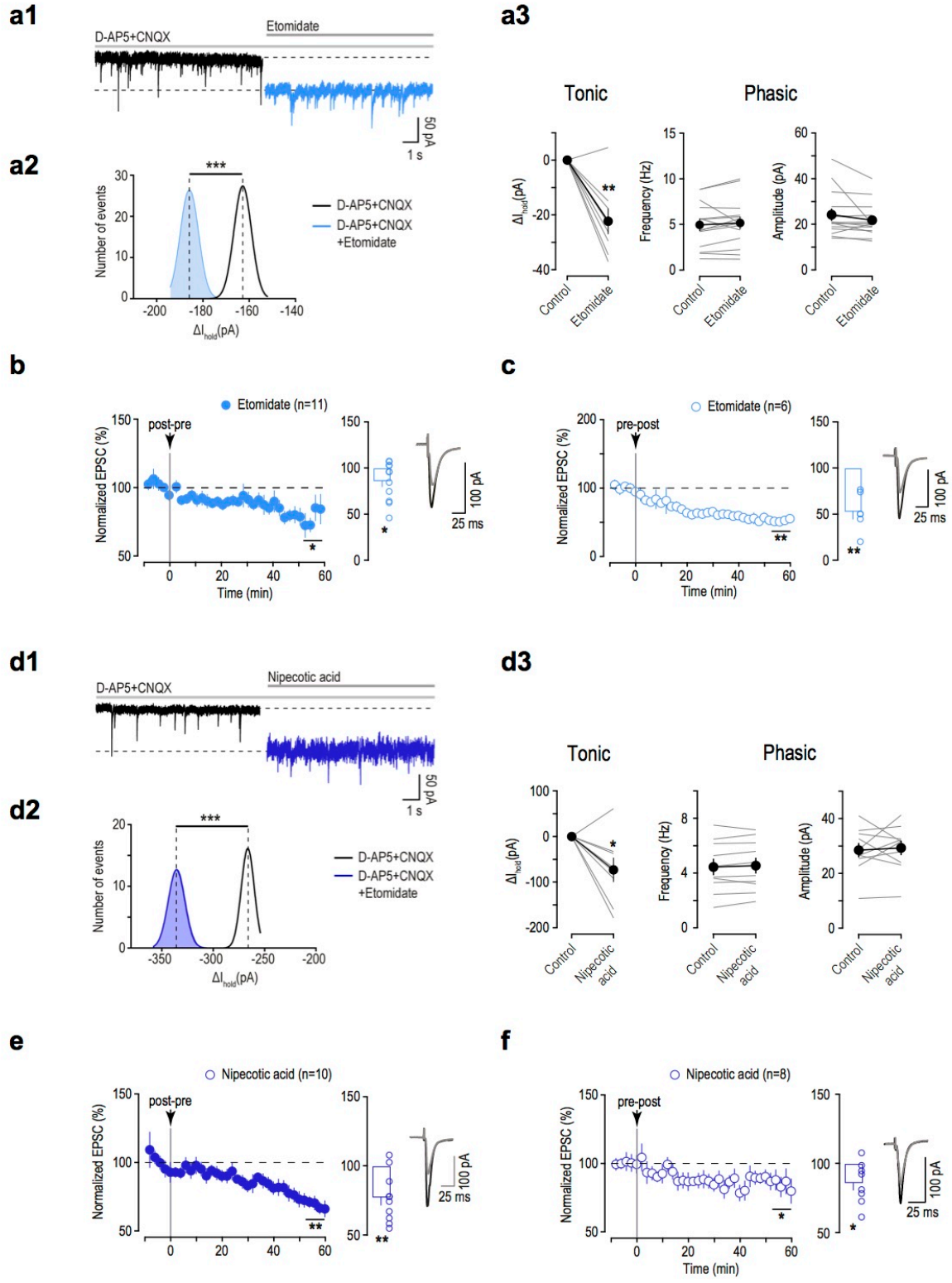
a1
D-AP5+CNQX
Etomidate
50 pA
1 s
a2
***
Number of events
D-AP5+CNQX
D-AP5+CNQX
+Etomidate
ΔI_hold(pA)
a3
Tonic
Phasic
ΔI_hold(pA)
Frequency (Hz)
Amplitude (pA)
Control
Etomidate
b
Etomidate (n=11)
post-pre
Normalized EPSC (%)
Time (min)
100 pA
25 ms
c
Etomidate (n=6)
pre-post
d1
D-AP5+CNQX
Nipecotic acid
d2
d3
Nipecotic acid
e
Nipecotic acid (n=10)
f
Nipecotic acid (n=8)

Figure 5

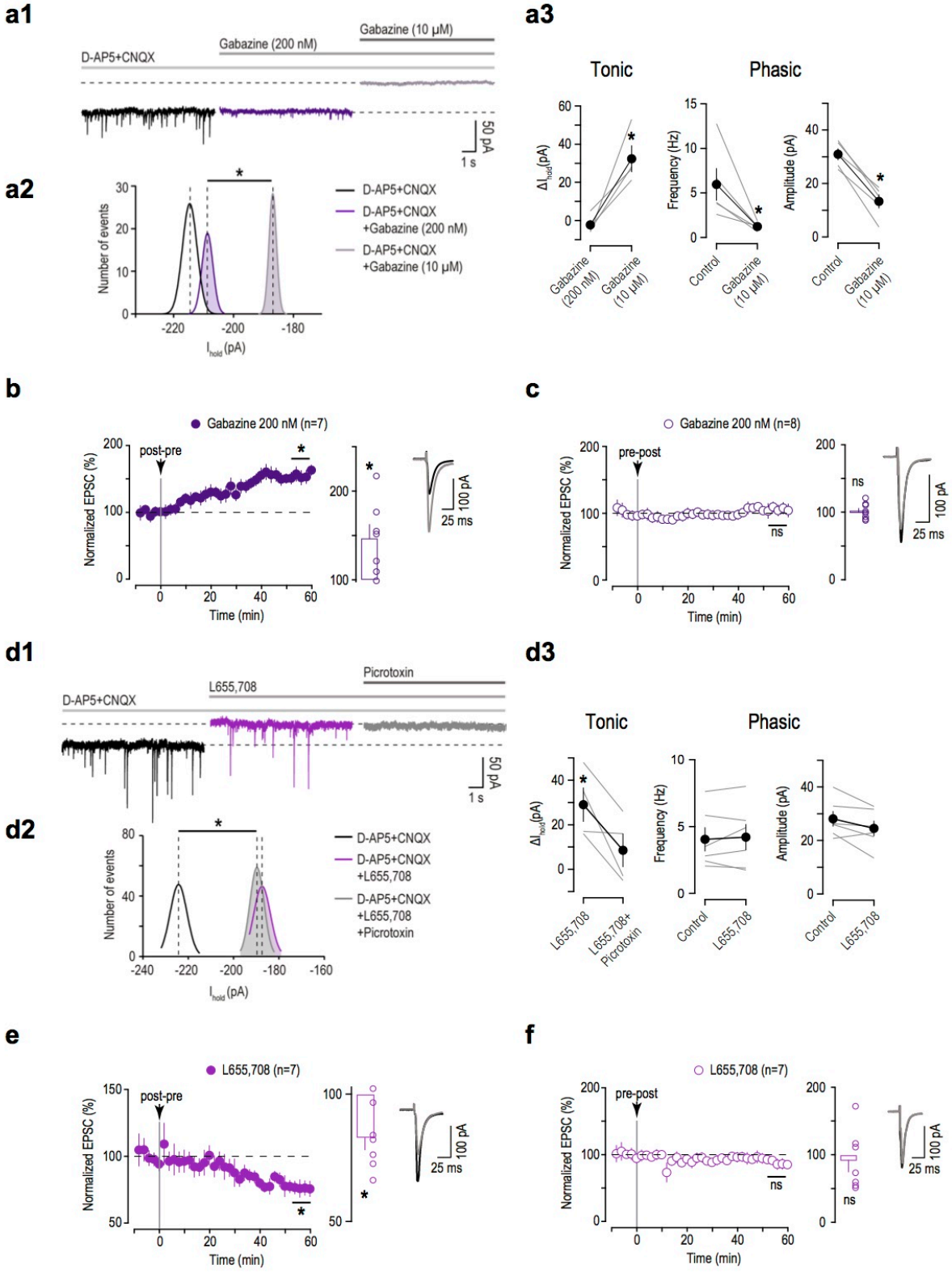
a1
Gabazine (10 µM)
Gabazine (200 nM)
D-AP5+CNQX
50 pA
1 s
a2
Number of events
D-AP5+CNQX
D-AP5+CNQX +Gabazine (200 nM)
D-AP5+CNQX +Gabazine (10 µM)
I_{hold} (pA)
a3
Tonic
Phasic
ΔI_{hold} (pA)
Frequency (Hz)
Amplitude (pA)
Gabazine (200 nM)
Gabazine (10 µM)
Control
b
Gabazine 200 nM (n=7)
Normalized EPSC (%)
post-pre
Time (min)
100 pA
25 ms
c
Gabazine 200 nM (n=8)
pre-post
ns
d1
Picrotoxin
L655,708
D-AP5+CNQX
d2
D-AP5+CNQX +L655,708
D-AP5+CNQX +L655,708 +Picrotoxin
d3
L655,708
L655,708+ Picrotoxin
e
L655,708 (n=7)
f
L655,708 (n=7)

Figure 6

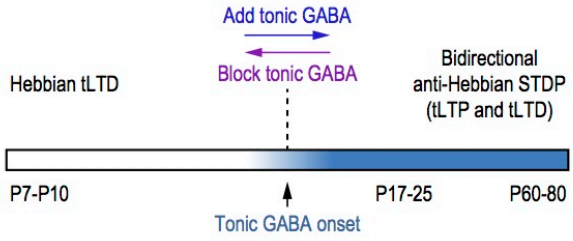
Add tonic GABA
Block tonic GABA
Hebbian tLTD
Bidirectional
anti-Hebbian STDP
(tLTP and tLTD)
P7-P10
P17-25
P60-80
Tonic GABA onset

RESULTS

Article II

Astrocytes gate Hebbian synaptic plasticity in the striatum

Valtcheva S and Venance L

(Nat Commun, in revision)

Astrocytes gate Hebbian synaptic plasticity in the striatum

Silvana VALTCHEVA[1,2] and Laurent VENANCE[1,2,*]

[1]Dynamics and Pathophysiology of Neuronal Networks Team, Center for Interdisciplinary Research in Biology, College de France, CNRS UMR7241/INSERM U1050, MemoLife Labex Paris, France

[2]Pierre et Marie Curie University, ED 158, Paris, France

[*]Correspondence: laurent.venance@college-de-france.fr

Conflict of interest: the authors have no competing financial interest to declare.

Running title: Astrocytes gate Hebbian plasticity

Abstract

Astrocytes, via excitatory amino-acid transporter type-2 (EAAT2), are the major sink for released glutamate and contribute to set the strength and timing of synaptic inputs. The conditions required for the emergence of Hebbian plasticity from distributed neural activity remain elusive. We investigated the role of EAAT2 in the expression of a major physiologically relevant form of Hebbian learning, spike-timing-dependent plasticity (STDP). We found that a transient blockade of EAAT2 disrupted the temporal contingency required for Hebbian synaptic plasticity. Indeed, STDP was replaced by aberrant non-timing-dependent plasticity occurring for uncorrelated events. Conversely, EAAT2 overexpression impaired the detection of correlated activity and precluded STDP expression. Our findings demonstrate that EAAT2 sets the appropriate glutamate dynamics for the optimal temporal contingency between pre- and postsynaptic activity required for STDP emergence, and highlight the role of astrocytes as gatekeepers for Hebbian synaptic plasticity.

Introduction

Fast excitatory transmission at central synapses is dependent on glutamate dynamics. Astrocytes play a major role in the precise regulation of glutamate concentration in the extracellular fluid, via their high-affinity glutamate transporters (excitatory amino-acid transporters, EAATs), which determine the extent of receptor stimulation by terminating the neurotransmitter signal[1,2,3,4]. Among the five subtypes of EAATs, the largest proportion of glutamate uptake (95%) in the adult forebrain is mediated by the astrocytic EAAT2[5,6,7,8]. Specific deletion of EAAT2 in astrocytes (which express 90% of total EAAT2) revealed that astrocytic EAAT2 contributes to most of the glutamate uptake and that specific EAAT2 deletion in neurons has to this day unidentified consequences[8,9]. Decreased levels of EAAT2 associated with increased ambient glutamate have been observed in neurodegenerative and psychiatric diseases[7,10,11] and in chronic exposure to drugs of abuse[12].

EAAT2 is of crucial importance in the maintenance of low glutamate concentrations and for ensuring a high signal-to-noise ratio in synaptic and extrasynaptic transmission[4,13]. Astrocytic glutamate uptake via EAAT2 affects both the fast component of the synaptic glutamate transient and slower components by limiting the spill-out to extrasynaptic receptors and the spillover to neighboring synapses[13,14,15]. Although, astrocytic glutamate transporters are not overwhelmed upon physiological activity[16], synaptic isolation is never reached[17]. Thus, fast removal of glutamate by astrocytes contributes to set the strength and timing of synaptic inputs by controlling peri- and extrasynaptic receptor activation during neuronal activity[18].

According to Hebbian theory, neural networks refine their connectivity by patterned firing of action potentials in pre- and postsynaptic neurons[19]. Spike-timing-dependent plasticity (STDP) is a synaptic Hebbian learning rule that has been the focus of considerable attention in experimental[19,20] and computational[21,22] neuroscience. STDP relies on the precise order and the millisecond timing of the paired activities on either side of the synapse[19,20]. However, the conditions required for the emergence of STDP from distributed neural activity remain unclear.

Temporal coding via STDP may be essential for the role of the striatum in learning of motor sequences in which sensory and motor events are associated in a precise time sequence. Corticostriatal long-term plasticity provides a fundamental mechanism for the function of the basal ganglia in procedural learning[23,24]. MSNs act as detectors of distributed patterns of cortical and thalamic activity. Thus, the physiological or pathological regulation of EAAT2 expression should play a major role in information processing in the basal ganglia, which is based on a precise time-coding process. EAAT2 is highly expressed in the striatum[7] and specific knockout of astrocytic EAAT2 in the striatum leads to pathological repetitive behaviors due to corticostriatal dysfunction[25]. We have previously shown, by dual astrocyte-neuron recordings, that EAAT2

controls corticostriatal transmission and short-term plasticity, and increases the strength of cortical input filtering by the striatum[26]. Here, we questioned the role of astrocytes (via EAAT2) in the control of Hebbian plasticity expression, and, more specifically, corticostriatal STDP.

RESULTS

Bidirectional STDP within a narrow temporal window

We investigated the effect of EAAT2 on STDP, using whole-cell recordings from striatal medium-sized spiny neurons (MSNs) in horizontal corticostriatal brain slices from juvenile rats as previously described[27] (Fig. 1a). Baseline excitatory postsynaptic currents (EPSCs) were recorded for 10 minutes in voltage-clamp mode and then recordings were switched to current-clamp mode to pair a single excitatory postsynaptic potential (EPSP) induced by presynaptic stimulation with a single postsynaptic spike induced by a brief depolarization of the MSN (Fig. 1b). The STDP protocol involved pairing pre- and postsynaptic stimulation with a certain fixed timing interval, Δt_{STDP} ($\Delta t_{STDP}<0$ indicating that postsynaptic stimulation preceded presynaptic stimulation and $\Delta t_{STDP}>0$ indicating that presynaptic stimulation preceded postsynaptic stimulation), repeated 100 times at 1 Hz. After the STDP protocol, recordings were obtained in voltage-clamp mode, and EPSCs were monitored for one hour.

Post- and presynaptic activities paired within a narrow time window ($-30<\Delta t_{STDP}<+30$ ms) induced bidirectional STDP in MSNs. An example of the timing-dependent long-term potentiation (t-LTP) induced by post-pre pairings ($\Delta t_{STDP}=-12$ ms) is illustrated in Figure 1c; the mean baseline EPSC amplitude was 155±6 pA before pairings, and increased by 360% to 711±22 pA one hour after pairings. Ri remained stable over this period. Conversely, pre-post pairings ($\Delta t_{STDP}=+13$ ms) induced timing-dependent long-term depression (t-LTD), as shown in the example in Figure 1d: the mean baseline EPSC amplitude, 474±10 pA, had decreased by 66%, to 318±7pA, one hour after pairing. To summarize, post-pre pairings ($-30<\Delta t_{STDP}<0$ms) induced t-LTP (mean EPSC amplitude recorded 60 min after protocol induction: 207±35% of baseline, p=0.0116, n=11; 9 of 11 cells displayed LTP), whereas pre-post pairings ($0<\Delta t_{STDP}<+30$ ms) induced t-LTD (61±5%, p=0.0001, n=7; 7/7 cells displayed LTD) (Fig. 1e,f,i), resulting in anti-Hebbian STDP. We have shown that GABA controls the polarity of corticostriatal STDP[28] and that Hebbian[29,30] or anti-Hebbian[27,31,32] STDP were observed, depending on whether $GABA_A$ receptor antagonists are used. The pairings for $\Delta t_{STDP}\sim-30$ ms and $\Delta t_{STDP}\sim+30$ ms did not induce plasticity (97±5%, p=0.6205, n=4 and 105±5%, p=0.4670, n=3). Less correlated pairings ($\Delta t_{STDP}<-30$ ms and $\Delta t_{STDP}>+30$ ms) failed to induce long-term synaptic efficacy changes. Indeed, for $-250<\Delta t_{STDP}<-100$ ms and $+100<\Delta t_{STDP}<+250$ ms, we observed no plasticity (98±6%, p=0.7931, n=7 and 91±4%, p=0.1067, n=5, respectively; Fig. 1g,i). Uncorrelated pairings up to ±500 ms, the maximum interval between the postsynaptic action potential and the presynaptic stimulation paired at 1Hz, also failed to induce long-term synaptic efficacy changes (103±5%, p=0.4577, n=7; Fig. 1h,i). Thus, post- and

presynaptic activities paired only within a narrow temporal window, spanning 60 ms (-30<Δt_{STDP}<+30 ms), efficiently induce bidirectional STDP (Fig. 1i).

EAAT2 gates the polarity and temporal window of STDP

Investigation of the role of astroctytic glutamate uptake in corticostriatal STDP required the transient blocking of EAAT2 during the STDP pairings (see Methods). We considered a pharmacological approach to be most appropriate for this purpose. We previously showed, by dual astroctyte-neuron recordings, that dihydrokainate (DHK; 300 μM), a selective non-transportable inhibitor of EAAT2[33], efficiently blocked most of the transporter-mediated currents in striatal astrocytes upon corticostriatal stimulation[26]. Brief EAAT2 blockade with DHK (300 μM) for 5 minutes resulted in a marked depolarization of the recorded MSN in current-clamp mode in the absence of cortical stimulation (22±2 mV, p<0.0001, n=14) (Fig. 2a). This effect was fully reversible after 15 minutes of DHK washout. These findings suggest that the slice contained sufficiently large amounts of glutamate to induce postsynaptic depolarization during EAAT2 blockade. DHK-induced depolarization involved AMPAR and type-I/II mGluR activation (Fig. 2a). Indeed, during the concomitant inhibition of AMPAR with CNQX (20 μM) and of type-I/II mGluR with MCPG (500 μM) no significant depolarization was observed (1±0.2 mV, p=0.5872, n=7). NMDAR inhibition with D-AP5 (50 μM) did not prevent DHK-induced depolarization (one-way repeated-measures ANOVA: p<0.0001; post hoc Bonferroni-corrected pairwise comparisons: DHK-D-AP5: p>0.05, DHK–CNQX: p<0.001, DHK-D-AP5+CNQX+MCPG: p<0.001) (Fig. 2a).

We then ensured that brief (5 minutes) EAAT2 blockade induced no long-term change in synaptic efficacy. A stable baseline was established over a period of 10 minutes. We then applied DHK for 5 minutes without STDP pairing. As exemplified in Figure 2b and 2c, we observed a transient decrease in EPSC amplitude (65±9%, p=0.0105, n=6) due to AMPAR desensitization, as previously reported[26], and an inward shift of $I_{holding}$ (-199±41 pA, p=0.0022) (Ri was not significantly affected, p=0.8182) (Fig.2c). These effects were fully reversed 15 minutes after DHK removal (93±9%, p=0.4749 and 11±16 pA, p=0.1797, respectively; Fig. 2c). Thus, transient EAAT2 blockade with DHK was compatible with the estimation of long-term changes in synaptic efficacy.

For transient EAAT2 blockade during STDP pairings, we observed a profound change in STDP, as synaptic plasticity extended over the entire temporal window: LTD for a narrow Δt_{STDP} (-70<Δt_{STDP}<+70 ms) and LTP for a broader Δt_{STDP} (-250<Δt_{STDP}<-100 ms, +100<Δt_{STDP}<+250 ms and Δt_{STDP}=±500 ms) (Fig. 2). An example of LTD induced by post-pre pairings (Δt_{STDP}=+38 ms) under transient EAAT2 blockade with DHK (300 μM) is shown in Figure 2d; the mean baseline

EPSC amplitude was 200±5 pA before pairings and had decreased by 38%, to 125±3 pA, one hour after pairings. Both post-pre and pre-post pairings induced LTD in a Δt_{STDP} spanning 140 ms (-70<Δt_{STDP}<+70 ms) (66±6%, p=0.0005, n=9; 8/9 cells displayed LTD for -70<Δt_{STDP}<0 ms and 63±5%, p=0.0008, n=6; 6/6 cells displayed LTD for 0<Δt_{STDP}<+70 ms; Fig. 2e and f). LTD was of similar amplitude for post-pre and pre-post pairings (p=0.7924). For more uncorrelated pairings (Δt_{STDP}<-70 ms and Δt_{STDP}>+70 ms), LTP extended over the entire temporal window until ±500 ms. Indeed, as exemplified in Figure 2g, we observed LTP for post-pairing with a Δt_{STDP}=-175 ms under transient EAAT2 blockade (mean baseline EPSC amplitude of 123±3pA before pairings, increasing by 66%, to 203±3 pA, one hour after pairings). In summary, we observed LTP for -250<Δt_{STDP}<-70 ms and +70<Δt_{STDP}<+250 ms (136±8%, p=0.0049, n=7; 6/7 cells displayed LTP and 144±14%, p=0.0148, n=8; 6/8 cells displayed LTP, respectively; Fig. 2h and j). We then assessed plasticity induction for the most uncorrelated Δt_{STDP} that could be achieved with a pairing frequency of 1 Hz (*i.e.* Δt_{STDP}=±500 ms), and we observed LTP (136±9%, p=0.0085, n=7; 6/7 cells displayed LTP; Figs. 2i and j). LTP was of similar amplitude for post-pre and pre-post pairings (p=0.6325). We previously showed that bidirectional STDP was equally frequent in MSNs involved in the direct and indirect pathways[28]. Here, the occurrence of plasticity under EAAT2 blockade indicates a lack of segregation between the two trans-striatal pathways.

To confirm these findings, we then used another EAAT2 inhibitor, WAY-213,613, structurally distinct from DHK. DHK and WAY-213,613 display different mechanisms of action onto EAAT2: DHK is a substrate inhibitor (non-transported)[33] whereas WAY-213,613 is a non-substrate inhibitor[34]. We ensured that transient EAAT2 blockade with WAY-213,613 was reversible and, thus, compatible with the estimation of long-term changes in synaptic efficacy. The bath application of WAY-213,613 (50 µM) for 5 minutes induced a transient, non-significant decrease in EPSC amplitude (with no change in Ri). This effect was fully reversible within 5 minutes (n=6; Supplementary Fig. 1a-c). For transient EAAT2 blockade with WAY-213,613 (50-100 µM) during STDP pairings (for -70<Δt_{STDP}<+70 ms and for Δt_{STDP}=±200 ms), we observed a profound modification of STDP (similar to that observed with DHK): LTD or no plasticity for a narrow Δt_{STDP} (-70<Δt_{STDP}<+70 ms) and LTP for a broader Δt_{STDP} (Δt_{STDP}=±200 ms) (Supplementary Fig. 1d-i). First, for -70<Δt_{STDP}<+70 ms with WAY-213,613 (50 µM), no plasticity was observed, as exemplified in the Supplementary Fig. 1d. Both post-pre and pre-post pairings (-70<Δt_{STDP}<+70 ms) failed to induce significant plasticity (104±5%, p=0.4600, n=5; 1/5 cells displayed LTD; Supplementary Fig. 1e). With 100 µM WAY-213,613, the incidence of LTD was higher, as exemplified in the Supplementary Fig. 1f, even though, in average no significant LTD was induced for pairings at -70<Δt_{STDP}<+70 ms (80±11%, p=0.1061, n=8; 5/8 cells showed LTD; Supplementary Fig. 1g). LTP was observed for uncorrelated pairings (Δt_{STDP}=±200 ms). An

example of LTP induced by post-pre pairings (Δt_{STDP}=-200 ms) during the transient blockade of EAAT2 with WAY-213,613 (50 μM) is shown in the Supplementary Fig. 1h. In summary, we observed LTP for Δt_{STDP}=±200 ms (165±21%, p=0.0150, n=8; 7/8 cells displayed LTP; Supplementary Fig. 1i).

Thus, during the transient blockade of EAAT2 with either DHK or WAY-213,613, any paired activity on either side of the synapse, regardless of Δt_{STDP}, was able to modify synaptic efficacy in the long term (Fig. 2j). This finding contrasts strongly with the STDP observed in control conditions, in which EAAT2 activity was unaffected. In conclusion, the correct functioning of EAAT2 allows the expression of a bidirectional order-dependent STDP during a restricted time window.

Postsynaptic DHK-induced depolarization cannot account for the plasticity observed under EAAT2 blockade

We investigated whether the observed plasticity was due to the transient depolarization induced by EAAT2 blockade. For this purpose, we maintained the recorded MSNs at -80 mV by intracellular current injection (close to MSN resting membrane potential) during STDP pairings, to prevent DHK-induced depolarization. In these conditions, pairings for -70<Δt_{STDP}<+70 ms and Δt_{STDP}=±200 ms induced LTD (77±7%, p=0.0233, n=5; 5/5 cells displayed LTD; Supplementary Fig. 2a) and LTP (186±28%, p=0.0382, n=5; 5/5 cells displayed LTP; Supplementary Fig. 2b), respectively. These results are similar to those obtained for the depolarization of DHK-treated neurons (Fig. 2). Thus, the depolarization of the postsynaptic MSN induced by EAAT2 blockade does not account for the observed plasticity.

We then investigated whether postsynaptic depolarization alone (without DHK) during STDP pairings mimicked the effects of transient EAAT2 blockade. When MSNs were held at -50 mV in the absence of DHK during the STDP protocol, pairings for -70<Δt_{STDP}<+70 ms and for Δt_{STDP}=±200 ms induced exclusively LTD (65±7%, p=0.0029, n=7, 7/7 cells displayed LTD and 62±6%, p=0.0011, n=7, 7/7 cells displayed LTD, respectively; Supplementary Figure 1c-d). This result is in accordance with LTD induced with sustained depolarization in visual cortex[35], and with hippocampal depolarization-induced LTD[36]. Thus, postsynaptic depolarization in the absence of DHK is not sufficient to reproduce the effects of transient EAAT2 blockade. Glutamate spillover is, therefore, likely to contribute to the observed plasticity.

The recruitment of GABAergic microcircuits under transient EAAT2 blockade induces LTD

We then investigated the receptors involved in the synaptic plasticity induced under transient EAAT2 blockade. We first investigated the receptors involved in the LTD observed for pairings at -70<Δt_{STDP}<+70 ms. In control conditions, corticostriatal t-LTD is mediated by CB_1R[16,17,18]. We, therefore, first determined whether the LTD observed under EAAT2 blockade was CB_1R-mediated. Following the bath application of a CB_1R-specific antagonist (AM251; 3 μM), LTD was still observed under EAAT2 blockade (69±8%, p=0.0019, n=11; 10/11 cells showed LTD; Supplementary Fig. 3a), indicating that LTD was not CB_1R-mediated. mGluRs and NMDARs located outside the synapse can be activated by glutamate spillover promoted by EAAT2 blockade[15,37,38,39,40]. We, therefore, investigated the involvement of mGluRs and NMDARs in LTD under EAAT2 blockade for pairings at -70<Δt_{STDP}<+70 ms. The inhibition of type I/II mGluRs with MCPG (500 μM) or of NMDARs with D-AP5 (50 μM) had no effect on the establishment of LTD (62±9%, p=0.0279, n=4; 4/4 cells displayed LTD and 61±5%, p=0.0003, n=7; 7/7 cells displayed LTD, respectively; Supplementary Fig. 3b). We then examined the involvement of L- and T-type voltage-sensitive calcium channels (VSCCs), which can be activated by DHK-induced depolarization. Under EAAT2 blockade, bath-applied mibefradil (20 μM), a specific antagonist of T-type VSCCs (also blocking L-type VSCCs at concentrations above 18 μM) not only prevented LTD, but also revealed potent LTP (207±13%, p=0.0002, n=7; 7/7 cells displayed LTP; Fig. 3a). This LTP, unmasked by VSCC inhibition, was mediated by NMDARs, because it was prevented by the co-application of mibefradil and D-AP5 (84±8%, p=0.0680, n=8; 1/8 cells displayed LTP; Supplementary Fig. 3c).

Given the involvement of VSCCs in the LTD observed under EAAT2 blockade, we investigated the calcium dependence of LTD at the level of the recorded MSN. To do so, we delivered intracellularly a fast calcium buffer, BAPTA, (i-BAPTA, 10mM) through the patch-clamp pipette in the recorded MSN. Under EAAT2 blockade, i-BAPTA had no effect on LTD (77±9%, p=0.0482, n=7; 5/7 cells displayed LTD at -70<Δt_{STDP}<+70 ms; Fig. 3b). Thus, LTD observed under EAAT2 blockade is not dependent on postsynaptic MSN calcium. These results indicate that network effects are involved in LTD expression. They also suggest that VSCCs involved are located on neurons other than the recorded MSN and are activated during EAAT2 blockade, due to glutamate spillover-induced depolarization.

We then investigated the involvement of inhibitory networks in LTD. DHK-induced depolarization would also affect GABAergic interneurons inhibitory tone[38]. Thus, the observed LTD might arguably arise from an increase in GABA release.

We investigated whether DHK application resulted in an increase in the inhibitory component recorded in MSNs. When MSNs were held at -50 mV, a membrane potential for measuring mainly inhibitory transmission, we observed an outward current of 21±4 pA (n=14) (Fig. 3c). In the presence of DHK, this outward current increased by 81%, reaching 37±6 pA, and was inhibited by a $GABA_AR$ blocker, picrotoxin (50 μM), (PSC after picrotoxin: 12±1 pA; one-way repeated-measures ANOVA: $p<0.002$; post hoc Bonferroni-corrected pairwise comparisons: control–DHK: $p<0.01$, DHK–picrotoxin: $p<0.001$). We tested the activation of GABAergic circuits under EAAT2 blockade directly, by making recordings on both striatal fast-spiking (FS) GABAergic interneurons and MSNs during EAAT2 blockade with DHK (Fig. 3d). In brain slices, both FS cells and MSNs are silent at rest, and DHK application led to marked depolarization in both cell types (FS cells: +29±2 mV, n=5; MSNs: +24±1 mV, n=6; Fig. 3e). Spontaneous firing activity during DHK application was observed only in FS cells (13±7 Hz, n=5) whereas MSNs remained silent (Fig. 3f). Cortical stimulation (of an intensity similar to that used for STDP pairings) evoked action potentials in all recorded FS cells whereas MSNs displayed subthreshold EPSPs (Fig. 3f). Thus, DHK application leads to the recruitment of GABAergic interneurons, resulting in an increase of the inhibitory weight exerted on the recorded MSN. An increase in inhibitory drive may, therefore, promote LTD.

We then bath-applied picrotoxin (50 μM) to investigate the involvement of GABAergic networks in LTD. For pairings at $-70<\Delta t_{STDP}<+70$ ms under EAAT2 blockade, picrotoxin application prevented LTD, instead promoting LTP (202±20%, p=0.0075, n=6; 6/6 cells displayed LTP; Fig. 3c). These findings suggest that LTD was dependent on $GABA_AR$ activation. Thus, an increase in inhibitory transmission, probably due to the recruitment of GABAergic interneurons under DHK treatment, is responsible for LTD. Surprisingly, the prevention of this GABAergic inhibition by picrotoxin did not result in the expected lack of plasticity. Instead, it promoted LTP. We analyzed the involvement of GABAergic circuits in LTD expression further, by inhibiting GABAergic transmission during transient DHK application. Co-application of gabazine (10 μM; with effects readily reversible by washout) and DHK prevented the expression of plasticity (94±3%, p=0.0974, n=5; 1/5 cells displayed LTD; Fig. 3i). Thus, GABAergic transmission during STDP pairings is determinant for LTD induction under transient EAAT2 blockade.

The LTD observed under transient EAAT2 blockade, for pairings at $-70<\Delta t_{STDP}<+70$ ms, is, thus, dependent on the activation of VSCCs, probably located on striatal GABAergic interneurons. The blockade of GABAergic transmission revealed potent LTP, similar to that observed for uncorrelated pairings ($-500<\Delta t_{STDP}<-70$ ms and $+70<\Delta t_{STDP}<+500$ ms). Thus, an impairment of EAAT2 function

leads to LTP over the entire range of Δt_{STDP}, with the exception of a narrow time window (-70<Δt_{STDP}<+70 ms), during which GABAergic microcircuits take over LTP and impose LTD.

LTP under transient EAAT2 blockade is dependent on extrasynaptic GluN2B-containing NMDARs located on the postsynaptic MSN

We then investigated the mechanism underlying the LTP observed under transient EAAT2 blockade, for pairings at -500<Δt_{STDP}<-70 ms and +70<Δt_{STDP}<+500 ms. For both Δt_{STDP}=±200 ms and Δt_{STDP}=±500 ms, LTP was mediated by NMDAR, as it was prevented by D-AP5 (50 μM) (98±7%, *p*=0.8330, *n*=8; 1/8 cells displayed LTP and 95±14%, *p*=0.7306, *n*=4; 1/4 cells displayed LTP, respectively; Fig. 4a). Glutamate spillover induced by EAAT2 blockade has been reported to mediate crosstalk between neighboring neurons via NMDARs[15,40]. We therefore investigated whether the observed LTP was dependent on the recruitment of NMDARs expressed on neighboring cells or solely on the NMDARs located on the postsynaptic MSN subjected to pairings. We used MK801, a use-dependent blocker of NMDARs, which we delivered intracellularly to the postsynaptic MSN used for recording via the patch-clamp pipette (i-MK801; 1 mM). i-MK801 prevented LTP (97±8%, *p*=0.6777, *n*=6; 1/6 cells displayed LTP; Fig. 4b). The NMDARs required for LTP were, therefore, located on the postsynaptic recorded MSN, and not on neighboring cells. We then aimed at identifying further the NMDARs involved in the LTP observed under transient EAAT2 blockade. Glutamate spillover activates high-affinity extrasynaptic NMDARs[14,15,39,40], which are enriched in the GluN2B subunit[41]. We thus explored the involvement of GluN2B-containing NMDARs in LTP with Ro25-6981, a selective non-competitive antagonist of the GluN2B subunit. Ro25-6981 treatment (10 μM) prevented long-term plasticity (93±10%, *p*=0.5320, *n*=6; 1/6 cells displayed LTP) (Fig. 4c), demonstrating the involvement of GluN2B-containing NMDARs in LTP expression under EAAT2 blockade.

The GluN2B subunit is predominantly expressed at extrasynaptic NMDARs but it has also been identified in synaptic NMDARs[41]. We applied memantine (10 μM), a low-affinity uncompetitive NMDAR antagonist that acts as an open-channel blocker with a fast off-rate (see Methods). Memantine preferentially blocks extrasynaptic NMDARs, without affecting synaptic transmission. Indeed, memantine blocks with a greater extend extrasynaptic NMDARs that are activated due to a low but prolonged elevation of glutamate concentration. By contrast, memantine is relatively inefficient to block NMDARs in the presence of higher synaptic concentrations of glutamate over periods of a few milliseconds, and thus does not interfere with synaptic activity[42]. For STDP during EAAT2 blockade, memantine treatment prevented LTP, as no significant plasticity was observed

(99±5%, p=0.8302, n=5; 1/5 cells displayed LTP; Fig. 4d). Extrasynaptic GluN2B-containing NMDARs located on the postsynaptic recorded striatal MSN are thus required for LTP induction under EAAT2 blockade.

We previously showed that corticostriatal t-LTP is dependent on postsynaptic NMDARs[31] and, more precisely, that the balance between GluN2A- and GluN2B-containing NMDARs shapes Δt_{STDP}[43]. We further investigated whether extrasynaptic NMDARs were required for t-LTP expression in control conditions, as observed for as for LTP observed under EAAT2 blockade. For this purpose, we performed STDP experiments with post-pre pairings at $-30<\Delta t_{STDP}<0$ ms (similar to the experiments in Fig. 1c,e), in presence of memantine (10 μM); LTP was still observed (222±44%, p=0.0271, n=8; 7/8 cells displayed LTP; Supplementary Fig. 4). Thus, in control conditions, extrasynaptic NMDARs are not required for t-LTP expression. This finding is consistent with the observation that, compared to t-LTP in control conditions, the LTP induced for uncorrelated pairings under transient EAAT2 blockade involves distinct signaling pathways.

EAAT2 blockade converts STDP into LTP, which does not rely on timing and order of paired activity

Under transient EAAT2 blockade, plasticity was observed even for highly uncorrelated pairings (up to Δt_{STDP}=±500 ms; Fig. 2g). This suggests that the induction of plasticity is not dependent on the timing or order of pre- and postsynaptic activity. Timing, order and paired activity are the cardinal features of STDP[11]. We, therefore, investigated whether the plasticity observed under transient EAAT2 blockade nevertheless followed STDP rules. We designed STDP protocols with each of 100 Δt_{STDP} pairings chosen randomly between -500 and +500 ms from a close-to-uniform distribution (see Methods; Fig. 5). Each of the random pairing protocols (n=8) was applied both to a MSN recorded in control conditions and to a MSN subjected to transient EAAT2 blockade. An example is shown in Figure 5a, with two MSNs (one in control conditions and the other under transient EAAT2 blockade) subjected to the same random pairing template. A single random Δt_{STDP} pattern (taken from the eight different randomly generated Δt_{STDP} patterns) did not trigger plasticity in the MSN in control conditions (the mean baseline EPSC amplitude, 119±3 pA, was not significantly different from the 120±5 pA one hour after pairings), but it did induce LTP in the MSN subjected to transient EAAT2 blockade (the mean baseline EPSC amplitude, 121±4 pA, increased by 152%, to 307±4pA, one hour after pairings). The histogram of the Δt_{STDP} random pairings (n=8) in Figure 5b illustrates that pairings were randomly distributed in a uniform manner. The application of the eight different randomly generated Δt_{STDP} patterns resulted in no significant

plasticity in control conditions (99±5%, p=0.8429, n=8; 2/8 cells displayed LTP; Fig. 5c), whereas these patterns induced LTP under transient EAAT2 blockade (165±22%, p=0.0226, n=8; 7/8 cells displayed LTP; Fig. 5d). Thus, plasticity under transient EAAT2 blockade does not depend on the timing or order of the paired activity on either side of the synapse and does not, therefore, meet the criteria for STDP.

LTP expressed under transient EAAT2 blockade does not require paired activity

The timing and order of pairings are crucial for STDP, but were not critical for the expression of plasticity under EAAT2 blockade. We investigated whether paired activity was required to induce plasticity under EAAT2 blockade, by determining whether unpaired activity consisting in postsynaptic spiking (a single postsynaptic action potential repeated 100 times at 1 Hz) without presynaptic stimulation could trigger long-term plasticity (Fig. 5e). In control conditions, this unpaired activity did not induce plasticity (101±5%, p=0.9074, n=6; 1/6 cells displayed LTP; Fig. 5f). By contrast, under transient EAAT2 blockade, this unpaired activity was sufficient to trigger LTP (156±17%, p=0.0152, n=7; 6/7 cells displayed LTP; Fig. 5g). This LTP was prevented by D-AP5 (50 μM) and was therefore NMDAR-mediated (96±10%, p=0.6693, n=6; 1/6 cells displayed LTP; Fig. 5g).

Finally, we investigated whether postsynaptic suprathreshold activity was required to induce plasticity under transient EAAT2 blockade. To do so, we induced subthreshold depolarization (repeated 100 times at 1 Hz without cortical stimulation) in the recorded MSN (Supplementary Fig. 5a). This subthreshold unpaired postsynaptic stimulation was not sufficient to trigger significant plasticity when the average of all experiments performed in these conditions was considered: 118±10% (p=0.1213, n=6; Supplementary Fig. 5b). However, four of the six recorded MSNs displayed significant LTP (see scatter plot in Supplementary Fig. 5b). The postsynaptic spike therefore seems to be required for the induction of potent NMDAR-mediated LTP under transient EAAT2 blockade.

Correct functioning of EAAT2 is, therefore, required for STDP expression. A cardinal feature for STDP is that it relies on the precise time-correlation between the activities on either side of the synapse. Plasticity under transient EAAT2 blockade therefore does not meet the criteria for STDP.

EAAT2 overexpression prevents striatal STDP expression

To estimate to what extent EAAT2 controls STDP expression, we next questioned if an overexpression of EAAT2 would have an impact on STDP. We used ceftriaxone, a beta-lactam antibiotic that increases EAAT2 levels and activity[44]. Indeed, immunohistochemistry showed that eight days of daily i.p. ceftriaxone (200 mg/kg) injections in rats (Fig. 6a significantly increased (p=0.0420) EAAT2 levels in the striatum (Fig. 6b). The control group consisted of rats receiving a daily injection of an equal volume of saline for eight days. We observed no significant difference between saline- and ceftriaxone-injected rats for passive and active membrane properties of MSNs (RMP, Ri, rheobase, intensity-frequency relationship) or transmission and short-term plasticity (Supplementary Fig. 6). We first verified that similar STDP was observed in saline-injected and control rats. The examples in Figure 6c and 6d show that post-pre pairings at Δt_{STDP}=-18 ms induced LTP (the mean baseline EPSC amplitude was 278±4 pA before pairings and had increased by 27%, to 354±3 pA, one hour after pairings; Fig. 6c) whereas pre-post pairings at Δt_{STDP}=+13 ms induced LTD (the mean baseline EPSC amplitude was 123±4 pA before pairings and had decreased by 63%, to 45±2 pA, one hour after pairings; Fig. 6d). In summary, saline-injected rats displayed bidirectional STDP similar to that observed in control rats: post-pre pairings induced LTP (179±28%, p=0.0295, n=7; 7/7 cells displayed LTP) and pre-post pairings triggered LTD (51±8%, p=0.0036, n=5; 5/5 cells displayed LTD; Fig. 6e,i). In ceftriaxone-treated rats, canonical pairings were unable to induce STDP. Indeed, as exemplified in Figure 6f, post-pre pairings at Δt_{STDP}=-10 ms failed to induce plasticity: no significant difference was observed before and after pairings (190±3 pA and 182±3 pA, respectively). Similarly, an absence of plasticity was observed for pre-post pairings at Δt_{STDP}=+10 ms because there was no significant difference before and after pairings (151±2 pA and 148±3 pA, respectively; Fig. 6g). In summary, MSNs recorded from ceftriaxone-treated rats displayed no STDP as both post-pre ($-30<\Delta t_{STDP}<0$ ms) and pre-post ($0<\Delta t_{STDP}<+30$ ms) pairings failed to induce significant plasticity (96±3%, p=0.3286, n=7, 0/7 cells displayed LTP and 97±5%, p=0.6279, n=7, 1/7 cells displayed LTD, respectively; Fig. 6h,i). In conclusion, EAAT2 overexpression impaired the detection of correlated activity and precluded the occurrence of a bidirectional STDP (Fig. 6i).

Discussion

Identifying the conditions required for the expression of Hebbian plasticity, such as STDP, is essential for a better understanding of the mechanisms underlying learning and memory. Our findings demonstrate that astrocytes play a key role in the establishment of STDP, through EAAT2-mediated glutamate uptake. Indeed, EAAT2 allows translating precise pre- and postsynaptic activity into a salient time-coded message. This is a key requirement for STDP, the main characteristic of which is a high degree of sensitivity to timing[19,20], a feature that was erased by the transient blockade of EAAT2. Under this blockade, STDP was replaced by a non-Hebbian form of plasticity that was not dependent on the timing or order of the activities on either side of the synapse and was even observed in cases of unpaired activity. By contrast, EAAT2 overexpression impaired the detection of correlated pre- and postsynaptic activity by MSNs, resulting in an absence of plasticity. Our results show that astrocytes gate the conversion from non-Hebbian to Hebbian plasticity via EAAT2, leading to the emergence of STDP (Fig. 7).

Astrocytes actively control various synaptic functions and, therefore, play a key role in the modulation of neuronal activity[11,12,45,46]. Control of neuronal computation by astrocytes is via the release and uptake of transmitters, such as glutamate. Glutamate release by astrocytes plays an important role in STDP at L4-L2/3 neocortical synapses, by controlling t-LTD through the activation of astrocytic CB_1R[47]. By contrast, the involvement of astrocytic glutamate uptake in a time-coding paradigm, such as STDP, has never been investigated. Previous reports indicate that rate-coded plasticity, induced by low- or high-frequency stimulation (LFS and HFS) or theta-burst stimulation (TBS), is sensitive to changes in astrocytic glutamate uptake[48,49,50,51,52,53]. In addition, neuronal EAAT3 regulates the balance between TBS-LTP and LFS-LTD[54] and cerebellar LTD is dependent on the patterned expression of neuronal EAAT4 on Purkinje cells[55]. This study is, to our knowledge, the first to assess the involvement of astrocytic glutamate uptake in the expression of time-coded plasticity, such as STDP. STDP relies on the precise timing and order of inputs on either side of the synapse. STDP thus constitutes a time-coding paradigm for plasticity induction[19,20] by contrast to rate-coding plasticity protocols. The detection of a temporal coincidence between pre- and postsynaptic activities is crucial for STDP expression. Astrocytic glutamate uptake is involved in setting the timing of synaptic inputs. We therefore explored the role of EAAT2 in STDP, by transiently inhibiting (with DHK or WAY-213,613) EAAT2 during STDP pairings. This allows an on-off manipulation compatible with STDP study, whereas genetic approaches (knockout) and long-lasting drug applications have potential long-term effects. DHK and WAY-213,613 have several advantages for studies of this type. In addition to their specificity for EAAT2 and their efficient washout, they are also non-transportable inhibitors of EAAT2, and

this property prevents artificial increases in extracellular glutamate concentration due to hetero-exchange[33,34]. We next overexpressed EAAT2 with ceftriaxone, which has been reported to increase EAAT2 expression and activity[44].

Astrocytic pools of EAAT2 are responsible for 90% of the glutamate uptake[8]. EAAT2 is also found on neurons but at much lower level (~10% of astrocytic EAAT2). The physiological role of neuronal EAAT2 remains uncertain based on their very low level of expression but also on their distribution in most of the axon-terminal membranes and not being concentrated in the synapses[9,56]. Specific deletion of EAAT2 in astrocytes induces dramatic effects, such as excess mortality, lower body weight and spontaneous seizures, whereas no detectable neurological abnormalities are observed with neuronal EAAT2 deletion[8,9]. Nevertheless, it would be interesting to test specifically the impact of neuronal EAAT2 (using neuronal EAAT2-KO mice) in STDP expression.

The key feature of STDP is its occurrence within a restricted time window. Uncorrelated events (>30 ms) therefore fail to trigger plasticity. When EAAT2 activity is transiently impaired, an aberrant form of plasticity occurs during time windows in which plasticity is not normally observed. Uncorrelated events can induce this aberrant plasticity and are considered as pertinent events for an engram. Unlike STDP, the non-Hebbian LTP induced under transient EAAT2 blockade did not depend on the timing or order of pre- and postsynaptic activity. t-LTP has been reported to be mainly dependent on NMDARs[19], which operate as molecular coincidence detectors[4]. By contrast, non-Hebbian LTP under EAAT2 blockade is dependent on postsynaptic GluN2B-containing NMDARs located extrasynaptically, and these receptors do not act as molecular coincident detectors. Supporting this, we found that even unpaired activity (consisting of a single postsynaptic action potential repeated 100 times at 1 Hz) induced non-Hebbian LTP under EAAT2 blockade. Molecular coincidence detectors, such as NMDARs, require concomitant signals to be activated, as in STDP, in which the postsynaptic back-propagating action potential is paired with presynaptic activity[19,20]. In the presence of transient EAAT2 blockade, this feature is lost, because a single signal, the postsynaptic back-propagating action potential removing Mg^{2+} blockade, becomes sufficient to trigger LTP, due to the high ambient glutamate levels present when EAAT2 is blocked.

GABAergic microcircuits are involved in plasticity occurring at specific time window ($-70<\Delta t_{STDP}<+70$ ms) resulting in LTD (by contrast to the non-timing-dependent LTP). In the presence of DHK, GABAergic inhibition was stronger, due to the recruitment of inhibitory neurons as a result of the increase in glutamate spillover. In the presence of blockers of $GABA_A$Rs or VSCCs, pairings for which $-70<\Delta t_{STDP}<+70$ ms unmasked NMDAR-mediated LTP. This LTP shares similar induction mechanism as that observed for larger time intervals.

We previously described the control of STDP polarity by GABA[28]. Here, different mechanisms are involved because concomitant transient blockade of GABAergic transmission and EAAT2 led to an absence of plasticity. GABAergic circuits are efficiently recruited by cortical stimulation in the presence of DHK. We hypothesize that the NMDAR-mediated LTP observed at large Δt_{STDP} is somehow shunted at narrow Δt_{STDP} by an additional pool of GABA, due to the recruitment of GABAergic interneurons by cortical stimulation. Indeed, NMDAR-mediated LTP at larger Δt_{STDP} was exclusively dependent on the postsynaptic spiking (Fig. 5g) and did not require presynaptic stimulation. By contrast, when cortical stimulation (and, thus, the recruitment of GABAergic interneurons) was paired with the postsynaptic spike for narrow Δt_{STDP}, the increased GABAergic transmission prevented LTP expression. Thus, NMDAR-mediated LTP may be expressed only at large Δt_{STDP}, when presynaptic stimulation occurs far from the postsynaptic spike and GABAergic evoked transmission does not interfere with LTP expression. As a result, the blocking of $GABA_A$ transmission revealed LTP. This LTP was similar to the non-timing-dependent LTP (NMDAR-mediated) induced for large Δt_{STDP}. Interestingly, pre-post t-LTD and post-pre t-LTP observed in control conditions are both dependent on VSCC activity[31], but their induction itself is not dependent on GABAergic transmission[28]. Thus, the t-LTD and t-LTP evoked in control conditions involve signaling mechanisms distinct from those involved in the plasticity observed under EAAT2 blockade.

EAAT2 overexpression by ceftriaxone prevented both t-LTP and t-LTD. We verified that ceftriaxone did not alter the passive and active electrophysiological properties of MSNs, as well as corticostriatal transmission and probability of glutamate release. Ceftriaxone can also mediate the upregulation of system x_c- (cystine/glutamate antiporter system)[57], which, together with EAAT2, is involved in the maintenance of glutamate homeostasis. However, the net effect of up- or downregulation and the precise balance between these two systems (glutamate uptake and export) remains to be determined. System x_c- modulates long-term synaptic plasticity in the nucleus accumbens through an increase of extracellular glutamate and activation of mGluR2/3 and mGluR5[58]. However, discerning the effects of ceftriaxone on either direct activation of system x_c- (due to off-target effects of system x_c- pharmacology) and an effect as a consequence of the alteration of EAAT2 function remains difficult to determine. We cannot, therefore, exclude the possibility that the observed effects of ceftriaxone arise from system x_c- upregulation. However, we hypothesize that enhanced glutamate clearance may prevent the activation of postsynaptic type-ImGluRs located perisynaptically, leading to t-LTD[31,43]. We have previously shown that the bidirectional corticostriatal STDP relies on two distinct signaling pathways[31,43]. Indeed, t-LTP is NMDAR-dependent, whereas t-LTD is mGluR-mediated. Both receptor subtypes can be localized outside the synaptic cleft[37,41] and thus compete with EAAT2 for the extracellular glutamate.

Therefore, enhancing glutamate uptake through EAAT2 overexpression with ceftriaxone, would reasonably result in a profound alteration of corticostriatal STDP expression. In line with that, increases in glutamate transporter expression have been shown to alter frequency-based plasticity, such as mGluR-dependent LFS-LTD and HFS-LTP in the hippocampus[53].

A few studies have reported effects of changes in EAAT2 expression on behavior[46]. The pharmacological blockade of EAAT2 with DHK impairs spatial memory and induces depression and anhedonia and ceftriaxone has been reported to display antidepressant effects[46]. EAAT2 downregulation in striatum is also found in a rat model of depression[59]. EAAT2 KO mice exhibit seizures and premature death[6,9]. An inducible astrocytic EAAT2 knockout in dorsal striatum was recently shown to be associated with pathological repetitive behaviors and an increase in corticostriatal excitatory transmission[25]. Moreover, this phenotype was reversed by memantine treatment, confirming that excessive glutamate spillover due to EAAT2 dysfunction, deregulating the corticostriatal pathway, was responsible for the observed repetitive behaviors. These findings are consistent with our results showing that memantine prevents aberrant LTP in conditions of EAAT2 blockade. Conversely, EAAT2 overexpression has been reported to impair hippocampal learning[60]. This observation is consistent with our results showing a lack of plasticity with ceftriaxone treatment.

EAAT2 dysfunction, associated with higher ambient glutamate levels, has been observed in neurodegenerative and psychiatric diseases including Huntington's, Parkinson's, Alzheimer's and schizophrenia in which cognitive functions are impaired[7,10,11]. Chronic exposure to drugs of abuse has also been shown to induce a downregulation of EAAT2 in the nucleus accumbens[12]. EAAT2 therefore appears to be a major target for the treatment of neurological diseases and addiction (by ceftriaxone), not only to combat glutamatergic neurotoxicity but also to prevent aberrant plasticity, which could be linked to cognitive deficits[10,11,12]. Thus, our results, showing the tight control of STDP by EAAT2, are of importance for linking the expression of timing-dependent plasticity with different physiological or pathological states.

Astrocyte function is not restricted to structural and metabolic support or homeostatic and protective functions. Through glutamate uptake, astrocytes are also involved in higher brain functions, such as learning and memory[11,45,46]. We demonstrate here that EAAT2 operates over a highly controlled range to allow the emergence of bidirectional STDP. If STDP is dependent on the efficiency of glutamate uptake, then we would expect STDP expression to be controlled by the precise location and density of transporter expression, and glial synaptic coverage, which may differ considerably between brain structures and can undergo experience-dependent remodelling[61] (Fig. 7). This work thus identifies astrocytes as key players in the establishment of synaptic Hebbian learning rule, such as STDP.

Methods

Animals

All experiments were performed in accordance with the guidelines of the local animal welfare committee (Center for Interdisciplinary Research in Biology Ethics Committee) and the EU (directive 2010/63/EU). Every precaution was taken to minimize stress and the number of animals used in each series of experiments. OFA rats P18-42 (Charles River, L'Arbresle, France) were used for brain slice electrophysiology. Animals were housed in standard 12-hour light/dark cycles and food and water were available *ad libitum*.

Brain slice preparation

Horizontal brain slices containing the somatosensory cortical area and the corresponding corticostriatal projection field were prepared as previously described[27,27,31,28]. Corticostriatal connections (between somatosensory cortex layer 5 and the dorsal striatum) are preserved in the horizontal plane. Horizontal brain slices (330 µm-thick) were prepared from rats with a vibrating blade microtome (VT1200S, Leica Micosystems, Nussloch, Germany). Brains were sliced in an ice-cold cutting solution (125 mM NaCl, 2.5 mM KCl, 25 mM glucose 25 mM $NaHCO_3$, 1.25 mM NaH_2PO_4, 2 mM $CaCl_2$, 1 mM $MgCl_2$, 1 mM pyruvic acid) through which 95% O_2/5% CO_2 was bubbled. The slices were transferred to the same solution at 34°C for one hour and then to room temperature.

Electrophysiology recordings

Patch-clamp recordings were performed as previously described[27,27,31,28]. Briefly, for whole-cell recordings, borosilicate glass pipettes of 6-8MΩ resistance were filled with (in mM): 105 K-gluconate, 30 KCl, 10 HEPES, 10 phosphocreatine, 4 Mg-ATP, 0.3 Na-GTP, 0.3 EGTA (adjusted to pH 7.35 with KOH). The composition of the extracellular solution was (mM): 125 NaCl, 2.5 KCl, 25 glucose, 25 $NaHCO_3$, 1.25 NaH_2PO_4, 2 $CaCl_2$, 1 $MgCl_2$, 10 µM pyruvic acid bubbled with 95% O_2 and 5% CO_2. Signals were amplified using with EPC9-2 and EPC10-4 amplifiers (HEKA Elektronik, Lambrecht, Germany). All recordings were performed at 34°C, using a temperature control system (Bath-controller V, Luigs & Neumann, Ratingen, Germany) and slices were continuously superfused with extracellular solution, at a rate of 2 ml/min. Slices were visualized under an Olympus BX51WI microscope (Olympus, Rungis, France), with a 4x/0.13 objective for

the placement of the stimulating electrode and a 40x/0.80 water-immersion objective for the localization of cells for whole-cell recordings. Current-clamp recordings were filtered at 2.5 kHz and sampled at 5 kHz and voltage-clamp recordings were filtered at 5 kHz and sampled at 10 kHz, with the Patchmaster v2x32 program (HEKA Elektronik).

Spike-timing-dependent plasticity protocols and random Δt_{STDP} patterns

Electrical stimulations were performed with a concentric bipolar electrode (Phymep, Paris, France and CBBSE75 FHC, Bowdoin, ME, USA) placed in layer 5 of the somatosensory cortex[15]. Electrical stimulations were monophasic, at constant current (ISO-Flex stimulator, AMPI, Jerusalem, Israel). Currents were adjusted to evoke 50-200 pA EPSCs. Repetitive control stimuli were applied at 0.1 Hz. STDP protocols consisted of pairings of pre- and postsynaptic stimulations (at 1 Hz) separated by a specific time interval (Δt_{STDP}). Presynaptic stimulations corresponded to cortical stimulations and the postsynaptic stimulation of an action potential evoked by a depolarizing current step (30 ms duration) in MSNs. $\Delta t_{STDP}<0$ ms for post-pre pairings, and $\Delta t_{STDP}>0$ ms for pre-post pairings. $\Delta t_{STDP}=\pm 500$ ms corresponds to post-pre and pre-post pairings performed around $\Delta t_{STDP}=-500$ ms and $\Delta t_{STDP}=+500$ ms. Note that for $\Delta t_{STDP}=-500$ ms and $\Delta t_{STDP}=+500$ ms, the order (post-pre *vs.* pre-post) was determined by the first pairing of the STDP protocol only, because, for the remaining pairings, the pre- and postsynaptic stimulations were separated by 500 ms and could therefore be considered as either post-pre or pre-post pairings at 1 Hz. We therefore pooled the data for $\Delta t_{STDP}=-500$ ms and $\Delta t_{STDP}=+500$ ms ($\Delta t_{STDP}=\pm 500$ms), which are presented as a single average on the figures. Recordings on neurons were made over a period of 10 minutes at baseline, and for at least 60 minutes after the SDTP protocols; long-term changes in synaptic efficacy were measured from 45 to 60 minutes. We individually measured and averaged 60 successive EPSCs, comparing the last 10 minutes of the recording with the 10-minute baseline recording. Neuron recordings were made in in voltage-clamp mode during baseline and for the 60 minutes of recording after the STDP protocol, and in current-clamp mode during STDP protocol. Experiments were excluded if input resistance (Ri) varied by more than 20%.

For the random Δt_{STDP} patterns, we used the following algorithm (programmed in Igor Pro 6.3 software, WaveMetrics): for each pairing, we first selected a time window with a randomly selected length between 500 and 1500 ms (with a uniform distribution) and located the presynaptic stimulation time in the middle of this window. The postsynaptic stimulation time was then randomly chosen within this window (with a uniform distribution). The Δt_{STDP} pattern was formed by the concatenation of 100 such windows. This generated both a close-to-uniform distribution of the Δt_{STDP} and a variable interval between two successive presynaptic stimulations.

Chemicals

All chemicals were purchased from Tocris (Ellisville, MO, USA), except for picrotoxin (Sigma). (2S,3S,4R)-2-Carboxy-4-isopropyl-3-pyrrolidineacetic acid (Dihydrokainic acid, DHK; 300 μM), DL-2-amino-5-phosphono-pentanoic acid (D-AP5; 50 μM), (1S,2S)-2-[2-[[3-(1H-benzimidazol-2yl)propyl]methylamino]ethyl]-6-fluoro-1,2,3,4-tetrahydro-1-(1-methylethyl)-2-naphthalenyl methoxyacetoacetate dihydrochloride (Mibefradil; 20 μM), 6-cyano-7-nitroquinoxaline-2,3-dione (CNQX; 20 μM), (αR,βS)-α-(4-hydroxyphenyl)-β-methyl-4-(phenylmethyl)-1-piperidinepropanol maleate (Ro 25-6981; 10 μM), SR 95531 hydrobromide (gabazine 10 μM) and 3,5-dimethyl-tricyclo[3.3.1.13,7]decan-1-amine hydrochloride (Memantine; 1 0μM) were dissolved directly in the extracellular solution and bath applied. N-(piperidin-1-yl)-5-(4-iodophenyl)-1-(2,4-dichlorophenyl)-4-methyl-1H-pyrazole-3-carboxamide (AM251; 3 μM) and picrotoxin (50 μM) were dissolved in ethanol and added to the external solution, such that the final concentration of ethanol was 0.01-0.1%. N-[4-(2-bromo-4,5-difluorophenoxy)phenyl]-L-asparagine (WAY-213,613; 50 and 100 μM) was dissolved in DMSO and added to the external solution such that the final concentration of DMSO was 0.05% and 0.1%, respectively. (S)-α-Methyl-4-carboxyphenylglycine (MCPG; 500 μM) was dissolved in 1.1 eq. NaOH and added to the external solution. BAPTA (10 mM) and dizocilpine maleate (i-MK801; 1 mM) were dissolved directly in the intracellular solution.

The contrasting activity patterns of synaptic and extrasynaptic NMDARs result in different degrees of memantine blockade[42]. Due to the agonist concentration-dependence of memantine blockade kinetics, slices were pre-incubated with low dose of memantine (10 μM) for at least one hour before recording, to allow sufficient time for equilibrium to be reached.

Transient EAAT2 blockade

Transient EAAT2 blockade was achieved with two structurally different molecules: DHK (300 μM), a selective substrate inhibitor (non-transportable) of EAAT2[33], and WAY-213,613 (50-100 μM), a selective non-substrate inhibitor (non-transportable) of EAAT2[34]. DHK was bath-applied for as short a period as possible, to ensure that its effect on Vm was compatible with the correct analysis of synaptic efficacy changes. Indeed, EAAT2 blockade resulted in a marked depolarization[21], potentially impairing the estimation of synaptic efficacy changes. A stable baseline was established over a period of 10 minutes. DHK was bath-applied for 5 minutes (the dark gray area in the figures). We systematically checked the efficacy of DHK application before applying the

STDP protocol. This depolarization (Fig. 2a) was used as an indicator of DHK efficiency. DHK was washed out at the STDP protocol offset. The full DHK washout took 15 minutes (the light gray area in the figures) and, during this period, a significant and transient decrease in EPSC magnitude (due to the DHK-induced inward shift in $I_{holding}$ and AMPAR desensitization[26]) was observed. Accordingly, in all figures, synaptic efficacy changes are illustrated from 15 minutes after the removal of DHK. Synaptic efficacy changes were evaluated 60 minutes after the start of the DHK washout (at least 30 minutes after the full recovery of baseline $I_{holding}$).

Electrophysiological data analysis

Off-line analysis was performed with Fitmaster (Heka Elektronik). Spontaneous post-synaptic currents (sPSCs) were identified using a semi-automated amplitude threshold based detection software (Mini Analysis 6.0.7 Program, Synaptosoft, Fort Lee, NJ, USA) and were visually confirmed. Statistical analysis was performed with Prism 5.02 software (San Diego, CA, USA). In all cases "n" refers to an experiment on a single cell from a single slice. All results are expressed as mean±SEM in the text and as mean±SD in the figures (except in Fig. 1f,i, 2g, 6i and Supplementary Fig. 2a: mean ± SEM), and statistical significance was assessed in unpaired *t* tests or in one-sample *t* tests, as appropriate, using the indicated significance threshold (*p*), or one-way ANOVA with Bonferroni correction, where specified.

Chronic ceftriaxone treatment

To increase the expression of EAAT2 chronic ceftriaxone treatment of the rats was performed as previously described[53]. Male OFA rats (P30-P42) received a daily intraperitoneal (i.p.) injection of ceftriaxone (Rocefin, Roche; 200 mg/kg per day dissolved in saline) or an equal volume of saline on eight consecutive days. Corticostriatal brain slices for electrophysiology were obtained from ceftriaxone- or saline-treated rats 24 hours after the final injection, and prepared as described above.

Immunohistochemistry

Rats were treated for eight days with daily i.p. injection of either saline (*n*=4 rats) or ceftriaxone (*n*=4 rats), as described above. Rats were anesthetized with pentobarbital 4% paraformaldehyde. Brains were postfixed in 4% paraformaldehyde and cut into 30 µm horizontal sections with a vibratome (Microm HM650V, ThermoScientific). Immunostaining was performed by incubating

free-floating sections with a guinea pig anti-EAAT2 antibody (1:5000; AB1783, Merck Millipore) for 48 hours at 4°C and then with a secondary Cyanine Cy™3-conjugated antibody (1:1000; Jackson Laboratories) dissolved in PBS 1X for one hour. Images were acquired with the SP5 confocal system (Leica, Germany).

References

1. Diamond, J. S. & Jahr, C. E. Transporters buffer synaptically released glutamate on a submillisecond time scale. *J Neurosci* 17, 4672-4687 (1997).
2. Kullmann, D. M. & Asztely, F. Extrasynaptic glutamate spillover in the hippocampus: evidence and implications. *Trends Neurosci* 21(1):8-14 (1998).
3. Takahashi, M. et al. The role of glutamate transporters in glutamate homeostasis in the brain. *J Exp Biol* 200(Pt 2):401-9 (1997).
4. Attwell, D. & Gibb, A. Neuroenergetics and the kinetic design of excitatory synapses. *Nat Rev Neurosci* 6(11):841-9 (2005).
5. Rothstein, J. D. et al. Knockout of glutamate transporters reveals a major role for astroglial transport in excitotoxicity and clearance of glutamate. *Neuron* 16, 675-686 (1996).
6. Tanaka, K. et al. Epilepsy and exacerbation of brain injury in mice lacking the glutamate transporter GLT-1. *Science* 276(5319):1699-702 (1997).
7. Danbolt, N.C. Glutamate uptake. *Prog Neurobiol* 65,1-105 (2001).
8. Danbolt, N. C., Furness, D.N. & Zhou, Y. Neuronal vs glial glutamate uptake: Resolving the conundrum. *Neurochem Int* 26. pii: S0197-0186(16)30108-5 (2016).
9. Petr, G. T. et al. Conditional deletion of the glutamate transporter GLT-1 reveals that astrocytic GLT-1 protects against fatal epilepsy while neuronal GLT-1 contributes significantly to glutamate uptake into synaptosomes. *J Neurosci* 1;35(13):5187-201 (2015).
10. Soni, N., Reddy, B. V. & Kumar, P. GLT-1 transporter: An effective pharmacological target for various neurological disorders. *Pharmacol Biochem Behav* 127C:70-81 (2014).
11. Chung, W. S., Welsh, C. A., Barres, B. A. & Stevens, B. Do glia drive synaptic and cognitive impairment in disease? *Nat Neurosci* 18(11):1539-45 (2015).
12. Scofield, M. D. & Kalivas, P. W. Astrocytic dysfunction and addiction: consequences of impaired glutamate homeostasis. *Neuroscientist* 20(6):610-22 (2014).
13. Tzingounis, A. V. & Wadiche, J. I. Glutamate transporters: confining runaway excitation by shaping synaptic transmission. *Nat Rev Neurosci* 8(12):935-47 (2007).
14. Arnth-Jensen, N., Jabaudon, D. & Scanziani, M. Cooperation between independent hippocampal synapses is controlled by glutamate uptake. *Nat Neurosci* 5(4):325-31 (2002).
15. Scimemi, A., Fine, A., Kullmann, D. M. & Rusakov, D. A. NR2B-containing receptors mediate cross talk among hippocampal synapses. *J Neurosci* 24(20):4767-77 (2004).
16. Diamond, J. S. & Jahr, C. E. Synaptically released glutamate does not overwhelm transporters on hippocampal astrocytes during high-frequency stimulation. *J Neurophysiol* 83(5):2835-43 (2000).

17. Asztely, F., Erdemli, G. & Kullmann, D. M. Extrasynaptic glutamate spillover in the hippocampus: dependence on temperature and the role of active glutamate uptake. *Neuron* 18(2):281-93 (1997).
18. Bergles, D. E. & Jahr, C. E. Synaptic activation of glutamate transporters in hippocampal astrocytes. *Neuron* 19(6):1297-308 (1997).
19. Feldman, D. E. The spike-timing dependence of plasticity. *Neuron* 75: 556-571 (2012).
20. Sjöström, P. J., Rancz, E. A., Roth, A. & Häusser, M. Dendritic excitability and synaptic plasticity. *Physiol Rev* 88: 769-840 (2008).
21. Clopath, C., Büsing, L., Vasilaki, E. & Gerstner, W. Connectivity reflects coding: a model of voltage-based STDP with homeostasis. *Nat Neurosci* 13(3):344-52 (2010).
22. Costa, R. P., Froemke, R. C., Sjöström, P. J. & van Rossum, M. C. Unified pre- and postsynaptic long-term plasticity enables reliable and flexible learning. *Elife* 26;4 (2015).
23. Di Filippo, M. et al. Short-term and long-term plasticity at corticostriatal synapses: implications for learning and memory. *Behav Brain Res* 199(1):108-18 (2009).
24. Yin, H. H. et al. Dynamic reorganization of striatal circuits during the acquisition and consolidation of a skill. *Nat Neurosci* 12:333-341 (2009).
25. Aida, T. et al. Astroglial glutamate transporter deficiency increases synaptic excitability and leads to pathological repetitive behaviors in mice. *Neuropsychopharmacology* 40(7):1569-79 (2015).
26. Goubard, V., Fino, E. & Venance, L. Contribution of astrocytic glutamate and GABA uptake to corticostriatal information processing. *J Physiol* 589(Pt 9): 2301-2319 (2011).
27. Fino, E., Glowinski, J. & Venance, L. Bidirectional activity-dependent plasticity at corticostriatal synapses. *J Neurosci* 25: 11279-11287 (2005).
28. Paillé, V. et al. GABAergic circuits control spike-timing-dependent plasticity. *J Neurosci* 29;33(22):9353-63 (2013).
29. Pawlak, V. & Kerr, J. N. Dopamine receptor activation is required for corticostriatal spike-timing-dependent plasticity. *J Neurosci* 28: 2435-2446 (2008).
30. Shen, W., Flajolet, M., Greengard, P. & Surmeier, D. J. Dichotomous dopaminergic control of striatal synaptic plasticity. *Science* 321: 848-851 (2008).
31. Fino, E. et al. Distinct coincidence detectors govern the corticostriatal spike timing-dependent plasticity. *J Physiol* 588: 3045-3062 (2010).
32. Schulz, J. M., Redgrave, P. & Reynolds, J. N. Cortico-striatal spike-timing dependent plasticity after activation of subcortical pathways. *Front Synaptic Neurosci* 2;2:23 (2010).

33. Arriza, J. L. et al. Functional comparisons of three glutamate transporter subtypes cloned from human motor cortex. *J Neurosci* 14, 5559-5569 (1994).

34. Dunlop, J. et al. WAY-163909 [(7bR, 10aR)-1,2,3,4,8,9,10,10a-octahydro-7bH-cyclopenta-[b][1,4]diazepino[6,7,1hi]indole], a novel 5-hydroxytryptamine 2C receptor-selective agonist with anorectic activity. *Pharmacol Exp Ther* 313(2):862-9 (2005).

35. Artola, A., Bröcher, S. & Singer, W. Different voltage-dependent thresholds for inducing long-term depression and long-term potentiation in slices of rat visual cortex. *Nature* 6;347(6288):69-72 (1990).

36. Lei, S., Pelkey, K. A., Topolnik, L., Congar, P., Lacaille, J. C. & McBain, C. J. Depolarization-induced long-term depression at hippocampal mossy fiber-CA3 pyramidal neuron synapses. *J Neurosci* 29;23(30):9786-95 (2003).

37. Baude, A., Nusser, Z., Roberts, J. D., Mulvihill, E., McIlhinney, R. A. & Somogyi. P. The metabotropic glutamate receptor (mGluR1 alpha) is concentrated at perisynaptic membrane of neuronal subpopulations as detected by immunogold reaction. *Neuron* 11(4):771-87 (1993).

38. Huang, Y. H., Sinha, S. R., Tanaka, K., Rothstein, J. D. & Bergles, D. E. Astrocyte glutamate transporters regulate metabotropic glutamate receptor-mediated excitation of hippocampal interneurons. *J Neurosci* 24(19):4551-9 (2004).

39. Lozovaya, N. A. et al. Extrasynaptic NR2B and NR2D subunits of NMDA receptors shape 'superslow' afterburst EPSC in rat hippocampus. *J Physiol* 15;558(Pt 2):451-63 (2004).

40. Chalifoux, J. R. & Carter, A. G. Glutamate spillover promotes the generation of NMDA spikes. *J Neurosci* 31(45):16435-46 (2011).

41. Paoletti, P., Bellone, C. & Zhou, Q. NMDA receptor subunit diversity: impact on receptor properties, synaptic plasticity and disease. *Nat Rev Neurosci* 14(6):383-400 (2013).

42. Xia, P., Chen, H. S., Zhang, D. & Lipton, S. A. Memantine preferentially blocks extrasynaptic over synaptic NMDA receptor currents in hippocampal autapses. *J Neurosci* 30(33):11246-50 (2010).

43. Evans, R. C. et al. The effects of NMDA subunit composition on calcium influx and spike timing-dependent plasticity in striatal medium spiny neurons. *PLoS Comput Biol* 8(4):e1002493 (2012).

44. Rothstein, J. D. et al. Beta-lactam antibiotics offer neuroprotection by increasing glutamate transporter expression. *Nature* 433(7021):73-7 (2005).

45. Fields, R. D., et al. Glial biology in learning and cognition. *Neuroscientist* 20(5):426-31 (2014).

46. Oliveira, J. F., Sardinha, V. M., Guerra-Gomes, S., Araque, A. & Sousa, N. Do stars govern our actions? Astrocyte involvement in rodent behavior. *Trends Neurosci* 38(9):535-49 (2015).

47. Min, R. & Nevian, T. Astrocyte signaling controls spike timing-dependent depression at neocortical synapses. *Nat Neurosci* 25;15(5):746-53 (2012).

48. Katagiri, H., Tanaka, K. & Manabe, T. Requirement of appropriate glutamate concentrations in the synaptic cleft for hippocampal LTP induction. *Eur J Neurosci* 14(3):547-53 (2001).

49. Pinard, A., Lévesque, S., Vallée, J. & Robitaille, R. Glutamatergic modulation of synaptic plasticity at a PNS vertebrate cholinergic synapse. *Eur J Neurosci* 18(12):3241-50 (2003).

50. Massey, P. V. et al. Differential roles of NR2A and NR2B-containing NMDA receptors in cortical long-term potentiation and long-term depression. *J Neurosci* 24(36):7821-8 (2004).

51. Tsvetkov, E., Shin, R. M. & Bolshakov, V. Y. Glutamate uptake determines pathway specificity of long-term potentiation in the neural circuitry of fear conditioning. *Neuron* 8;41(1):139-51 (2004).

52. Wang, Z. Y., Zhang, Y. Q. & Zhao, Z. Q. Inhibition of tetanically sciatic stimulation-induced LTP of spinal neurons and Fos expression by disrupting glutamate transporter GLT-1. *Neuropharmacology* 51(4):764-72 (2006).

53. Omrani, A. et al. Up-regulation of GLT-1 severely impairs LTD at mossy fiber-CA3 synapses. *J Physiol* 587(Pt 19):4575-88 (2009).

54. Scimemi, A., Tian, H. & Diamond, J. S. Neuronal transporters regulate glutamate clearance, NMDA receptor activation, and synaptic plasticity in the hippocampus. *J Neurosci* 29(46):14581-95 (2009).

55. Wadiche, J. I. & Jahr, C. E. Patterned expression of Purkinje cell glutamate transporters controls synaptic plasticity. *Nat Neurosci* 8(10):1329-34 (2005).

56. Furness, D. N. et al. A quantitative assessment of glutamate uptake into hippocampal synaptic terminals and astrocytes: new insights into a neuronal role for excitatory amino acid transporter 2 (EAAT2). *Neuroscience* 11;157(1):80-94 (2008).

57. Lewerenz, J. et al. Induction of Nrf2 and xCT are involved in the action of the neuroprotective antibiotic ceftriaxone in vitro. *Neurochem* 111(2):332-43 (2009).

58. Moussawi, K., Pacchioni, A., Moran, M., Olive, M. F., Gass, J. T., Lavin, A. & Kalivas, P. W. N-Acetylcysteine reverses cocaine-induced metaplasticity. *Nat Neurosci* 12(2):182-9 (2009).

59. Almeida, R. F. et al. Effects of depressive-like behavior of rats on brain glutamate uptake. *Neurochem Res* 35(8):1164-71 (2010).

60. Matos-Ocasio, F., Hernández-López, A. & Thompson, K. J. Ceftriaxone, a GLT-1 transporter activator, disrupts hippocampal learning in rats. *Pharmacol Biochem Behav* 122:118-21 (2014).

61. Bernardinelli. Y., Muller, D. & Nikonenko, I. Astrocyte-synapse structural plasticity. *Neural Plast* 2014:232105 (2014).

Author Contributions: SV and LV conceived and designed the experiments; SV performed experiments and analysis; SV and LV wrote the manuscript; LV supervised the project.

Acknowledgments: We thank the members of the LV laboratory, Hugues Berry, Olivier Manzoni and Christian Giaume, for helpful suggestions and critical comments. We thank Giuseppe Gangarossa and Sylvie Perez for assistance with immunohistochemistry. SV is a Research Fellow of the MRT and the LabEx MemoLife. This work was supported by grants from INSERM, *Collège de France*, CNRS and *Fondation de France*.

Competing Financial Interests statement: the authors have no competing financial interests to declare.

Figure Legends

Figure 1. Bidirectional corticostriatal STDP expression occurs within a restricted time window.

(**a**) Scheme of the recording and stimulating sites in corticostriatal slices. (**b**) STDP pairings: a single spike evoked in the recorded striatal MSN was paired with a single cortical stimulation; this pairing being repeated 100 times at 1 Hz. Δt_{STDP} indicates the time between pre- and postsynaptic stimulations. $\Delta t_{STDP}<0$ and $\Delta t_{STDP}>0$ refer to post-pre and pre-post pairings, respectively. (**c**) Example of LTP induced by 100 post-pre pairings. Top, EPSC strength before and after pairings. Bottom, time course of Ri (baseline: 67±0.3MΩ and 50-60 min after pairings: 79±0.8MΩ; change of 18%). Postsynaptic EPSC traces during 10 minutes of baseline (1) and 60 minutes after the STDP protocol (arrow) (2). (**d**) Example of LTD induced by 100 pre-post pairings (Ri, baseline: 106±0.5MΩ; 50-60 min after pairings: 116±0.5MΩ; change of 9%). (**e**) Averaged time-course of LTP induced by 100 post-pre pairings and LTD induced by 100 pre-post pairings. (**f**) Bidirectional STDP occurred in a narrow time window: post-pre pairings ($-30<\Delta t_{STDP}<0$ ms) induced LTP, whereas pre-post pairings ($0<\Delta t_{STDP}<+30$ ms) induced LTD. Synaptic strength was determined 45-60 minites after pairings (empty circles: individual neurons; black circle: average). The *y*-axis is discontinuous for clarity; plasticity amplitudes above the interruption are 312 pA, 367 pA and 424 pA. (**g**) Uncorrelated post-pre ($-250<\Delta t_{STDP}<-100$) and pre-post ($+100<\Delta t_{STDP}<+250$ ms) pairings induced no significant plasticity. (**h**) Post-pre or pre-post pairings with $\Delta t_{STDP}\sim\pm500$ ms induced no significant plasticity. (**i**) Graph summarizing STDP occurrence. Bidirectional plasticity was induced over a narrow time window ($-30<\Delta t_{STDP}<+30$ ms), whereas no plasticity was observed with uncorrelated pairings ($-500<\Delta t_{STDP}<-30$ ms and $+30<\Delta t_{STDP}<+500$ ms).

Insets correspond to a mean of 60 EPSCs during baseline and 1 hour after STDP pairings. Error bars represent the SD (except in panel i: SEM). *: $p<0.05$; **: $p<0.01$; ***: $p<0.001$; ns: not significant.

Figure 2. EAAT2 activity gates STDP polarity and time window

(**a**) Current-clamp recording of MSN in the absence of cortical stimulation showing that brief DHK application (300 µM for 5min) induced significant depolarization, indicating the presence of ambient glutamate in the slice. This depolarization was fully reversed after 15 minutes of DHK washout and was dependent on AMPAR and type-I/II mGluR, but not NMDAR. (**b-c**) DHK application had no effect on long-term synaptic efficacy changes estimated from 15 minutes after DHK washout (example in b and averaged time-course of experiments in c). The brief application of DHK without the STDP protocol induced a transient decrease in EPSC amplitude and an inward shift in $I_{holding}$ (light gray area). Both EPSC amplitude and $I_{holding}$ had fully recovered 15 minutes

after DHK washout. Ri remained unchanged during and after DHK application. The effects of DHK were fully reversible and, thus, compatible with the estimation of long-term synaptic efficacy changes. (**d**) Example of LTD induced by 100 pre-post pairings (Δt_{STDP}=+38 ms) with a transient blockade of EAAT2 by DHK (300 μM for 5 min, dark gray area; the light gray area indicates DHK washout). Top, EPSC strength before and after pairings. Bottom, time course of Ri (baseline, 47±0.2MΩ; 50-60 min after pairings, 51±0.1MΩ; change of 10%). (**e**) Averaged time-course of experiments with the transient blockade of EAAT2 with DHK, showing the induction of LTD for both post-pre (-70<Δt_{STDP}<0 ms) and pre-post (0<Δt_{STDP}<+70 ms) pairings. (**f**) LTD expression for -70<Δt_{STDP}<+70 ms with DHK. Synaptic strength was assessed 45-60 minutes after pairings (light blue circles: individual neurons; dark blue circle: average). (**g**) Example of LTP induced by 100 post-pre pairings (Δt_{STDP}=-175 ms) during the transient blockade of EAAT2 with DHK (Ri, baseline: 136±0.5MΩ; 50-60 min after pairings: 145±1MΩ; change of 6%). (**h**) Averaged time-course of experiments with transient EAAT2 blockade with DHK during pairings, inducing LTP for both post-pre (-250<Δt_{STDP}<-100 ms) and pre-post (+100<Δt_{STDP}<+250 ms) pairings. (**i**) Averaged time-course of experiments with transient EAAT2 blockade with DHK during pairings, inducing LTP for Δt_{STDP}~±500 ms. (**j**) Time window for long-term synaptic strength for post-pre and pre-post pairings (-500<Δt_{STDP}<+500 ms) in control conditions and in the presence of DHK. In controls, bidirectional plasticity was induced over a narrow time window (-30<Δt_{STDP}<+30 ms) and no plasticity was observed with uncorrelated pairings (-500<Δt_{STDP}<-30 ms and +30<Δt_{STDP}<+500 ms). During transient EAAT2 blockade in the STDP protocol, plasticity was observed regardless of the Δt_{STDP} value: LTD for narrow Δt_{STDP} (-70<Δt_{STDP}<+70) and LTP for a larger Δt_{STDP} (-500<Δt_{STDP}<-70 ms and +70<Δt_{STDP}<+500 ms).

Insets correspond to the mean of 60 EPSCs during baseline and 1 hour after STDP pairings. Error bars represent the SD (except in panel g: SEM) *: p<0.05; **: p<0.01; ***: p<0.001. ns: not significant.

Figure 3. The recruitment of GABAergic microcircuits under transient EAAT2 blockade induces LTD

(**a**) Blocking L- and T-type VSCCs with mibefradil (20 μM) under transient EAAT2 blockade impaired LTD and revealed potent LTP. (**b**) i-BAPTA did not impair the LTD observed under transient EAAT2 blockade. (**c**) Inhibitory currents recorded in MSNs held at -50 mV in control conditions, with DHK and with DHK+picrotoxin (50 μM) (n=14). (**d**) Top, characteristic voltage responses of one FS cell and one MSN to a series of 500 ms current pulses. Bottom, depolarization of FS cells and MSNs induced by DHK application. Left: example of changes in Vm before, during and after DHK application, in one FS cell and one MSN; right: mean values. (**e**) DHK-induced

depolarization led to firing activity in FS cells but not in MSNs. (**f**) Under EAAT2 blockade, cortical stimulation evoked an action potential in all recorded FS cells whereas subthreshold EPSPs were observed in MSNs. (**g**) Picrotoxin (50 μM) prevented the LTD induced by pairings at -70<Δt_{STDP}<+70 ms under EAAT2 blockade, and revealed LTP. (**h**) Co-application of gabazine (10 μM) with DHK during STDP pairings prevented the expression of LTD.
Insets correspond to the mean of 60 EPSCs during baseline and 1 hour after STDP pairings. Error bars represent the SD. *: p<0.05; **:p<0.01; ***: p<0.001; ns: not significant.

Figure 4: LTP under transient EAAT2 blockade is dependent on extrasynaptic GluN2B-containing NMDARs located on the postsynaptic MSN

(**a**) The LTP induced under EAAT2 blockade for Δt_{STDP}=±200 ms and Δt_{STDP}=±500 ms was mediated by NMDARs, because it was prevented by D-AP5 (50 μM) application. (**b**) The LTP induced under transient EAAT2 blockade for Δt_{STDP}=±200 ms was prevented by blocking postsynaptic NMDARs with i-MK801 (1 mM) applied intracellularly in the recorded MSN. (**c**) The inhibition of GluN2B-containing NMDARs with Ro25-6981 (10 μM) prevented the induction of LTP. (**d**) The inhibition of extrasynaptic NMDARs with memantine (10 μM) prevented LTP under transient EAAT2 blockade. Extrasynaptic GluN2B-containing NMDARs located on the postsynaptic MSN are thus required for the induction of LTP under transient EAAT2 blockade.
Insets correspond to the mean of 60 EPSCs during baseline and 1 hour after STDP pairings. Error bars represent SD. ns: not significant.

Figure 5. Paired activity is not required for LTP expression under transient EAAT2 blockade.

(**a-c**) Example of one random Δt_{STDP} pairing in control conditions and of one such pairing under transient EAAT2 blockade. (**a**) Scatter plot of a single random Δt_{STDP} pattern (comprising 100 consecutive random Δt_{STDP} pairings between -500 and +500 ms) together with the CC traces of 7 successive random pairings. Example of experiments performed in two separate MSNs, showing that the same random Δt_{STDP} pattern failed to induce plasticity in control conditions, whereas LTP was observed under transient EAAT2 blockade. (**b**) Histogram of the Δt_{STDP} from the n=8 random protocols, showing a uniform distribution. (**b-d**) Eight random Δt_{STDP} patterns were generated and each was applied to two MSNs, one in control conditions (**c**) and the other under EAAT2 blockade (**d**). In summary, random Δt_{STDP} patterns failed to induce plasticity in control cells, but resulted in LTP under transient EAAT2 blockade. Thus, under transient EAAT2 blockade, plasticity is not dependent on the timing and order of the paired activity. (**e**) Experimental design depicting a cell conditioning protocol consisting of a postsynaptic spike without paired presynaptic stimulation, repeated 100 times at 1 Hz; (**f**) This protocol did not induce plasticity in control conditions. (**g**)

Postsynaptic suprathreshold activity is sufficient to induce potent LTP under transient EAAT2 blockade. This LTP was mediated by NMDARSs, as it was prevented by D-AP5 (50 μM).
Insets correspond to the mean of 60 EPSCs during baseline and 1 hour after STDP pairings. Error bars represent the SD. *: $p<0.05$; ***: $p<0.001$; ns: not significant.

Figure 6. EAAT2 overexpression by ceftriaxone treatment impairs STDP

(**a**) Experimental design: ceftriaxone (or saline) was daily injected for 8 days; electrophysiology and immunohistochemistry experiments were performed 24 h after the last injection. (**b**) Immunohistochemistry revealed an increase of EAAT2-positive puncta in striatal slices from ceftriaxone-injected rats than in slices from saline-injected rats. Scale bar: 10 μm. (**c**) Example of LTP induced by 100 post-pre pairings recorded in a saline-injected rat. Top, EPSC strength before and after pairings. Bottom, time course of Ri (baseline: 50±0.2MΩ; 50-60 min after pairings: 48±0.2MΩ; change of -5%). (**d**) Example of LTD induced by 100 pre-post pairings recorded in a saline-injected rat (Ri, baseline: 60±0.3MΩ; 50-60 min after pairings: 61±0.4MΩ; change of 0.4%). (**e**) Averaged time-course of experiments performed in saline-injected rats, showing bidirectional STDP: LTP was induced for post-pre ($-30<\Delta t_{STDP}<0$ ms) and LTD for pre-post ($0<\Delta t_{STDP}<+30$ ms) pairings. (**f**) Example of the lack of plasticity observed with 100 post-pre pairings recorded from a ceftriaxone-treated rat. Top, EPSC strength was not significantly different before and after pairings. Bottom, time course of Ri (baseline: 75±0.3MΩ; 40-50 min after pairings: 69±0.5MΩ; change of -8%). (**g**) Example of the absence of plasticity observed with 100 pre-post pairings from a ceftriaxone-treated rat. EPSC strength did not differ significantly before and after pairings (Ri, baseline: 149±0.6MΩ; 40-50 min after pairings 163±10MΩ; change of 10%). (**h**) Averaged time course of experiments performed on ceftriaxone-treated rats, showing an absence of STDP for both post-pre and pre-post pairings. **(i)** Time window for long-term synaptic strength for post-pre and pre-post pairings ($-30<\Delta t_{STDP}<+30$ ms) in saline- and ceftriaxone-treated rats. Synaptic strength was assessed 45-60 min after pairings (empty circles: individual neurons; gray or purple circles: average). Bidirectional plasticity was induced in saline-injected rats, whereas no plasticity was observed in ceftriaxone-treated rats.
Insets correspond to the average of 60 EPSCs during baseline and 1 hour after STDP pairings. Error bars represent the SD (except in panel i: SEM). *: $p<0.05$; **: $p<0.01$; ***: $p<0.001$; ns: not significant.

Figure 7. Schematic representation of the impact of astrocytes, via their EAAT2 expression, on Hebbian plasticity in the striatum

(**a**) Transient EAAT2 blockade prevents the expression of STDP, instead favoring non-Hebbian plasticity (timing-independent LTP). LTP is mediated by extrasynaptic NMDAR and LTD is dependent on the activation of striatal GABAergic microcircuits. In these conditions, unpaired activity is sufficient to induce LTP. (**b**) The physiological expression of EAAT2 allows the emergence of Hebbian plasticity (bidirectional STDP). Pairings on either side of the synapse induced NMDAR-mediated t-LTP (and non-dependent on extrasynaptic NMDARs) and endocannabinoid-mediated t-LTD. (**c**) EAAT2 overexpression by limiting glutamate spillover prevents STDP expression.

Thus, the efficiency of glutamate uptake, most through astrocytic EAAT2, gates the expression of Hebbian synaptic plasticity in the striatum.

Supplementary Figure Legends

Supplementary Figure 1. The transient inhibition of EAAT2 by WAY-213,613 disrupts STDP

(**a-c**) WAY-213,613 application had no effect on the changes in synaptic efficacy estimated from WAY-213,613 washout (example in a, and averaged time-course of experiments in b and c). The brief application of WAY-213,613 induced a non-significant transient decrease in EPSC amplitude, with no change in Ri. The effect of WAY-213,613 on synaptic transmission was, thus, compatible with the estimation of long-term synaptic efficacy changes. (**d**) Example of the lack of plasticity observed with 100 pre-post pairings (Δt_{STDP}=+44 ms) during the transient blockade of EAAT2 with WAY-213,613 (50 μM for 5 min, gray area). Top, EPSC strength before and after pairings. Bottom, time course of Ri (baseline, 79±1MΩ; 50-60 min after pairings, 81±0.2MΩ; change of 2%). (**e**) Averaged time-course of experiments with a transient blockade of EAAT2 with WAY-213,613 (50 μM), with the absence of plasticity induction for pairings at -70<Δt_{STDP}<+70 ms. (**f**) Example of LTD induced by 100 pre-post pairings (Δt_{STDP}=+20 ms) with a transient blockade of EAAT2 with WAY-213,613 (100 μM). Top, EPSC strength before and after pairings. Bottom, time course of Ri (baseline, 84±0.2MΩ; 50-60 min after pairings, 92±0.2MΩ; change of 11%). (**g**) Averaged time-course of experiments with a transient blockade of EAAT2 with WAY-213,613 (50 μM), with no significant induction of plasticity for pairings at -70<Δt_{STDP}<+70 ms. However, it should be noted that LTD was more frequent (5/8 cells) when induced with 100 μM WAY-213,613 than when induced with 50 μM WAY-213,613 (1/5 cells). (**h**) Example of LTP induced by 100 post-pre pairings (Δt_{STDP}=-200 ms) with a transient blockade of EAAT2 with WAY-213,613 (50 μM) (Ri, baseline: 54±0.3MΩ; 50-60 min after pairings: 52±0.3MΩ; change of -4%). (**h**) Example of LTP induced by 100 post-pre pairings (Δt_{STDP}=-200 ms) with a transient blockade of EAAT2 with WAY-213,613 (50 μM). Top, EPSC strength before and after pairings. Bottom, time course of Ri (baseline, 54±0.3MΩ; 50-60 min after pairings, 52±0.3MΩ; change of -4%). (**i**) Averaged time-course of experiments with transient EAAT2 blockade with WAY-213,613 during pairings, inducing LTP for Δt_{STDP}=±200 ms pairings.

Insets correspond to the average of 60 EPSCs during baseline and 1 hour after STDP pairings. Error bars represent the SD. *: p<0.05; ***: p<0.001. ns: not significant.

Supplementary Figure 2. The plasticity observed under EAAT2 blockade is not dependent on postsynaptic DHK-induced depolarization

(**a, b**) Averaged time-course of STDP experiments with the recorded MSN maintained at -80 mV by intracellular current injection during the STDP pairings. LTD and LTP were induced with pairings at -70<Δt_{STDP}<+70 ms (**a**) and Δt_{STDP}=±200 ms (**b**), respectively. The prevention of DHK-induced depolarization did not impair the plasticity observed when MSN was depolarized. (**c**, **d**)

Summary of STDP experiments in which the recorded MSN was held at -50 mV, performed with pairings at $-70<\Delta t_{STDP}<+70$ ms (**c**) and $\Delta t_{STDP}=\pm 200$ ms (**d**), respectively; in these conditions, only LTD was observed.

Insets correspond to the average of 60 EPSCs during baseline and 1 hour after STDP pairings. Error bars represent the SD. *: $p<0.05$; **: $p<0.01$.

Supplementary Figure 3. LTD under transient EAAT2 blockade is not dependent on the activation of CB_1Rs, type I/II mGluRs or NMDARs

(**a**) LTD under transient EAAT2 blockade for pairings at $-70<\Delta t_{STDP}<+70$ ms was not dependent on CB_1R activation, because AM251 (3 μM) failed to prevent LTD. (**b**) LTD was not mediated by type-I/II mGluR or NMDAR, because MCPG (500 μM) or D-AP5 (50 μM) failed to block LTD. (**c**) The LTP observed with transient EAAT2 blockade during pairings for $-70<\Delta t_{STDP}<+70$ ms in the presence of mibefradil was NMDAR-mediated, because it was prevented by the application of mibefradil (20 μM) together with D-AP5 (50 μM).

Insets correspond to the average of 60 EPSCs during baseline and 1 hour after STDP pairings. Error bars represent the SD. *: $p<0.05$; **:$p<0.01$; ***: $p<0.001$; ns: not significant.

Supplementary Figure 4. t-LTP in control conditions is not dependent on extrasynaptic NMDARs

Memantine (10 μM) did not affect t-LTP for pairings at $-30<\Delta t_{STDP}<0$ ms.

Insets correspond to the average of 60 EPSCs during baseline and 1 hour after STDP pairings. Error bars represent the SD. *: $p<0.05$.

Supplementary Figure 5. Under EAAT2 blockade, postsynaptic subthreshold activity fails to induce plasticity

(a) Protocol consisting of postsynaptic subthreshold depolarization without paired presynaptic stimulation repeated 100 times at 1 Hz, under EAAT2 blockade. (b) This protocol did not induce plasticity.

ns: not significant.

Supplementary Figure 6. The electrophysiological properties of MSNs and corticostriatal transmission did not differ between saline- and ceftriaxone-injected rats

(**a**, **b**) The passive electrophysiological properties, RMP (**a**) and Ri (**b**), of MSNs did not differ between saline- and ceftriaxone-injected rats (n=20 in both groups). (**c**) Characteristic voltage responses of MSNs from saline- and ceftriaxone-injected rats to a series of 500 ms current pulses.

(**d**) The rheobase of MSNs did not differ between saline- and ceftriaxone-injected rats (*n*=20 in both groups). (**e**) Number of elicited spikes plotted as a function of 500 ms current pulses of increasing amplitude in saline- and ceftriaxone-injected rats. No difference was found between the two groups. (**f**) Paired-pulse ratio at 20 Hz induced facilitation did not differ between saline- and ceftriaxone-injected rats (*n*=13 and *n*=16, respectively). (**g**) Traces of sPSCs from saline- and ceftriaxone-injected rats. (**h**, **i**) No difference was found in the amplitude (**h**) and frequency (**i**) of sPSCs between the two groups (*n*=13 and *n*=12, respectively).
ns: not significant.

Figure 1

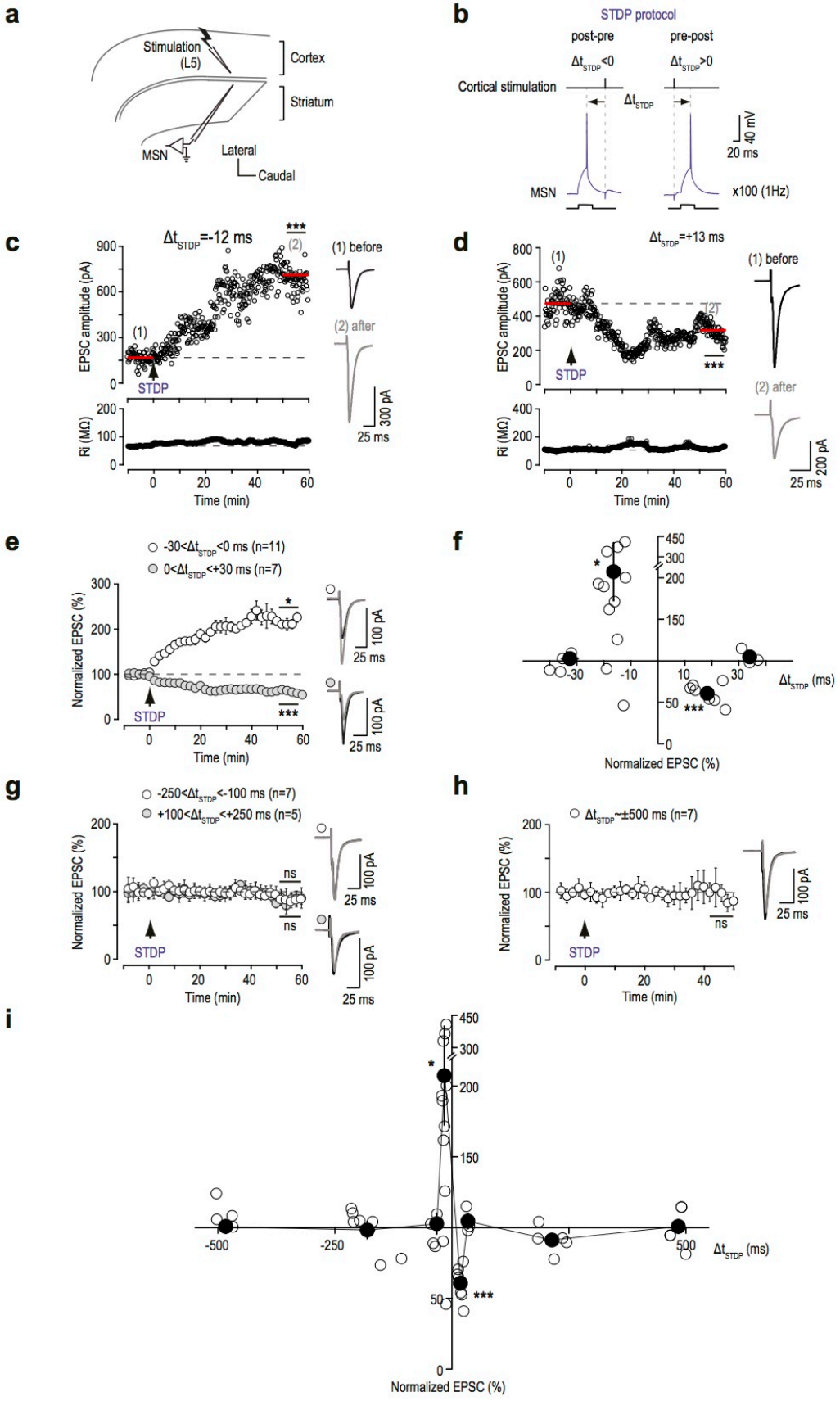
a
Stimulation (L5)
Cortex
Striatum
MSN
Lateral
Caudal
b
STDP protocol
post-pre
pre-post
Δt_STDP<0
Δt_STDP>0
Cortical stimulation
Δt_STDP
40 mV
20 ms
MSN
x100 (1Hz)
c
Δt_STDP=-12 ms
EPSC amplitude (pA)
(1)
(2)
STDP
Ri (MΩ)
Time (min)
(1) before
(2) after
300 pA
25 ms
d
Δt_STDP=+13 ms
EPSC amplitude (pA)
(1)
(2)
STDP
Ri (MΩ)
Time (min)
(1) before
(2) after
200 pA
25 ms
e
-30<Δt_STDP<0 ms (n=11)
0<Δt_STDP<+30 ms (n=7)
Normalized EPSC (%)
STDP
Time (min)
100 pA
25 ms
f
Δt_STDP (ms)
Normalized EPSC (%)
g
-250<Δt_STDP<-100 ms (n=7)
+100<Δt_STDP<+250 ms (n=5)
Normalized EPSC (%)
ns
STDP
Time (min)
100 pA
25 ms
h
Δt_STDP~±500 ms (n=7)
Normalized EPSC (%)
ns
STDP
Time (min)
100 pA
25 ms
i
Δt_STDP (ms)
Normalized EPSC (%)

Figure 2

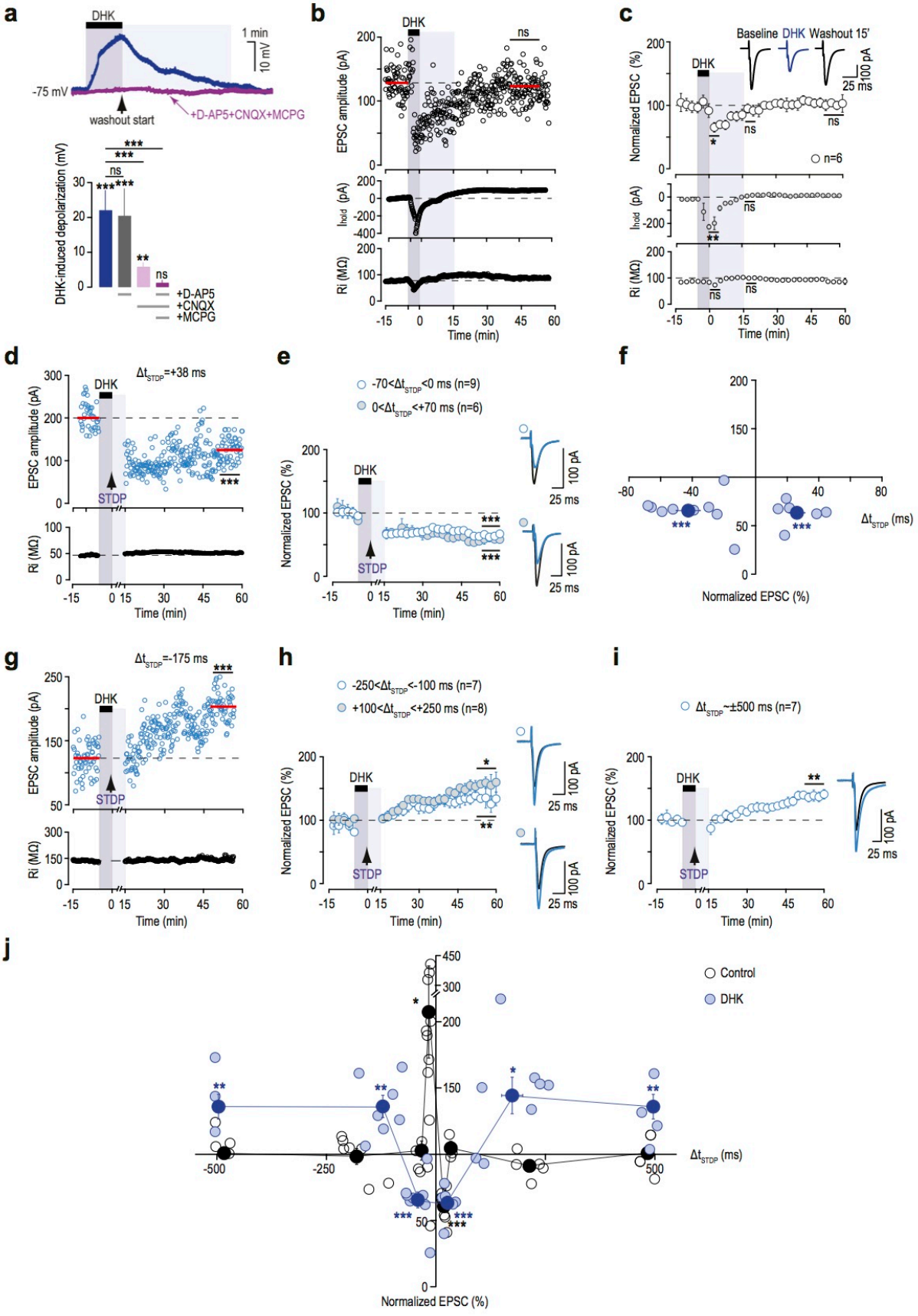
a
DHK
1 min
10 mV
-75 mV
washout start
+D-AP5+CNQX+MCPG
DHK-induced depolarization (mV)
+D-AP5
+CNQX
+MCPG
b
DHK
ns
EPSC amplitude (pA)
Ihold (pA)
Ri (MΩ)
Time (min)
c
Baseline DHK Washout 15'
100 pA
25 ms
Normalized EPSC (%)
n=6
d
Δt_STDP=+38 ms
STDP
e
-70<Δt_STDP<0 ms (n=9)
0<Δt_STDP<+70 ms (n=6)
f
Δt_STDP (ms)
Normalized EPSC (%)
g
Δt_STDP=-175 ms
h
-250<Δt_STDP<-100 ms (n=7)
+100<Δt_STDP<+250 ms (n=8)
i
Δt_STDP~±500 ms (n=7)
j
Control
DHK
Δt_STDP (ms)
Normalized EPSC (%)

Figure 3

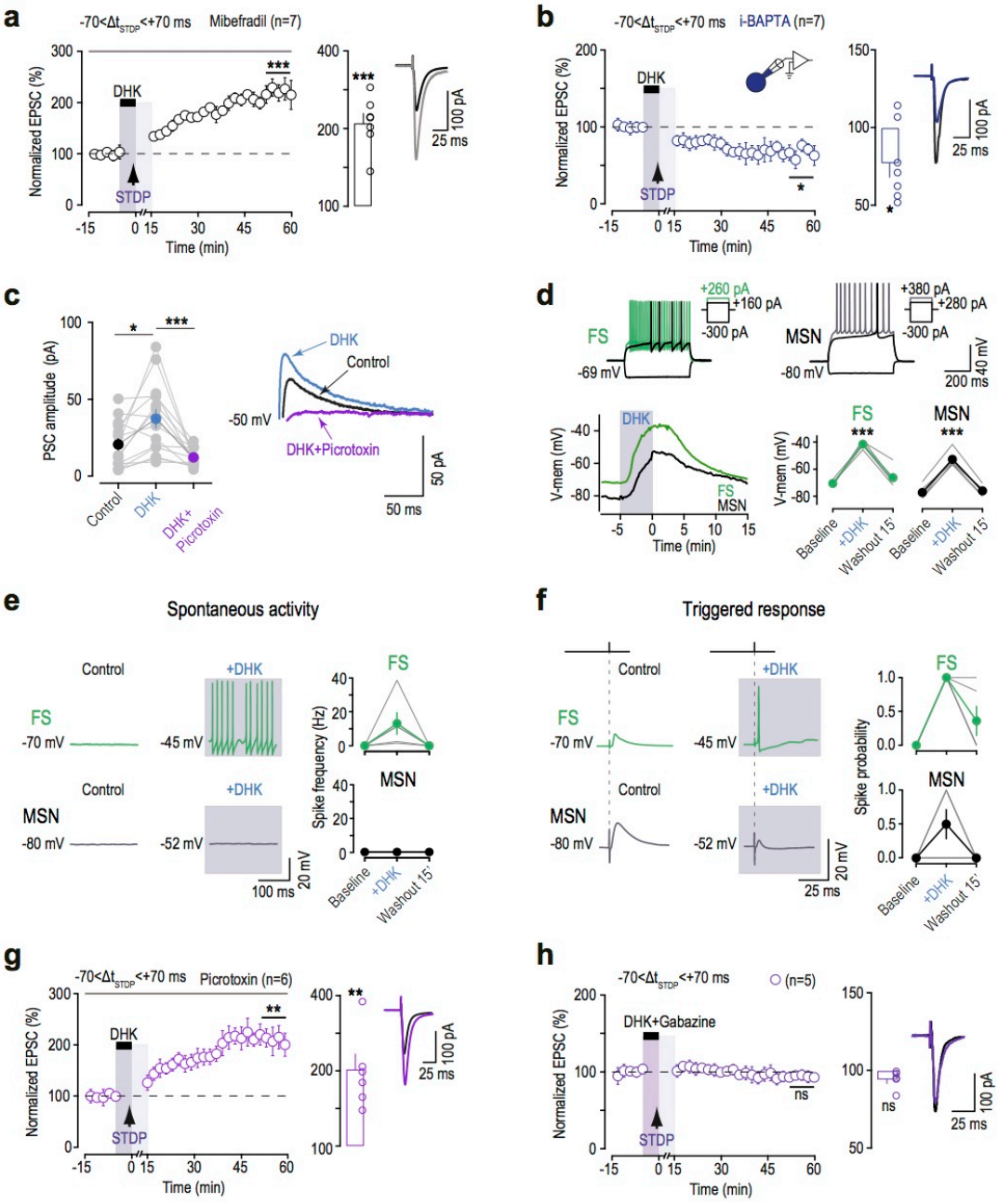
a
-70<Δt_STDP<+70 ms Mibefradil (n=7)
Normalized EPSC (%)
DHK
STDP
Time (min)
***
100 pA
25 ms
b
-70<Δt_STDP<+70 ms i-BAPTA (n=7)
Normalized EPSC (%)
DHK
STDP
Time (min)
*
100 pA
25 ms
c
PSC amplitude (pA)
Control
DHK
DHK+ Picrotoxin
-50 mV
DHK
Control
DHK+Picrotoxin
50 pA
50 ms
d
FS
+260 pA
+160 pA
-300 pA
-69 mV
MSN
+380 pA
+280 pA
-300 pA
-80 mV
40 mV
200 ms
V-mem (mV)
DHK
FS
MSN
Time (min)
Baseline
+DHK
Washout 15'
e
Spontaneous activity
Control
+DHK
FS
-70 mV
-45 mV
MSN
-80 mV
-52 mV
20 mV
100 ms
Spike frequency (Hz)
Baseline
+DHK
Washout 15'
f
Triggered response
Control
+DHK
FS
-70 mV
-45 mV
MSN
-80 mV
-52 mV
20 mV
25 ms
Spike probability
Baseline
+DHK
Washout 15'
g
-70<Δt_STDP<+70 ms Picrotoxin (n=6)
Normalized EPSC (%)
DHK
STDP
Time (min)
**
100 pA
25 ms
h
-70<Δt_STDP<+70 ms (n=5)
DHK+Gabazine
Normalized EPSC (%)
STDP
Time (min)
ns
100 pA
25 ms

Figure 4

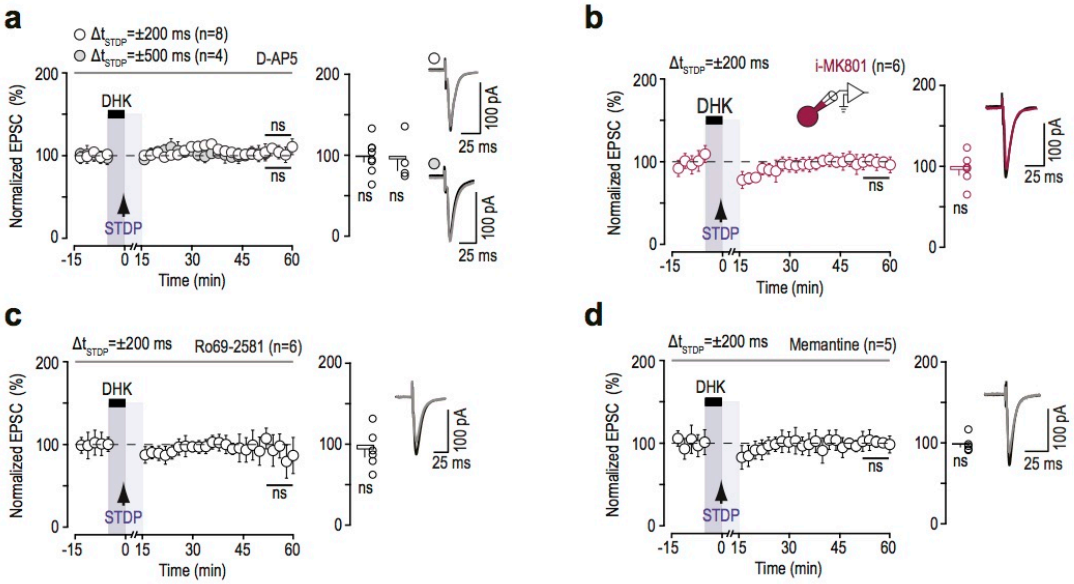
a
Δt_STDP=±200 ms (n=8)
Δt_STDP=±500 ms (n=4)
D-AP5
DHK
STDP
ns
Normalized EPSC (%)
Time (min)
100 pA
25 ms
b
Δt_STDP=±200 ms
i-MK801 (n=6)
c
Δt_STDP=±200 ms
Ro69-2581 (n=6)
d
Δt_STDP=±200 ms
Memantine (n=5)

Figure 5

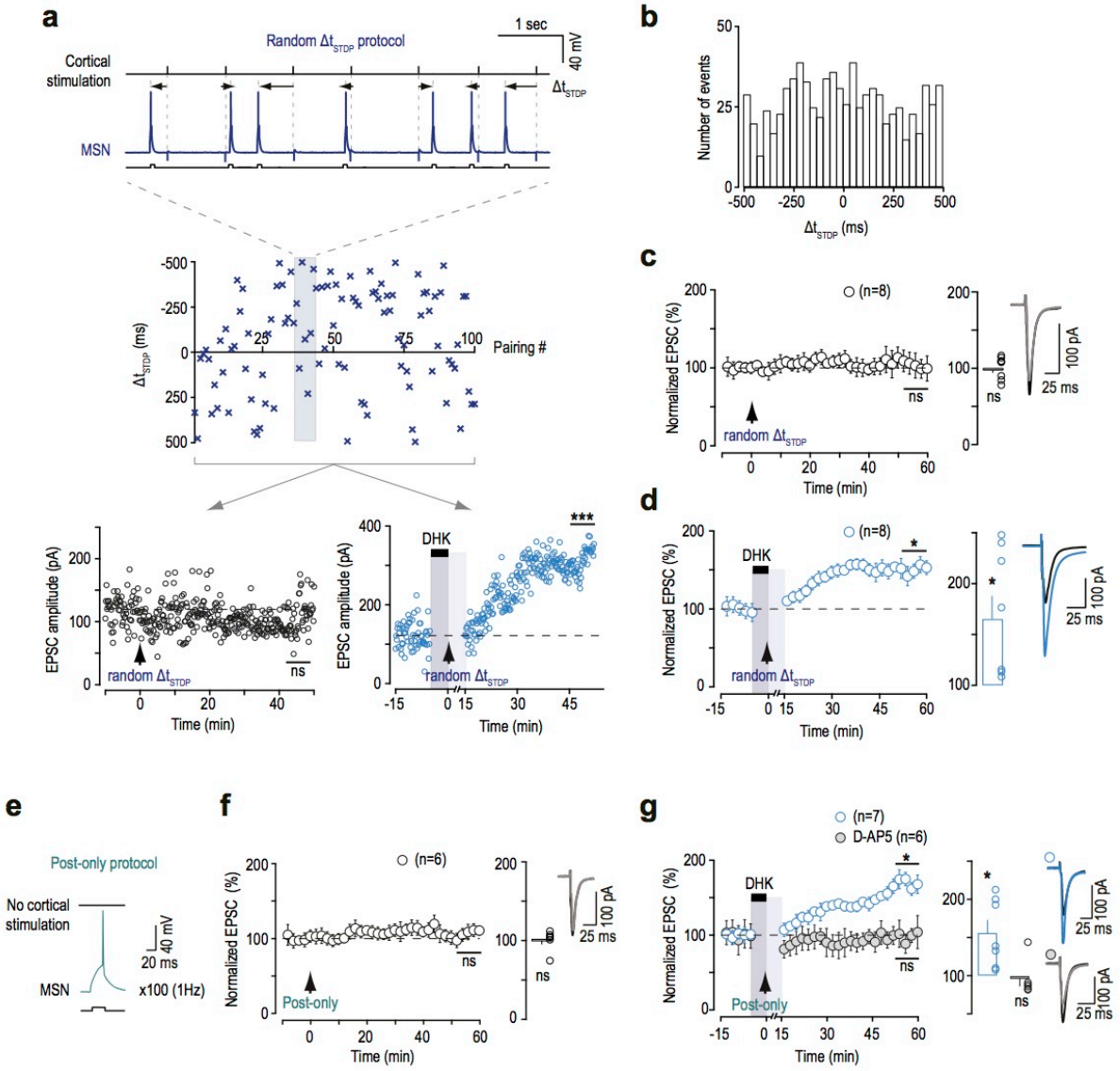
a
Random Δt_STDP protocol
1 sec
40 mV
Cortical stimulation
MSN
Δt_STDP
Δt_STDP (ms)
Pairing #
EPSC amplitude (pA)
random Δt_STDP
ns
Time (min)
DHK
***
b
Number of events
Δt_STDP (ms)
c
(n=8)
Normalized EPSC (%)
100 pA
25 ms
d
*
e
Post-only protocol
No cortical stimulation
40 mV
20 ms
MSN
x100 (1Hz)
f
(n=6)
Post-only
g
(n=7)
D-AP5 (n=6)

Figure 6

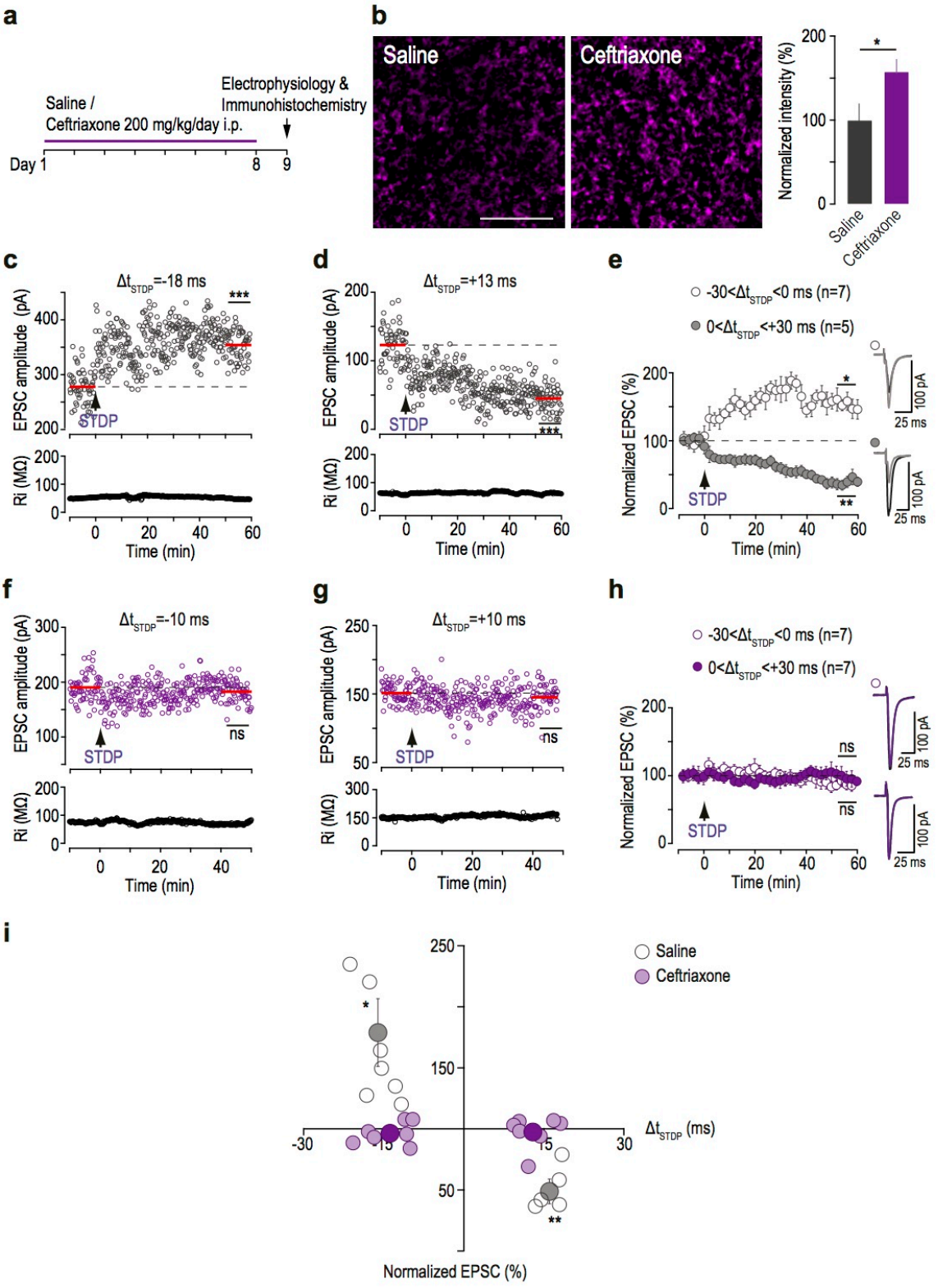
a
Saline /
Ceftriaxone 200 mg/kg/day i.p.
Electrophysiology &
Immunohistochemistry
Day 1
8
9
b
Saline
Ceftriaxone
Normalized intensity (%)
200
100
0
*
Saline
Ceftriaxone
c
Δt_STDP=-18 ms
***
EPSC amplitude (pA)
400
300
200
STDP
Ri (MΩ)
200
100
0
0
20
40
60
Time (min)
d
Δt_STDP=+13 ms
EPSC amplitude (pA)
200
100
0
STDP
***
Ri (MΩ)
200
100
0
0
20
40
60
Time (min)
e
○ -30<Δt_STDP<0 ms (n=7)
● 0<Δt_STDP<+30 ms (n=5)
Normalized EPSC (%)
200
100
0
*
**
STDP
100 pA
25 ms
100 pA
25 ms
0
20
40
60
Time (min)
f
Δt_STDP=-10 ms
EPSC amplitude (pA)
300
200
100
STDP
ns
Ri (MΩ)
200
100
0
0
20
40
Time (min)
g
Δt_STDP=+10 ms
EPSC amplitude (pA)
250
150
50
STDP
ns
Ri (MΩ)
300
150
0
0
20
40
Time (min)
h
○ -30<Δt_STDP<0 ms (n=7)
● 0<Δt_STDP<+30 ms (n=7)
Normalized EPSC (%)
200
100
0
ns
ns
STDP
100 pA
25 ms
100 pA
25 ms
0
20
40
60
Time (min)
i
250
150
50
*
**
-30
-15
15
30
Δt_STDP (ms)
Saline
Ceftriaxone
Normalized EPSC (%)

Figure 7

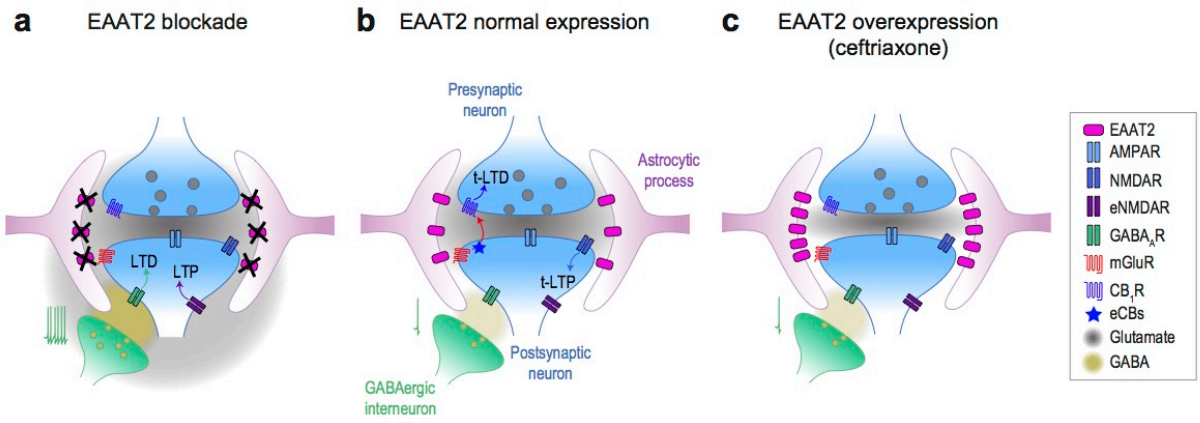

no STDP
timing-independent LTP
GABA-dependent LTD

non-Hebbian plasticity

bidirectional STDP
timing-dependent LTP and LTD

Hebbian plasticity

no STDP
no plasticity

Supplementary figure 1

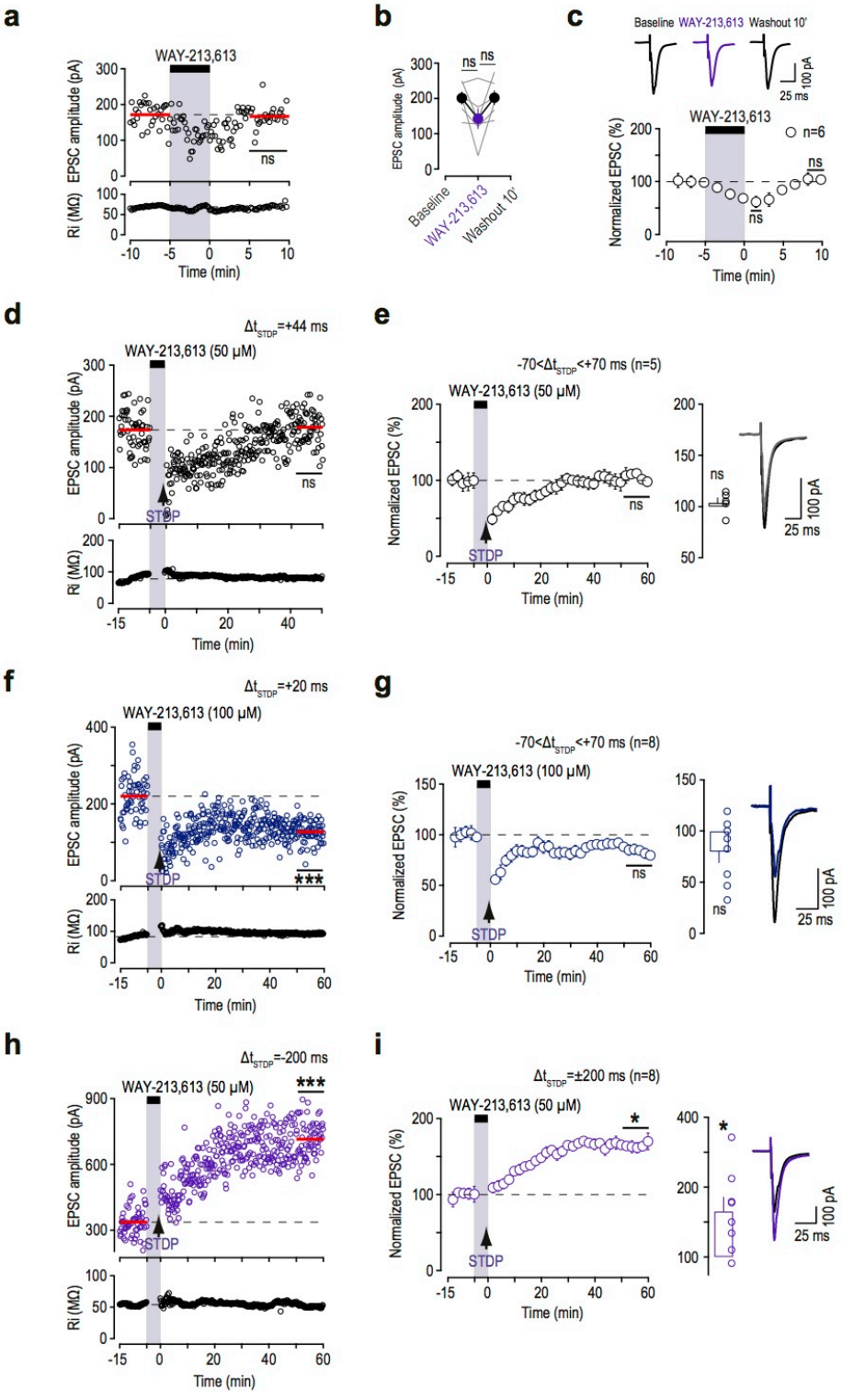

Supplementary figure 2

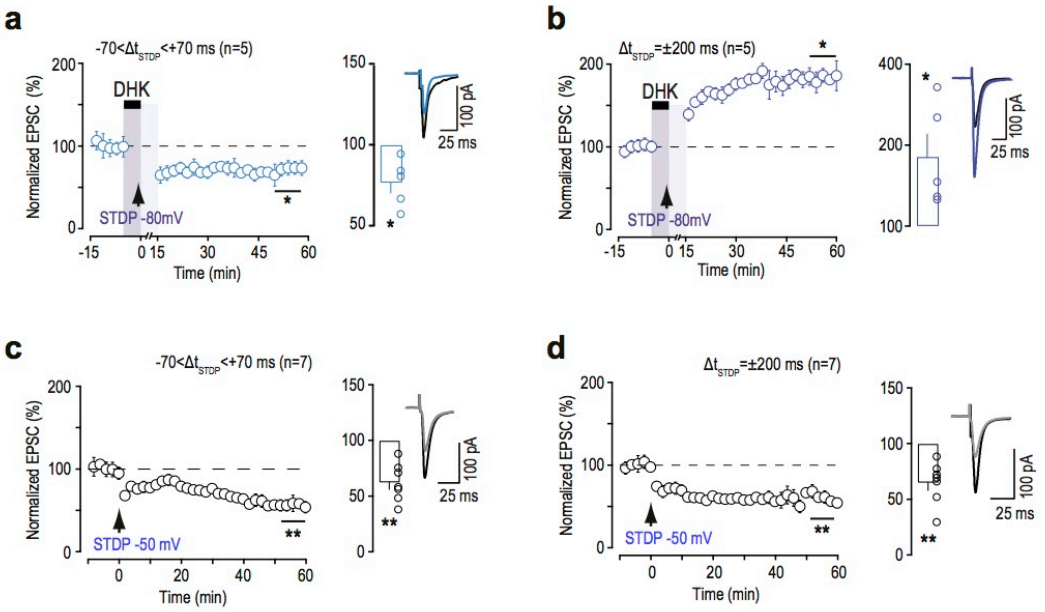

Supplementary figure 3

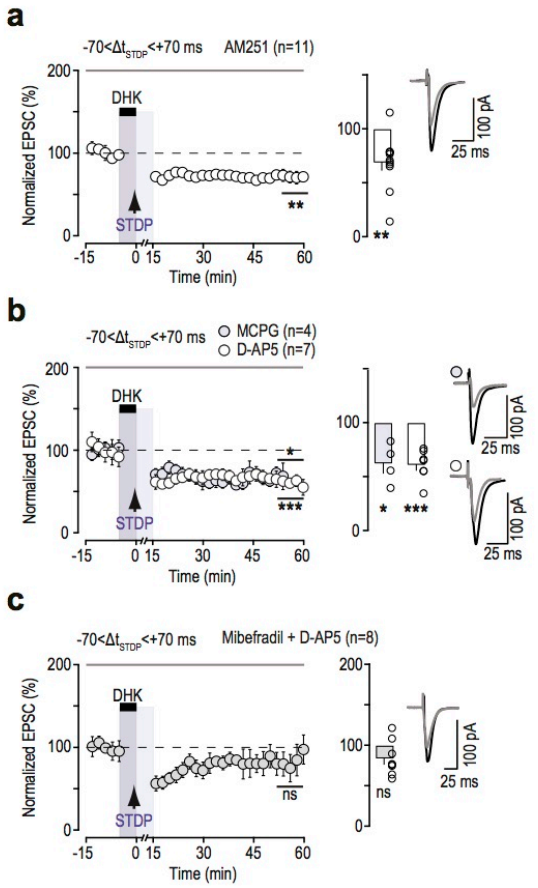

Supplementary figure 4

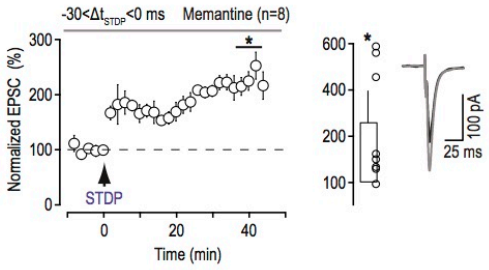

Supplementary figure 5

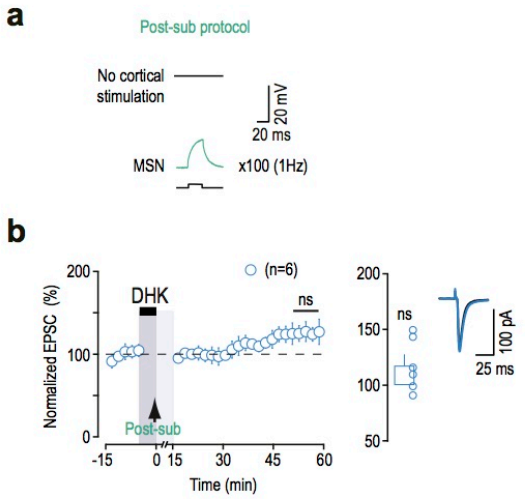

Supplementary figure 6

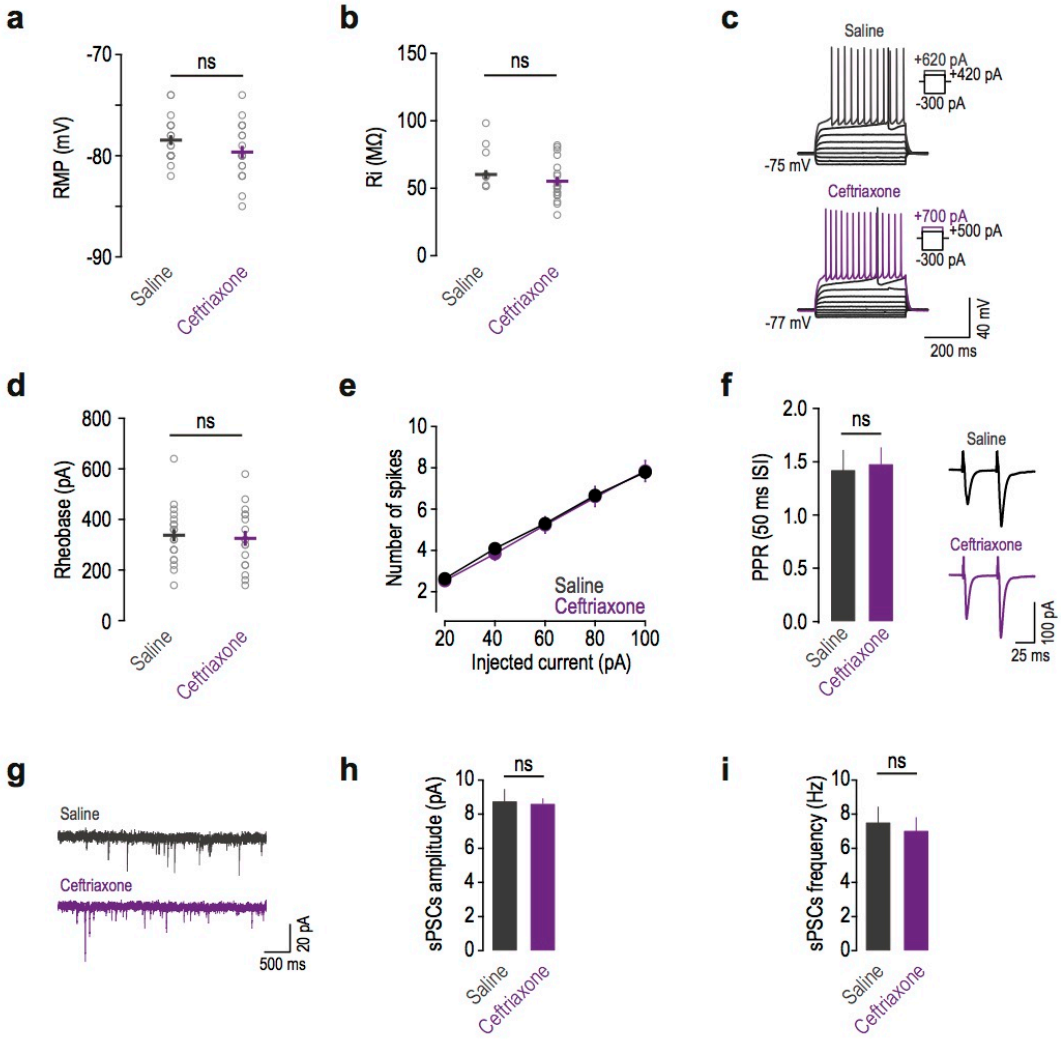

GENERAL DISCUSSION

GENERAL DISCUSSION

I. ARTICLE 1

Developmental control of spike-timing-dependent plasticity polarity by tonic GABAergic signaling in striatum

Valtcheva S*, Paillé V*, Ganagarossa G, Perez S, Dembitskaya Y, Fino E and Venance L

(in preparation)

1 - Comparison with previous studies

(1) STDP polarity

Temporally asymmetric and unidirectional learning rules governing changes in synaptic strength have been rarely described (*see Introduction, Part III - STDP*) and therefore their computation advantages are poorly understood. Associative long-term plasticity (t-LTP or t-LTD) can occur for a fixed temporal order of pairings, whereas the reverse sequence of pairings fails to influence synaptic efficacy. Such timing rules exist in the mammalian CNS (Tzounopoulos et al. 2004; Shin et al. 2006; Tzounopoulos et al. 2007; Cui et al. 2015; Cui et al. 2016) and PNS (Li & Baccei 2016); as well as in the electrosensory lobe of the electric fish (Bell et al. 1997).

Both unidirectional asymmetric Hebbian and anti-Hebbian plasticity rules have been described with the specificity that mainly pre-post pairings are efficient to trigger plasticity. Pre-post pairings trigger t-LTP in the case of unidirectional asymmetric Hebbian STDP (Shin et al. 2006; Li & Baccei 2016). Conversely, the same pre-post order triggers t-LTD in the case of unidirectional asymmetric anti-Hebbian STDP (Bell et al. 1997; Tzounopoulos et al. 2004; Tzounopoulos et al. 2007; Li & Baccei 2016). Just recently, unidirectional anti-Hebbian t-LTP, induced for post-pre pairings, has been found at corticostriatal synapses (Cui et al. 2015; Cui et al. 2016).

With respect to previous studies, the corticostriatal STDP at early developmental stages described in our study (*see Results – Article 1*), has remarkable characteristics in that it occurs exclusively for post-pre pairings, resulting in tLTD.

(2) STDP during development

Developmental regulation of STDP expression has been previously investigated in the cerebral cortex. Developmental switch in STDP occurs at the end of the second postnatal week in

somatosensory cortex, when unidirectional symmetric STDP (t-LTP only) at L4–L2/3 cortical synapses is transformed to bidirectional Hebbian STDP (Itami & Kimura 2012). In addition, thalamocortical terminals to L2/3 pyramidal cells display unidirectional order-independent STDP (t-LTP only) that is transformed to t-LTD only between the first and the second postnatal week (Itami et al. 2016).

Nevertheless, to our knowledge, our current study is the first to assess the contribution of tonic GABAergic signaling in the developmental switch of STDP timing rule. We showed that tonic GABAergic component is absent in the immature striatum and promoting it, partially restores anti-Hebbian STDP in young animals. More importantly, preventing tonic GABAergic signaling in juvenile animals results in Hebbian t-LTD similar to what we observed in young animals (*see Results – Article 1*).

One study investigated the contribution of tonic GABA for STDP expression in hippocampus exclusively in juvenile animals (Groen et al. 2014). In this case, tonic GABAergic inhibition regulates dendritic bAP in juvenile, but not in younger animals. Moreover, blockade of the tonic GABAergic component leads to higher threshold for STDP induction in juvenile animals but without changing the polarity of STDP (Groen et al. 2014).

Therefore, our study is the first to report a flip in STDP polarity along development and that this transition is operated by maturation of the tonic GABAergic signaling.

(3) Possible explanations of the observed results

Our results show that the reversal potential of the $GABA_AR$-mediated current ($E_{GABA(A)}$), although depolarizing in both cases, is different in young compared to juvenile animals (-35 mV vs -60 mV) (Paillé et al. 2013) (*see Results – Article 1*). However, the RMP of MSNs in young animals is also shifted to more depolarized values (data not shown). Therefore, the shunting inhibition operated by GABAergic signaling should increase the membrane conductance in an identical manner. This will result in a similar reduction in the membrane time constant and therefore less temporal integration of inputs in both young and juvenile animals. This suggests that the information transfer regarding temporal coding at early developmental stages is expected to be similar in mature animals. Therefore, the change in $E_{GABA(A)}$ alone cannot account for the observed changes in the corticostriatal STDP rule.

The apparent resistance of corticostriatal synapses to t-LTP may be restricted to the STDP pairing protocol used in our studies (*see Methods*). Therefore, it is not excluded that other activity-

dependent regimes such as high-frequency stimulation or theta-burst stimulation; or – alternatively – increasing the rate and/or number of STDP pairings, would be efficient in unraveling corticostriatal LTP in the immature brain. In line with that, unopposed t-LTD at corticostriatal synapses would eventually result in the saturation of these synapses and a loss in the ability of MSNs to efficiently encode cortical information. In this case, homeostatic mechanisms could contribute to the scaling down of synaptic connections.

2 - Physiological relevance

A central question is what would be the computational advantage of such asymmetric learning rule early in development?

The spontaneous activity of the brain provides a context within which incoming sensory signals are processed. This emphasizes the importance of establishing a certain degree of filtering which is mainly operated by GABAergic signaling. GABAergic networks mature parallel to the stabilization of synaptic connections and play an important role in maintaining the excitation/inhibition balance. Early in development, when the tonic GABAergic component is absent, the filtering of arriving inputs would be weaker and thus the signal-to-noise ratio would be decreased. Due to this noisy environment, synaptic connections would tend to be preferentially depressed by Hebbian t-LTD. This could contribute to the filtering of irrelevant inputs and narrowing the repertoire of pertinent information, thus helping network maturation.

Specifically, at the level of the striatum, presynaptic activity from the thalamus representing upcoming sensory inputs, followed by cortical activity, will result in a post-pre sequence. Considering our results, this temporal order of activation will depress corticostriatal synapses at the level of the MSNs. Nevertheless, corticostriatal STDP exhibit marked cell-specific features (Fino et al. 2005; Fino et al. 2008; Fino et al. 2009) and thus, the striatal output is shaped by the interplay between the strengthening and weakening of synapses onto different neuronal populations. Therefore, it would be difficult to speculate about the net result of Hebbian t-LTD on striatal output early in development, without exploring STDP expression in other neuronal types (GABAergic and cholinergic interneurons for example). In addition, thalamo-striatal STDP displays Hebbian features (unpublished data) in juvenile and adult animals, thus being ‘complementary’ to anti-Hebbian STDP at corticostriatal synapses, but it still remains to explore its developmental regulation.

3 – Open questions

(1) Coincidence detectors

We showed that corticostriatal Hebbian t-LTD occurs in young animals. An appealing question would be what molecular mechanisms underlie this form of plasticity? Bidirectional anti-Hebbian STDP at corticostriatal synapses in juvenile animals relies on two distinct coincidence detectors (Fino et al. 2010). In addition, these signaling pathways are preserved in the absence of GABAergic signaling (Paillé et al. 2013). More precisely, t-LTP is mediated by NMDARs, and t-LTD requires PLCβ and (IP3R)-gated calcium stores resulting in retrograde endocannabinoid signaling (Fino et al. 2010). In addition, endocannabinoids can trigger both anti-Hebbian t-LTP and t-LTD in striatum (Cui et al. 2015; Cui et al. 2016). Therefore, it would be interesting to test weather endocannabinoids can also gate Hebbian t-LTD in the immature striatum.

(2) Sources of tonic inhibition

The origins of tonic GABA have been subject to a debate (Glykys & Mody 2007a). Vesicular release and spillout of GABA from synaptic to extrasynaptic compartments have been suggested (Glykys & Mody 2007b). Astrocytes have been also shown to release GABA through anion-channels (Lee et al. 2010). Considering the vesicular origin of tonic GABA, its absence in young animals could be due either (1) to a significantly lower degree of spillout; (2) incomplete maturation of inhibitory interneurons (Chesselet et al. 2007); or (3) to a different localization of $GABA_AR$s where the sensing of tonic GABA would be less efficient. Astrocytic release on the other hand, would imply that (1) astrocytic wrapping of synapses is weaker, or (2) the mechanisms of GABA release by astrocytes are immature. In addition the expression of GATs is developmentally regulated (Conti et al. 2004). It would be thus tempting to explore the possible reasons for the absence of tonic GABA at early developmental stages and potentially try to induce bidirectional anti-Hebbian STDP in young animals by playing with these mechanisms.

II. ARTICLE 2

Astrocytes gate Hebbian synaptic plasticity in striatum

Valtcheva S and Venance L

(Nat Commun, in revision)

1 – Novelty of the study

Few other previous studies have addressed the effects of glutamate uptake in the expression of synaptic plasticity. All reports in the current literature have been focused on rate-coded plasticity, induced with low- and high-frequency stimulation (LFS and HFS) or theta-burst stimulation (TBS), showing that rate-coded plasticity is sensitive to alterations of glutamate uptake (Katagiri et al. 2001; Pinard et al. 2003; Massey et al. 2004; Wang et al. 2006; Omrani et al. 2009; Scimemi et al. 2009). Nevertheless, our study is the first one to focus on time-coded plasticity using explicitly a synaptic Hebbian learning rule such as STDP, which is currently viewed as the finest way to trigger physiological plasticity and could account for experience-dependent changes in neural networks (Feldman 2012).

Our study constitutes the first report demonstrating not only that astrocytic glutamate uptake allows the emergence and the expression of STDP but also that it prevents the occurrence of aberrant plasticity. In all previous studies, glutamate uptake has been shown to control in different extent rate-coded plasticity but our study is the first to shows that EAAT2 glutamate uptake is responsible for the shift from STDP to other form of plasticity which is not timing-dependent. The role of EAAT2 has never been assessed in STDP paradigm, which strongly differs from frequency-based protocols (HFS, LFS, TBS) and which constitutes a Hebbian synaptic learning rule relying on precise time coding. Since its discovery, STDP has been attracting substantial interest in experimental (Feldman 2012) as well in computational neuroscience (Clopath et al. 2010; Costa et al. 2015).

The key point of our study is coming from a pending and debated question: how STDP emerge out of distributed neural activity. Our findings demonstrate that EAAT2 sets the glutamate dynamics allowing for optimal temporal contingency between pre- and postsynaptic activity necessary for STDP emergence and highlight the role of astrocytes as gatekeepers for Hebbian synaptic plasticity.

Up to our knowledge, there are only few studies investigating the effects of glutamate uptake on long-term synaptic plasticity. It has been reported that a long lasting inhibition of glutamate uptake precludes HFS-LTP in spinal cord (Wang et al. 2006), enhances HFS-LTD at neuromuscular junction (Pinard et al. 2003), has a permissive role for the expression of LFS-LTD in cerebral cortex

(Massey et al. 2004) or induces heterosynaptic LTP in amygdala (Tsvetkov et al. 2004). Note that Pinard et al., Tsvetkov et al., or Massey et al. studies tested the role of glutamate uptake in general, not specifically EAAT2, by using unspecific glutamate transporter antagonist (TBOA). Using genetic approach, impairment of HFS-LTD has been reported in hippocampus from EAAT2 KO mice (Katagiri et al. 2001). Furthermore, increased EAAT2 expression has been shown to alter frequency-based plasticity such as mGluR-dependent LFS-LTD and HFS-LTP in the hippocampus (Omrani et al. 2009).

Concerning the neuronal EAAT3 transporter, it has been shown that it regulates the balance between TBS-LTP and LFS-LTD (Scimemi et al. 2009). In addition, this study shows that the structural and diffusion properties of the hippocampal neuropil are not altered by genetic deletion of EAAT3 since they are similar in wild-type and EAAT3 KO mice. The main finding of this study is that EAAT3 acts primarily as a buffer, rapidly binding glutamate and then releasing it back in the extracellular space without significantly diminishing the total amount of glutamate taken up by astrocytes.

When compared with our study, we can quote several major differences with these studies. First, we investigated the role of EAAT2 in STDP, as a canonical paradigm for synaptic Hebbian learning rule (as discussed above). We show for the first time that specific EAAT2 inhibition (with either DHK or WAY-213,613) does not only prevent STDP expression but unveils another form of plasticity, which does not rely on spike-timing. Our manuscript is the first report addressing the specific control of STDP emergence by EAAT2. Indeed, the question of the appropriate conditions of the emergence of STDP out of distributed neural activity remains unsolved. Here we show that EAAT2 is a key actor for allowing the expression of STDP and counteracting spurious plasticity. Second, a major advance of our study is that we transiently inhibit EAAT2 with two specific inhibitors (DHK or WAY-213,613) exclusively during the pairing protocol to evaluate the impact of glutamate uptake on STDP induction. This strategy allows for the first time exerting an on-off manipulation compatible with STDP study in contrast to previous reports using long-lasting drug application (Pinard et al. 2003; Massey et al. 2004; Tsvetkov et al. 2004; Wang et al. 2006) or genetic approaches (Katagiri et al. 2001) having potential long-term effects.

To our knowledge, the present results constitute the first report of the erasure of STDP to the profit of a distinct form of plasticity, which does not rely on the precise timing or order of paired activity. Astrocytes via a subtle control of glutamate uptake (and consequently glutamate spillover extent) ensures the expression of STDP. Thus, astrocytic glutamate uptake *via* EAAT2 does not only gate STDP but also places astrocytes as a key player in the establishment of Hebbian synaptic plasticity and in counteracting aberrant plasticity.

2 - Technical challenge

(1) EAAT2 transient blockade

Astrocytic glutamate uptake is involved in setting the precise timing of synaptic inputs. We therefore explored the role of EAAT2 in STDP, first by transiently inhibiting (with DHK or WAY-213,613) EAAT2 during STDP pairings. This allows an on-off manipulation compatible with STDP investigation. In contrast, as aforementioned genetic approaches (knockout) (Tanaka et al. 2008; Katagiri et al. 2001; Petr et al. 2015) and long-lasting drug applications (Pinard et al. 2003; Massey et al. 2004; Tsvetkov et al. 2004; Wang et al. 2006) would have potential long-term effects. DHK and WAY-213,613 have several advantages for studies of this type. In addition to their specificity for EAAT2 and their efficient washout, they are also non-transportable inhibitors of EAAT2, and this property prevents artificial increases in extracellular glutamate concentration due to hetero-exchange (Arriza et al. 1994; Dunlop et al. 2005). We confirmed our initial findings with DHK, by using another specific EAAT2 inhibitor, WAY-213,613 which is structurally distinct from DHK. DHK and WAY-213,613 display different mechanisms of action onto EAAT2: DHK is a substrate inhibitor (non-transported) (Arriza et al. 1994), whereas WAY-213,613 is a non-substrate inhibitor (Dunlop et al. 2005).

(2) Ceftriaxone chronic treatment

When ceftriaxone (Sigma) adapted to *in vitro* cell culture research was first used, we obtained radically different results than when ceftriaxone (Roche) specifically designed for injections was used later in our study (data not shown). In addition, marked difference in results outcome and variability was observed in both ceftriaxone and saline groups when rats were chronically I.P. injected for 8 days with either ceftriaxone (200mg/kg) or equal volumes of saline before weaning, when group housed with an adult female rat (data not shown). Notably, control corticostriatal STDP could not be reproduced in saline-injected rats before weaning when housed with their mother. Only when rats were group housed separately from their mother and injections started at least 2 days after separation and at least 8-10 days after weaning age (~P28-30), control STDP could be observed in saline-injected rats and ceftriaxone-injected rats displayed homogeneous and reproducible results. Thus, chronic daily injections regardless of the injected compound (saline or ceftriaxone) seem to be an important stress factor in young rats. Therefore, ceftriaxone treatment is efficient only in older animals.

3 - Physiological and pathological implications of the study

Although, the aim of our study was not to mimic a pathological state but rather to reveal the role of EAAT2 in the expression of Hebbian plasticity such as STDP, there are several important implications for our study in a physiological as well as in pathological frame.

We showed that EAAT2 activity in a physiological range is crucial for STDP expression. Indeed, there is a shift from STDP to a non-timing-dependent plasticity (when EAAT2 is blocked) or to the lack of plasticity (when EAAT2 is overexpressed with ceftriaxone). It indicates that timing-dependent plasticity, such as STDP, depends on different levels of EAAT2 expression or/and function.

EAAT2 expression levels can vary in different physiological states and pathological conditions:

(1) Physiological processes

EAAT2 expression varies along development with lower EAAT2 levels in early stages (Furuta et al. 1997; Ullensvang et al. 1997). Glutamate transport in the neonatal cortex is shown to be slow and therefore not limiting NMDAR activation (Hanson et al. 2015). In contrast, glutamate uptake becomes more important later in development and in the adult cortex LTD could be induced exclusively by blocking glutamate transport (Massey et al. 2004). In addition, EAAT2 expression decreases with aging (Potier et al. 2010) and EAAT2 upregulation prevents age-related cognitive decline (Pereira et al. 2014).

At corticostriatal synapses, physiological stimulation has been shown to enhance glutamate spillover (Zhang & Sulzer 2003). Interestingly, the authors show similar results by blocking EAATs with different blockers including DHK at 300µM, when monitoring the effect of such spillover on dopamine release.

Moreover, EAAT2 function can vary with experience. Astroglial wrapping of neurons controlling glutamate clearance is plastic and can be modulated by different physiological processes such as lactation or dehydration (Oliet et al. 2001; Boudaba et al. 2003; Bernardinelli et al. 2014). Sensory experience can increase the enwrapping of synapses and EAAT2 expression in sensory cortex (Genoud et al. 2006).

Negative experience also regulates EAAT2 expression. EAAT2 downregulation in striatum and habenula was found in a rat model of depression (Almeida et al. 2010; Zink et al. 2010; Cui et al. 2014; Choudary et al. 2005; Bernard et al. 2011). Blockade of EAAT2 in the prefrontal cortex induces anhedonia (John et al. 2012) and blockade of EAAT2 in amygdala alters social behavior

(Lee et al. 2007). Moreover, ceftriaxone has been reported to display antidepressant-like effects (Mineur et al. 2007). On the contrary, glucocorticoids or chronic stress either increase or decrease EAAT2 expression (Reagan et al. 2004; Popoli et al. 2012).

(2) Pathological processes

Specific knockout of astrocytic EAAT2 in dorsal striatum and an increased corticostriatal excitatory transmission leads to pathological repetitive behaviors (Aida et al. 2015). Furthermore, this phenotype was reversed by memantine (*see Results – Article 2*), which is in accordance with our results showing that memantine prevents the expression of aberrant LTP observed under EAAT2 blockade.

EAAT2 downregulation is also observed in various neurodegenerative diseases including Parkinson's, Huntington's and Alzheimer's. In this context, ceftriaxone appears as a new drug strategy for treatment (Soni et al. 2014; Fontana 2015). On the contrary, upregulation of EAAT2 is found in the prefrontal cortex of schizophrenics (Matute et al. 2005).

In addition, chronic exposure to drugs of abuse or alcohol consumption has been shown to induce a downregulation of EAAT2 in the nucleus accumbens (Scofield & Kalivas 2014). Ceftriaxone constitutes a promising tool to restore glutamate homeostasis, to reverse drug-induced plasticity and to inhibit drug seeking (Scofield & Kalivas 2014).

Thus, our results, showing the tight control of STDP by EAAT2, might be of importance for linking the expression of timing-dependent plasticity with experience or pathological states.

4 - Potential drawbacks of the study

(1) Discerning between astrocytic and neuronal EAAT2 pools

DHK and ceftriaxone treatment affect not only astrocytic pools of EAAT2 but also possibly neuronal ones. The fact that astrocytic pools of EAAT2 are certainly involved in shaping STDP (since they are responsible for 90% of the glutamate uptake, (Lehre & Danbolt 1998) does not exclude a contribution of neuronal EAAT2.

Nerve terminal uptake of glutamate has been debated and indeed constitutes a controversial issue for decades. In hippocampus, EAAT2 has been detected in axon terminals (Furness et al. 2008; Holmseth et al. 2012; Petr et al. 2015; Danbolt et al. 2016). However, the physiological role of neuronal EAAT2 remains uncertain based first on its very low level of expression (~10% of that

expressed in astrocytes) but also on its distribution in most of the axon-terminal membranes and not being concentrated in the synapses (Furness et al. 2008; Danbolt et al. 2016). Therefore, the density of neuronal EAAT2 is not expected to be sufficient to capture any major proportion of released glutamate.

Astrocytic EAAT2 deletion (Tanaka et al. 2008; Petr et al. 2015) results in dramatic effects such as excess mortality, lower body weight, and spontaneous seizures whereas no detectable neurological abnormalities could be observed with neuronal EAAT2 deletion. However, contradicting these observations, Petr et al. found that neuronal EAAT2 but not astrocytic EAAT2 contributed significantly to glutamate uptake in crude synaptosomes. It seems that this is not due to differential rates of net uptake and heteroexchange (Zhou et al. 2014). These surprising results may arise from differences in mechanical properties of the cells, i.e. neuronal membrane give more easily « synaptosomes » than astrocytes (astrocytic EAAT2 is not proportionately represented by the synaptosomal uptake assay). Indeed, an important caveat of synaptosomal preparation is that the rapid release from presynaptic terminals and reuptake by nearby transporters that characterize synaptic transmission, are both lost with biochemical uptake assays. Furthermore, the uptake of exogenous substrates in the brains slices and synaptosomal preparations mostly occurs in the nerve terminals rather than in astrocytes (Furness et al. 2008; Petr et al. 2015). An additional explanation brought by Petr and coll. is that a subset of astrocytic EAAT2 « just » bind glutamate with a low net transport (due to mitochondria distribution). It has been estimated that glutamate transporters display transport and binding/unbinding of glutamate with comparable probability (Tzingounis & Wadiche 2007). Thus, it is unlikely that neuronal EAAT2 would have a significant functional contribution (contrarily to EAAT3; see (Scimemi et al. 2009).

Furthermore, specific knockout of astrocytic EAAT2 in the dorsal striatum has a profound impact on behavior. EAAT2-KO mice have an increased corticostriatal excitatory transmission together with pathological repetitive behaviors, which are an indication of corticostriatal dysfunction (Aida et al. 2015). This finding suggests that astrocytic EAAT2 in striatum has a cardinal role in the regulation of corticostriatal information processing.

The aim of our paper was to inhibit EAAT2 exclusively during the STDP pairing protocol to examine the role of glutamate uptake onto STDP induction phase. Indeed, canonical form of STDP (100 pairings at 1Hz) is induced with protocol lasting for 100 seconds. It is the reason why we chose a pharmacological strategy (due to a lack of current tools providing possibility for an on-off manipulation of EAAT2 activity, like optogenetics for example) instead of genetic approach. However, testing the mouse lines with astrocytic or neuronal EAAT2 deletion would be highly interesting to firmly conclude concerning the putative functional role of neuronal EAAT2 in STDP.

(2) Ceftriaxone treatment

The use of ceftriaxone can be viewed as problematic because it implies a chronic treatment (8 days of daily injections) with all putative multiple concomitants of EAAT2 overexpression it can involve. However, it seems that ceftriaxone displays a quite specific effect on EAAT2 expression. To our knowledge, the only other target for ceftriaxone, which has been reported is the system x_c^- (cystine/glutamate antiporter system) (Lewerenz et al. 2013). Ceftriaxone-mediated upregulation of system x_c^- occurs by transcriptional regulation of its specific subunit xCT and is dependent on the increase of nuclear Nrf2 levels induced by ceftriaxone.

When EAAT2 expression is decreased (by cocaine for example), the system x_c^- is decreased in parallel, and vice versa. Thus the system x_c^- participates to the glutamate homeostasis and brings an opposite effect than EAAT2. However, the net effect following either up- or downregulation and the exact balance between these two systems (glutamate uptake and export) remains to be determined.

System x_c^- modulates synaptic plasticity in the nucleus accumbens (Moussawi et al. 2009). Indeed, expression of LTP and LTD of PFC afferents to the nucleus accumbens is altered in cocaine-withdrawn animals and treatment with N-acetylcysteine (a cysteine prodrug that activates system x_c^-) restores both LTP and LTD. This effect is due to an increase of extracellular glutamate and activation of mGluR2/3 and mGluR5 as a consequence of the activation of system x_c^-.

To our knowledge, all pharmacological substances used to study system x_c^- display off-target effects (all x_c^- inhibitors have cross-reactivity, especially with ionotropic and metabotropic glutamate receptors, due to their structural similarity to glutamate) making problematic the direct study of the potential involvement of system x_c^- in synaptic plasticity. Also, discerning between direct effect on system x_c^- activity (and/or system x_c^- expression) and an effect as a consequence of the alteration of EAAT2 function remains difficult to access.

(3) EAAT2 upregulation but not side-effects of ceftriaxone treatment is responsible for the lack of STDP

The possibility to occlude ceftriaxone effect on STDP by preventing EAAT2 upregulation is not easy to address. Stereotaxic siRNA injections could be an attempt to "normalize" the effect of ceftriaxone by bringing back to baseline the expression levels of EAAT2. However, the only commercially available EAAT2 siRNA (Santa Cruz, EAAT2 siRNA sc-270106) is specifically designed for *in vitro* cell culture transfection studies. *In vivo* experiments require 5 to 50 µM concentrated siRNA, and the Santa Cruz siRNA is sold and packed for cell culture experiments with

an already-made dilution preventing *in vivo* utilization. However, it would be interesting to design EAAT2 siRNA allowing in vivo use to conclude about the specific effect of upregulation of EAAT2 via ceftriaxone treatment.

III. FUTURE DIRECTIONS

EXPERIENCE-DEPENDENT PLASTICITY IN STRIATUM

Corticostriatal long-term plasticity is itself a plastic phenomenon as shown in the present manuscript (*see Results*). STDP undergoes developmental transformation, shifting from Hebbian t-LTD in the immature brain, to bidirectional anti-Hebbian STDP in the juvenile and adult brain (*see Results - Article 1*). Furthermore, synaptic environment also plays a crucial role in the establishment of bidirectional anti-Hebbian STDP at corticostriatal synapses. More precisely, we showed that astrocytes *via* EAAT2 tightly control STDP expression (*see Results - Article 2*). A primary driving force for brain plasticity in the intact behaving organism is learning and experience. Experience-dependent remodeling of synaptic circuits underlies changes in perception and behavior. Therefore, a cardinal question to ask would be how corticostriatal transmission and plasticity can vary depending on the context and experience.

1 - Decision-making and chronic stress

Life experience could be negative and maladaptive responses to persistent negative experience can produce changes in the brain and affect cognitive processes, attention and executive functions. Specifically in the dorsal striatum, chronic stress impairs cognitive functions and affects decision-making (Hollon et al. 2015). More specifically, chronic unpredictable stress alters the flexibility in shifting between the two types of behavioral strategies (goal-directed vs habitual) (*see Introduction, Part IV - Striatum*) in rodents (Dias-Ferreira et al. 2009) as well in humans (Soares et al. 2012).

Thus, stress induces a bias in decision-making strategies and promotes a shift to habitual behavior. Moreover, automatization of recurring decision processes into stereotypic behaviors or habits caused by exposure to stress could be advantageous. This could increase behavioral efficiency by releasing cognitive resources for more demanding tasks.

2 - Dorsal striatum and chronic stress

These changes in behavior are paralleled by morphological changes in the both subregions of the dorsal striatum (Dias-Ferreira et al. 2009). More specifically, dendritic atrophy was observed in the DMS and mPFC (forming the associative network), coupled with hypertrophy in the DLS. In human subjects, sMRI study showed morphological hypertrophy and increased activity and volume

of the putamen (=DLS in rodents), and an atrophy and reduced activity in the caudate (=DMS in rodents) (Soares et al. 2012).

3 - Neural substrates underlying effects of chronic stress on decision-making

These changes reflect an imbalanced activation of the networks that govern decision processes, shifting activation from the associative to the sensorimotor circuits.
However, electrophysiology data are missing and the underlying mechanisms of the potential network remodeling in dorsal striatum are still to be investigated. We can speculate that cell excitability, corticostriatal transmission and short- and long-term plasticity are differentially regulated in the two dorsal striatum subregions (DLS and DMS) following chronic stress. Precisely, we would expect increased cell excitability and strengthened corticostriatal transmission in DLS compared to DMS, thus favoring a bias towards habitual behavioral strategies. Concerning the underlying mechanisms, they could be of various natures. Indeed, increased presynaptic release, altered postsynaptic receptor expression together with the complex role of neuromodulatory and neurotrophic factors, and structural changes of the synapse, could play a role in shaping corticostriatal synaptic transmission following chronic stress (Popoli et al. 2012; Mcewen et al. 2015).

4 - EAAT2 expression and chronic stress

EAAT2 expression levels are subject to experience-dependent changes (Oliet et al. 2001; Boudaba et al. 2003; Genoud et al. 2006; Cui et al. 2014). Importantly, negative states like stress can alter EAAT2 expression. Similar to the inverted U-shape of the physiological responses to stressors, EAAT2 expression also varies as the function of the persistence of the stressors. Allostasis is defined as the active process of adaptation to stressors. In the case of protective allostasis (or allostatic load), acute stress (and acute glucocorticoid treatments) induce adaptive changes that lead to increased glutamate clearance, thereby preventing spillover of the excessive release of presynaptic glutamate into the extrasynaptic space (Popoli et al. 2012); but see (Yang et al. 2005). In the contrary, in the case of damaging allostasis (or allostatic overload), chronic stress leads to increased basal levels of serum corticosterone (Popoli et al. 2012) and leads to the downregulation of EAAT2 and reduced glutamate clearance (Olivenza et al. 2000; de Vasconcellos-Bittencourt et al. 2011); but see (Reagan et al. 2004). Furthermore, the cumulative pathophysiology of chronic exposure to life stressors is one of the most reliable precipitating factors in the development of a depressive episode (Hill et al. 2012) and ceftriaxone has been reported to display antidepressant-like

effects (Mineur et al. 2007; Hashimoto 2009). Altogether, these findings stand for a crucial role of EAAT2 in shaping glutamate transmission and responses to stress.

5 - EAAT2 expression may underlie dorsal striatum alterations following chronic stress

Given the (1) strong evidence of the importance of EAAT2 in shaping corticostriatal transmission (Goubard et al. 2011) and long-term plasticity (*see Results - Article 2*); (2) EAAT2 susceptibility to alterations following chronic stress (Popoli et al. 2012); and (3) the antidepressant-like effects of EAAT2 upregulation (Mineur et al. 2007), we hypothesize that EAAT2 might be involved in the dorsal striatum network remodeling following exposure to chronic stress. More precisely, on a molecular level, we would expect that EAAT2 is downregulated in DLS, thus promoting excessive spillover resulting in strengthening of the corticostriatal synaptic transmission. Furthermore, we would expect that these alterations in EAAT2 expression levels will trigger parallel electrophysiological changes in DLS and DMS corticostriatal synaptic transmission and plasticity. We would thus expect that restoring proper EAAT2 expression levels and function with chronic ceftriaxone treatment during the chronic stress exposure will rescue the corticostriatal synaptic transmission and plasticity. Finally, we speculate that these molecular and physiological changes would reflect imbalanced activation of the sensorimotor vs associative circuits, and thus, result in a lack of flexibility in shifting between goal-directed vs habitual behavior. Therefore, we would expect that ceftriaxone treatment would rescue adequate decision-making, and that, on the contrary, local DHK infusion in the DLS would promote habit-biased behavior in non-stress exposed control animals.

In conclusion, it would be of a great significance to explore the modulation of corticostriatal plasticity in a chronic stress paradigm, therefore further demonstrating its susceptibly to undergo plastic changes with experience, together with the already demonstrated developmental changes (*see Results - Article 1*) and astrocytic involvement in its expression (*see Results - Article 2*).

ANNEX

ANNEX
INTRODUCTION

The main focus of this PhD work was the investigation of the proper conditions for STDP emergence in striatum. In addition, I was also involved in two other collaborative projects with colleagues working in the fields of computational neuroscience and biophysics. These projects can be viewed as a follow up of a first collaborative project about the determination of the extent to which obstructions (fiber bundles, blood vessels, glial cells, …) affect electrical signal propagation on a microscale (Nelson et al., 2013).

I. ARTICLE 1

Intracellular impedance measurements reveal non-ohmic properties of the extracellular medium around neurons.

Gomès* JM, Bédard* C, Valtcheva S, Nelson M, Khokhlova V, Pouget P, Venance L, Bal T and Destexhe A, *Biophys J* Jan 5;110(1):234-46 (2016).

The first project includes a quantitative study of the electrical properties of the extracellular space around neurons (Gomes et al., 2016).

Introduction and rationale:

Understanding the genesis of extracellular potentials and their exact source localization is a critical issue in experimental neuroscience where extracellular recordings are broadly used as readout of neural activity. Nevertheless, interpretation of such extracellular data may be a sensitive issue. The propagation of electric signals in brain tissue depends on its electric properties. It is classically admitted that the extracellular medium presents ohmic properties (i.e. resistive medium). This assumption mainly relies on data collected with metal electrodes (Logothetis et al., 2007).

A previous study involving our team, indicated a marked frequency dependence of the brain tissue (Nelson et al., 2013). Indeed, dependent on the nature of the inhomogeneties, present in the extracellular medium, the electrical signal propagation is differently distorted. Such inhomogeneties (cell bodies, blood vessels, striatal fibers) impose a significant frequency filtering of the extracellular signal. These findings present an indirect evidence for nonresistive nature of the extracellular medium.

Results and conclusions:

Here, we combined *in vitro* and *in vivo* whole-cell recordings with computational modeling to address the question of the exact biophysical nature of the extracellular medium. We introduced a method to measure the impedance of the tissue by preserving the intact cell-medium interface using whole-cell *in vivo* and *in vitro*. We found that neural tissue has marked non-ohmic and frequency-filtering properties, which are, thus, not consistent with resistive medium as previously assumed. Furthermore, our computational model showed that the impact of such frequency-filtering properties might be important for the generation of local field potentials, as well as for the cable properties of neurons.

II. ARTICLE 2

A recording circuit for cross-talk between recording channels and its implications for electrophysiology experimentation.

Nelson M, Valtcheva S and Venance L *(in preparation)*

In this second study, we addressed the issue of possible cross-talk which could arise from the simultaneous recording from two or more electrodes.

Introduction and rationale:

Using two or more electrodes for simultaneous intracellular and extracellular recordings or stimulation could have complications in interpreting the collected data as these methods are susceptible to capacitive cross-talk. However, estimations of the exact extend and the importance of suck cross-talk for neuroscience experimentation is still lacking.

Results and conclusions:

Here, we described a simplified electrical circuit to model simultaneous recording or stimulation with two or more electrodes. We further validated the model by using *in vitro* whole-cell recordings in brain slices where we could experimentally observe the occurrence of cross-talk. Our experimental data show that cross-talk increases with higher frequencies and with higher electrode impedance of the channel receiving the cross-talk. Nevertheless, cross-talk amplitudes remain a small fraction of the originating signal. The result would thus be negligible when both originating and receiving electrodes record signals of the same magnitude, as with multiple electrode extracellular recordings for example. However this effect can be noticeable in extracellular recordings when intracellular signals are recorded simultaneously on nearby channels, or in some cases when stimulation and simultaneous recording is applied, because of the different orders of magnitude of the two signals.

ANNEX

Article I

Intracellular impedance measurements reveal non-ohmic properties of the extracellular medium around neurons

Gomès* JM, Bédard* C, Valtcheva S, Nelson M, Khokhlova V, Pouget P, Venance L, Bal T and Destexhe A

(Biophys J 2016)

Article

Intracellular Impedance Measurements Reveal Non-ohmic Properties of the Extracellular Medium around Neurons

Jean-Marie Gomes,[1] Claude Bédard,[1] Silvana Valtcheva,[2] Matthew Nelson,[3] Vitalia Khokhlova,[1] Pierre Pouget,[3] Laurent Venance,[2] Thierry Bal,[1] and Alain Destexhe[1,*]

[1]Unité de Neurosciences, Information et Complexité, Centre National de la Recherche Scientifique, Gif-sur-Yvette, France; [2]Centre Interdisciplinaire de Recherche en Biologie, Centre National de la Recherche Scientifique UMR 7241, Institut National de la Santé et de la Recherche Médicale U1050, Collège de France, Paris, France; and [3]Institut du Cerveau et de la Moelle Epinière, Centre National de la Recherche Scientifique UMR 7225, Institut National de la Santé et de la Recherche Médicale UMRS 975, Hôpital de la Salpétrière, Université Pierre et Marie Curie, Paris, France

ABSTRACT Determining the electrical properties of the extracellular space around neurons is important for understanding the genesis of extracellular potentials, as well as for localizing neuronal activity from extracellular recordings. However, the exact nature of these extracellular properties is still uncertain. Here, we introduce a method to measure the impedance of the tissue, one that preserves the intact cell-medium interface using whole-cell patch-clamp recordings in vivo and in vitro. We find that neural tissue has marked non-ohmic and frequency-filtering properties, which are not consistent with a resistive (ohmic) medium, as often assumed. The amplitude and phase profiles of the measured impedance are consistent with the contribution of ionic diffusion. We also show that the impact of such frequency-filtering properties is possibly important on the genesis of local field potentials, as well as on the cable properties of neurons. These results show non-ohmic properties of the extracellular medium around neurons, and suggest that source estimation methods, as well as the cable properties of neurons, which all assume ohmic extracellular medium, may need to be reevaluated.

INTRODUCTION

The genesis and propagation of electric signals in brain tissue depend on its electric properties, which can be simply resistive (ohmic) or more complex, such as capacitive, polarizable, or diffusive. The exact nature of these electric properties is important, because nonresistive media will necessarily impose frequency-filtering properties upon electric signals (1,2), and therefore will influence any source localization. These electric properties were measured using metal electrodes, which provided measurements suggesting that the brain tissue is essentially resistive (3–5). However, the electrical behavior of tissue and electrodes can be easily confused (6); efforts in the direction of distinguishing or separating them abound (7–9). Another experimental approach using very low-impedance probes revealed a marked frequency dependence of conductivity and permittivity (10,11). Indirect evidence for nonresistive media was also obtained (12–14), and also indicated a marked frequency dependence.

To explain these discrepancies, we hypothesize that the apparently contradictory results are due to the fact that different measurement methods were used. The use of metal electrodes represents a nonphysiological interface for interacting with the surrounding tissue, while in reality, neurons interact with the extracellular medium by exchanging ions through membrane ion channels and pumps. To respect as much as possible these natural conditions, we have measured the tissue impedance using a neuron as a current source, thereby respecting the natural interface. This intracellular measurement provides a measurement of a global cell impedance, which contains the membrane impedance and the impedance of the extracellular medium. This global, intracellularly measured impedance can also be defined as the impedance as seen by the cell.

Fig. 1 illustrates this concept and the recording setup needed to record this global impedance intracellularly, in vitro (Fig. 1 *A*) or in vivo (Fig. 1 *B*). Fig. 1 *C* gives two circuit configurations for this system, emphasizing three impedances: Z_i is the impedance of the intracellular medium (cytoplasm); Z_e is the extracellular impedance; and Z_{RC} is the membrane impedance, represented by a simple resistance-capacitance (RC) circuit (*left*), or a more complex circuit including dendritic compartments all described by different RC circuits (*right*). An intracellular electrode will measure a global combination of these impedances. In the following text, we will call this global impedance the "global intracellular impedance".

A central point of our study is that this global intracellular impedance is different from the electrical impedances measured by metal electrodes, which we refer to here as

Submitted July 22, 2015, and accepted for publication November 10, 2015.

*Correspondence: destexhe@unic.cnrs-gif.fr

Jean-Marie Gomes and Claude Bédard contributed equally to this work.

Matthew Nelson's present address is Cognitive Neuroimaging Unit, INSERM U992, NeuroSpin Center, Commissariat à l'Energie Atomique, Gif-sur-Yvette, France.

Editor: Ian Forster.

0006-3495/16/01/0234/13

http://dx.doi.org/10.1016/j.bpj.2015.11.019

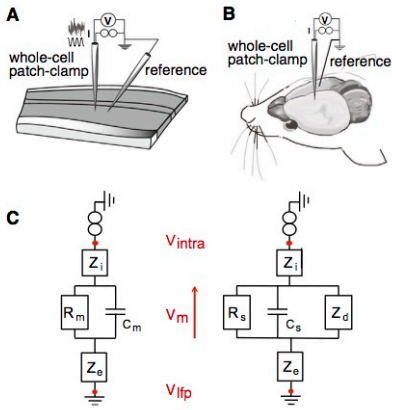

FIGURE 1 Scheme of the experimental setup for measuring the global intracellular impedance. (*A* and *B*) Placement of electrodes in vitro and in vivo. In each case, a cell is recorded in patch-clamp whole-cell configuration using a micropipette, where the reference electrode is a micropipette located in the extracellular medium at a short distance from the recording (*A*), or a silver wire in the contralateral hemisphere (*B*). (*C*) Equivalent circuits corresponding to this experimental setup, in two different configurations: the cell is either considered as a single compartment (*left*), or with dendrites (*right*), resulting in a slightly more complicated circuit. The membrane is modeled as an RC circuit, where R_m and C_m are the global membrane resistance and capacitance of the cell (*left*), respectively, or R_s and C_s are the resistance and capacitance of the somatic membrane (*right*). The value Z_i is the macroscopic intracellular impedance (including the electrode-cytosol interface), and Z_e is the macroscopic extracellular impedance. In the resistive models, Z_e is modeled as a simple resistance R_e; in the diffusive models, it is a function of three parameters (*A*, *B*, and *k*, respectively, scaling the modulus, phase, and cutoff frequency of the diffusive impedance; see Materials and Methods). In the right circuit, Z_d is the equivalent input impedance of the dendritic tree seen by the soma; it is a function of l_d, the equivalent length of the dendritic tree. In both circuits, V_{intra} represents the intracellular potential, and V_{lfp} is the potential in extracellular space. To see this figure in color, go online.

"metal-electrode impedance". We will investigate whether the intracellularly measured impedance reveals more complex electrical properties than with metal electrodes, which could possibly explain the discrepancies described above. The global intracellular impedance provides not only a realistic estimate of the electrical properties of the extracellular medium, but it is also closer to the natural conditions; it could be a useful physical parameter to determine a more-precise source localization of cerebral electric signals, and to model the propagation of electrical signals in the extracellular space or in dendritic trees, as we illustrate here.

MATERIALS AND METHODS

Animals

Maintenance, surgery, and all experiments were performed in accordance with the local animal welfare committees (the Center for Interdisciplinary Research in Biology and European Union Guidelines, under Directive No. 2010/63/EU; and the Regional Ethics Committee, Ile-de-France Sud, under Certificate No. 05-003). Every precaution was taken to minimize stress and the number of animals used in each series of experiments. Animals were housed in standard 12 h light/dark cycles and food and water were available ad libitum.

In vitro electrophysiology

Brain slice preparation

Visual cortex. A quantity of 300-μm-thick coronal brain slices of juvenile mice (P_{12-16} Swiss mice bred in the CNRS Animal Care facility, Gif-sur-Yvette, France; under French Agriculture Ministry Authorization No. B91-272-105) were obtained with a VT1200S microtome (Leica Biosystems, Wetzlar, Germany). Slices were prepared at 4°C in the following medium: choline chloride 110 mM, KCl 2.55 mM, NaH_2PO_4 1.65, $NaHCO_3$ 25 mM, dextrose 20 mM, $CaCl_2$ 0.5 mM, and $MgCl_2$ 7 mM. Slicing started 2 mm from the posterior limit of olfactory bulb, and ended 3.9 mm further. Before recordings, slices were incubated at 34°C in artificial cerebro-spinal fluid (ACSF) of the following composition: NaCl 126 mM, KCl 3 mM, $NaHCO_3$ 26 mM, NaH_2PO_4 1.25 mM, myo-inositol 3 mM, sodium pyruvate 2 mM, L-ascorbate de sodium 0.4 mM, and dextrose 10 mM. The slicing and recording solution was bubbled with 95% O_2 and 5% CO_2, for a final pH of 7.4.

Dorsal striatum. Horizontal brain slices with a thickness of 330 μm were prepared from rats (P_{23-30} OFA rats (Charles River, L'Arbresle, France), using a vibrating blade microtome (VT1200S; Leica Biosystems). Brains were sliced in a 95% O_2/5% CO_2-bubbled, ice-cold cutting solution containing: NaCl 125 mM, KCl 2.5 mM, glucose 25 mM, $NaHCO_3$ 25 mM, NaH_2PO_4 1.25 mM, $CaCl_2$ 1 mM, $MgCl_2$ 1 mM, and pyruvic acid 1 mM, and then transferred into the same solution at 34°C.

Electrophysiological recordings

Patch-clamp recordings in pyramidal cells of visual cortex from mice were performed as followed. Slices were superfused at 2 mL/min with the same ACSF solution that was used for incubation. Bath temperature of the submerged chamber was maintained at 34°C using a TC-344B temperature controller (Warner Instruments, Hamden, CT). Neurons in slices of the mouse visual cortex (P_{12-16}) were identified with an upright microscope (Axioscope FS; Carl Zeiss, Jena, Germany), an infrared camera (No. C750011; Hamamatsu Photonics, Boston, MA), and an infrared filter. Patch-clamp in the whole-cell current-clamp configuration in layer V pyramidal neurons was performed simultaneously with an extracellular recording using a 3-MΩ patch pipette (Fig. 1 *A*). The latter was located within a close vicinity ($\approx$3 μm) of the patched cell. All results were indifferent to the distance between the reference electrode and the patched cells, as potential variations on the extracellular electrode did not exceed 1% of the variations of the intracellular potential. Borosilicate pipettes (No. 1B150F4; World Precision Instruments, Sarasota, FL) of 5–8 MΩ impedance were used for whole-cell recordings and contained the intracellular solution: HEPES 10 mM, EGTA 1 mM, K-gluconate 135 mM, $MgCl_2$ 5 mM, and $CaCl_2$ 0.1 mM, with osmolarity of 308 mOsm and a pH of 7.3. Serial resistance was not compensated for. Recordings were performed with a Multiclamp 700B amplifier (Axon Instruments, Union City, CA), filtered at 10 kHz with a built-in Bessel filter, and sampled at 25 kHz. Data acquisition and stimulation were performed with a National Instruments BNC 2090 A card, and the software Elphy (G. Sadoc, Centre National de la Recherche Scientifique, Unit of Neuroscience, Information and Complexity, Gif-sur-Yvette, France).

Patch-clamp recordings in medium-sized spiny neurons of dorsal striatum from rats were performed as previously described in Paille et al. (15). Briefly, borosilicate glass pipettes of 6–8 M impedance contained

for whole-cell recordings: K-gluconate 105 mM, KCl 30 mM, HEPES 10 mM, phosphocreatine 10 mM, ATP-Mg 4 mM, GTP-Na 0.3 mM, and EGTA 0.3 mM (adjusted to pH 7.35 with KOH). The composition of the extracellular solution was NaCl 125 mM, KCl 2.5 mM, glucose 25 mM, $NaHCO_3$ 25 mM, NaH_3PO4 1.25 mM, $CaCl_2$ 2 mM, $MgCl_2$ 1 mM, and pyruvic acid 10 mM, bubbled with 95% O_2 and 5% CO_2. Signals were amplified using EPC10-3 amplifiers (HEKA Elektronik, Lambrecht, Germany). All recordings were performed at 34°C using a temperature control system (Bath-Controller V; Luigs & Neumann, Ratingen, Germany) and slices were continuously superfused at 2 mL/min with the extracellular solution. Slices were visualized on a BX51WI microscope (Olympus, Rungis, France) using a 4×/0.13 objective for the placement of the stimulating electrode and a 40×/0.80 water-immersion objective for localizing cells for whole-cell recordings. During the experiment, individual striatal and cortical neurons were identified using infrared-differential interference contrast microscopy with a charge-coupled device camera (model No. VX45; Optronis, Kehl, Germany). Serial resistance was not compensated for. Current-clamp recordings were filtered at 2.9 kHz and sampled at 16.7 kHz using the Patchmaster v2x73 program (HEKA Elektronik). Stimuli in current-clamp mode underwent a high-cut, 10 kHz filter before being applied. Recordings were made with EPC 10-3 amplifiers (HEKA Elektronik) with a very high input impedance (1 TΩ) to ensure there was no appreciable signal distortion imposed by the high impedance electrode (16). Sinusoidal stimuli were then introduced in whole-cell patch-clamp to the patched cell.

This configuration enables estimating the extracellular impedance, according to the circuit displayed in Fig. 1 *C*. To this end, a white-noise current stimulus was injected into the recorded cell and the impedance was calculated based on this current injection (see Fig. 2 A). A quantity of 20–120 s of Gaussian white noise with zero mean and 100 pA variance was injected (results were similar for 30 and 200 pA variance). For each cell, we injected 15–30 times the same sequence of white noise (i.e., frozen noise) and averaged the measured voltages. This enhanced the signal/noise without altering the results. Fig. 2 *A* (*right panel*) shows the very low autocorrelation of the injected currents, being thus a good approximation of white noise. To verify that the same results can be obtained using a different protocol, we also performed slice experiments using sinusoid current stimuli, at different frequencies. This set of experiments was performed using the methods previously published in Nelson et al. (14,16). Namely, sine waves of 12 different frequencies were tested, varying approximately evenly on a logarithmic scale ranging from 6 to 926 Hz. Up to 500 traces of 100–1500 ms in length were averaged before recording the data to disk for offline analyses. Longer stimulus lengths and more traces were necessary for the low-frequency stimuli. The order of the presentation of the frequencies was randomized. Stimuli were introduced with the patch electrode in current-clamp mode. The injected current amplitudes ranged from 200 to 300 pA. Before conducting experiments, we verified via control recordings with an external signal generator in the bath without a slice that any amplitude changes or phase shifts in the recordings across frequencies induced by the amplifier and recording hardware were negligible (16).

In vivo electrophysiology

Surgical preparation of animals

Adult rats (P40–P90) were placed in a stereotaxic apparatus (Unimecanique, Asnières, France) after anesthesia induction with a 400 mg/kg

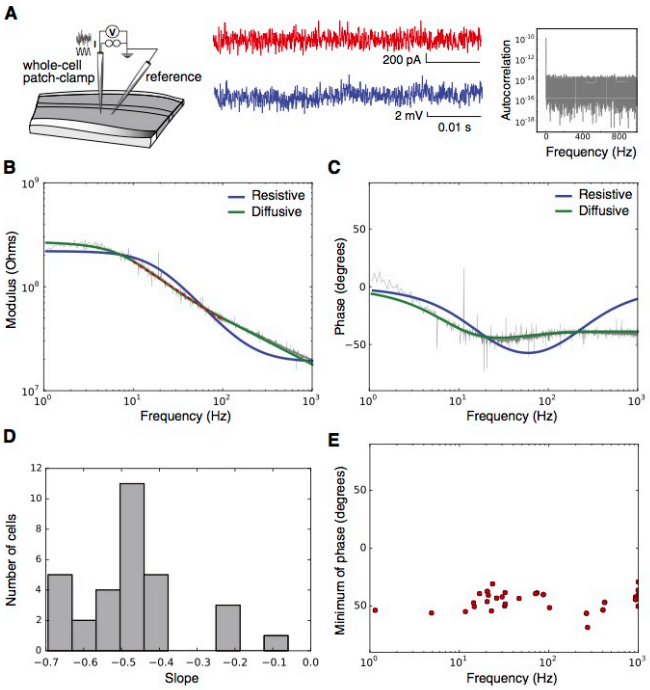

FIGURE 2 Global intracellular impedance of cortical neurons recorded in vitro (current-clamp). (*A*) (*Left*) Scheme of the experimental setup; (*middle*) example signals. A Gaussian white-noise current signal (*red*, amplitude: ± 100 pA) was injected repeatedly into patched neurons while recording the intracellular potential (*blue*). For each 20 s period, we computed the impedance as the ratio of measured voltage on injected current ($Z_{mes} = V_{intra}/i_{inj}$) and averaged on 30 periods. Acquisition was performed at 20 kHz. (*Right*) Autocorrelation of the injected white-noise current in Fourier space. (*B*) Modulus of Z_{eq} (log scale) represented as a function of frequency ($\log_{10}(f)$), for white-noise current injection. (*C*) Fourier phase of Z_{eq}, in the same experiment. The different curves shows the best fit of two models to the experimental data (*blue*, resistive; *green*, diffusive). Parameters of the models: (*resistive*) $R_m = 200$ MΩ, $C_m = 45$ pF, and $R_e = 19$ MΩ; (*diffusive*) $R_m = 180$ MΩ, $C_m = 110$ pF, $A = 99$ MΩ, $B = 3.8$ MΩ, and $f_W = 36$ Hz. (*A*, *B*, and f_W are parameters of the diffusive impedance scaling; respectively, its amplitude, phase, and cutoff frequency.) (*D*) Distribution of the slopes of Z_{eq} fitted between 20 and 200 Hz (linear fit, *red dashed lines* on the figures). (*E*) Coordinates of the minima of the Fourier phases for each cell. To see this figure in color, go online.

intraperitoneal injection of chloral hydrate (Sigma-Aldrich, Saint-Quentin Fallavier, France). A deep anesthesia maintenance was ensured by intraperitoneal infusion on demand of chloral hydrate delivered with a peristaltic pump set at 60 mg/kg/h turned on 1 h after induction. Proper depth of anesthesia was assessed regularly by testing the cardiac rhythm, EcoG activity, the lack of response of mild hindpaw pinch, and the lack of vibrissae movement. The electrocardiogram was monitored throughout the experiment and body temperature was maintained at 36.5°C by a homeothermic blanket.

Two craniotomies were performed, one for the insertion of a reference electrode in the somatosensory cerebral cortex (layer 2/3) and one to allow the whole-cell recordings in the contralateral cortex (layer 5). For whole-cell recordings, a 2×2 mm craniotomy was made to expose the left posteromedial barrel subfield at the following coordinates: posterior 3.0–3.5 mm from the bregma, lateral 4.0–4.5 mm from the midline. The dura was opened and the craniotomy space was filled with low-melting-point paraffin after each time lowering a recording pipette. To increase recording stability, the cisterna magna was drained.

Electrophysiological recordings

Borosilicate glass pipettes of 5–8 MΩ impedance for blind whole-cell recordings contained: K-gluconate 105 mM, KCl 30 mM, HEPES 10 mM, phosphocreatine 10 mM, ATP-Mg 4 mM, GTP-Na 0.3 mM, and EGTA 0.3 mM (adjusted to pH 7.35 with KOH). Signals were amplified using an EPC10-plus-2 amplifier (HEKA Elektronik). Series resistance was not compensated for. Current-clamp recordings were filtered at 2.5 kHz and sampled at 5 kHz using the Patchmaster v2x32 program (HEKA Elektronik). Whole-cell recordings were performed in pyramidal cells of the somatosensory cortex in layer IV/V (depth from the dura: 0.8–1.2 mm) (Fig. 1 *B*). Recorded cells were identified as pyramidal cells according to their characteristic spiking pattern. The reference was a silver wire placed in the contralateral hemisphere. Note that for both in vivo and in vitro experiments, the reference electrode is passive, just measuring the extracellular voltage, and thus the exact nature of this reference is not critical. Accordingly, the same configuration using a silver microwire gave similar results in vitro (not shown).

It is important, however, that the reference electrode be placed in the brain tissue, so that the estimated extracellular impedance is not influenced by other tissues. Thus, as in the in vitro experiments, this intracellular-extracellular configuration enables estimating the extracellular impedance. An important difference with in vitro, is that in vivo the current can flow more freely in three dimensions, and is closer to natural conditions. Another difference is that in vivo, the system is not silent but displays prominent spontaneous activity. To limit this contribution, we have used a frozen-noise protocol, where identical sequences of white-noise stimuli were injected repetitively, and the sequences averaged.

The main purpose of this experiment was to estimate Z_{eq}, the equivalent impedance between the Ag-AgCl electrode and the ground. In the case of a simple, single-compartment neuron, it can be formally defined as $Z_{eq} = Z_i + Z_{RC} + Z_e$. This was achieved by applying two protocols of subthreshold current injection.

1) The frozen-noise protocol consisting, in the same template, of 20 s of a white-noise current (repeated 50 times with 2 s intervals between stimulations and averaged). Sequences in which spikes were induced were discarded.
2) Sinusoidal current at fixed frequencies ranged from 6 Hz to 926 Hz (similar to those used in in vitro experiments). The order of the presentation of the frequencies was randomized.

For the frozen noise and sinusoidal stimuli, the injected currents, tuned for each neuron to evoke voltage response of magnitude, ranged between 2 and 6 mV. Note that in some experiments we injected a hyperpolarizing current (of maximum amplitude −150 pA) to prevent suprathreshold activity during application of stimuli.

Analysis

All analyses were performed using the software Python (Python Software Foundation, Wolfeboro Falls, NH) and the Scipy Stack and Spyder (Pierre Raybaut, The Spyder Development Team).

In vitro and in vivo patch-clamp: sine-wave experiments

For each frequency and current intensity, the recorded voltages and injected intensities were averaged and fit with sines using the optimize package included in Scipy. The adequation between data and the fitted sine waves was checked by human intervention for every set of data. The voltage and current were represented, respectively, as $V(t, f) = V_0\sin(2\pi ft + \phi_v)$ and $I(t, f) = I_0\sin(2\pi ft + \phi_i)$. The impedance for a given frequency was thus given by $Z(f) = (V_0/I_0)e^{i(\phi_v - \phi_i)}$.

In vitro and in vivo patch-clamp: white-noise experiments

Several models were fit to the experiments. First, we used a purely resistive model (Fig. 1, *bottom left*) in which the intracellular impedance Z_i can be considered zero and the extracellular impedance Z_e was a small resistance (R_e). The equivalent impedance is thus given by

$$Z_{eq,1}(\omega) = \frac{R_m}{1 + i\omega\tau_m} + R_e. \quad (1)$$

Second, we combined Z_i and Z_e as a diffusive term. Rather than trying to find an elusive general solution for the usual Nernst-Planck equation (17), we used a first-order approximation for ionic diffusion. The impedance of an electrolyte showing nonnegligible ionic diffusion was derived by Warburg (18,19), and yielded a modulus scaling in $1/\sqrt{\omega}$ and a constant phase. Similar derivations have been performed in different symmetries (20–22). Note that the latter derivations model the impedance of ionic accumulations close to the membrane, by using a first-order approximation of the electric potential generated by ionic species after Boltzmann distributions.

This diffusion impedance has been observed experimentally (reviewed in Geddes (7)), and can be modeled in spherical symmetry by two components scaling the modulus and phase (A and B), and a cutoff frequency $f_W = \omega_W/2\pi$:

$$Z_W(\omega) = \frac{A + iB}{1 + \sqrt{\omega/\omega_W}}. \quad (2)$$

This leads to the following expression for the equivalent impedance:

$$Z_{eq,2}(\omega) = \frac{R_m}{1 + i\omega\tau_m} + \frac{A + iB}{1 + \sqrt{i\frac{\omega}{\omega_W}}}. \quad (3)$$

To take into account the fact that some of the current can flow through the dendrites of the cell, we define a dendritic input impedance Z_d (see Fig. 1 *D*, *right*), namely the impedance of the dendritic tree seen by currents leaving the soma. These currents will flow the gradient potential downwards from the intracellular potential (V_{intra}) to the reference ($V_{\text{ref}} = 0$). Thus, Z_d is defined by $V_{\text{intra}}/i^g{}_d$, where $i^g{}_d$ is the generalized axial current in the dendrite at the level of the soma, and V_{intra} is the intracellular potential at the soma. Note that we consider here V_{intra} as not necessarily equal to the transmembrane potential (V_m) because we take V_e, the potential of the extracellular medium, into account. We then consider separately the resistance and capacitance of the soma (R_s, C_s) and the impedance of the dendrite. The equivalent impedance is then $Z_{eq,3-4}(\omega) = (Z_dZ_s/Z_d + Z_s) + Z_i + Z_e$, where $Z_s(\omega) = R_s/1 + i\omega\tau_m$ is the impedance of the soma, and $Z_{eq,3}$ and $Z_{eq,4}$ are the impedances for resistive and diffusive media, respectively. A description of these different models can be found in the next section; parameters for each of these models are listed in Table 1.

TABLE 1 Parameters Used for the Four Models

Model type	Resistive	Diffusive
No dendrite	R_m, C_m, R_e	R_m, C_m, A, B, f_W
Dendrite	R_s, C_m, R_s, C_s, R_e, l_d	R_s, C_s, A, B, f_W, l_d

The value l_d is the length of the dendritic compartment; R_e is the extracellular resistance.

Fitting models with and without dendrites

Two types of models were fit to the experimental measurements, as illustrated in Fig. 1 *C*: a single-compartment model and a model including a dendritic segment. Dendritic filtering has been proposed to explain the frequency-dependence of local field potential (LFP) (23,24); thus, current flowing in the dendrites could be involved in shaping the measured impedance, which would in turn influence the frequency-dependence of local field potentials. We tested this possible influence by considering models that include an equivalent dendritic compartment, which has been shown to be electrically equivalent to a full dendritic tree (25,26), leading to a ball-and-stick type model (see *right circuit* in Fig. 1 *C*).

To fit the models to experimental data, several traditional fitting methods were tested (e.g., Newton-Gauss, Levenberg-Marquardt, conjugate gradient, simplex…), but were plagued with three main problems: a long computation time (with four parameters or more), a tendency to get trapped in local minima, and an extreme sensitivity to the first estimation of model parameters. We thus developed a probabilistic, noniterative method that had none of these problems.

We proceeded as follows. 1) For each parameter, we defined a domain of acceptable values, keeping it very large (too much restriction on a parameter is a symptom of analytical bias). 2) We drew random sets of parameters (between 500 and 5000), e.g., $P_j = (R_m, C_m, A, B, f_W\ldots)$, and computed the theoretical impedance spectra they predicted with a given model. 3) We computed the squared error $E_j(P_j)$ between the theoretical and measured impedances; the error was computed as the sum of squared errors on real and imaginary parts. 4) The couple $(P_j, E_j(P_j))$ that had the smallest errors over all tries was kept as the best fit.

Random drawing removed the sensitivity to local minima and initial parameters that is intrinsic to traditional iterative methods. It allowed a thorough exploration of the parameter space, and with high reliability and acceptable efficiency. Empirically, this method was found to be much faster than a systematic exploration, but just as reliable.

Modeling the contribution of dendrites

To model the impedance of the cell including the contribution of dendrites, we use the generalized cable formalism (FO model in Bédard and Destexhe (27)), which reads

$$\lambda^2 \frac{\partial^2 V_m(x,\omega)}{\partial x^2} = \kappa^2 V_m(x,\omega), \tag{4}$$

where

$$\begin{cases} \lambda^2 &= \dfrac{r_m}{\bar{z}_i} \\ \kappa^2 &= 1 + i\omega\tau_m \end{cases} \tag{5}$$

for a cylindrical compartment. Here, the quantity $\bar{z}_i$ is an equivalent impedance, which depends on the model considered. The value $\bar{z}_i = r_i + r_e$ for the standard (resistive) cable model, defined from the intracellular and extracellular resistivities of r_i and r_e, respectively. In the case of a frequency-dependent impedance, $\bar{z}_i$ is more complex and is given by

$$\bar{z}_i = z_i \Big/ \left[1 + \frac{z_e^{(m)}}{r_m}(1 + i\omega\tau_m)\right],$$

where z_i and z_e are the intracellular (cytoplasm) and extracellular impedance densities, respectively; r_m is the membrane resistivity; and τ_m is the membrane time constant. The estimation of these parameters from the experimental measurements is given in Appendix S1 in the Supporting Material.

When including a dendritic segment, the equivalent impedance (circuit shown in Fig. 1 *C*, *right*) is given by

$$Z_{eq}^{3,4}(\omega) = Z_i + \frac{(Z_s + Z_e)Z_d}{Z_s + Z_e + Z_d}, \tag{6}$$

where $Z_s = R_s/1 + i\omega\tau_m$ is the impedance of the somatic membrane, and $Z_{eq}{}^3(\omega)$ and $Z_{eq}{}^4(\omega)$ correspond to resistive and diffusive media, respectively. Note that in these models, we have considered $Z_i \approx 0$ (see Fig. 1 *C*) because the cytoplasm impedance of the soma is negligible compared to the membrane impedance.

If $i^g{}_d$ is the current flowing in the dendritic tree, the dendritic impedance (as seen by the soma) is

$$Z_d = \frac{V_{\text{intra}}}{i_d^g} = \frac{V_{\text{intra}}}{V_m}\frac{V_m}{i_d^g}. \tag{7}$$

Taking into account $V_{\text{intra}} = V_m + V_e$, we obtain

$$\frac{V_{\text{intra}}}{V_m} = 1 + \frac{V_e}{V_m} = 1 + \frac{Z_e}{Z_s}$$

because the conservation law for the generalized current implies $V_e = Z_e(i^g - i^g{}_d)$ and $V_m = Z_s(i^g - i^g{}_d)$. Note that these equalities would not make sense with the free-charge current, because the variations of V_m may imply charge accumulation around the membrane (dendrite and soma), and thus there is no guarantee of conservation of the free-charge current.

The second part of the fraction represents the input impedance of the dendrite Z_{in}, which is given by

$$\frac{V_m}{i_d^g} = Z_{in} = \frac{\bar{z}_i}{\kappa_\lambda}\coth(\kappa_\lambda l_d), \tag{8}$$

where κ_λ is the cable parameter of the dendrite. Thus,

$$Z_d = \left(1 + \frac{Z_e}{Z_s}\right)\frac{\bar{z}_i}{\kappa_\lambda}\coth(\kappa_\lambda . l_d). \tag{9}$$

Note that the values of parameters (κ_λ and $z_e{}^{(m)}$) in the models considered above correspond to an open-circuit configuration, which also corresponds to these experiments; the cable equation for the open-circuit configuration, with an arbitrarily complex extracellular medium, was given previously in Bédard and Destexhe (27).

The intermediate formulas and variables for each model are listed in Table 2.

Statistics on population data

Different models call for different sets of parameters. For example, the membrane resistance and capacitance of a resistive model are similar but not identical to their counterparts in a model that features a Warburg impedance (e.g., some of the frequency-filtering properties can come from this supplementary impedance). Thus, for a single neuron, we allowed membrane resistance and capacitance to differ across models.

TABLE 2 Intermediate Variables

Model Type	$Z_i = z_i l_s$	Z_e	$z_e(m)$	$\kappa^2\lambda$
Standard	Zils	negligible	negligible	$\frac{r_i}{r_m}(1+i\omega\tau_m)$
Diffusive	$\frac{r_i}{(1+i)\sqrt{\omega}} l_s$	$\frac{A+iB}{1+\sqrt{i\omega/\omega_W}}$	$\frac{0.5\tau_m}{2\pi a C_m(1+i)\sqrt{\omega}}$	$\frac{z_i(1+i\omega\tau_m)}{r_m\left[1+\frac{z_e^{(m)}}{r_m}(1+i\omega\tau_m)\right]}$

The values Z_i and Z_e are, respectively, the intracellular and extracellular impedances; $z_e(m)$ is the input resistance of the extracellular medium seen by the dendrite (in Ω/m); and $\kappa^2\lambda$ is the cable parameter of the system. Constants: the values r_i and r_e are the linear density of resistance in the cytoplasm and extracellular medium (estimated to 28 × 109 and 18 × 109 Ω/m), respectively; z_i is the linear density of impedance in the dendrite; l_s and l_d are the length of the soma and dendrite, respectively; a is the diameter of the dendrite; τ_m is the time constant of the membrane (~10 ms); and C_m is the specific membrane capacitance (10−2 F/m^2). We also have $r_m = \tau_m/2\pi a_m C_m$, where $1/r_m$ is the linear density of membrane conductance (S/m).

To determine which model was best to describe experimental data, we used the following classical procedure.

1) For each cell and each model, we computed the residual sum of squares (RSS) between the experimental curves (y_{exp}) and theoretical curves (y_{th}):

$$RSS_{cell} = \sum_{frequencies} \left(y_{exp} - y_{th}\right)^2.$$

For each cell, we normalized this distance by the distance obtained by the best fit. The distance between experimental and theoretical curves for a given model was thus:

$$RSS_{model} = \sum_{cells} RSS.$$

2) We want to compare the RSS across models. A raw comparison would be unfair, as a model with more parameters is more capable of fitting a given data set. Choosing for reference the diffusive model with dendrites (DD), we thus formed, for every other model M, the null hypothesis: The model M explains the observed curves. If the model DD has smaller RSS, it is only because it has more parameters than the model M.
3) We chose $\alpha < 0.05$ as threshold for rejecting H_0.
4) We used the extra sum of squares F-test, which is able to account for the discrepancy in degrees of freedom across models. We computed the parameter F, using an F-distribution under H_0,

$$F = \frac{RSS_M - RSS_{DD}}{RSS_{DD}} \frac{DF_{DD}}{DF_M - DF_{DD}},$$

where DF is the degrees of freedom (number of cells minus number of parameters) of a given model.

5) The F cumulative distribution function (*fcdf*) allows us to compute the likelihood of H_0 (see Fig. 5):

$$p = 1 - fcdf(F).$$

If $p < \alpha$, we reject the null hypothesis: the diffusive model with dendrites is significantly better than the other model, and this cannot be explained by the surplus of parameters alone.

Computational models using the measured impedances

Two types of models were used to test possible consequences of the measurements. First, we used a model of the genesis of the extracellular potential. To this end, a current waveform corresponding to the total membrane current generated $I_{AP}(t)$ by an action potential was computed from the Hodgkin-Huxley model in the NEURON simulation environment (28). This current waveform was used as a current source to calculate the extracellular potential, using a formalism that is valid for any extracellular impedance. We calculated the extracellular potential by using the impedance measurements made in this article. According to step 2 of the classical procedure above, we have

$$Z_e(\omega) = \frac{A+iB}{1+\sqrt{i\omega/\omega_W}}, \quad (10)$$

where $A = 151 \times 10^6\ \Omega$, $B = 2.54 \times 10^6\ \Omega$, and $\omega_W = 335$ rad.s^{-1} for a distance of a few micrometers. The extracellular potential $V(t)$ was calculated using the convolution

$$V(t) = \int_{-\infty}^{+\infty} \overline{Z}_e(t-\tau) I_{AP}(\tau) d\tau, \quad (11)$$

where $\overline{Z}_e(t)$ is the inverse Fourier transform of $Z_e(\omega)$.

Second, we simulated a ball-and-stick model using the generalized cable equation (27) (see Eq. 5).

A zero-mean Gaussian white-noise current waveform was injected into the dendrite, and the generalized cable was used to compute the membrane potential in dendrites and in the soma (see details of the methods in Bédard and Destexhe (27)).

RESULTS

We start by outlining the measurement paradigm and the notion of global intracellular impedance, then we successively describe the results obtained in vitro and in vivo. Finally, we illustrate consequences of these findings on two fundamental properties: the genesis of extracellular potentials and the voltage attenuation along neuronal dendrites.

The global intracellular impedance

Here, we explore the hypothesis that the extracellular impedance is fundamentally different if measured in natural conditions where the interface between the neuronal membrane and extracellular medium is respected, compared to metal electrodes, which rely on an artificial metal-medium interface. In natural conditions, the neuronal membrane's interface with the medium involves the opening/closing of

ion channels, ionic concentration differences, and ionic diffusion, whereas metal electrodes involve a different type of ion exchange with the medium, which consists of a chemical reaction between the metal and the ions in the medium. To measure the impedance in natural conditions, it is therefore necessary to use an intact neuron as the interface with the medium, to respect the correct ionic exchange conditions. To do this, we performed whole-cell patch-clamp recordings, using neurons as natural current sources in the surrounding medium.

This measurement paradigm is illustrated in Fig. 1, *A* and *B*, and consists of a whole-cell patch-clamp recording coupled to a micropipette measuring the potential in the extracellular medium close to the recorded neuron, in vitro (Fig. 1 *A*) or in vivo (Fig. 1 *B*). In all cases, the recorded neuron is driven by current injection and serves as a natural current source in the medium. In this configuration, relating the signals of the two electrodes gives a direct access to the extracellular impedance, as shown by the equivalent circuits (Fig. 1 *C*).

According to this equivalent circuit, we have

$$V_{\text{intra}} = Z_{eq}.i^{g}, \tag{12}$$

where i_g is the generalized current injected by the patch-clamp electrode. The use of the generalized current is essential here because it is the only current that is conserved if the media have arbitrarily complex impedances (27), and therefore abides by Kirchhoff's current laws in this general case. Note that the current provided by the current generator is also a generalized current because capacitive or nonresistive effects are negligible in modern generators.

In contrast, the conservation of the classic free-charge current would apply only with resistive impedances. The previous equation gives, for the left circuit (single-compartment cell),

$$Z_{eq}(\omega) = Z_i + \frac{R_m}{1 + i\omega\tau_m} + Z_e, \tag{13}$$

and for the right circuit (cell consisting of a soma and an equivalent dendrite),

$$Z_{eq}(\omega) = Z_i + \frac{(Z_s + Z_e)Z_d}{Z_s + Z_e + Z_d}, \tag{14}$$

where Z_{eq} is the equivalent impedance of each of the two circuits, and Z_i and Z_e are the macroscopic impedances of the cytosol and the extracellular medium, respectively. The value R_m is the global input resistance of the cell and τ_m is the global membrane time constant (*left circuit*); $Z_s = R_m/1 + i\omega\tau_m$ is the impedance of the soma membrane (*right circuit*); and Z_d is the input impedance of an equivalent dendrite, as seen by the soma, including the extracellular medium surrounding it.

In the standard model, Z_i and Z_e are usually modeled by a lumped and resistive impedance. In the following, Z_{eq} will be called the "global intracellular impedance" of the circuit, because in such a recording configuration the neuron acts as a current source in the brain tissue. It represents the impedance of the system as seen by the intracellular side of the neuron.

The value Z_e is the impedance of the extracellular medium as seen by the neuron (extracellular component of the intracellularly measured global impedance). We will test here whether the latter impedance is negligible or constant, as usually assumed. We will consider resistive and diffusive versions of this impedance, and check which one better fits the data.

The value Z_i includes the impedance of the interface between the tip of the electrode and the intracellular medium. This interface will be different in whole-cell patch or sharp-electrode recording configurations, because of the location and impedance of the pipettes themselves. So, the interpretation of the measured impedances may be different in sharp-electrode and whole-cell recordings, and we indeed have observed such differences (not shown here). In particular, we made sure that the interface of the silver-silver chloride electrodes, used for patching and as a reference, does not contribute significantly to the equivalent impedance: it is negligible compared to other impedances in the circuit and has little frequency dependence between 1 and 1000 Hz (Fig. 3).

To measure Z_{eq}, we injected a current intracellularly, and measured the intracellular potential V_{intra} with respect to a reference. Ideally, this reference is a micropipette in the extracellular medium (V_{LFP}; see scheme in Fig. 1 *A*). In the in vivo experiments, the reference was a silver electrode inserted in the contralateral somatosensory cortex as in Fig. 1 *B*. For subthreshold currents, the system can be considered linear in frequency: injecting current at an arbitrary frequency yields voltage variations only at that frequency (see Appendix S2 in the Supporting Material). This linearity of the system is illustrated in Fig. 4. First, for the subthreshold range of V_m considered, the membrane V-I relation is linear (Fig. 4 *A*). Second, a combination of four sine-wave currents of fixed frequency generate V_m variations that have strictly the same frequencies (Fig. 4 *B*), showing that the linear approximation is valid: sine waves appear as sharp spectral lines in Fourier space, two orders of magnitude above baseline. Thus, there seems to be no significant impact of nonlinear membrane ion channels on the recordings. Indeed, no action potentials were present in the recordings analyzed here.

We used two protocols of current injection, either injection of a series of sinusoidal currents of different fixed frequencies (6–926 Hz) or injection of a broad-band (white-noise) current, with a flat spectrum between 1 and 10 kHz. In this case, several instances of the same noisy current trace were injected into the cell (frozen-noise protocol),

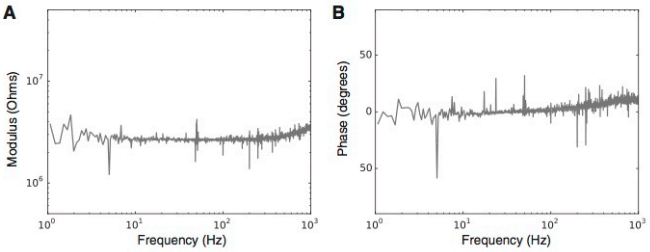

FIGURE 3 Impedance of a silver-silver chloride electrode inserted in a typical ($\approx$3 $M\Omega$) patch pipette, measured in ACSF. (*A*) Modulus (measured in ohms); (*B*) phase (measured in degrees).

which allowed us to take an average and increase the signal/noise of the measurements. This is particularly useful in vivo, to limit the contamination of the measurement by spontaneous synaptic activity, which can be very strong in vivo.

In vitro measurements of the global intracellular impedance

Measurements were first performed in vitro by using an experimental setup consisting of a whole-cell patch-clamp recording of a neuron, together with an extracellular recording in the nearby tissue in the cortical slice (see Fig. 2 *A*). Using this recording configuration, we computed the global intracellular impedance (Z_{eq} in Eq. 12; see Materials and Methods) by using either white-noise current injection, or injected sinusoidal currents. The results of a representative cell ($N = 31$) is shown in Fig. 2, *B* and *C*. Both the modulus amplitude and Fourier phase of the impedance are represented. The colored curves in Fig. 2, *B* and *C*, show the best fits of different models to the experimental data. One can see that the purely resistive model (RC membrane + resistive extracellular medium, *blue curves*) does not capture the data. We read from Eq. 1 that $|Z_{eq}(\omega)|$ scales as $1/\omega$ in the resistive model, which corresponds to a slope of -1, while the experimental modulus yields a slope of -0.5 ± 0.1 (Fig. 2 *D*). The resistive model has a phase similar to $\arctan(k\omega)$ with a minimum of $\sim -90°$ at high frequencies, which contrasts with the $-50°$ observed in the data (Fig. 2 *E*).

So frequency dependence is clearly different from that predicted by the RC-circuit membrane model. The best fits of a model taking into account ionic diffusion (22) can account significantly better for most of this frequency dependence in different cells (*green curves*; see also Fig. 5). In particular, the $1/\sqrt{\omega}$ frequency scaling predicted by the diffusive model (Eq. 3) corresponds to the actually observed -0.5 slope of the

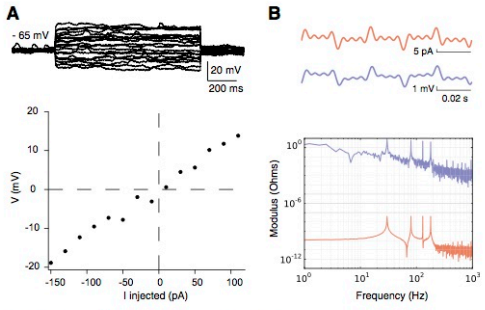

FIGURE 4 Linearity in temporal and frequency space. (*A*) Injection of hyperpolarizing and depolarizing pulses in a cortical neuron patched in vivo, around resting membrane potential. The V-I relation indicated is roughly linear in this subthreshold range. (*B*) Sine waves of current with four different frequencies were injected simultaneously in a patched neuron in vivo (*top*, *red curve*). The voltage was recorded (*top*, *blue curve*). The modulus of the Fourier transform of both signals is shown here, as a function of frequency (Hz): current (*red*, *A*); voltage (*blue*, *V*). The frequencies corresponding to the peaks on both signals illustrate the linearity in frequency of the system, here tested between 1 and 1000 Hz. To see this figure in color, go online.

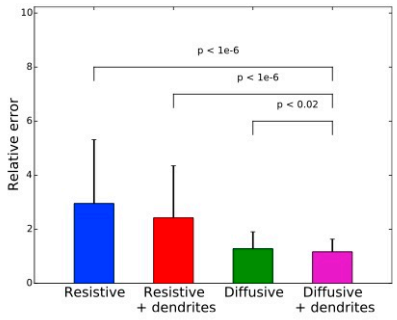

FIGURE 5 Average fitting error of the four models. The figure shows the average goodness of fit for four different models investigated (*Resistive*, *Resistive + dendrites*, *Diffusive*, and *Diffusive + dendrites*).The error bars are standard deviations of fitting errors. The testing variable used to compare the quality of these fits takes into account their different number of variables. Of all models, the diffusive models give the smallest error in all cases tested. The best fit is provided by the diffusive model with dendrite, although it is only marginally better than the diffusive model in a single-compartment model. To see this figure in color, go online.

modulus. The phase modulations can also be remarkably well captured by the diffusive model.

We also tested the possible influence of dendrites, by including an equivalent dendritic compartment in the circuit (Fig. 1 *C*, *right*). This addition could not rescue the resistive model, which was still unable to match the observations (Fig. 6). We have considered variations of dendritic parameters, including very long dendritic segments and different axial and leak conductances, and did not see any significant improvement by the addition of dendrites. In the diffusive model, taking the dendrites in account only enhanced marginally the agreement between experimental and theoretical curves. Statistical analysis showed that the improvement in quality from the resistive to the diffusive model was significant, and not due simply to a higher number of parameters. Furthermore, the apparent smaller number of parameters in resistive models can come from hidden assumptions, such as homogeneity and low resistivity of the extracellular medium.

These results were replicated in striatal neurons using purely sinusoidal input currents from 6 to 926 Hz (see Fig. 7; $N = 18$), thereby confirming that the global shape of the global cell impedance does not depend on the stimulation protocol. In addition, we tested a capacitive (RC) model of the extracellular space, but this model did not account for the modulus and the phase modulations (it was the worst fit of all models tested; not shown).

We also checked whether the quality of seals could affect the global intracellular impedance measurements. Indeed, if the cell membrane is bypassed, the impedance is no longer measured through the natural interface of a neuron membrane. The average of neurons with good seals (>1 GΩ) yields a slope of -0.5 ± 0.1 (see Fig. 2 *D*); in comparison, cells with extremely poor seals (e.g., 200 MΩ, not included in the data shown here) yielded a flatter impedance, with a slope between 0 and −0.3. This can be easily explained by replacing Z_{RC} by a resistance in the expression of Z_{eq}.

Finally, we checked whether part of the observed frequency dependence could be due to the recording pipette. We found that the frequency dependence of the patching pipette and silver-silver chloride electrode is negligible in ACSF (Fig. 3). These measurements show that the observed frequency dependence of the impedance cannot be attributed to the silver-electrode interface, and probably stems from the properties of the extracellular medium.

Global intracellular impedance in vivo

In a second set of experiments, the measurements were performed in vivo with whole-cell patch-clamp recordings of pyramidal cells of the somatosensory cortex, layer V (see scheme in Fig. 8 *A* and details in Materials and Methods). Similarly to Fig. 2, the modulus and the phase of the impedance were estimated by white-noise current injection (Fig. 8, *B* and *C*). Although the data display a high degree of noise (due to spontaneous synaptic inputs in vivo), they were in qualitative agreement with in vitro results on $N = 18$ cells. The resistive model did not capture the modulus amplitude, nor the phase of the global intracellular impedance of the neuron. The diffusive model was able to capture the essential variations, both in amplitude (modulus) and phase domain. Similar to in vitro measurements, the modulus yields a slope of -0.4 ± 0.1 (Fig. 8 *D*), and a minimum phase at ~−50° (Fig. 8 *E*), which significantly deviate from predictions of a resistive model.

As in the in vitro experiments, the addition of an equivalent dendritic compartment did not improve these differences. The resistive model with dendrites was also unable to account for the measurements, while the diffusive model provided acceptable fits to the data.

One must keep in mind that the in vivo measurements were made in the presence of low-frequency spontaneous activity, typical of anesthetized states. This synaptic bombardment probably explains the mismatch of all impedance models at low frequencies in vivo. Such a mismatch was not present in vitro.

Possible consequences of these measurements

Finally, to evaluate possible consequences of these measurements, we have considered two situations where the extracellular impedance can have strong consequences. A first consequence is the fact that the diffusive nature of the medium will necessarily impose frequency filtering properties on

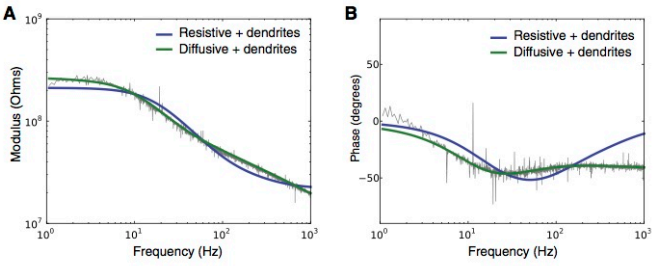

FIGURE 6 (*A* and *B*) Dendritic contribution to the global intracellular impedance of a cortical neuron recorded in vitro (current-clamp). Same arrangement of panels as in Fig. 2, except that the different curves show the best fit of two models to the experimental data (*blue*, resistive, *green*, diffusive), and both models included an equivalent dendritic compartment. Parameters of the models: (*resistive*) $R_s = 240$ MΩ, $C_s = 37$ pF, $R_e = 21$ MΩ, and $l_{dend} = 390$ μm; (*diffusive*) $R_s = 150$ MΩ, $C_s = 89$ pF, $A = 130$ MΩ, $B = -12$ MΩ, $f_W = 30$ Hz, and $l_{dend} = 12$ μm. (*A*, *B*, and f_W are parameters of the diffusive impedance scaling; respectively, its amplitude, phase, and cutoff frequency.) To see this figure in color, go online.

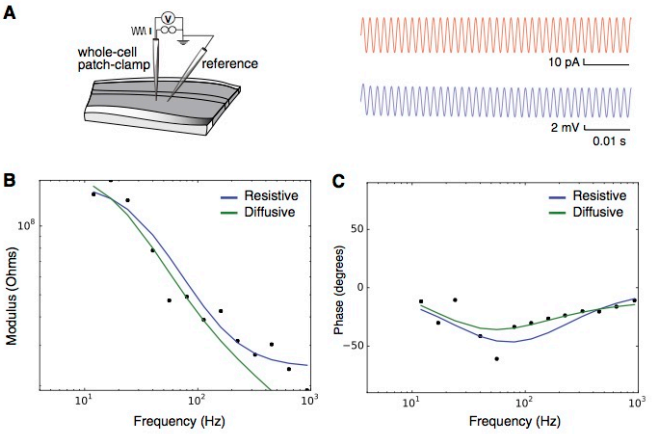

FIGURE 7 Global intracellular impedance measurements of a striatal neuron recorded in vitro (current-clamp) and stimulated with sinusoid inputs from 6 to 926 Hz. (*A*) Sine waves of current (*top*, *red*; minimum 25 samples and 20 cycles per sample) were injected in patched neurons while recording the intracellular potential (*top*, in *blue*; 16.7 kHz sampling). (*B*) Modulus of Z_{eq} (log scale) represented as a function of frequency ($\log_{10}(f)$), for sine wave current injection (600 pA amplitude). (*C*) Fourier phase of Z_{eq} in the same experiment. Parameters of the models: (*resistive*) $R_m = 120$ MΩ, $C_s =$ 46 pF, and $R_e = 28$ MΩ; (*diffusive*) $R_m = 130$ MΩ, $C_m = 59$ pF, $A = 58$ MΩ, $B = 43$ MΩ, and $f_W =$ 30 Hz. (A, B, and f_W are parameters of the diffusive impedance scaling; respectively, its amplitude, phase, and cutoff frequency.) Representative of $N = 18$ cells. To see this figure in color, go online.

extracellular potentials, which affects measurements made with extracellular electrodes. To illustrate this point, we simulated extracellular potentials generated by a current source corresponding to the total membrane current generated by an action potential (using the Hodgkin-Huxley model). We then calculated the extracellular potential at a distance from this current source, using either a resistive model, or a diffusive model (Fig. 9 *A*). Interestingly, one can see that the extracellular signature of the spike has a slower time course in diffusive conditions. A similar situation was also simulated

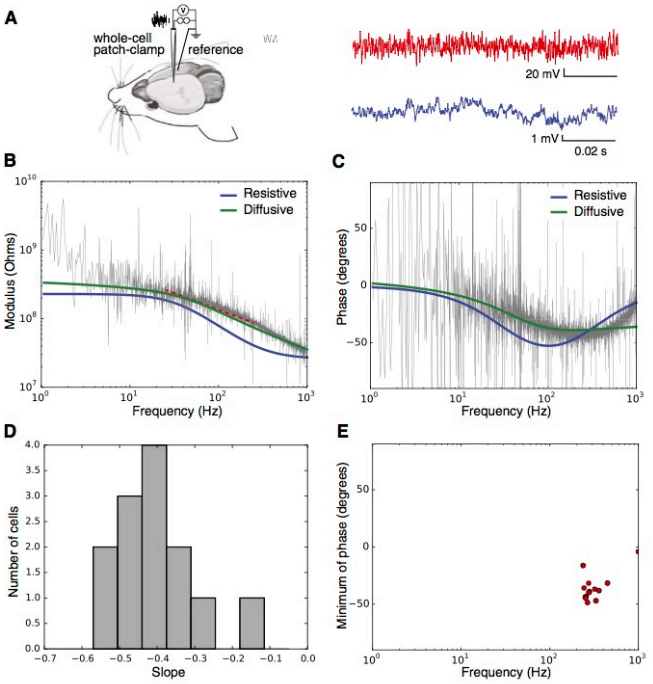

FIGURE 8 Global intracellular impedance of cortical neurons recorded in vivo in current-clamp. (*A*) Scheme of the recording configuration, with a similar representation as in Fig. 2 *A*, but performed in rat somatosensory cortex in vivo (with a contralateral reference electrode), using white-noise current injection. For these experiments, we injected 20 times the same Gaussian white-noise current trace (*top*, in *red*), then recorded at 20 kHz and averaged the intracellular potential (*top*, in *blue*). We calculated the impedance seen by the neuron. (*B*) Modulus of the impedance obtained, as a function of frequency. (*C*) Phase of the impedance. Parameters of the models: (*resistive*) $R_m = 230$ MΩ, $C_s = 28$ pF, and $R_e = 29$ MΩ; (*diffusive*) $R_m =$ 100 MΩ, $C_m = 21$ pF, $A = 250$ MΩ, $B = 24$ MΩ, and $f_W = 20$ Hz. (A, B, and f_W are parameters of the diffusive impedance scaling; respectively, its amplitude, phase, and cutoff frequency.) Representative of $N = 18$ cells. (*D*) Distribution of the slopes of Z_{eq} fitted between 25 and 250 Hz (linear fit, *red dashed lines* on the figures). (*E*) Coordinates of the minima of the Fourier phases for each cell. To see this figure in color, go online.

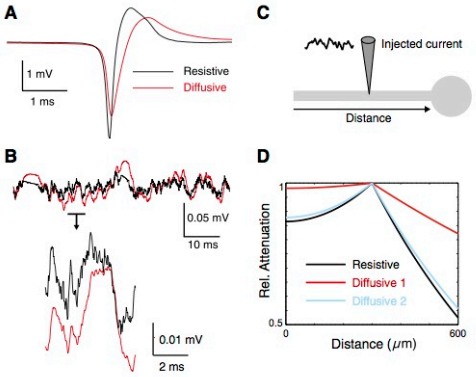

FIGURE 9 Consequences of the diffusive nature of the extracellular medium. (*A*) Simulation of LFP in the extracellular medium (10 μm from the soma) after injection of current after a spike waveform. The panel compares the extracellular spike obtained for a resistive medium (*black*), compared to a diffusive medium (*red*), where the filtering is evident. (*B*) Same simulation as in (*A*), but using injection of the combined current of noisy excitatory and inhibitory (subthreshold) inputs. In this case, the LFP values obtained in resistive and diffusive media are also differentially filtered. (*C*) Scheme of a ball-and-stick neuron model where a noisy current waveform was injected into the middle of the dendrite. (*D*) Relative voltage attenuation profile obtained (at 5 Hz) when the neuron is simulated in resistive (*black*) or diffusive (*red*, *blue*) media. Two diffusive configurations were simulated: (*diffusive 1*) diffusive intracellular and extracellular media (*red curves*); (*diffusive 2*) diffusive extracellular medium with resistive intracellular medium (*blue curves*). Using diffusive media results in a reduced voltage attenuation. In all cases, the resistive or diffusive media were simulated using the best fits to the impedances measured in vitro. To see this figure in color, go online.

using subthreshold noisy excitatory and inhibitory synaptic activity (Fig. 9 *B*). In both cases, the nature of the medium influences the shape and propagation of the LFP, for both extracellular spikes and LFP resulting from synaptic activity.

A second possible consequence is on the cable properties of neurons. This point was illustrated by simulating a ball-and-stick model subject to injection of a noisy current waveform in the dendritic cable (Fig. 9 *C*). As shown in Fig. 9 *D*, the attenuation of the voltage along the dendrite can be drastically different in a diffusive medium compared to a resistive medium, as noted previously in Bédard and Destexhe (27). Including a diffusive extracellular medium reduced voltage attenuation (Fig. 9 *D*, *blue curve*), but this reduction was the strongest when both intracellular and extracellular media were diffusive (*red curves*). Thus, the nature of the medium will also influence the shape and propagation of potentials in dendrites.

DISCUSSION

We have provided here, to our knowledge, the first experimental measurements of the impedance of the extracellular medium in natural conditions, both in vitro and in vivo. We found that not only is the estimated extracellular impedance higher compared to traditional metal-electrode measurements, it is also more frequency-dependent. The standard model, considering the medium as resistive, can account for metal electrode measurements, but not for natural impedance measurements. In contrast, we found that a diffusive model can account for most measurements, both in modulus amplitude and in phase. We also checked whether the inclusion of dendrites could affect these conclusions, but it did not qualitatively change these results.

It is noteworthy that these measurements are made between a neuron, and a reference electrode in the nearby tissue. Therefore, the current presumably flows in the entire tissue, and thus, the impedance measured can be considered macroscopic. From the different experiments realized here, we estimate that the impedance is determined by the region close to the membrane, within distances of approximately hundreds of microns in cerebral cortex.

The apparent inconsistency with the previous metal-electrode measurements can be resolved by considering that each kind of electrode has a specific interface and impedance, depending on its physical nature (7). Classical impedance measurement studies tackle this problem offline with a normalization by a measure in saline (3,10), online by removing the effect of the interface using the saturation due to large currents (5), or by minimizing the interface (6,29). In physiological conditions, neurons have an electrical interface with the extracellular medium, as a part of their normal environment. This interface should therefore not be removed when using neurons to evaluate the impedance of the extracellular medium, as it is one of the keys to explaining the electric field produced by an active cell.

The system presented here deals with the usual problems of electrode recordings (see Robinson (29)) in unusual ways, which solves some classical issues but raises new interrogations. First, the electrode—or neuron—must be standardized. It is remarkable to see that, despite the considerable cell-to-cell variability in size or morphology, we obtained here very consistent measurements, with very similar amplitude and phase profiles from cell to cell. These measurements can be captured with accuracy with a limited number of parameters, most of which are well known (R_m, C_m, ...). How the cellular morphology influences these results, and why this influence seems so small, constitute interesting subjects for future extensions of this work. Second, the spatial scale concerned by potential measurement and current injection is a gray area in the literature (see Nunez and Srinivasan (30)). We believe that the scale of a single neuron may be as relevant as the tip of traditional recording electrodes, of arbitrary size and position in an inhomogeneous medium, which can affect recordings significantly (14). Third, the interface of the electrode and its behavior must be linear and well understood within the measurement range, which we discussed previously.

Provided the system is operated with all necessary precautions, linearity is maintained (Fig. 4); the path of the injected currents in neuron compartments does not seem to be a crucial matter (Fig. 4) and injected currents splitting between different forms (free or bound charges, electric flux…) is not a problem within the generalized current formalism. Furthermore, the traditional four-electrode setup is designed to separate voltage recording from possible filtering by the interface generated when injecting current (6). In the system presented here, the silver-silver chloride wire has a very resistive interface (Fig. 3) and is negligible with respect to the main, relevant interface of the recorded neuron.

A possible explanation for the prominent role of ionic diffusion is that when a neuron acts as a current source, the electric field lines will not, in general, match the complex geometry of the extracellular medium. The trajectory of ions would thus be affected by obstacles such as cells and fibers (14), which would yield local variations in ionic concentrations. Ionic diffusion would therefore exert an important force on ions in the extracellular medium. A linear approximation of this phenomenon allows one to model this contribution by a Warburg-type impedance, scaling as $1/\sqrt{\omega}$. In addition, ionic diffusion is involved in membrane potential changes, and participates as well in maintaining the Debye layer surrounding the membrane (31). Taken together, these factors could explain why these measurements are in such good agreement with the diffusive model.

Despite this agreement, the participation of diffusive phenomena can vary with age and experimental conditions. As the brain gets older, the extracellular volume fraction shrinks, which could make ionic diffusion even stronger and thus reinforce the Warburg component of the natural impedance. Furthermore, in vivo tissue may be more confined than in vitro, with a similar result on the importance of ionic diffusion. One can thus reasonably expect Z_W to be stronger in P30 rats in vivo ($N = 18$) than in P12–P16 mice in vitro ($N = 31$). Indeed, the components A and B of Z_W are significantly stronger in vivo in P30 rats than in vitro in P12–P16 mice (comparing the medians $\pm$ the standard error of the mean: respectively, 96 $\pm$ 12 MΩ vs. 138 $\pm$ 16 MΩ for A, and 6.6 $\pm$ 2.7 MΩ vs. 28 $\pm$ 3.7 MΩ for B). Thus, the age of the subject and the type of recording need to be taken into account when using measured values of the natural impedance. In particular, it may lead to an underestimation of Z_W in this article, because we mainly focused on in vitro recordings in young mice; our conclusions on the importance of ionic diffusion are thus rather conservative. It is noteworthy that in between these two sets of observations, the Warburg frequency remains the same: 43 $\pm$ 3 Hz in vitro versus 42 $\pm$ 3 Hz in vivo.

Our results do not disqualify the previous measurements, but are complementary. We suggest that for all cases where the current sources are generated by natural conditions (i.e., by neurons), the global intracellular impedance should be used. This is the case, for example, when analyzing the LFP signal, or with current source density (CSD) analysis. In cases where a metal electrode is used to inject current, the metal-electrode impedance would be relevant, for example, in deep-brain-stimulation paradigms.

Note that, although the diffusive model accounts very well for the modulus and phase variations of the global intracellular impedance, small deviations do exist—particularly at high frequencies. The latter may be due to a number of phenomena, including variability in neuron geometry or limitations of the linear approximations used here. The existence of shunt-type structures due to the liquid around the electrodes is also not to be excluded. Further studies should be designed to identify the contribution of such factors, e.g., pharmacological inactivation of nonlinear channels. Two arguments suggest that this formalism is satisfactory: the strong reproducibility of results across 31 recorded neurons in vitro, despite intrinsic biological variability; and the coherence between the diffusive model and experimental data.

The exact boundaries of the domain where these results apply are still to be determined. For example, in Fig. 9 we are extrapolating into a nonlinear region to make implications about the shape of the action potential. We think this extrapolation is acceptable because nonlinear behavior is mostly happening in the highest frequencies, barely overlapping with the LFP frequency range (see also Appendix S2 in the Supporting Material), but one should be aware of that caveat.

Finally, using computational models, we illustrated consequences of the medium nonresistivity on extracellular and intracellular potentials. A number of fundamental theoretical equations used in neuroscience, such as CSD analysis (32), or neuronal cable equations (25,26), were originally derived under the assumption that the extracellular medium is resistive. If the medium is nonresistive, these equations are no longer valid and must be generalized. Attempts for such generalizations were proposed recently for CSD analysis (22) and cable equations (27), but they were not constrained by measurements. The simulations provided here show that including a diffusive impedance based on these measurements has significant consequences, both for extracellular potentials and for the electrotonic properties of neurons. The shape of the extracellular spike may be affected by the nature of the medium (Fig. 9 *A*), assuming that one can extrapolate these results to the nonlinear region of the V_m. This shows that the sharpness of the extracellular spike may be influenced by the properties of the medium, which constitutes another factor that could complicate the identification of neurons from spike shape. The dendritic attenuation is also reduced in the presence of a diffusive medium (Fig. 9, *D* and *E*), as shown in Bédard and Destexhe (27). Upon extrapolating these results, it seems that the sources estimated by CSD analysis could be greatly affected by the nature of the extracellular medium; this constitutes a direct extension of this study. Similarly, source reconstruction methods from the EEG are also likely to be affected

by the nature of the medium, and thus, these methods may need to be reevaluated as well.

SUPPORTING MATERIAL

Two appendices are available at http://www.biophysj.org/biophysj/supplemental/S0006-3495(15)01176-5.

AUTHOR CONTRIBUTIONS

J.-M.G., S.V., M.N., P.P., and T.B. performed the in vitro experiments; L.V. performed the in vivo experiments; analyses were designed by A.D. and C.B. and were performed by J.-M.G., C.B., M.N., V.K., and A.D.; and A.D., T.B., and L.V. co-supervised the work.

ACKNOWLEDGMENTS

We thank Sylvie Perez for technical assistance with the in vivo experiments.

Research was supported by the Centre National de la Recherche Scientifique (CNRS), the Paris-Saclay Excellence Network (IDEX), the Institut National de la Santé et de la Recherche Médicale (INSERM), Collège de France, Fondation Brou de Laurière, Fondation Roger de Spoelberch, the French Ministry of Research, the French National Research Agency (ANR, the Complex-V1 project), the Eiffel Excellence Grants program, and the European Community (BrainScales No. FP7-269921, Magnetrodes No. FP7-600730, and the Human Brain Project No. FP7-604102).

SUPPORTING CITATIONS

References (33,34) appear in the Supporting Material.

REFERENCES

1. Makarova, J., M. Gómez-Galán, and O. Herreras. 2008. Variations in tissue resistivity and in the extension of activated neuron domains shape the voltage signal during spreading depression in the CA1 in vivo. *Eur. J. Neurosci.* 27:444–456.
2. Buzsáki, G., C. A. Anastassiou, and C. Koch. 2012. The origin of extracellular fields and currents—EEG, ECoG, LFP and spikes. *Nat. Rev. Neurosci.* 13:407–420.
3. Ranck, J. B., Jr. 1963. Analysis of specific impedance of rabbit cerebral cortex. *Exp. Neurol.* 7:153–174.
4. Nicholson, C. 2005. Factors governing diffusing molecular signals in brain extracellular space. *J. Neural Transm. (Vienna).* 112:29–44.
5. Logothetis, N. K., C. Kayser, and A. Oeltermann. 2007. In vivo measurement of cortical impedance spectrum in monkeys: implications for signal propagation. *Neuron.* 55:809–823.
6. Schwan, H. P. 1968. Electrode polarization impedance and measurements in biological materials. *Ann. N. Y. Acad. Sci.* 148:191–209.
7. Geddes, L. A. 1997. Historical evolution of circuit models for the electrode-electrolyte interface. *Ann. Biomed. Engin.* 25:1–14.
8. McAdams, E. T., and J. Jossinet. 2000. Nonlinear transient response of electrode-electrolyte interfaces. *Med. Biol. Eng. Comput.* 38:427–432.
9. Schwan, H. P. 1966. Alternating current electrode polarization. *Biophysik.* 3:181–201.
10. Gabriel, S., R. W. Lau, and C. Gabriel. 1996. The dielectric properties of biological tissues: II. Measurements in the frequency range 10 Hz to 20 GHz. *Phys. Med. Biol.* 41:2251–2269.
11. Wagner, T., U. Eden, …, A. Valero-Cabré. 2014. Impact of brain tissue filtering on neurostimulation fields: a modeling study. *Neuroimage.* 85:1048–1057.
12. Bédard, C., S. Rodrigues, …, A. Destexhe. 2010. Evidence for frequency-dependent extracellular impedance from the transfer function between extracellular and intracellular potentials: intracellular-LFP transfer function. *J. Comput. Neurosci.* 29:389–403.
13. Dehghani, N., C. Bédard, …, A. Destexhe. 2010. Comparative power spectral analysis of simultaneous electroencephalographic and magnetoencephalographic recordings in humans suggests non-resistive extracellular media. *J. Comput. Neurosci.* 29:405–421.
14. Nelson, M. J., C. Bosch, …, P. Pouget. 2013. Microscale inhomogeneity of brain tissue distorts electrical signal propagation. *J. Neurosci.* 33:2821–2827.
15. Paille, V., E. Fino, …, L. Venance. 2013. GABAergic circuits control spike-timing-dependent plasticity. *J. Neurosci.* 33:9353–9363.
16. Nelson, M. J., P. Pouget, …, J. D. Schall. 2008. Review of signal distortion through metal microelectrode recording circuits and filters. *J. Neurosci. Methods.* 169:141–157.
17. Pods, J., J. Schönke, and P. Bastian. 2013. Electrodiffusion models of neurons and extracellular space using the Poisson-Nernst-Planck equations—numerical simulation of the intra- and extracellular potential for an axon model. *Biophys. J.* 105:242–254.
18. Warburg, E. 1899. Ueber das verhalten sogenannter unpolarisir Barer elektroden gegen wechselstrom. *Wied. Ann.* 67:493–499.
19. Warburg, E. 1901. Ueber die polarisations kapazitaet des platins. *Ann. Phys.* 6:125–135.
20. Bisquert, J., G. Garcia-Belmonte, …, P. Bueno. 1999. Theoretical models for AC impedance of finite diffusion layers exhibiting low frequency dispersion. *J. Electroanal. Chem.* 475:152–163.
21. Bédard, C., and A. Destexhe. 2009. Macroscopic models of local field potentials and the apparent 1/*f* noise in brain activity. *Biophys. J.* 96:2589–2603.
22. Bédard, C., and A. Destexhe. 2011. Generalized theory for current-source-density analysis in brain tissue. *Phys. Rev. E Stat. Nonlin. Soft Matter Phys.* 84:041909.
23. Pettersen, K. H., and G. T. Einevoll. 2008. Amplitude variability and extracellular low-pass filtering of neuronal spikes. *Biophys. J.* 94:784–802.
24. Lindén, H., K. H. Pettersen, and G. T. Einevoll. 2010. Intrinsic dendritic filtering gives low-pass power spectra of local field potentials. *J. Comput. Neurosci.* 29:423–444.
25. Rall, W. 1962. Electrophysiology of a dendritic neuron model. *Biophys. J.* 2:145–167.
26. Rall, W. 1995. The Theoretical Foundations of Dendritic Function. MIT Press, Cambridge, MA.
27. Bédard, C., and A. Destexhe. 2013. Generalized cable theory for neurons in complex and heterogeneous media. *Phys. Rev. E Stat. Nonlin. Soft Matter Phys.* 88:022709.
28. Hines, M. L., and N. T. Carnevale. 1997. The NEURON simulation environment. *Neural Comput.* 9:1179–1209.
29. Robinson, D. 1968. The electrical properties of metal microelectrodes. *Proc. IEEE.* 56:1065–1071.
30. Nunez, P. L., and R. Srinivasan. 2005. Electric fields of the brain. *In* The Neurophysics of EEG, 2nd Ed.. Oxford University Press, Oxford, UK.
31. Hille, B. 2001. Ionic Channels of Excitable Membranes. Sinauer, Sunderland, MA.
32. Mitzdorf, U. 1985. Current source-density method and application in cat cerebral cortex: investigation of evoked potentials and EEG phenomena. *Physiol. Rev.* 65:37–100.
33. Rudin, W. 1976. Principles of Mathematical Analysis. McGraw-Hill, New York.
34. White, S. H. 1970. A study of lipid bilayer membrane stability using precise measurements of specific capacitance. *Biophys. J.* 10:1127–1148.

ANNEX

Article II

A recording circuit for cross-talk between recording channels and its implications for electrophysiology experimentation

Nelson M, Valtcheva S and Venance L
(in preparation)

A recording circuit for cross-talk between recording channels and its implications for electrophysiology experimentation

Matthew J. NELSON[1], Silvana VALTCHEVA[2], Laurent VENANCE[2]

[1] NeuroSpin Center, Cognitive Neuroimaging Unit, INSERM U992, Commissariat à l'Energie Atomique (CEA), Gif-sur-Yvette, France

[2] Centre Interdisciplinaire de Recherche en Biologie (CIRB), CNRS UMR 7241 - Inserm U1050, Collège de France, Paris, France;

Running head:

Cross-talk circuit and implications for neuroscience

Address for correspondence:

Matthew Nelson (matthew.nelson@cea.fr)

ABSTRACT

Modern neurophysiological experiments are being performed in an increasingly parallel fashion with simultaneous recordings from many channels often separated by very small distances. A unique methodological concern for multiple electrode experiments is that of capacitive coupling (cross-talk) between channels, to which such recordings would potentially be susceptible. Yet the nature of the cross-talk recording circuit is not widely known in the field and the extent to which it might practically affect the experiments being conducted today in neuroscience has never been investigated. Here we describe a simplified electrical circuit to model simultaneous recording or stimulation with two or more electrodes. We demonstrate the validity of the model across a range of experimental configurations, both intracellularly and extracellularly and for both *in vitro* brain slice and *in vivo* whole-brain preparations. Consistent with the model, cross-talk increases with higher frequencies and with higher electrode impedance of the channel receiving the cross-talk. Recorded cross-talk signals are characteristically positively phase shifted, leading the originating signal up to 90 degrees. Nevertheless, cross-talk amplitudes remain a small fraction of the originating signal. For a typical extracellular recording electrode recording in our tests, .0006 of the original signal amplitude was transferred between channels at 900 Hz. The result would thus be negligible when both originating and receiving electrodes record signals of the same magnitude, as with multiple electrode extracellular recordings for example. However this effect can be noticeable in extracellular traces when intracellular signals are recorded simultaneously on nearby channels, or in some cases when stimulation and simultaneous recording is applied, because of the different orders of magnitude of the two signals. We experimentally demonstrate observable cross-talk of action potential waveforms between intracellular and extracellular channels. We then discuss some techniques for detecting and experimentally reducing cross-talk.

INTRODUCTION

Once upon a time in neuroscience, neurophysiological experiments were performed on a single channel at a time, including extracellular (Mountcastle 1957) and intracellular (Hodgkin et al. 1952) experiments. Today neurophysiological experiments are performed in an increasingly parallel fashion with simultaneous recordings from many channels (Buzsáki 2004). Beyond merely increasing the throughput of a given experiment, multiple channel experiments afford unique inferences not available to single channel studies (Borst et al. 1995; Debanne et al. 2008).

A unique methodological concern for multiple electrode experiments is that of capacitive coupling (cross-talk) between channels. This coupling occurs along the lengths of electrode shanks located close to each other and is artificially introduced into the naturally occurring electrical circuits of the brain whenever simultaneous multiple electrode recordings are performed. Modern multi-channel neuronal recording methods have been becoming increasingly parallel with increasingly smaller inter-electrode distances (Khodagholy et al. 2015), raising the question of whether cross-talk would ever create a problem for these designs. Additionally, cross-talk will be more apparent for experiments involving large differences in amplitudes between signals (Nagaoka et al. 1992), with the larger amplitude signal more easily contaminating the smaller amplitude signal. This is precisely the case for simultaneous intracellular and extracellular experiments, which have seen increased interest in recent years (Hasenstaub et al. 2005; Poulet and Petersen 2008; Atallah and Scanziani 2009; Glickfeld et al. 2009; Poo and Isaacson 2009; Trevelyan 2009; Bazelot et al. 2010; Okun et al. 2010; Anastassiou et al. 2011, 2015; Nelson et al. 2013; Blot and Barbour 2014; Gomes et al. 2016; Haider et al. 2016), among other situations.

Some neurophysiologists may be aware of the existence of cross-talk, but the nature of the cross-talk recording circuit is not widely known in the field and the extent to which it might practically affect the types experiments being conducted today in neuroscience has never been fully investigated. In reviewing the literature, we were only able to find the issue discussed in depth with respect to surface EMGs (Kilner et al., 2002; Farina et al., 2004, but see Nagaoka et al., 1992). Further, a mention of the potential concerns for cross-talk rarely appears in even the methodology sections of any papers (but see Blot and Barbour, 2014).

We sought to explore the topic of cross-talk in and present the details of import for neurophysiology experimenters and anyone interpreting multiple channel electrophysiological data. Here we review the signatures of cross-talk and present a simplified circuit and concurrent model to estimate cross-talk between channels. We experimentally verify the behavior of such circuits and describe the practical implications of cross-talk for present-day neurophysiology experiments.

METHODS

All experiments involving animals were performed in accordance with the local animal welfare committee (Center for Interdisciplinary Research in Biology) and EU guidelines (directive 86/609/EEC).

Recording procedures- Brain slice recordings

Extracellular or whole-cell recordings of striatal neurons were performed in horizontal brain slices (330 μm) from Oncins France Strain A (OFA) rats (Charles River, L'Arbresle, France) (postnatal days P_{17-30}), using procedures described previously (Fino et al. 2009). Using a temperature control system (Bathcontroller V, Luigs&Neumann, Ratingen, Germany) recordings were performed at 34°C. Slices were continuously superfused at 1.5-2 ml/min with an extracellular solution similar to cerebro-spinal fluid. The composition was (mM): 125 NaCl, 2.5 KCl, 25 glucose, 25 $NaHCO_3$, 1.25 NaH_2PO_4, 2 $CaCl_2$, 1 $MgCl_2$, 10 μM pyruvic acid bubbled with 95% O_2 and 5% CO_2. Pipettes used for whole-cell recordings were filled with (mM): 105 K-gluconate, 30 KCl, 10 HEPES, 10 phosphocreatine, 4 ATP-Mg, 0.3 GTP-Na, 0.3 EGTA (adjusted to pH 7.35 with KOH). Pipettes used for extracellular recordings or stimulation were filled with the same extracellular solution used to bathe the slice. Recordings were made with EPC 10-3 amplifiers (HEKA Elektronik; Lambrecht, Germany) with a very high input impedance (~1 TΩ) to ensure there was no appreciable signal distortion imposed by the high impedance electrodes (Nelson et al. 2008). For all experiments, a circular reference electrode surrounding the slice was used to avoid biasing current travel in any direction.

During the experiments, individual neurons and the microscale local composition of the extracellular space were identified using infrared-differential interference contrast video-microscopy with a CCD camera (Optronis VX45; Kehl, Germany). For experiments that involved whole-cell recordings, target cells were chosen avoiding obvious extracellular obstructions (blood vessels, fiber bundles, etc.) that would not bias the amounts of obstructions in the slice in any direction (Nelson et al. 2013). Recorded neurons were identified as striatal output neurons based on apparent cell morphology, current-voltage relationships and specific firing patterns (Fino et al. 2005, 2008).

Recording pipettes of varying impedances across experiments (ranging from 1.7 to 17.2 MΩ) were inserted into the slice via a micromanipulator, and either were used for whole-cell recordings or remained suspended in the extracellular space within the slice 100 μm below the surface of the slice. With the recording pipette in place, a signal pipette (6-8 MΩ impedance) filled with extracellular solution was placed suspended in the air above the bath, with its tip approximately 50 microns away in a lateral direction from the recording pipette shaft. Sinusoidal

stimuli were then driven through the signal pipette as described below. For the recording in Figure 1, we varied the location of the recording pipette between recordings while maintaining the signal pipette in the same position.

To calculate pipette impedance across frequencies, sinusoidal stimuli (see below for details) were applied with the pipette in the slice without other pipettes present. The pipette impedance for each frequency was taken as the ratio of voltage to current. For some recordings this was done while performing whole-cell recordings with that electrode.

Recording procedures- In vivo recordings

In vivo experiments were conducted in adult male Sprague-Dawley rats (Charles River, L'Arbresle, France) weighing 275-300g. Rats were placed in a stereotaxic apparatus (Unimecanique, Asniere, France) after anesthesia induction with a 400mg/kg intra-peritoneal injection of chloral hydrate (Sigma-Aldrich, Saint-Quentin Fallavier, France). A deep anesthesia maintenance was ensured by intra-peritoneal infusion on demand of chloral hydrate delivered with a peristaltic pump set at 60mg/kg/hour turned on one hour after induction. Proper depth of anesthesia was assessed regularly by testing the cardiac rhythm, EcoG activity, the lack of response of mild hindpaw pinch and the lack of vibrissae movement. The electrocardiogram was monitored throughout the experiment and body temperature was maintained at 36.5° C by a homeothermic blanket.

Two craniotomies were performed, one for the insertion of a reference electrode in the somatosensory cerebral cortex (layer2/3) and one to allow the recording of activity from within the cortex. For the recording electrode, a 2x2 mm craniotomy was made to expose the left posteromedial barrel subfield at the following coordinates: posterior 3.0-3.5 mm from the bregma, lateral 4.0-4.5 mm from the midline. To increase recording stability the cistern was drained.

Recording pipettes of varying impedances across experiments (ranging from 1.7 to 9.2 MΩ) filled with extracellular solution were inserted into the brain and lowered 1.5 mm below the cortical surface. With the recording pipette in place, a signal pipette (6-8 MΩ impedance) filled with extracellular solution was placed suspended in the air above the brain, with a tip approximately 50 microns away in a lateral direction from the recording pipette shaft. Sinusoidal stimuli were then driven through the signal pipette as described below.

Stimuli-sinusoids

Sine waves of 13 different frequencies were tested, varying approximately evenly on a logarithmic scale ranging from 6 Hz to 905 Hz. Specific frequencies tested were: 6, 12, 24, 40, 57, 80, 113, 160, 225, 320, 450, 640 and 905 Hz. For some experimental configurations, not all

frequencies were gathered. Recordings were sampled at 16.7 kHz. 100 to 300 traces of 100 to 1500 ms in length were averaged before recording the data to disk for offline analyses. Longer stimulus lengths and more traces were recorded for low frequency stimuli for which the cross-talk signal-to-noise ratio was lower. The order of the presentation of the frequencies was randomized for each recording.

For most configurations, stimuli were introduced with the signal electrode in voltage clamp mode in order to ensure constant voltage amplitude, regardless of the impedance from the signal electrode to ground. This was particularly important when the signal electrode was suspended in the air. The signal amplitudes for most configurations were 300 mV for frequencies from 6 Hz to 113 Hz, and 50 mV for frequencies from 160 Hz to 926 Hz. For select experiments indicated, amplitudes of 100 μV across all frequencies were used to mimic typical extracellular LFP recording amplitudes. For the impedance measurements of the pipette in series with a neuron while the pipette performed a whole-cell recording, we used a constant current stimulus of 300 pA at every frequency to ensure that the current levels would not damage the recorded neuron. Intracellular and extracellular voltages were recorded completely unfiltered. Before conducting experiments, we verified via control recordings with an external signal generator in the bath without a slice that any amplitude changes or phase shifts introduced by the equipment into the recordings across frequencies were negligible.

Natural LFP recordings

Extracellular recordings of natural LFPs were performed for both in-vitro slice preparations and in vivo whole-brain preparations. A recording pipette was suspended in the air approximately 50 μm away from the shaft of the signal originating electrode which passively recorded potentials in two conditions: suspended in the air above the neural preparation (in vivo or in vitro), or inserted in the neural preparation at the same depths described above for the sinusoidal recordings for each preparation. For the in vitro preparation, dihydrokainic acid (Tocris Bioscience) (DHK, 300uM) was added to the slice to increase the spontaneous LFP activity by blocking glutamate re-uptake and neuronal depolarization. 5 minutes of spontaneous activity was recorded in both conditions.

Natural action potential recordings

To record the cross-talk effect of natural action potential waveforms, a recording electrode was placed submerged in the aCSF bath, but above the slice, 50 microns away laterally from the shaft of a pipette performing a whole-cell recording of a neuron. Repeated step-function current injections of 620 pA for 350 ms were applied to the neuron in order to elicit a large number of

spikes while recording the voltage continuously on both channels. These recordings were sampled at 50 kHz.

Analyses

Offline analyses were conducted in Matlab (Natick, MA). The amplitude and phase of each digitized recording at the known stimulus frequency were determined using techniques previously describe (Nelson et al. 2013). Noise levels were estimated for each experiment at each frequency by averaging across all the recordings in the experiment when the given frequency was not the frequency of the stimulus sinusoid. When averaging across experiments, the phase and amplitude of each measurement were first combined and averages were then performed in the complex plane, although we observed that for these data results were the same when calculating the average amplitude and circular average phase individually.

For the analysis of natural LFPs, spectra were calculated using the function pwelch from matlab's signal processing toolbox, dividing the data into 8 equal-length segments with 50% overlap. Segments were windowed with a Hamming window. The resulting spectra were smoothed on a log-log scale with each point showing the average spectrum over a width of 0.25 in base 10 log of frequency space, at a sampling distance of 0.25 in base 10 log of frequency. Results near 50 Hz were omitted.

Equipment sources of cross-talk

We tested to rule-out equipment sources of cross-talk downstream of the amplifiers-electrodes circuits we present here. This was done one channel at a time by attaching a BNC shorting cap to each channel and recording from that channel while the stimulation channel delivered sinusoidal current in the same manner as in the rest of our experiments. The resulting signal was flat on the shorted channel for all frequencies and configurations.

RESULTS

We observed that when one electrode in a bath is placed near another electrode suspended in the air that is made to carry a sine wave voltage, some amount of the sine wave at the same frequency becomes present in the electrode in the bath (Figure 1A). Since the electrode from which the signal originates is suspended in the air, we can be certain that the voltage present in the second electrode in this situation results only from capacitive cross-talk between the electrodes. Importantly, this cross-talk would still be present in the case of simultaneous recordings with two or more electrodes placed in a neural preparation and might need to be considered when interpreting such data. Interestingly, after removing the second pipette from the bath, the recorded cross-talk signal increases considerably (Figure 1 B) and becomes instead in-phase with the original signal. When the electrode is moved far enough away, the recorded cross talk can be made to disappear entirely beneath the noise floor of the channel (Figure 1C).

Equivalent circuit

We present a simplified recording circuit (Figure 2) to describe simultaneous recording of more than one channel. Additional complications could always be added to the circuit to improve precision, but this circuit suffices to describe the phenomena we explore here, which are the practical implications of cross-talk in neuroscience. To describe the implications of the circuit, we recall the behavior of a voltage divider shown in Figure 2C, which yields the resulting relationship:

$$\frac{V_B(\omega)}{V_A(\omega)} = \frac{Z_B(\omega)}{Z_A(\omega)+Z_B(\omega)} \qquad (1)$$

where (ω) indicates that the given variable is a function of frequency. Thus, the ratio of V_B to a signal that is present at V_A connected in series along a path to ground is equal to the ratio of the impedance of the portion of the path following V_B (i.e. Z_B) to the impedance of the entire path $(Z_A + Z_B)$. This relation follows from the application of Ohm's law and a conservation of current.

We apply this basic concept to the circuit shown in Figure 2A and B which applies to both in vitro slice recordings or grounded in vivo whole brain recordings in order to derive an expression for the cross-talk voltage recorded. We denote the voltage present in the signal originating electrode to be V_{elec1}. This voltage could arise from recording neural activity intracellularly or extracellularly as is shown in the circuit of Figure 2A, or from externally applied stimulation for example. A second electrode records a cross-talk voltage from the first electrode, which we denote as V_{elec2}. Note that either electrode could be performing whole-cell recordings, as shown for electrode 1 in Figure 2A. Doing so would just add a component to the effective impedance at the electrode's tip, but would not change the behavior of the overall circuit. The cross-talk voltage ratio can be reduced to the approximation in equation 2:

$$\frac{V_{elec2}(\omega)}{V_{elec1}(\omega)} = \frac{(Z_{elec2\prime}+Z_{extra3}\|(Z_{extra2}+Z_{extra1}))\|Z_a}{Z_{cross}+(Z_{elec2\prime}+Z_{extra3}\|(Z_{extra2}+Z_{extra1}))\|Z_a} = \frac{Z_{elec2\prime\prime}\|Z_a}{Z_{cross}+Z_{elec2\prime\prime}\|Z_a} \approx \frac{Z_{elec2\prime\prime}(\omega)}{Z_{cross}(\omega)+Z_{elec2\prime\prime}(\omega)}$$

(2)

where $\|$ represents impedances adding in parallel, and the effective electrode impedance is written as $Z_{elec2\prime\prime} = Z_{elec2\prime} + Z_{extra3}\|(Z_{extra2} + Z_{extra1})$, which incorporates the impedance in the neural preparation downstream of the electrode. The (ω) is omitted for intermediate variables for brevity above, but it should be known that every variable can potentially vary with frequency. $Z_{elec2\prime}$ corresponds to the potential inclusion of Z_{intra} and Z_m in series with Z_{elec2} if the electrode is used for whole-cell recordings. The approximation in the rightmost side of the equation holds if $Z_a \gg Z_{elec2\prime\prime}$, which is typically the case for the high input-impedance amplifiers used in brain slice recordings. In our setup, Z_a is reported to be ~1TΩ (HEKA Elektronik, Lambrecht, Germany) which is several orders of magnitude over our measured values of $Z_{elec2\prime\prime}$.

This circuit and equation indicates that the current contributing to cross-talk voltages crosses a capacitance between the electrode shafts and then, rather than only traveling to ground through the amplifier input impedance, much of the current travels through the second electrode tip into the neural preparation en route to ground, as indicated in Figure 2A. V_{elec2} is thus in between the impedances Z_{cross} and $Z_{elec2\prime\prime}$ in a complete path to ground, and the resulting cross-talk voltage is describe by a voltage divider between those two impedances. This capacitive current traveling through the neural preparation is of course artificially introduced by the addition of these multiple electrodes and would not otherwise be present. Moreover, if $Z_{cross} \gg Z_{elec2\prime\prime}$ a final simplifying approximation of:

$$\frac{V_{elec2}(\omega)}{V_{elec1}(\omega)} \approx \frac{Z_{elec2\prime\prime}(\omega)}{Z_{cross}(\omega)} \quad (3)$$

can be considered, and the cross talk voltage magnitude will scale approximately linearly with the effective electrode impedance magnitude.

Equations 2 and 3 explain the increase in amplitude in Figure 1B when the electrode is removed from the bath, as this would have the effect of adding an additional very large capacitive impedance in series with Z_{elec2}, effectively raising the magnitude of $Z_{elec2\prime\prime}$ a large amount. Note that the behavior of this circuit stands in contrast with the circuit for single-channel electrode recording described in (Robinson 1968) and (Nelson et al. 2008), where the recorded voltage is effectively electrically independent of electrode impedance when high input-impedance initial amplifiers are used.

The phase of the signal is also well described by the above equations. Z_{cross} will always have a phase angle of -90°. Equations 2 and 3 predict that the phase of the resulting ratio will thus

be approximately the phase angle of $Z_{elec2''}$ plus 90°. Glass micropipettes are well described electrically by a simple frequency-independent resistance at the tip (see Figure 5) which has a phase of 0° across all frequencies. V_{elec2} for these electrodes would thus be phase shifted +90° relative to V_{elec1}, indicating the cross-talk component of V_{elec2} would *lead* V_{elec1} by that amount. This is precisely what is found in the example of Figure 1A. When the glass pipette is removed from the bath, $Z_{elec2''}$ effectively becomes dominated by large capacitive impedances to ground. The phase of $Z_{elec2''}$ effectively becomes -90°, equal to that of Z_{cross}. The cross-talk observed in V_{elec2} will thus be in-phase with V_{elec1} as well as a higher in amplitude, as is observed in Figure 1B. The resulting cross-talk phase recorded by metal microelectrodes will be positive but less than +90°, because the impedance phase of metal microelectrode tips are frequency dependent but between 0 and -90° for the frequencies of interest to neuroscientists (Nelson et al. 2008).

As described above, to perform a measurement that approximately isolates the cross-talk component of V_{elec2}, we placed the electrode carrying the source voltage above the bath. In the generalized circuit we present here, this would have the effect of adding an additional very large capacitive impedance in series with $Z_{elec1'}$, effectively leaving that portion of the circuit open, though for absolute precision, some current would still travel via this route into the bath or slice. This current would contribute to the voltage recorded by the second pipette in the bath or slice, combining additively with the cross-talk signal described in equations 2 and 3 above. However this contribution would be expected to be very low, as the relative voltage induced in the bath in this configuration is given by $\frac{Z_{bath}}{Z_{elec1}+Z_{cap1}+Z_{bath}}$, where Z_{cap1} is the capacitive impedance added by raising the first pipette above the water, and Z_{bath} is the impedance to reach ground after entering the bath. . Because Z_{bath} is expected to be much lower than the series combination of Z_{elec1} and Z_{cap1}, this contribution to V_{elec2} should be relatively negligible.

Demonstrating and testing the equivalent circuit

Figure 3 demonstrates the existence of cross-talk recorded in an extracellular electrode when a voltage signal is sent through a nearby channel suspended in the air. At the signal levels tested here, the cross-talk rises above the noise, with higher magnitudes at higher frequencies and a phase that leads the originating signal voltage by about 90° across frequencies. We showed that this same effect is present in in vivo extracellular recordings across a range of electrode impedances (Figure 4A). Specifically, the recorded cross-talk amplitude increased as the extracellular electrode impedance increased. Application of the model (equation 2) with the known impedance of the pipette permitted calculation of the cross-talk impedance, Z_{cross} (Figure 4B). The values were nearly identical across electrodes, with some slight systematic differences across electrodes likely

resulting from differential effects of stray capacitance unaccounted for in the simplified model. Z_{cross} decreases linearly with frequency on a log-log scale with an approximate slope of -1 and a phase of nearly -90°, as anticipated for the impedance of a simple capacitance. Using the average value for Z_{cross} and the known impedance of each extracellular electrode, we used the rightmost expression of equation 2 to predict the expected voltage ratio. These yielded close results to the observed data (solid versus dashed lines in Figure 4A), indicating that the quantitative predictions of the model are held in these data. Across frequencies and electrodes for this configuration we estimated the capacitance underlying Z_{cross} to be 87 pF.

The calculations described above to determine the predicted values in Figure 4A assume that the pipette impedance is resistive and constant across frequencies, using the value estimated from Patchmaster software (HEKA Elektronik, Lambrecht, Germany) using a square biphasic pulse of 5 ms duration per phase. We verified the assumption by performing single electrode tests measuring pipette impedances across for frequencies for a range of pipette impedances (Figure 5). The impedance of these pipettes is generally resistive (with phases near zero) and constant across frequencies. Some effects of stray capacitances can be observed though at high frequencies for high impedance pipettes, which causes a negative phase shift and depressed impedance moduli over those ranges. These effects are seen over these ranges because both higher frequencies and higher pipette resistances result in the parallel stray capacitive routes becoming increasingly less impeding relative to the direct route through the pipette tip. Note that observation that the impedance of glass micropipettes surrounding a metallic filament is well described as a constant resistance across frequencies stands in stark contrast to the impedance of metal microelectrodes, which are well modeled by resistance and capacitance in parallel (Robinson 1968; Grimnes and Martinsen 2008; Nelson et al. 2008). Considering that glass pipettes involve recording with a metallic inner filament, this can be explained by the fact that there is a low overall resistance in the very large metal to saline contact over the wire inside the pipettes. The impedance of the pipette is then dominated by the impedance at the pipette tip, which becomes large because of the microscopically small conductive opening there. This impedance through saline along a narrow passage still involves the transfer of ions through saline, which is resistive across frequencies (Grimnes and Martinsen 2008) thus resulting in the overall resistive and frequency independent nature of the glass pipettes used in slice electrophysiology.

Cross-talk recorded on an intracellular channel

Cross-talk originating from a nearby channel can also affect intracellular recordings, drawing current into the recorded neuron and later the bath via the electrode performing the recordings in the same manner demonstrated above for extracellular recordings. Figure 6 shows that

signals originating from an electrode suspended in air were transmitted above noise levels across frequencies to a nearby electrode that was performing a whole-cell recording. The recorded voltage effects had a positive phase shift as in Figure 3, but that phase shift was less than 90 degrees, resulting from the negative phase of the impedance of the recorded neuron. We explored this further by directly measuring the total impedance of a pipette performing a whole-cell recording in a slice (Figure 7A) in a subsample of cells for which cross-talk recordings were later performed. The impedance rose over lower frequencies, with moderate negative phases near -30°, and local phase minima at about 40 Hz. These impedances reflect the value of Z_{elec2}, in the model, as the pipette performing a whole-cell recording is considered as the recording pipette in this analysis. This impedance corresponds to the impedance of the pipette, the neuron and the extracellular space of the slice in series, and explains the observed phase shifts in the cross-talk voltages. The phase shifts predicted by the model approximation (equation 3) are 90° plus the phase of Z_{elec2}, which matches reasonably well with the observed values, including the shape of the cross-talk phase across frequencies (Figure 7B).

Practical Implications of the equivalent circuit

One can observe in Figure 3 that the overall ratio of recorded cross-talk voltage to the voltage in the originating signal is very low, peaking at 10^-3 at the highest frequencies we tested (~1 kHz), with even lower ratios than this for low frequencies. Are these ratios likely to cause a problem for multiple channel extracellular recordings? To test this we re-performed the same experiment as shown in Figure 3 for one experiment with lower originating signal peak-to-peak amplitudes of 200 μV, mimicking what would be a large voltage observed during an extracellular recording. Figure 8 shows that the cross-talk signal voltages do not exceed the noise level in the same recordings, for both the in vitro (Figure 8A) and in vivo preparations (Figure 8B). Importantly, these results indicate that even at close distances (here 50 μm of lateral separation at the pipette tips), there is no appreciable effect of cross-talk between extracellular recording channels for the amplitudes typically encountered for these recordings.

We tested the cross-talk transfer of spontaneous LFPs recorded from in vitro and in vivo preparations. For each preparation, a recording pipette was suspended in the air 50 microns away from the shaft of a signal pipette under two conditions: when the signal pipette was suspended in the air as well or when it was placed in a slice or brain recording spontaneous LFPs. There was no appreciable difference in the power spectra recorded between the two conditions for both slice and in vivo preparations, and the condition where LFPs were recorded in the signal electrode actually showed slightly less power across frequencies (Figure 9). The extracellular potentials recorded by the signal electrode were too weak to have an appreciable effect through cross-talk.

However, when performing simultaneous intracellular and extracellular recordings, the amplitudes differ by several orders of magnitude. Are the effects of cross-talk from natural signals in this situation observable? We tested this by recording a neuron in whole-cell mode with one pipette and eliciting it to spike using step injections of current while measuring the spike-triggered average resulting potentials recorded from a second pipette submerged in the bath but not in the slice. Figure 10 shows the average waveform recorded on the recording pipette, which matches the predicted waveform by equation 2. The recorded cross-talk waveform is a distorted version of the intracellular waveform, and is distinct in shape from extracellular spike waveforms recorded in absence of cross-talk which are typically negative going at their largest amplitude point. The waveform peaks before the intracellular waveform, resulting from the positive phase shift across frequencies described above. The peak cross-talk waveform voltage recorded here was 6.7 μV.

Note though that the intracellular spikes appear to have a baseline of -30 mV roughly, because we excited the neuron to this elevated baseline level. Completely natural spikes without this elevated baseline potential would be expected to have larger amplitudes and equally large resulting cross-talk waveforms.

DISCUSSION

We have demonstrated the existence of cross-talk between multiple channels in typical neuroscience preparations. We have presented a simplified electrical circuit model to explain the behavior of this circuit and developed simple equations to capture the bulk of the circuit's behavior. We demonstrated experimentally both in in vitro slice preparations and in vivo whole brain preparations that this model accurately describes cross-talk and amplitudes and phases. We have shown that the equations we describe can be used to predict cross-talk waveforms in novel situations. This cross-talk recorded on a given electrode will increase with its impedance and will have a positive phase shift so that the cross-talk voltage leads the originating signal voltage. We find that for a 1.7 MΩ pipette, a fraction of 0.0006 of the originating signal amplitude is recorded when separated by 50 μm from the signal pipette in our experiment (Figure 4A). This ratio will increase for higher frequencies and with less separation between the shafts of the recording electrodes. We have shown with artificial and natural stimuli that recordings of similar amplitude levels will not be affected by appreciably affected. However signals of largely differing amplitudes including simultaneous intracellular and extracellular recordings, or simultaneous stimulation and recording can have appreciable cross-talk effects that should be considered by experimenters and readers interpreting these data.

Practical implications of cross-talk in neuroscience

We find that multiple extracellular recordings are likely not to be affected by cross-talk considerably, nor are as far as we can tell EEG recordings. The results in Figures 8 and 9 are of course good news for modern multiple-electrode recording designs (e.g. (Maynard et al. 1997; Khodagholy et al. 2015) which have increasingly smaller separations between recording channels. Here we tested a distance of 50 μm and found no noticeable cross-talk for signals at approximate amplitude of typical LFPs. We do note however that the 50 μm that we mention here is the minimum distance between channels in our experiments. More so than just the minimum distance between channels, the integrated distance of the entire electrical paths between the channels up until the initial headstage amplifiers is the critical factor in the determination of cross-talk magnitude. The collection of wires across the multiple channels leading to the headstage for modern multiple-electrode arrays is likely to be the limiting factor that would lead to cross-talk problems for these designs if they are to occur, which we did not investigate here.

Cross-talk may warrant special consideration for simultaneous intracellular and extracellular experiments however. Intracellular experiments vary on the order of tens of millivolts, with peak-to-peak action potential amplitudes exceeding 100 mV, while extracellular potentials on the order of tens of microvolts can be of interest in extracellular recordings. In consideration of spike shapes in

particular, we note that the distorted, positive-peaked spike shape resulting from cross-talk will be one noticeable sign of potential cross-talk. Recording of classically-shaped negative-peaked action potentials that match the extracellular spike shape in recordings when the intracellular electrode is not present is a positive sign that the resulting waveform was not a result of cross-talk, though cross-talk waveforms could have impacted the precision of the resulting waveform measurement. Describing tests for cross-talk and indication of what cross-talk amplitudes were in these experiments would allow the user to better assess the precision of the resulting measurement.

Some of the most important results in the literature involving simultaneous intra- and extracellular measurements are classical studies from Gyori Buzsáki's group (Buzsáki et al. 1996; Henze et al. 2000) as well as recent work from (Anastassiou et al. 2015). In these papers the extracellular waveforms recorded are perfectly in line with waveforms recorded in scores of other extracellular recording only experiments. Through personal communication with the authors, we know that they were aware of the issue when conducting the experiment and took steps to reduce cross-talk, but this or what they did was not mentioned in the published text. Recent work continues these works in an impressive fashion in slice recordings

The questions we raise are not imply that all articles employing this methodology are certain to have cross-talk concerns, or that such concerns if they exist necessarily invalidate every conclusion of the paper. Taking one recent example in the literature, (Haider et al. 2016) used a regularized linear regression technique to explore coupling between simultaneously recorded intracellular and extracellular data. The distances between their electrodes (from 0.2 to 1.1 mm, on average 0.5 mm) may be sufficiently large to avoid concern, in addition to the fact that much of their results are driven by lower frequencies where cross-talk is less of a concern, especially for the pipettes they use to perform extracellular recordings. Our intention here is to review the cross-talk effect, which we feel may not be well-known by everyone in the field and implore readers and experimenters to then consider the effect in the future when it is appropriate.

Stimulation with simultaneous recording paradigms may also be susceptible to this in the same fashion (Anastassiou et al. 2011; Nelson et al. 2013), since the stimulating electrodes and extracellular recording electrodes may have vastly differing voltage magnitudes. Other techniques averaging over many events to reveal a small signal may also be susceptible to concern (Bakkum et al. 2013; Teleńczuk et al. 2015).

Signs of the occurrence of cross talk

There are some signals that experimenters can look for in their data as potential red flags for the presence of cross-talk.

A positive phase shift between a recording and a potential cross-talk source is one sign. This phase will be 90° if the signal is recorded with a glass pipette, but between 0 and 90° with more variation across frequencies if the signal is recorded with typical metal microelectrodes because of the phase of metal microelectrode impedances (Nelson et al. 2008).

Another cross-talk red flag is if the effect increases with electrode impedance across experiments where that parameter varied. Note this increase of voltage with electrode impedance is different from the single-channel behavior of recording a signal from the neural preparation in series with the electrode tip (Nelson et al. 2008). If using the correctly designed amplifiers, this will be independent of electrode impedance. Though both this circuit and the cross-talk circuit we describe here operate essentially as voltage dividers, the pipette impedance is on opposite sides of the mid-point voltage along the shaft of the electrode, which is what gets recorded during the experiments. In the cross-talk circuit, the current in the electrode shaft flows in the *reverse* direction to what is typically considered; after going across Z_{cross} the current flows across the electrode tip and back into the neural preparation and towards the ground there. Z_{elec2},, thus takes the place of Z_{a}, from the single electrode circuit (Nelson et al. 2008) and Z_{cross} takes the place of Z_{e},.

If the recorded amplitude decreases with an increase in distance from a suspected cross-talk voltage source, this would indicate the presence of cross-talk. However in many cases this dependence on distance may be difficult to disentangle from an effect of the distance from the desired signal source. For example, consider the measurements in (Anastassiou et al. 2015) simultaneously recording spike waveforms of the same neuron with an intracellular and extracellular electrode. Showing that the recorded potential in this instance decreases as the distance between the two electrodes increases likely gives no information about the presence of cross-talk since this decrease would happen to both cross-talk and desired voltage signal sources of the recorded voltage. In this case, maintaining the electrode tip position while varying the extracellular electrode orientation to be as perpendicular as possible to the intracellular electrode would affect the recording of cross-talk but not recording from the intended signal voltage. The authors may have even performed this very test, but it's not mentioned in the article, so it's difficult to say.

How to prevent and deal with cross talk

Here we review some ways to help address the issue of crosstalk for a study where it could be a concern. Distance of a recording electrode to potential cross-talk sources should be maximized, especially if the potential cross-talk source has a much larger amplitude than the signals of interest or the noise floor of the recording on the second channel being made. To this end, we note that the capacitance, which is to be minimized, will be proportional to the area of overlap between the two electrodes. Therefore the integrated distance between channels along the entire path of current

traveled between each electrode's tip and the primary headstage of the recording equipment should be maximized in instances where cross-talk is a concern. To maximize this distance for given recordings at two distinct points in space, the electrode shafts should be made to be as perpendicular as possible given the physical constraints of the recording.

As we have shown here, minimizing electrode impedance is another way to decrease the amplitude of cross-talk. Doing so however will decrease the noise floor of the electrode by roughly the same amount considering thermal noise, which will not make the cross-talk less visible relative to that. However both the thermal noise and cross-talk will be decreased in amplitude relative to the target signal being recorded, so minimizing electrode impedance inasmuch as it does not interfere with other aims of the study at hand is generally a good idea.

Inferences involving neural activity over lower frequencies will be less susceptible to cross-talk. This dependence will be stronger when the channel potentially receiving cross-talk is a micro-pipette as opposed to metal microelectrodes. The dominant element giving rise to the impedance of glass micropipettes is an essentially pure resistance at the narrow pipette tip. This is constant in amplitude and has a phase of 0° across frequencies, which data we present here verifies (Figure 5). Equations 2 and 3 shows that cross-talk at lower frequencies will thus be attenuated because Z_{cross} increases with lower frequencies, as it reflects the ratio of the recording electrode impedance to Z_{cross}. In contrast, the impedance of metal microelectrodes rises at lower frequencies, but not as steeply as Z_{cross}. Z_{cross} is a purely capacitive impedance that increases with lower frequencies, with a slope of -1 on a log-log scale. The slope of common metal-microelectrode impedance against frequency is less steep, and is roughly -0.6 with some differences at different frequencies (Nelson et al. 2008). Thus there is expected to be some increase in cross-talk for higher frequencies for metal microelectrode recordings, but less frequency dependence than glass pipette recordings.

If cross-talk has been recorded between two channels, in some cases the contamination can be removed after recording using a 'blind signal separation' algorithm described in (Kilner et al. 2002).

Implications, continued

People should write in their methods everything an outside person reading the article would need to reproduce it. We are aware that describing this type of information might not always make for the sexiest, most captivating prose in the world, but the details can be included in supplementary materials for example free of cost and journal space and without distracting from the message/story of the main text for the majority of interested readers. Particularly with increased attention to replication issues in science, the field needs to realize that the success of a particular study does not come merely when it is published, but rather when it is published and reproduced in an unrelated

laboratory. When publishing results, neuroscientists should be eager to help others to replicate their finding, not to show off an impossible feat that only the authors of the paper with their expertise are able to accomplish. Including all of the methodological details necessary for someone to do this we view is an important part of this process. It is our experience broadly in the neuroscience literature that this often does not happen.

Acknowledgements

We would like to thank Ueli Rutishauser for helpful conversations and comments on the manuscript.

REFERENCES

Anastassiou CA, **Perin R**, **Buzsáki G**, **Markram H**, **Koch C**. Cell type-and activity-dependent extracellular correlates of intracellular spiking. *J Neurophysiol* 114: 608–623, 2015.

Anastassiou CA, **Perin R**, **Markram H**, **Koch C**. Ephaptic coupling of cortical neurons. *Nat Neurosci* 14: 217–223, 2011.

Atallah BV, **Scanziani M**. Instantaneous Modulation of Gamma Oscillation Frequency by Balancing Excitation with Inhibition. *Neuron* 62: 566–577, 2009.

Bakkum DJ, **Frey U**, **Radivojevic M**, **Russell TL**, **Müller J**, **Fiscella M**, **Takahashi H**, **Hierlemann A**. Tracking axonal action potential propagation on a high-density microelectrode array across hundreds of sites. *Nat Commun* 4: 2181, 2013.

Bazelot M, **Dinocourt C**, **Cohen I**, **Miles R**. Unitary inhibitory field potentials in the CA3 region of rat hippocampus. *J Physiol* 588: 2077–2090, 2010.

Blot A, **Barbour B**. Ultra-rapid axon-axon ephaptic inhibition of cerebellar Purkinje cells by the pinceau. *Nat Neurosci* 17: 289–295, 2014.

Borst JG, **Helmchen F**, **Sakmann B**. Pre- and postsynaptic whole-cell recordings in the medial nucleus of the trapezoid body of the rat. *J Physiol* 489: 825–840, 1995.

Buzsáki G. Large-scale recording of neuronal ensembles. *Nat Neurosci* 7: 446–451, 2004.

Buzsáki G, **Penttonen M**, **Nádasdy Z**, **Bragin A**. Pattern and inhibition-dependent invasion of pyramidal cell dendrites by fast spikes in the hippocampus in vivo. *Proc Natl Acad Sci U S A* 93: 9921–9925, 1996.

Debanne D, **Boudkkazi S**, **Campanac E**, **Cudmore RH**, **Giraud P**, **Fronzaroli-Molinieres L**, **Carlier E**, **Caillard O**. Paired-recordings from synaptically coupled cortical and hippocampal neurons in acute and cultured brain slices. *Nat Protoc* 3: 1559–1568, 2008.

Farina D, **Merletti R**, **Indino B**, **Graven-Nielsen T**. Surface EMG crosstalk evaluated from experimental recordings and simulated signals. Reflections on crosstalk interpretation, quantification and reduction. *Methods Inf Med* 43: 30–35, 2004.

Fino E, **Deniau J-M**, **Venance L**. Cell-specific spike-timing-dependent plasticity in GABAergic and cholinergic interneurons in corticostriatal rat brain slices. *J Physiol* 586: 265–282, 2008.

Fino E, **Deniau J-M**, **Venance L**. Brief subthreshold events can act as Hebbian signals for long-term plasticity. *PLoS One* 4: e6557, 2009.

Fino E, **Glowinski J**, **Venance L**. Bidirectional activity-dependent plasticity at corticostriatal synapses. *J Neurosci Off J Soc Neurosci* 25: 11279–11287, 2005.

Glickfeld LL, **Roberts JD**, **Somogyi P**, **Scanziani M**. Interneurons hyperpolarize pyramidal cells along their entire somatodendritic axis. *Nat Neurosci* 12: 21–23, 2009.

Gomes J-M, **Bédard C**, **Valtcheva S**, **Nelson M**, **Khokhlova V**, **Pouget P**, **Venance L**, **Bal T**, **Destexhe A**. Intracellular impedance measurements reveal non-ohmic properties of the extracellular medium around neurons. *Biophys J* 110: 234–246, 2016.

Grimnes S, **Martinsen ØG**. Chapter 2 - ELECTROLYTICS [Online]. In: *Bioimpedance and Bioelectricity Basics (Second Edition)*. Academic Press, p. 7–55. http://www.sciencedirect.com/science/article/pii/B9780123740045000027 [9 Apr. 2016].

Haider B, **Schulz DPA**, **Häusser M**, **Carandini M**. Millisecond Coupling of Local Field Potentials to Synaptic Currents in the Awake Visual Cortex. *Neuron* 90: 35–42, 2016.

Hasenstaub A, **Shu Y**, **Haider B**, **Kraushaar U**, **Duque A**, **McCormick DA**. Inhibitory Postsynaptic Potentials Carry Synchronized Frequency Information in Active Cortical Networks. *Neuron* 47: 423–435, 2005.

Henze DA, **Borhegyi Z**, **Csicsvari J**, **Mamiya A**, **Harris KD**, **Buzsáki G**. Intracellular Features Predicted by Extracellular Recordings in the Hippocampus In Vivo. *J Neurophysiol* 84: 390–400, 2000.

Hodgkin AL, **Huxley AF**, **Katz B**. Measurement of current-voltage relations in the membrane of the giant axon of Loligo. *J Physiol* 116: 424–448, 1952.

Khodagholy D, **Gelinas JN**, **Thesen T**, **Doyle W**, **Devinsky O**, **Malliaras GG**, **Buzsáki G**. NeuroGrid: recording action potentials from the surface of the brain. *Nat Neurosci* 18: 310–315, 2015.

Kilner JM, **Baker SN**, **Lemon RN**. A novel algorithm to remove electrical cross-talk between surface EMG recordings and its application to the measurement of short-term synchronisation in humans. *J Physiol* 538: 919–930, 2002.

Maynard EM, **Nordhausen CT**, **Normann RA**. The Utah Intracortical Electrode Array: A recording structure for potential brain-computer interfaces. *Electroencephalogr Clin Neurophysiol* 102: 228–239, 1997.

Mountcastle VB. Modality and Topographic Properties of Single Neurons of Cat's Somatic Sensory Cortex. *J Neurophysiol* 20: 408–434, 1957.

Nagaoka T, **Walker DD**, **Seaba PJ**, **Yamada T**. "Cross-talk" in recording evoked potentials. *Electroencephalogr Clin Neurophysiol* 84: 473–476, 1992.

Nelson MJ, **Bosch C**, **Venance L**, **Pouget P**. Microscale inhomogeneity of brain tissue distorts electrical signal propagation. *J Neurosci* 33: 2821–2827, 2013.

Nelson MJ, **Pouget P**, **Nilsen EA**, **Patten CD**, **Schall JD**. Review of signal distortion through metal microelectrode recording circuits and filters. *J Neurosci Methods* 169: 141–157, 2008.

Okun M, **Naim A**, **Lampl I**. The Subthreshold Relation between Cortical Local Field Potential and Neuronal Firing Unveiled by Intracellular Recordings in Awake Rats. *J Neurosci* 30: 4440–4448, 2010.

Poo C, **Isaacson JS**. Odor Representations in Olfactory Cortex: "Sparse" Coding, Global Inhibition, and Oscillations. *Neuron* 62: 850–861, 2009.

Poulet JFA, **Petersen CCH**. Internal brain state regulates membrane potential synchrony in barrel cortex of behaving mice. *Nature* 454: 881–885, 2008.

Robinson D. The electrical properties of metal microelectrodes. *Proc IEEE* 56: 1065–1071, 1968.

Teleńczuk B, **Baker SN**, **Kempter R**, **Curio G**. Correlates of a single cortical action potential in the epidural EEG. *NeuroImage* 109: 357–367, 2015.

Trevelyan AJ. The Direct Relationship between Inhibitory Currents and Local Field Potentials. *J Neurosci* 29: 15299–15307, 2009.

FIGURE LEGENDS

Figure 1. Evidence of cross-talk between channels. The same 40 Hz sine wave signal is sent through the electrode on the left while it is suspended in the air and a second recording micropipette records signals at three different locations. A: In the bath. B: Just above the surface of the bath, near the signal electrode. C: Above the bath and far away from the signal electrode. Data traces show raw single recordings. Note the y-axis scaling of the recorded signal at each location. The same x-axis scaling is used for all plots.

Figure 2. Equivalent circuit model for simultaneous intracellular and extracellular recordings. A: A hypothetical simultaneous recording with two glass micropipette electrodes is illustrated, with the pipette on the left performing a whole-cell recording of a neuron while the pipette on the right records extracellularly. The equivalent recording circuit model in black is overlaid on the illustration of the experiment. Both pipettes are connected to amplifiers with input impedances Z_a recording signals V_{elec1} and V_{elec2}, respectively. This diagram and circuit could describe the behavior of either a slice recording or an in vivo recording with a grounded reference in contact with the neural tissue. Grounding in the bath as for a slice preparation is indicated. The arrow labeled I_{cross} indicates the path of current flow that gives rise to the cross-talk contamination added to V_{elec2}. B: Schematic of the recording circuit diagram shown in A with impedance elements of arbitrary phases replacing parallel combinations of capacitance and resistance. Z_{elec1}, and Z_{elec2}, correspond to the potential inclusion of Z_{intra} and Z_m in series with Z_{elec1} or Z_{elec2} if either channel is performing a whole-cell recording. The equivalent circuit otherwise functions the same with or without a neuron recording taking place on either channel. C: Abstract schematic of a voltage divider circuit. This simple circuit leads to the relations shown in equation 1.

Figure 3. Recorded cross-talk across frequencies by an extracellular electrode. Blue traces show the voltage recorded across frequencies with a pipette recording extracellularly in a slice while sinusoidal signals of different frequencies are sent through a nearby signal electrode suspended above the bath a fixed distance away from the extracellular electrode (50 μm laterally). Red traces correspond to estimates of the noise levels obtained from the same recordings, using the recordings when no signal was present for each frequency. Five recordings were made with similar impedances of both pipettes. The shaded regions show the standard errors of the mean across recordings. The top plot shows the amplitude ratio of the voltage, specifically the recording channel amplitude divided by the signal channel amplitude. The bottom plot shows the phase of the recording channel relative to the phase of the signal channel. The dashed line indicates a phase of 90°.

Figure 4. Cross-talk recordings in extracellular electrodes in vivo across a range of impedances. A: Amplitude (top) and phase (bottom) of an extracellular electrode recording from the cortex of an anesthetized rat while sinusoidal signals are sent through a second electrode suspended above the rat's brain near the first electrode. Extracellular electrodes with impedances of 1.7, 4.8 and 9.2 MΩ across frequencies were used in separate recordings, with the darker traces corresponding to higher impedances. Blue traces show the voltage at the frequency used to drive the signal in the suspended electrode. Red traces correspond to estimates of the noise levels obtained from the same recordings, using the recordings when no signal was present for each frequency. Dashed blue lines show the amplitude values predicted by the model given each electrode's known impedance value. The expected voltage phase of 90° is shown with a horizontal dashed line in the lower panel. B: Estimations of the amplitude (top) and phase (bottom) of Z_{cross} for each electrode using these same data. The average value for Z_{cross} across all three electrodes was used to derive the predicted voltage ratios shown with dashed lines in the left panel. The dashed black line in the upper plot shows the regression line approximating the average Z_{cross} amplitude, and the horizontal dashed line in the lower plots marks the phase of -90°, which is expected for the impedance across a simple capacitance.

Figure 5. Pipette impedances. Impedance amplitude (top) and phase (bottom) measured from single pipettes suspended in a brain slice. The impedance is generally resistive and constant across frequencies, with some stray capacitance causing a negative phase shift and depressed impedance moduli observed at high frequencies for high impedance pipettes.

Figure 6. Cross-talk recorded in pipettes performing intracellular recordings. Blue traces correspond to signal frequency voltage recorded by a pipette performing a whole-cell recording while sinusoidal signals of different frequencies are sent through a nearby signal-originating electrode suspended above the bath a fixed distance away (50 μm laterally). Red traces correspond to estimates of the noise levels in the recording channel obtained from the same recordings, based on the recordings where no signal was present at that frequency for each frequency. 6 different neurons were recorded with similar impedances of both pipettes. The shaded regions show the standard errors of the mean across recordings. The top plot shows the amplitude of the voltage while the bottom plot shows the phase. The dashed line indicates a phase of 90°.

Figure 7. Whole-cell recording impedance and resulting cross talk. A: The impedance of a whole-cell recording configuration was measured across frequencies for 2 different whole-cell recordings, following the same procedure as in Figure 5. The top panel shows the absolute impedance

amplitude and the bottom panel shows the impedance phase. B: Cross-talk recorded from a nearby electrode suspended in the air in the same 2 whole-cell recordings. The upper panel shows the amplitude ratio (the whole-cell recording channel amplitude divided by the amplitude of the signal channel suspended in air). The lower panel shows the phase of the whole-cell recording channel relative to the phase of the signal channel suspended in air. The dashed lines in the lower panel indicate the predicted phase across frequencies, given the measurements shown in A.

Figure 8. Cross-talk of signals at amplitudes seen during extracellular recordings does not exceed noise levels. A: An example in vitro recording session using stimuli woth peak-to-peak amplitudes of 200 μV and a recording pipette impedance of 1.1 MΩ. B: Example in vivo recording sessions using stimuli of amplitude 200 μV for the same pipettes shown in Figure 4 (1.7, 4.8 and 9.2 MΩ).

Figure 9. Recorded natural LFP fluctuations are too weak to create appreciable cross-talk voltages in neighboring electrodes. A: Power spectral density across frequencies recorded on a 1.4 MΩ pipette suspended in the air next to a signal originating electrode that was either suspended in the air, or recording spontaneous LFPs from a slice preparation. B: The same for a 0.8 MΩ pipette with a signal originating electrode alternately placed in the air or in the brain in an in vivo preparation.

Figure 10. Intracellular spike waveforms lead to cross-talk on nearby extracellular channels. A neuron was recorded in a whole-cell configuration and elicited to spike with a second 7.5 MΩ recording pipette submerged in the bath above the slice, at a 50 μm lateral distance from the shaft of the pipette used for whole-cell recordings. The top panel shows the intracellular waveform averaged over 2648 elicited spikes. The bottom panel solid line shows the waveform of the recording pipette in the bath averaged over the same spikes. The dashed line shows the cross-talk waveform predicted by equation 2 from the recorded intracellular waveform given the recording pipette's measured impedance and estimates of the inter-channel capacitance at that distance from other recordings.

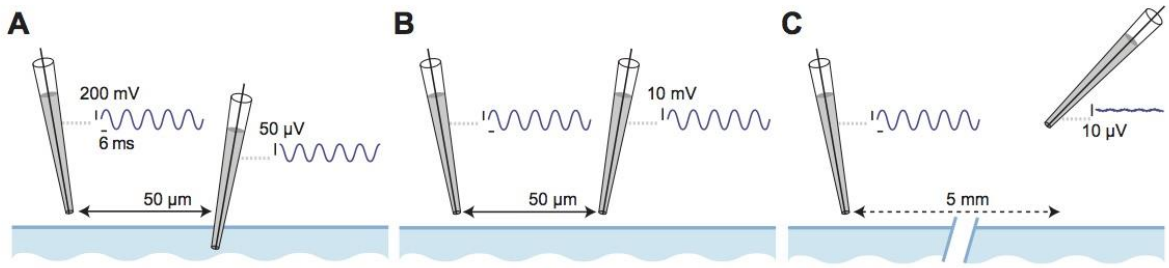

Nelson, Valtcheva, & Venance
Figure 1

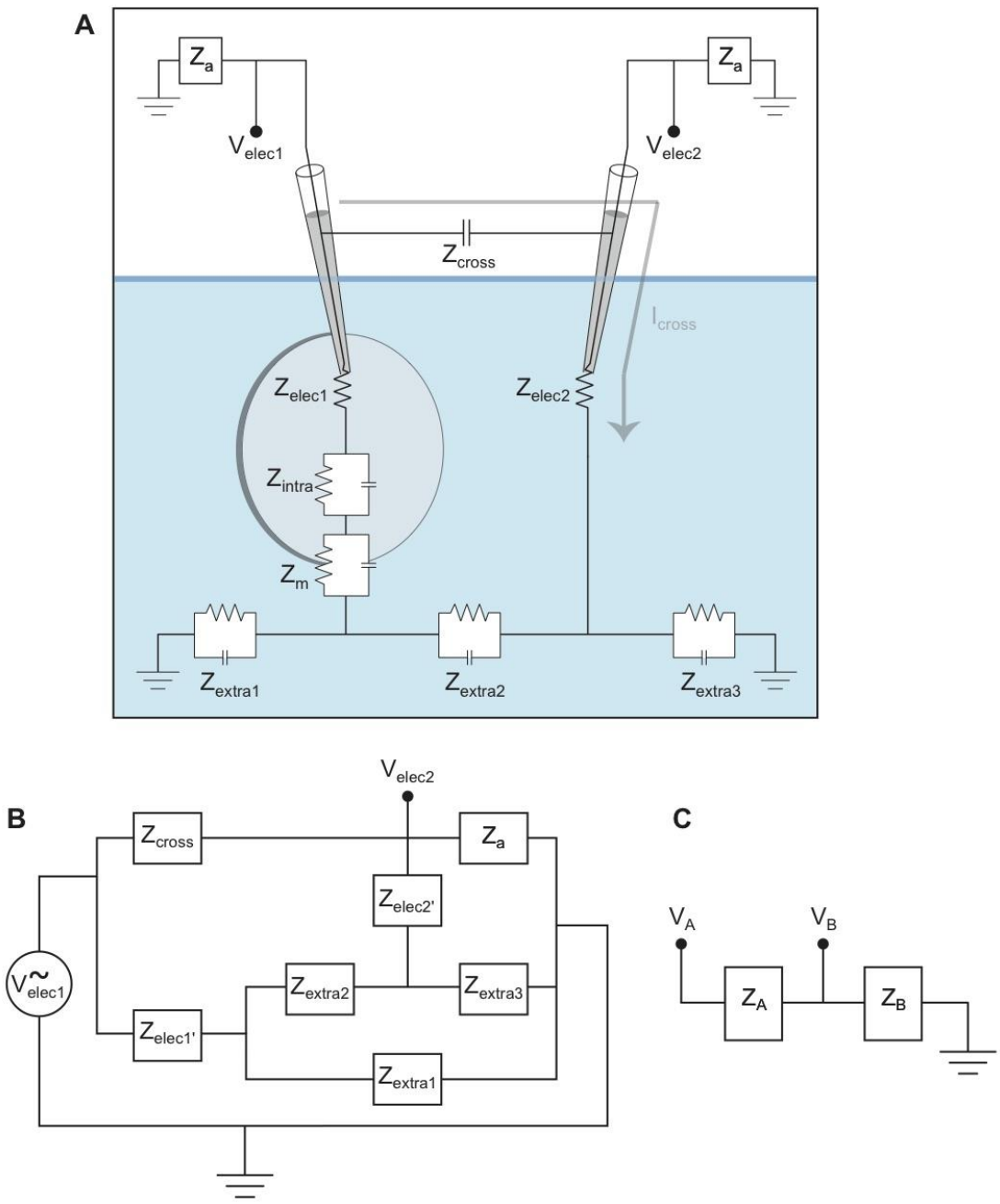

Nelson, Valtcheva, & Venance
Figure 2

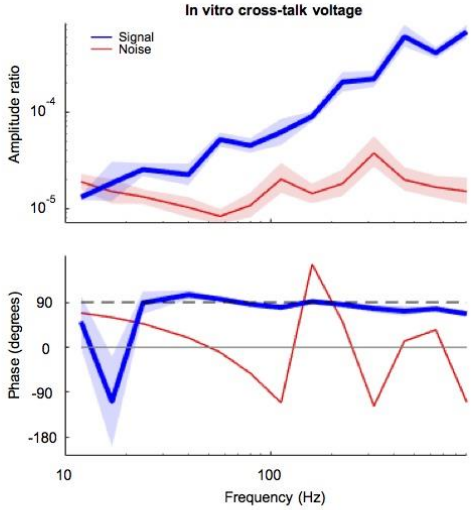

Nelson, Valtcheva, & Venance
Figure 3

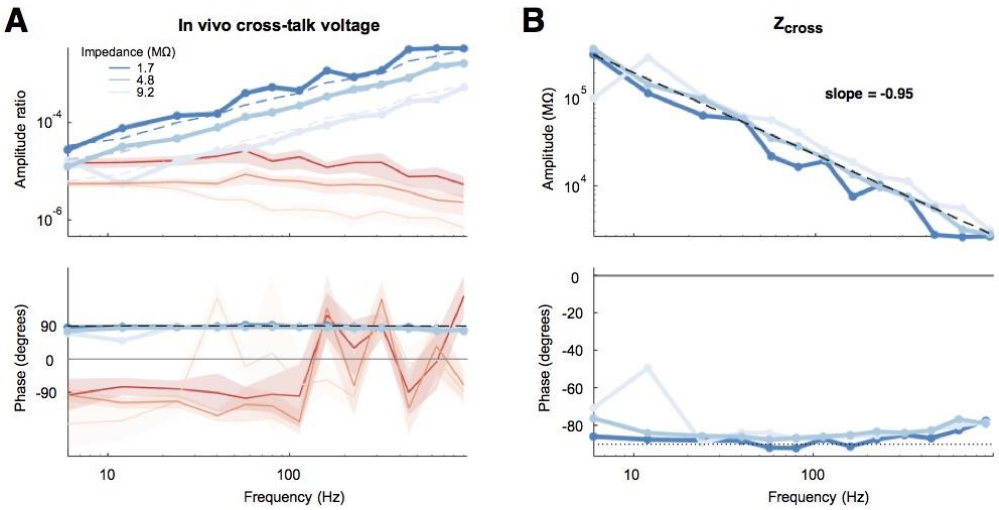

Nelson, Valtcheva, & Venance
Figure 4

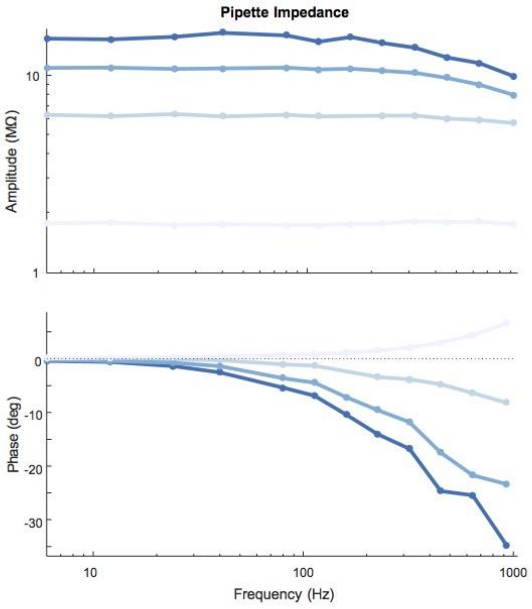

Nelson, Valtcheva, & Venance
Figure 5

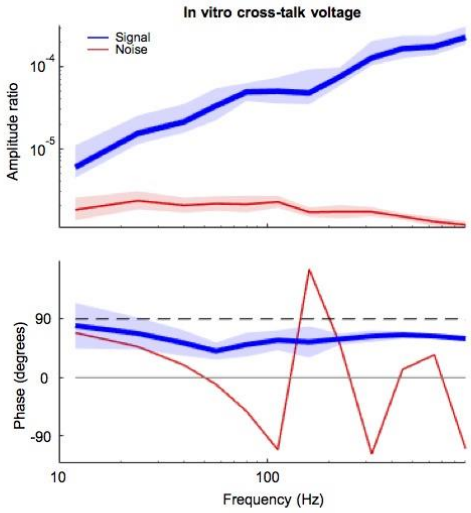

Nelson, Valtcheva, & Venance
Figure 6

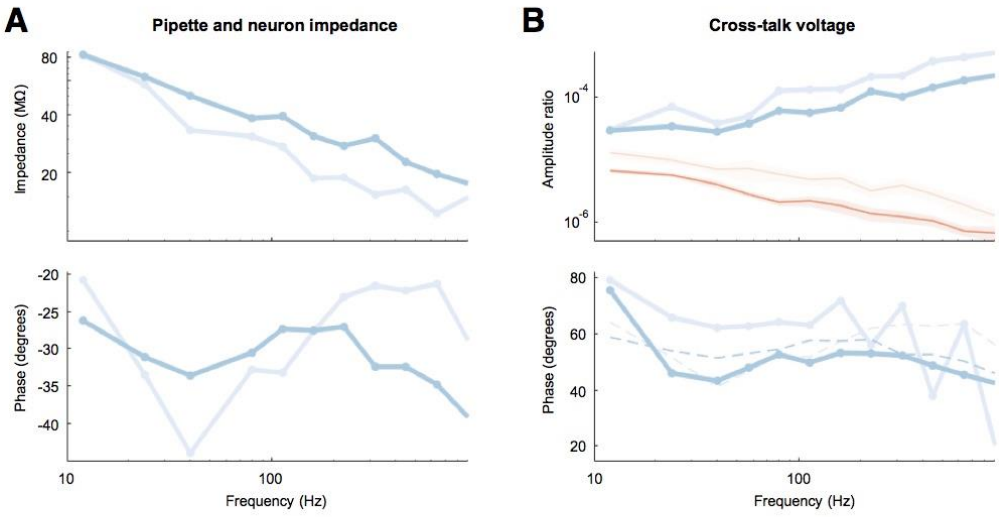

Nelson, Valtcheva, & Venance
Figure 7

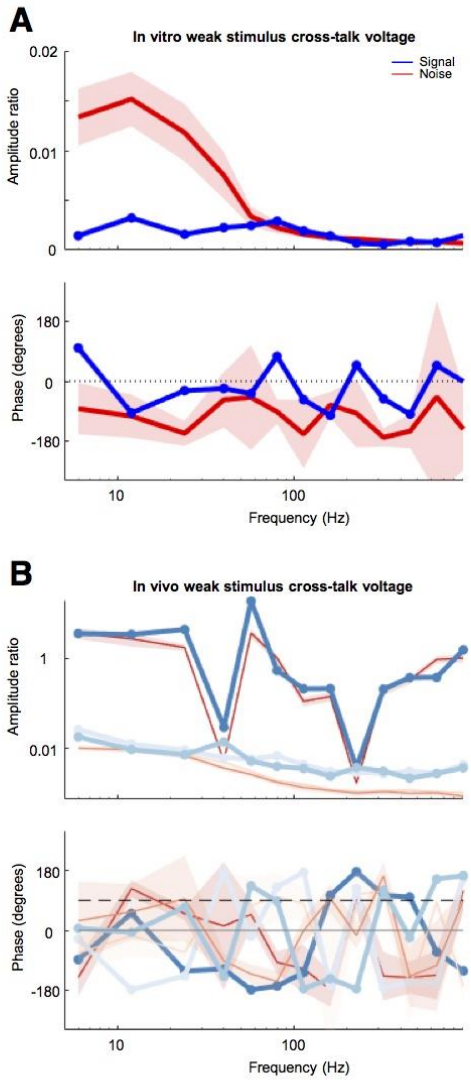

Nelson, Valtcheva, & Venance
Figure 8

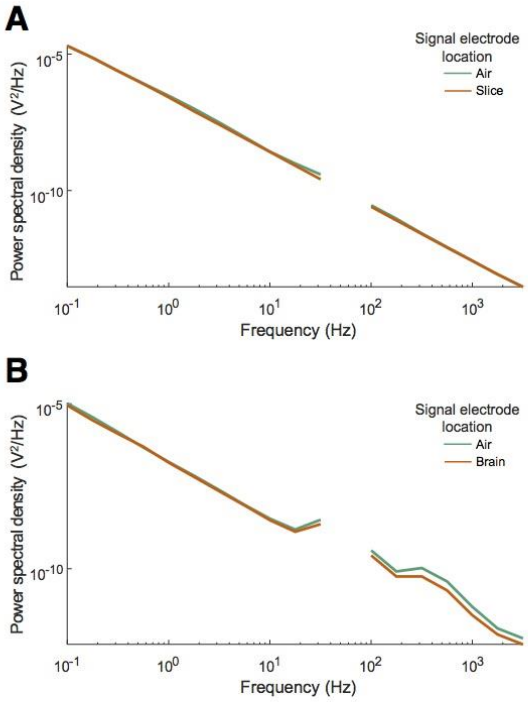

Nelson, Valtcheva, & Venance
Figure 9

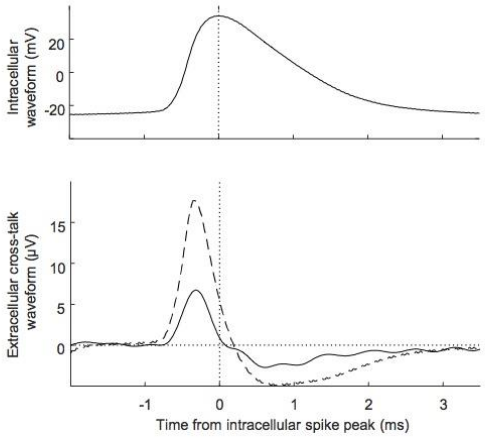

Nelson, Valtcheva, & Venance
Figure 10

REFERENCES

REFERENCES

Part I - Glutamate dynamics (In and out of the cleft)

Alberstein, R., Grey, R., Zimmet, A., Simmons, D.K., Mayer, M.L., 2015. Glycine activated ion channel subunits encoded by ctenophore glutamate receptor genes. Proc. Natl. Acad. Sci. 201513771. doi:10.1073/pnas.1513771112

Ametamey, S.M., Kessler, L.J., Honer, M., Wyss, M.T., Buck, A., Hintermann, S., Auberson, Y.P., Gasparini, F., Schubiger, P. a, 2006. Radiosynthesis and preclinical evaluation of 11C-ABP688 as a probe for imaging the metabotropic glutamate receptor subtype 5. J. Nucl. Med. 47, 698–705.

Angulo, M.C., Kozlov, A.S., Charpak, S., Audinat, E., 2004. Glutamate released from glial cells synchronizes neuronal activity in the hippocampus. J. Neurosci. 24, 6920–7. doi:10.1523/JNEUROSCI.0473-04.2004

Arnth-Jensen, N., Jabaudon, D., Scanziani, M., 2002. Cooperation between independent hippocampal synapses is controlled by glutamate uptake. Nat. Neurosci. 5, 325–31. doi:10.1038/nn825

Asztely, F., Erdemli, G., Kullmann, D.M., 1997. Extrasynaptic Glutamate Spillover in the Hippocampus: Dependence on Temperature and the Role of Active Glutamate Uptake 18, 281–293.

Attwell, D., Barbour, B., Szatkowski, M., 1993. Nonvesicular release of neurotransmitter. Neuron 11, 401–407. doi:10.1016/0896-6273(93)90145-H

Attwell, D., Gibb, A., 2005. Neuroenergetics and the kinetic design of excitatory synapses. Nat. Rev. Neurosci. 6, 841–9. doi:10.1038/nrn1784

Baker, D.A., Xi, Z., Shen, H., Swanson, C.J., Kalivas, P.W., 2002. The Origin and Neuronal Function of In Vivo Nonsynaptic Glutamate 22, 9134–9141.

Barbour, B., 2001. An evaluation of synapse independence. J. Neurosci. 21, 7969–7984. doi:21/20/7969 [pii]

Barbour, B., Häusser, M., 1997. Intersynaptic diffusion of neurotransmitter 377–384.

Baude, A., Nusser, Z., Roberts, J.D.B., Mulvihill, E., Jeffrey Mcllhinney, R.A., Somogyi, P., 1993. The metabotropic glutamate receptor (mGluR1 alpha) is concentrated at perisynaptic membrane of neuronal subpopulations as detected by immunogold reaction. Neuron 11, 771–787. doi:10.1016/0896-6273(93)90086-7

Benveniste, H., Drejer, J., Schousboe, a, Diemer, N.H., 1984. Elevation of the extracellular concentrations of glutamate and aspartate in rat hippocampus during transient cerebral ischemia monitored by intracerebral microdialysis. J. Neurochem. 43, 1369–1374. doi:10.1111/j.1471-4159.1984.tb05396.x

Bergles, D.E., Diamond, J.S., Jahr, C.E., 1999. Clearance of glutamate inside the synapse and beyond. Curr. Opin. Neurobiol. 9, 293–298. doi:10.1016/S0959-4388(99)80043-9

Bergles, D.E., Dzubay, J. a, Jahr, C.E., 1997. Glutamate transporter currents in bergmann glial cells follow the time course of extrasynaptic glutamate. Proc. Natl. Acad. Sci. U. S. A. 94, 14821–5.

Bergles, D.E., Jahr, C.E., 1997. Synaptic activation of glutamate transporters in hippocampal astrocytes. Neuron 19, 1297–308.

Bezzi, P., Carmignoto, G., Pasti, L., Vesce, S., Rossi, D., Rizzini, B.L., Pozzan, T., Volterra, A., 1998. Prostaglandins stimulate calcium-dependent glutamate release in astrocytes. Nature 391, 281–5. doi:10.1038/34651

Boudaba, C., Linn, D.M., Halmos, K.C., Tasker, J.G., 2003. Increased tonic activation of presynaptic metabotropic glutamate receptors in the rat supraoptic nucleus following chronic dehydration. J. Physiol. 551, 815–23. doi:10.1113/jphysiol.2003.042739

Bouvier, M., Szatkowski, M., Amato, A., Attwell, D., 1992. The glial cell glutamate uptake carrier countertransports pH-changing anions. Nature 360, 40–46.

Bramham, C.R., Torp, R., Zhang, N., Storm-Mathisen, J., Ottersen, O.P., 1990. Distribution of glutamate-like immunoreactivity in excitatory hippocampal pathways: a semiquantitative electron microscopic study in rats. Neuroscience 39, 405–17.

Bridges, R., Lutgen, V., Lobner, D., Baker, D.A., 2012. Thinking Outside the Cleft to Understand Synaptic Activity : Contribution of the Cystine-Glutamate Antiporter (System x c □) to Normal and Pathological Glutamatergic Signaling 64, 780–802.

Burger, P.M., Mehl, E., Cameron, P.L., Maycox, P.R., Baumert, M., Lottspeich, F., De Camilli, P., Jahn, R., 1989. Synaptic vesicles immunoisolated from rat cerebral cortex contain high levels of glutamate. Neuron 3, 715–720. doi:10.1016/0896-6273(89)90240-7

Carter, A.G., Regehr, W.G., 2000. Prolonged synaptic currents and glutamate spillover at the parallel fiber to

stellate cell synapse. J. Neurosci. 20, 4423–4434.
Cavelier, P., Attwell, D., 2005. Tonic release of glutamate by a DIDS-sensitive mechanism in rat hippocampal slices. J. Physiol. 564, 397–410. doi:10.1113/jphysiol.2004.082131
Chanda, S., Xu-Friedman, M.A., 2011. Excitatory Modulation in the Cochlear Nucleus through Group I Metabotropic Glutamate Receptor Activation. J. Neurosci. 31, 7450–7455. doi:10.1523/JNEUROSCI.1193-11.2011
Clements, J.D., Lester, R. a, Tong, G., Jahr, C.E., Westbrook, G.L., 1992. The time course of glutamate in the synaptic cleft. Science 258, 1498–501.
Diamond, J.S., Jahr, C.E., 2000. Synaptically Released Glutamate Does Not Overwhelm Transporters on Hippocampal Astrocytes During High-Frequency Stimulation. J Neurophysiol 2835–2843.
Diamond, J.S., Jahr, C.E., 1997. Transporters buffer synaptically released glutamate on a submillisecond time scale. J. Neurosci. 17, 4672–87.
DiGregorio, D.A., Nusser, Z., Silver, R.A., 2002. Spillover of glutamate onto synaptic AMPA receptors enhances fast transmission at a cerebellar synapse. Neuron 35, 521–533. doi:10.1016/S0896-6273(02)00787-0
Dubois, C.J., Lachamp, P.M., Sun, L., Mishina, M., Liu, S.J., 2016. Presynaptic GluN2D receptors detect glutamate spillover and regulate cerebellar GABA release. J. Neurophysiol. 115, 271–285. doi:10.1152/jn.00687.2015
Dulla, C., Tani, H., Okumoto, S., Frommer, W.B., Reimer, R.J., Huguenard, J.R., 2009. Imaging of Glutamate in Brain Slices Using FRET Sensors Chris 27, 417–428. doi:10.1055/s-0029-1237430.Imprinting
Featherstone, D.E., Shippy, S.A., 2008. Regulation of synaptic transmission by ambient extracellular glutamate. Neurosci. 14, 171–81. doi:10.1177/1073858407308518
Fellin, T., Pascual, O., Gobbo, S., Pozzan, T., Haydon, P.G., Carmignoto, G., Biomediche, S., Colombo, G., Hall, S., Walk, H., 2004. Neuronal Synchrony Mediated by Astrocytic Glutamate through Activation of Extrasynaptic NMDA Receptors 43, 729–743.
Fleming, T.M., Scott, V., Naskar, K., Joe, N., Brown, C.H., Stern, J.E., 2011. State-dependent changes in astrocyte regulation of extrasynaptic NMDA receptor signalling in neurosecretory neurons. J. Physiol. 589, 3929–3941. doi:10.1113/jphysiol.2011.207340
Hascup, E.R., Hascup, K.N., Stephens, M., Pomerleau, F., Huettl, P., Gratton, A., Gerhardt, G.A., 2010. Rapid microelectrode measurements and the origin and regulation of extracellular glutamate in rat prefrontal cortex. J. Neurochem. 115, 1608–1620. doi:10.1111/j.1471-4159.2010.07066.x
Herman, M. a, Jahr, C.E., 2007. Extracellular glutamate concentration in hippocampal slice. J. Neurosci. 27, 9736–41. doi:10.1523/JNEUROSCI.3009-07.2007
Herman, M. a, Nahir, B., Jahr, C.E., 2011. Distribution of extracellular glutamate in the neuropil of hippocampus. PLoS One 6, e26501. doi:10.1371/journal.pone.0026501
Herring, B.E., Silm, K., Edwards, R.H., Nicoll, R. a., 2015. Is Aspartate an Excitatory Neurotransmitter? J. Neurosci. 35, 10168–10171. doi:10.1523/JNEUROSCI.0524-15.2015
Hires, S.A., Zhu, Y., Tsien, R.Y., 2008. Optical measurement of synaptic glutamate spillover and reuptake by linker optimized glutamate-sensitive fluorescent reporters. Proc. Natl. Acad. Sci. U. S. A. 105, 4411–4416. doi:10.1073/pnas.0712008105
Innocenti, B., Parpura, V., Haydon, P., 2000. Imaging extracellular waves of glutamate during calcium signaling in cultured astrocytes. J Neurosci 20, 1800–1808.
Isaacson, J.S., 1999. Glutamate Spillover Mediates Excitatory Transmission in the Rat Olfactory Bulb ates reciprocal feedback excitation via a different excit. Neuron 23, 377–384. doi:10.1016/S0896-6273(00)80787-4
Jabaudon, D., SHIMAMOTO, K., YASUDA-KAMATANI, Y., SCANZIANI, M., Gahwiler, B.H.G., GERBER, U., 1999. Inhibition of uptake unmasks rapid extracellular turnover of glutamate of nonvesicular origin. PNAS 96, 8733–8738.
Karakossian, M.H., Otis, T.S., 2004. Excitation of cerebellar interneurons by group I metabotropic glutamate receptors. J. Neurophysiol. 92, 1558–65. doi:10.1152/jn.00300.2004
Kőszeghy, Á., Kovács, A., Bíró, T., Szücs, P., Vincze, J., Hegyi, Z., Antal, M., Pál, B., 2014. Endocannabinoid signaling modulates neurons of the pedunculopontine nucleus (PPN) via astrocytes. Brain Struct. Funct. 220, 3023–3041. doi:10.1007/s00429-014-0842-5
Kullmann, D.M., Asztely, F., 1998. Extrasynaptic glutamate spillover in the hippocampus: evidence and implications. Trends Neurosci. 21, 8–14.
Kullmann, D.M., Erdemli, G., Asztély, F., 1996. LTP of AMPA and NMDA receptor-mediated signals:

evidence for presynaptic expression and extrasynaptic glutamate spill-over. Neuron 17, 461–74.
Le Meur, K., Galante, M., Angulo, M.C., Audinat, E., 2007. Tonic activation of NMDA receptors by ambient glutamate of non-synaptic origin in the rat hippocampus. J. Physiol. 580, 373–383. doi:10.1113/jphysiol.2006.123570
Lehre, K.P., Danbolt, N.C., 1998. The number of glutamate transporter subtype molecules at glutamatergic synapses: chemical and stereological quantification in young adult rat brain. J. Neurosci. 18, 8751–8757.
Lehre, K.P., Rusakov, D.A., 2002. Asymmetry of Glia near Central Synapses Favors Presynaptically Directed Glutamate Escape 83, 125–134.
Levy, L.M., Warr, O., Attwell, D., 1998. Stoichiometry of the glial glutamate transporter GLT-1 expressed inducibly in a Chinese hamster ovary cell line selected for low endogenous Na+-dependent glutamate uptake. J. Neurosci. 18, 9620–8.
Lewerenz, J., Hewett, S.J., Huang, Y., Lambros, M., Gout, P.W., Kalivas, P.W., Massie, A., Smolders, I., Methner, A., Pergande, M., Smith, S.B., Ganapathy, V., Maher, P., 2013. The cystine/glutamate antiporter system x(c)(-) in health and disease: from molecular mechanisms to novel therapeutic opportunities. Antioxid. Redox Signal. 18, 522–55. doi:10.1089/ars.2011.4391
M, S., PA, S., KE, V., RC, M., RA, N., 1997. Use-dependent increases in glutamate concentration activate presynaptic metabotropic glutamate receptors.
Magistretti, P.J., 2009. Role of glutamate in neuron-glia metabolic coupling. Am. J. Clin. Nutr. 90, 875–880. doi:10.3945/ajcn.2009.27462CC
Marcaggi, P., Billups, D., Attwell, D., 2003. The role of glial glutamate transporters in maintaining the independent operation of juvenile mouse cerebellar parallel fibre synapses. J. Physiol. 552, 89–107. doi:10.1113/jphysiol.2003.044263
Martinez, D., Slifstein, M., Nabulsi, N., Grassetti, A., Urban, N.B.L., Perez, A., Liu, F., Lin, S.F., Ropchan, J., Mao, X., Kegeles, L.S., Shungu, D.C., Carson, R.E., Huang, Y., 2014. Imaging glutamate homeostasis in cocaine addiction with the metabotropic glutamate receptor 5 positron emission tomography radiotracer [11C]ABP688 and magnetic resonance spectroscopy. Biol. Psychiatry 75, 165–171. doi:10.1016/j.biopsych.2013.06.026
Marvin, J.S., Borghuis, B.G., Tian, L., Cichon, J., Harnett, M.T., Akerboom, J., Gordus, A., Renninger, S.L., Chen, T.-W., Bargmann, C.I., Orger, M.B., Schreiter, E.R., Demb, J.B., Gan, W.-B., Hires, S.A., Looger, L.L., 2013. An optimized fluorescent probe for visualizing glutamate neurotransmission. Nat. Methods 10, 162–70. doi:10.1038/nmeth.2333
Marx, M.-C., Billups, D., Billups, B., 2015. Maintaining the presynaptic glutamate supply for excitatory neurotransmission. J. Neurosci. Res. 96, 1031–1044. doi:10.1002/jnr.23561
Min, M., Rusakov, D.A., Kullmann, D.M., 1998. Activation of AMPA, Kainate, and Metabotropic Receptors at Hippocampal Mossy Fiber Synapses: Role of Glutamate Diffusion. Neuron 21, 561–570.
Miyake, N., Skinbjerg, M., Easwaramoorthy, B., Kumar, D., Girgis, R.R., Xu, X., Slifstein, M., Abi-Dargham, A., 2011. Imaging changes in glutamate transmission in vivo with the metabotropic glutamate receptor 5 tracer [11C] ABP688 and N-acetylcysteine challenge. Biol. Psychiatry 69, 822–824. doi:10.1016/j.biopsych.2010.12.023
Moussawi, K., Riegel, A., Nair, S., Kalivas, P.W., 2011. Extracellular Glutamate: Functional Compartments Operate in Different Concentration Ranges. Front. Syst. Neurosci. doi:10.3389/fnsys.2011.00094
Namiki, S., Sakamoto, H., Iinuma, S., Iino, M., Hirose, K., 2007. Optical glutamate sensor for spatiotemporal analysis of synaptic transmission. Eur. J. Neurosci. 25, 2249–2259. doi:10.1111/j.1460-9568.2007.05511.x
Nicholls, D., Attwell, D., 1990. The release and uptake of excitatory amino acids. TIPS 22.
Nicholls, D.G., Sihra, T.S., 1986. Synaptosomes possess an exocytotic pool of glutamate. Nature 319, 402–403.
Nicholson, C., Sykova, E., 1998. Extracellular space structure revealed by diffusion analysis. Trends Neurosci. 21, 207–215.
Nie, H., Zhang, H., Weng, H.-R., 2010. Bidirectional neuron-glia interactions triggered by deficiency of glutamate uptake at spinal sensory synapses. J. Neurophysiol. 104, 713–725. doi:10.1152/jn.00282.2010
Nielsen, T.A., DiGregorio, D.A., Silver, R.A., 2004. Modulation of glutamate mobility reveals the mechanism underlying slow-rising AMPAR EPSCs and the diffusion coefficient in the synaptic cleft. Neuron 42, 757–771. doi:10.1016/j.neuron.2004.04.003
Okubo, Y., Iino, M., 2011. Visualization of glutamate as a volume transmitter. J. Physiol. 589, 481–488.

doi:10.1113/jphysiol.2010.199539
Okubo, Y., Sekiya, H., Namiki, S., Sakamoto, H., Iinuma, S., Yamasaki, M., Watanabe, M., Hirose, K., Iino, M., 2010. Imaging extrasynaptic glutamate dynamics in the brain. Proc. Natl. Acad. Sci. U. S. A. 107, 6526–31. doi:10.1073/pnas.0913154107
Okumoto, S., 2010. Imaging approach for monitoring cellular metabolites and ions using genetically encoded biosensors. Curr. Opin. Biotechnol. 21, 45–54. doi:10.1016/j.copbio.2010.01.009
Oldenziel, W.H., van der Zeyden, M., Dijkstra, G., Ghijsen, W.E.J.M., Karst, H., Cremers, T.I.F.H., Westerink, B.H.C., 2007. Monitoring extracellular glutamate in hippocampal slices with a microsensor. J. Neurosci. Methods 160, 37–44. doi:10.1016/j.jneumeth.2006.08.003
Oliet, S.H., Piet, R., Poulain, D. a, 2001. Control of glutamate clearance and synaptic efficacy by glial coverage of neurons. Science 292, 923–6. doi:10.1126/science.1059162
Pál, B., 2015. Astrocytic Actions on Extrasynaptic Neuronal Currents 9. doi:10.3389/fncel.2015.00474
Paoletti, P., Bellone, C., Zhou, Q., 2013. NMDA receptor subunit diversity: impact on receptor properties, synaptic plasticity and disease. Nat. Rev. Neurosci. 14, 383–400. doi:10.1038/nrn3504
Parsons, M.P., Vanni, M.P., Woodard, C.L., Kang, R., Murphy, T.H., Raymond, L.A., 2016. Real-time imaging of glutamate clearance reveals normal striatal uptake in Huntington disease mouse models. Nat. Commun. 7, 11251. doi:10.1038/ncomms11251
Patneau, K., Mayer, L., 1990. Structure-Activity Relationships for Amino Candidates Acting at IV-MethybAspartate Receptors Acid Transmitter and Quisqualate 2385–2399.
Piet, R., Bonhomme, R., Theodosis, D.T., Poulain, D. a., Oliet, S.H.R., 2003. Modulation of GABAergic transmission by endogenous glutamate in the rat supraoptic nucleus. Eur. J. Neurosci. 17, 1777–1785. doi:10.1046/j.1460-9568.2003.02611.x
Pomerleau, F., Day, B., Huettl, P., Burmeister, J., Gerhardt, G., 2003. Real time in vivo measures of L-glutamate in the rat central nervous system using ceramic-based multisite microelectrode arrays. Ann N Y Acad Sci 320, 9–12.
Riveros, N., Fiedler, J., Lagos, N., Muñoz, C., Orrego, F., 1986. Glutamate in rat brain cortex synaptic vesicles: influence of the vesicle isolation procedure. Brain Res. 386, 405–8. doi:10.1016/0006-8993(86)90181-2
Rusakov, D.A., Kullmann, D.M., 1998. Extrasynaptic Glutamate Diffusion in the Hippocampus: Ultrastructural Constraints, Uptake, and Receptor Activation. J. Neurosci. 18, 3158–3170.
Rutledge, E.M., Aschner, M., Kimelberg, H.K., Eric, M., Harold, K., 1998. H] aspartate release from primary astrocyte cultures Pharmacological characterization of swelling-induced D - [3 H] aspartate release from primary astrocyte cultures. Am. J. Physiol.
Ryan, T.J., Grant, S.G.N., 2009. The origin and evolution of synapses. Nat. Rev. Neurosci. 10, 701–12. doi:10.1038/nrn2717
Sah, P., Hestrin, R., Nicoll, R.A., 1988. Tonic Activation of NMDA Receptors by Ambient Glutamate Enhances Excitability of Neurons. Science (80-.).
Sandiego, C., Nabulsi, N., Lin, S., 2013. Studies of the metabotropic glutamate receptor 5 radioligand ABP688 with N-acetylcysteine challenge in rhesus monkeys. Synapse 67, 489–501. doi:10.1002/syn.21656.Studies
Sasaki, T., Beppu, K., Tanaka, K.F., Fukazawa, Y., Shigemoto, R., Matsui, K., 2012. Application of an optogenetic byway for perturbing neuronal activity via glial photostimulation. Proc. Natl. Acad. Sci. U. S. A. 109, 20720–5. doi:10.1073/pnas.1213458109
Semyanov, a, Kullmann, D.M., 2000. Modulation of GABAergic signaling among interneurons by metabotropic glutamate receptors. Neuron 25, 663–672. doi:10.1016/S0896-6273(00)81068-5
Shupliakov, O., Brodin, L., Cullheim, S., Ottersen, O.P., Storm-Mathisen, J., 1992. Immunogold quantification of glutamate in two types of excitatory synapse with different firing patterns. J. Neurosci. 12, 3789–3803.
Sjöström, P.J., Rancz, A., Roth, A., Häusser, M., 2010. Dendritic Excitability and Synaptic Plasticity. Physiol. Rev. 1–28. doi:10.1152/physrev.00016.2007.
Sperlágh, B., Köfalvi, A., Deuchars, J., Atkinson, L., Milligan, C., Buckley, N., Vizi, E., 2002. Involvement of P2X7 receptors in the regulation of neurotransmitter release in the rat hippocampus. J. Neurochem. 81, 1196–1211. doi:10.1046/j.1471-4159.2002.00920.x
Sylantyev, S., Savtchenko, L.P., Niu, Y.-P., Ivanov, A.I., Jensen, T.P., Kullmann, D.M., Xiao, M.-Y., Rusakov, D.A., 2008. Electric Fields Due to Synaptic Currents Sharpen Excitatory Transmission 467, 1845–1849.
Szapiro, G., Barbour, B., 2007. Multiple climbing fibers signal to molecular layer interneurons exclusively

via glutamate spillover. Nat. Neurosci. 10, 735–742. doi:10.1038/nn1907
Takamori, S., Holt, M., Stenius, K., Lemke, E.A., Grønborg, M., Riedel, D., Urlaub, H., Schenck, S., Brügger, B., Ringler, P., Müller, S.A., Rammner, B., Gräter, F., Hub, J.S., De Groot, B.L., Mieskes, G., Moriyama, Y., Klingauf, J., Grubmüller, H., Heuser, J., Wieland, F., Jahn, R., 2006. Molecular Anatomy of a Trafficking Organelle. Cell 127, 831–846. doi:10.1016/j.cell.2006.10.030
Takumi, Y., Matsubara, A., Rinvik, E., Ottersen, O.P., 1999. The arrangement of glutamate receptors in excitatory synapses. Ann. N. Y. Acad. Sci. 868, 474–482. doi:10.1111/j.1749-6632.1999.tb11316.x
Westerink, B.H.C., 1995. Brain microdialysis and its application for the study of animal behaviour. Behav. Brain Res. 70, 103–124. doi:10.1016/0166-4328(95)80001-8
Yang, Y., Xu-Friedman, M. a, 2015. Different pools of glutamate receptors mediate sensitivity to ambient glutamate in the cochlear nucleus. J. Neurophysiol. jn.00693.2014. doi:10.1152/jn.00693.2014
Ye, Z.-C., Wyeth, M.S., Baltan-Tekkok, S., Ransom, B.R., 2003. Functional hemichannels in astrocytes: a novel mechanism of glutamate release. J. Neurosci. 23, 3588–3596. doi:23/9/3588 [pii]
Zerangue, N., Kavanaugh, M.P., 1996. Flux coupling in a neuronal glutamate transporter. Nature. doi:10.1038/383634a0
Zhang, S., Takeda, Y., Hagioka, S., Takata, K., Aoe, H., Nakatsuka, H., Yokoyama, M., Morita, K., 2005. Measurement of GABA and glutamate in vivo levels with high sensitivity and frequency. Brain Res. Protoc. 14, 61–66. doi:10.1016/j.brainresprot.2004.03.005
Zheng, K., Scimemi, A., Rusakov, D. a, 2008. Receptor actions of synaptically released glutamate: the role of transporters on the scale from nanometers to microns. Biophys. J. 95, 4584–4596. doi:10.1529/biophysj.108.129874
Zhou, Y., Danbolt, N.C., 2014. Glutamate as a neurotransmitter in the healthy brain. J. Neural Transm. 121, 799–817. doi:10.1007/s00702-014-1180-8
Zuber, B., Nikonenko, I., Klauser, P., Muller, D., Dubochet, J., 2005. The mammalian central nervous synaptic cleft contains a high density of periodically organized complexes. Proc. Natl. Acad. Sci. U. S. A. 102, 19192–19197. doi:10.1073/pnas.0509527102

Part II - Glutamate uptake

Abousaab, A., Warsi, J., Elvira, B., Alesutan, I., Hoseinzadeh, Z., Lang, F., 2015. Down-Regulation of Excitatory Amino Acid Transporters EAAT1 and EAAT2 by the Kinases SPAK and OSR1. J. Membr. Biol. doi:10.1007/s00232-015-9826-5
Aida, T., Yoshida, J., Nomura, M., Tanimura, A., Iino, Y., Soma, M., Bai, N., Ito, Y., Cui, W., Aizawa, H., Yanagisawa, M., Nagai, T., Takata, N., Tanaka, K.F., Takayanagi, R., Kano, M., Götz, M., Hirase, H., Tanaka, K., 2015. Astroglial Glutamate Transporter Deficiency Increases Synaptic Excitability and Leads to Pathological Repetitive Behaviors in Mice. Neuropsychopharmacology 1, 1–11. doi:10.1038/npp.2015.26
Almeida, R.F., Thomazi, A.P., Godinho, G.F., Saute, J.A.M., Wofchuk, S.T., Souza, D.O., Ganzella, M., 2010. Effects of depressive-like behavior of rats on brain glutamate uptake. Neurochem. Res. 35, 1164–1171. doi:10.1007/s11064-010-0169-4
Aoyama, K., Suh, S.W., Hamby, A.M., Liu, J., Chan, W.Y., Chen, Y., Swanson, R. a, 2006. Neuronal glutathione deficiency and age-dependent neurodegeneration in the EAAC1 deficient mouse. Nat. Neurosci. 9, 119–126. doi:10.1038/nn1609
Arnth-Jensen, N., Jabaudon, D., Scanziani, M., 2002. Cooperation between independent hippocampal synapses is controlled by glutamate uptake. Nat. Neurosci. 5, 325–31. doi:10.1038/nn825
Arriza, J.L., Eliasof, S., Kavanaugh, M.P., Amara, S.G., 1997. Excitatory amino acid transporter 5, a retinal glutamate transporter coupled to a chloride conductance. Proc. Natl. Acad. Sci. U. S. A. 94, 4155–4160. doi:10.1073/pnas.94.8.4155
Arriza, J.L., Fairman, W.A., Amara, S.G., Kavanaugh, P., Wadiche, I., Murdoch, H., 1994. Functional Comparisons of Three Glutamate Cloned from Human Motor Cortex Transporter 14, 5559–5569.
Asztely, F., Erdemli, G., Kullmann, D.M., 1997. Extrasynaptic Glutamate Spillover in the

Hippocampus: Dependence on Temperature and the Role of Active Glutamate Uptake 18, 281–293.
Bar-Peled, O., Ben-Hur, H., Biegon, a, Groner, Y., Dewhurst, S., Furuta, a, Rothstein, J.D., 1997. Distribution of glutamate transporter subtypes during human brain development. J. Neurochem. 69, 2571–2580.
Barakat, L., Bordey, a, 2002. GAT-1 and reversible GABA transport in Bergmann glia in slices. J. Neurophysiol. 88, 1407–1419. doi:10.1152/jn.01002.2001.
Barbour, B., Szatkowski, M., Ingledew, N., Attwell, D., 1989. Arachidonic acid induces a prolonged inhibition of glutamate uptake into glial cells. Nature.
Baude, A., Nusser, Z., Roberts, J.D.B., Mulvihill, E., Jeffrey Mcllhinney, R.A., Somogyi, P., 1993. The metabotropic glutamate receptor (mGluR1 alpha) is concentrated at perisynaptic membrane of neuronal subpopulations as detected by immunogold reaction. Neuron 11, 771–787. doi:10.1016/0896-6273(93)90086-7
Bazargani, N., Attwell, D., 2016. Astrocyte calcium signaling: the third wave. Nat. Neurosci. 19, 182–189. doi:10.1038/nn.4201
Beart, P.M., O'Shea, R.D., 2007. Transporters for L-glutamate: an update on their molecular pharmacology and pathological involvement. Br. J. Pharmacol. 150, 5–17. doi:10.1038/sj.bjp.0706949
Bechtholt-Gompf, A.J., Walther, H. V, Adams, M.A., Carlezon, W.A., Öngür, D., Cohen, B.M., 2010. Blockade of Astrocytic Glutamate Uptake in Rats Induces Signs of Anhedonia and Impaired Spatial Memory. Neuropsychopharmacology 35, 2049–2059. doi:10.1038/npp.2010.74
Benediktsson, A.M., Marrs, G.S., Tu, J.C., Worley, P.F., Rothstein, J.D., Bergles, D.E., Dailey, M.E., 2012. Neuronal activity regulates glutamate transporter dynamics in developing astrocytes. Glia 60, 175–188. doi:10.1002/glia.21249
Berger, U. V., Hediger, M.A., 2000. Distribution of the glutamate transporters GLAST and GLT-1 in rat circumventricular organs, meninges, and dorsal root ganglia. J. Comp. Neurol. 421, 385–399. doi:10.1002/(SICI)1096-9861(20000605)421:3<385::AID-CNE7>3.0.CO;2-S
Bergles, D.E., Dzubay, J. a, Jahr, C.E., 1997. Glutamate transporter currents in bergmann glial cells follow the time course of extrasynaptic glutamate. Proc. Natl. Acad. Sci. U. S. A. 94, 14821–5.
Bergles, D.E., Jahr, C.E., 1998. Glial contribution to glutamate uptake at Schaffer collateral-commissural synapses in the hippocampus. J. Neurosci. 18, 7709–16.
Bergles, D.E., Jahr, C.E., 1997. Synaptic activation of glutamate transporters in hippocampal astrocytes. Neuron 19, 1297–308.
Bernardinelli, Y., Muller, D., Nikonenko, I., Bernardinelli, Y., Muller, D., Nikonenko, I., 2014. Astrocyte-Synapse Structural Plasticity. Neural Plast. 2014, 1–13. doi:10.1155/2014/232105
Billups, D., Marx, M.-C., Mela, I., Billups, B., 2013. Inducible presynaptic glutamine transport supports glutamatergic transmission at the calyx of Held synapse. J. Neurosci. 33, 17429–34. doi:10.1523/JNEUROSCI.1466-13.2013
Boudaba, C., Linn, D.M., Halmos, K.C., Tasker, J.G., 2003. Increased tonic activation of presynaptic metabotropic glutamate receptors in the rat supraoptic nucleus following chronic dehydration. J. Physiol. 551, 815–23. doi:10.1113/jphysiol.2003.042739
Brasnjo, G., Otis, T.S., 2001. Neuronal glutamate transporters control activation of postsynaptic metabotropic glutamate receptors and influence cerebellar long-term depression. Neuron 31, 607–616. doi:10.1016/S0896-6273(01)00377-4
Bridges, R., Lutgen, V., Lobner, D., Baker, D.A., 2012. Thinking Outside the Cleft to Understand Synaptic Activity : Contribution of the Cystine-Glutamate Antiporter (System x c ☐) to Normal and Pathological Glutamatergic Signaling 64, 780–802.
Cammack, J.N., Schwartz, E. a, 1993. Ions required for the electrogenic transport of GABA by horizontal cells of the catfish retina. J. Physiol. 472, 81–102.
Carter, A.G., Regehr, W.G., 2000. Prolonged synaptic currents and glutamate spillover at the parallel fiber to stellate cell synapse. J. Neurosci. 20, 4423–4434.

Casado, M., Bendahan, a, Zafra, F., Danbolt, N.C., Aragón, C., Giménez, C., Kanner, B.I., 1993. Phosphorylation and modulation of brain glutamate transporters by protein kinase C. J. Biol. Chem. 268, 27313–27317.
Cavelier, P., Attwell, D., 2005. Tonic release of glutamate by a DIDS-sensitive mechanism in rat hippocampal slices. J. Physiol. 564, 397–410. doi:10.1113/jphysiol.2004.082131
Chalifoux, J.R., Carter, A.G., 2011. Glutamate spillover promotes the generation of NMDA spikes. J. Neurosci. 31, 16435–46. doi:10.1523/JNEUROSCI.2777-11.2011
Chanda, S., Xu-Friedman, M.A., 2011. Excitatory Modulation in the Cochlear Nucleus through Group I Metabotropic Glutamate Receptor Activation. J. Neurosci. 31, 7450–7455. doi:10.1523/JNEUROSCI.1193-11.2011
Chatton, J.Y., Marquet, P., Magistretti, P.J., 2000. A quantitative analysis of L-glutamate-regulated Na+ dynamics in mouse cortical astrocytes: Implications for cellular bioenergetics. Eur. J. Neurosci. 12, 3843–3853. doi:10.1046/j.1460-9568.2000.00269.x
Chaudhry, F.A., Lehre, K.P., Lookeren Campagne, M. van, Ottersen, O.P., Danbolt, N.C., Storm-Mathisen, J., 1995. Glutamate transporters in glial plasma membranes: Highly differentiated localizations revealed by quantitative ultrastructural immunocytochemistry. Neuron 15, 711–720. doi:10.1016/0896-6273(95)90158-2
Chen, S., Diamond, J.S., 2002. Receptors on Cells in the Ganglion Cell Layer of Rat Retina. Stimulus 22, 2165–2173. doi:22/6/2165 [pii]
Cholet, N., Pellerin, L., Magistretti, P.J., Hamel, E., 2002. Similar perisynaptic glial localization for the Na+,K+-ATPase alpha 2 subunit and the glutamate transporters GLAST and GLT-1 in the rat somatosensory cortex. Cereb. Cortex 12, 515–25. doi:10.1093/cercor/12.5.515
Clark, B. a, Barbour, B., 1997. Currents evoked in Bergmann glial cells by parallel fibre stimulation in rat cerebellar slices. J. Physiol. 502 (Pt 2, 335–50.
Clark, B.A., Cull-Candy, S.G., 2002. Activity-dependent recruitment of extrasynaptic NMDA receptor activation at an AMPA receptor-only synapse. J. Neurosci. 22, 4428–4436. doi:20026509
Clements, J.D., Lester, R. a, Tong, G., Jahr, C.E., Westbrook, G.L., 1992. The time course of glutamate in the synaptic cleft. Science 258, 1498–501.
Coddington, L., Rudolph, S., VandeLune, P., Overstreet-Wadiche, L., Wadiche, J., 2013. Spillover-Mediated Feedforward Inhibition Functionally Segregates Interneuron Activity. Neuron 78, 1050–1062. doi:10.1016/j.neuron.2013.04.019
Coddington, L.T., Nietz, A.K., Wadiche, J.I., 2014. The contribution of extrasynaptic signaling to cerebellar information processing. Cerebellum 13, 513–520. doi:10.1007/s12311-014-0554-7
Conti, F., Debiasi, S., Minelli, A., Jeffrey, D., Melone, M., 1998. EAAC1, a high-affinity glutamate tranporter, is localized to astrocytes and gabaergic neurons besides pyramidal cells in the rat cerebral cortex. Cereb. Cortex 108–116.
Cui, W., Mizukami, H., Yanagisawa, M., Aida, T., Nomura, M., Isomura, Y., Takayanagi, R., Ozawa, K., Tanaka, K., Aizawa, H., 2014. Glial Dysfunction in the Mouse Habenula Causes Depressive-Like Behaviors and Sleep Disturbance. J. Neurosci. 34, 16273–16285. doi:10.1523/JNEUROSCI.1465-14.2014
Danbolt, Storm-Mathisen, Kanner, 1992. AN [N a + + K +] COUPLED L-GLUTAMATE TRANSPORTER PURIFIED FROM RAT BRAIN IS LOCATED IN GLIAL CELL PROCESSES 51, 295–310.
Danbolt, N.C., 2001. Glutamate uptake. Prog. Neurobiol. 65, 1–105. doi:10.1016/S0301-0082(00)00067-8
Danbolt, N.C., Furness, D.N., Zhou, Y., 2016. Neuronal vs glial glutamate uptake: Resolving the conundrum. Neurochem. Int. doi:10.1016/j.neuint.2016.05.009
Dehnes, Y., Chaudhry, F. a, Ullensvang, K., Lehre, K.P., Storm-Mathisen, J., Danbolt, N.C., 1998. The glutamate transporter EAAT4 in rat cerebellar Purkinje cells: a glutamate-gated chloride channel concentrated near the synapse in parts of the dendritic membrane facing astroglia. J. Neurosci. 18, 3606–3619.

Devaraju, P., Sun, M.-Y., Myers, T.L., Lauderdale, K., Fiacco, T. a, 2013. Astrocytic group I mGluR-dependent potentiation of astrocytic glutamate and potassium uptake. J. Neurophysiol. 109, 2404–14. doi:10.1152/jn.00517.2012
Diamond, J.S., 2001. Neuronal glutamate transporters limit activation of NMDA receptors by neurotransmitter spillover on CA1 pyramidal cells. J. Neurosci. 21, 8328–8338. doi:21/21/8328 [pii]
Diamond, J.S., Bergles, D.E., Jahr, C.E., 1998. Glutamate Release Monitored with Astrocyte Transporter Currents during LTP. Neuron 21, 425–433. doi:10.1016/S0896-6273(00)80551-6
Diamond, J.S., Jahr, C.E., 2000. Synaptically Released Glutamate Does Not Overwhelm Transporters on Hippocampal Astrocytes During High-Frequency Stimulation. J Neurophysiol 2835–2843.
Diamond, J.S., Jahr, C.E., 1997. Transporters buffer synaptically released glutamate on a submillisecond time scale. J. Neurosci. 17, 4672–87.
Dzubay, J.A., Otis, T.S., 2002. Climbing fiber activation of metabotropic glutamate receptors on cerebellar purkinje neurons. Neuron 36, 1159–1167. doi:10.1016/S0896-6273(02)01052-8
El Mestikawy, S., Wallen-Mackenzie, A., Fortin, G.M., Descarries, L., Trudeau, L.E., 2011. From glutamate co-release to vesicular synergy: vesicular glutamate transporters. Nat Rev Neurosci 12, 204–216. doi:10.1038/nrn2969
Eliasof, S., Jahr, C.E., 1996. Retinal glial cell glutamate transporter is coupled to an anionic conductance. Proc. Natl. Acad. Sci. U. S. A. 93, 4153–4158. doi:10.1073/pnas.93.9.4153
Erecińska, M., Silver, I.A., 1990. Metabolism and role of glutamate in mammalian brain. Prog. Neurobiol. 35, 245–296. doi:10.1016/0301-0082(90)90013-7
Fahlke, C., Kortzak, D., Machtens, J.P., 2016. Molecular physiology of EAAT anion channels. Pflugers Arch. Eur. J. Physiol. 468, 491–502. doi:10.1007/s00424-015-1768-3
Fairman, W.A., Vandenberg, R.J., Arriza, J.L., Kavanaugh, M.P., Amara, S.G., 1995. An excitatory amino-acid transporter with properties of a ligand-gated chloride channel. Nature. doi:10.1038/375599a0
Featherstone, D.E., Shippy, S.A., 2008. Regulation of synaptic transmission by ambient extracellular glutamate. Neurosci. 14, 171–81. doi:10.1177/1073858407308518
Figiel, M., Allritz, C., Lehmann, C., Engele, J., 2007. Gap junctional control of glial glutamate transporter expression. Mol. Cell. Neurosci. 35, 130–137. doi:10.1016/j.mcn.2007.02.009
Figiel, M., Engele, J., 2000. Pituitary adenylate cyclase-activating polypeptide (PACAP), a neuron-derived peptide regulating glial glutamate transport and metabolism. J. Neurosci. 20, 3596–3605.
Filosa, A., Paixão, S., Honsek, S.D., Carmona, M. a, Becker, L., Feddersen, B., Gaitanos, L., Rudhard, Y., Schoepfer, R., Klopstock, T., Kullander, K., Rose, C.R., Pasquale, E.B., Klein, R., 2009. Neuron-glia communication via EphA4/ephrin-A3 modulates LTP through glial glutamate transport. Nat. Neurosci. 12, 1285–1292. doi:10.1038/nn.2394
Fleming, T.M., Scott, V., Naskar, K., Joe, N., Brown, C.H., Stern, J.E., 2011. State-dependent changes in astrocyte regulation of extrasynaptic NMDA receptor signalling in neurosecretory neurons. J. Physiol. 589, 3929–3941. doi:10.1113/jphysiol.2011.207340
Fontana, A.C.K., 2015. Current approaches to enhance glutamate transporter function and expression. J. Neurochem. n/a–n/a. doi:10.1111/jnc.13200
Foran, E., Rosenblum, L., Bogush, A., Pasinelli, P., Trotti, D., 2014. Sumoylation of the astroglial glutamate transporter EAAT2 governs its intracellular compartmentalization. Glia 62, 1241–1253. doi:10.1002/glia.22677
Furness, D.N., Dehnes, Y., Akhtar, a Q., Rossi, D.J., Hamann, M., Grutle, N.J., Gundersen, V., Holmseth, S., Lehre, K.P., Ullensvang, K., Wojewodzic, M., Zhou, Y., Attwell, D., Danbolt, N.C., 2008. A quantitative assessment of glutamate uptake into hippocampal synaptic terminals and astrocytes: new insights into a neuronal role for excitatory amino acid transporter 2 (EAAT2). Neuroscience 157, 80–94. doi:10.1016/j.neuroscience.2008.08.043
Furuta, A., Rothstein, J.D., Martin, L.J., 1997. Glutamate Transporter Protein Subtypes Are

Expressed Differentially during Rat CNS Development 17, 8363–8375.
Gameiro, A., Braams, S., Rauen, T., Grewer, C., 2011. The discovery of slowness: Low-capacity transport and slow anion channel gating by the glutamate transporter EAAT5. Biophys. J. 100, 2623–2632. doi:10.1016/j.bpj.2011.04.034
Gegelashvili, G., Danbolt, N.C., Schousboe, a, 1997. Neuronal soluble factors differentially regulate the expression of the GLT1 and GLAST glutamate transporters in cultured astroglia. J. Neurochem. 69, 2612–5.
Gegelashvili, G., Dehnes, Y., Danbolt, N.C., Schousboe, a, 2000. The high-affinity glutamate transporters GLT1, GLAST, and EAAT4 are regulated via different signalling mechanisms. Neurochem. Int. 37, 163–70.
Gegelashvili, G., Robinson, M.B., Trotti, D., Rauen, T., 2001. Regulation of glutamate transporters in health and disease. Prog. Brain Res. 132, 267–286. doi:10.1016/S0079-6123(01)32082-4
Genoud, C., Quairiaux, C., Steiner, P., Hirling, H., Welker, E., Knott, G.W., 2006. Plasticity of astrocytic coverage and glutamate transporter expression in adult mouse cortex. PLoS Biol. 4, 2057–2064. doi:10.1371/journal.pbio.0040343
Ghosh, M., Yang, Y., Rothstein, J.D., Robinson, M.B., 2011. Nuclear Factor- B Contributes to Neuron-Dependent Induction of Glutamate Transporter-1 Expression in Astrocytes. J. Neurosci. 31, 9159–9169. doi:10.1523/JNEUROSCI.0302-11.2011
Ginsberg, S.D., Martin, L.J., Rothstein, J.D., 1995. Regional deafferentation down-regulates subtypes of glutamate transporter proteins. J. Neurochem. 65, 2800–3.
Goubard, V., Fino, E., Venance, L., 2011. Contribution of astrocytic glutamate and GABA uptake to corticostriatal information processing. J. Physiol. 589, 2301–19. doi:10.1113/jphysiol.2010.203125
Grewer, C., Rauen, T., 2005. Electrogenic glutamate transporters in the CNS: Molecular mechanism, pre-steady-state kinetics, and their impact on synaptic signaling. J. Membr. Biol. 203, 1–20. doi:10.1007/s00232-004-0731-6
Grewer, C., Watzke, N., Wiessner, M., Rauen, T., 2000. Glutamate translocation of the neuronal glutamate transporter EAAC1 occurs within milliseconds. Proc. Natl. Acad. Sci. U. S. A. 97, 9706–11. doi:10.1073/pnas.160170397
Hanson, E., Armbruster, M., Cantu, D., Andresen, L., Taylor, A., Danbolt, N.C., Dulla, C.G., 2015. Astrocytic glutamate uptake is slow and does not limit neuronal NMDA receptor activation in the neonatal neocortex. Glia n/a–n/a. doi:10.1002/glia.22844
Hertz, L., Dringen, R., Schousboe, A., Robinson, S.R., 1999. Astrocytes: Glutamate producers for neurons. J. Neurosci. Res. 57, 417–428. doi:10.1002/(SICI)1097-4547(19990815)57:4<417::AID-JNR1>3.0.CO;2-N
Holmseth, S., Dehnes, Y., Huang, Y.H., Follin-Arbelet, V. V., Grutle, N.J., Mylonakou, M.N., Plachez, C., Zhou, Y., Furness, D.N., Bergles, D.E., Lehre, K.P., Danbolt, N.C., 2012. The Density of EAAC1 (EAAT3) Glutamate Transporters Expressed by Neurons in the Mammalian CNS. J. Neurosci. 32, 6000–6013. doi:10.1523/JNEUROSCI.5347-11.2012
Holmseth, S., Scott, H. a., Real, K., Lehre, K.P., Leergaard, T.B., Bjaalie, J.G., Danbolt, N.C., 2009. The concentrations and distributions of three C-terminal variants of the GLT1 (EAAT2; slc1a2) glutamate transporter protein in rat brain tissue suggest differential regulation. Neuroscience 162, 1055–1071. doi:10.1016/j.neuroscience.2009.03.048
Huang, Y.H., 2004. Climbing Fiber Activation of EAAT4 Transporters and Kainate Receptors in Cerebellar Purkinje Cells. J. Neurosci. 24, 103–111. doi:10.1523/JNEUROSCI.4473-03.2004
Huang, Y.H., Bergles, D.E., 2004. Glutamate transporters bring competition to the synapse. Curr. Opin. Neurobiol. 14, 346–52. doi:10.1016/j.conb.2004.05.007
Huang, Y.H., Sinha, S.R., Tanaka, K., Rothstein, J.D., Bergles, D.E., 2004. Glutamate Receptor-Mediated Excitation of Hippocampal Interneurons 24, 4551–4559. doi:10.1523/JNEUROSCI.5217-03.2004
Isaacson, J.S., 1999. Glutamate Spillover Mediates Excitatory Transmission in the Rat Olfactory Bulb ates reciprocal feedback excitation via a different excit. Neuron 23, 377–384.

doi:10.1016/S0896-6273(00)80787-4
Jabaudon, D., SHIMAMOTO, K., YASUDA-KAMATANI, Y., SCANZIANI, M., Gahwiler, B.H.G., GERBER, U., 1999. Inhibition of uptake unmasks rapid extracellular turnover of glutamate of nonvesicular origin. PNAS 96, 8733–8738.
Jensen, A.A., Fahlke, C., Bjørn-yoshimoto, W.E., Bunch, L., 2015. Excitatory amino acid transporters : recent insights into molecular mechanisms , novel modes of modulation and new therapeutic possibilities. Curr. Opin. Pharmacol. 20, 116–123. doi:10.1016/j.coph.2014.10.008
Jiménez, E., Núñez, E., Ibáñez, I., Draffin, J.E., Zafra, F., Giménez, C., 2014. Differential regulation of the glutamate transporters GLT-1 and GLAST by GSK3β. Neurochem. Int. 79, 33–43. doi:10.1016/j.neuint.2014.10.003
John, C.S., Smith, K.L., Van't Veer, A., Gompf, H.S., Carlezon, W.A., Cohen, B.M., Öngür, D., Bechtholt-Gompf, A.J., 2012. Blockade of astrocytic glutamate uptake in the prefrontal cortex induces anhedonia. Neuropsychopharmacology 37, 2467–75. doi:10.1038/npp.2012.105
Kalandadze, A., Wu, Y., Robinson, M.B., 2002. Protein kinase C activation decreases cell surface expression of the GLT-1 subtype of glutamate transporter: Requirement of a carboxyl-terminal domain and partial dependence on serine 486. J. Biol. Chem. 277, 45741–45750. doi:10.1074/jbc.M203771200
Kanai, Y., Hediger, M.A., 1992. Primary structure and functional characterization of a high-affinity glutamate transporter. Nature 360, 467–71. doi:10.1038/360467a0
Kanner, B.I., Borre, L., 2002. The dual-function glutamate transporters: Structure and molecular characterisation of the substrate-binding sites. Biochim. Biophys. Acta - Bioenerg. 1555, 92–95. doi:10.1016/S0005-2728(02)00260-8
Katagiri, H., Tanaka, K., Manabe, T., 2001. Requirement of appropriate glutamate concentrations in the synaptic cleft for hippocampal LTP induction. Eur J Neurosci 14, 547–553.
Kim, K., Lee, S.-G., Kegelman, T.P., Su, Z.-Z., Das, S.K., Dash, R., Dasgupta, S., Barral, P.M., Hedvat, M., Diaz, P., Reed, J.C., Stebbins, J.L., Pellecchia, M., Sarkar, D., Fisher, P.B., 2011. Role of excitatory amino acid transporter-2 (EAAT2) and glutamate in neurodegeneration: opportunities for developing novel therapeutics. J. Cell. Physiol. 226, 2484–93. doi:10.1002/jcp.22609
Kirischuk, S., Héja, L., Kardos, J., Billups, B., 2015. Astrocyte sodium signaling and the regulation of neurotransmission. Glia n/a–n/a. doi:10.1002/glia.22943
Kirischuk, S., Parpura, V., Verkhratsky, A., 2012. Sodium dynamics: another key to astroglial excitability? Trends Neurosci. 35, 497–506. doi:10.1016/j.tins.2012.04.003
Kullmann, D.M., Asztely, F., 1998. Extrasynaptic glutamate spillover in the hippocampus: evidence and implications. Trends Neurosci. 21, 8–14.
Le Meur, K., Galante, M., Angulo, M.C., Audinat, E., 2007. Tonic activation of NMDA receptors by ambient glutamate of non-synaptic origin in the rat hippocampus. J. Physiol. 580, 373–383. doi:10.1113/jphysiol.2006.123570
Lee, S.G., Su, Z.Z., Emdad, L., Gupta, P., Sarkar, D., Borjabad, A., Volsky, D.J., Fisher, P.B., 2008. Mechanism of ceftriaxone induction of excitatory amino acid transporter-2 expression and glutamate uptake in primary human astrocytes. J. Biol. Chem. 283, 13116–13123. doi:10.1074/jbc.M707697200
Lee, Y., Gaskins, D., Anand, A., Shekhar, A., 2007. Glia mechanisms in mood regulation: A novel model of mood disorders. Psychopharmacology (Berl). 191, 55–65. doi:10.1007/s00213-006-0652-4
Lehre, K.P., Danbolt, N.C., 1998. The number of glutamate transporter subtype molecules at glutamatergic synapses: chemical and stereological quantification in young adult rat brain. J. Neurosci. 18, 8751–8757.
Lehre, K.P., Levy, L.M., Storm-mathisen, J., Ottersen, O.P., Danbolt, N.C., 1995. Differential Expression of Two Glial Glutamate Transporters in the Rat Brain : Quantitative and lmmunocytochemical Observations. J. Neurosci.
Levenson, J., Weeber, E., Selcher, J.C., Kategaya, L.S., Sweatt, J.D., Eskin, A., 2002. Long-term

potentiation and contextual fear conditioning increase neuronal glutamate uptake. Nat. Neurosci. 5, 155–61. doi:10.1038/nn791
Levy, L.M., Warr, O., Attwell, D., 1998. Stoichiometry of the glial glutamate transporter GLT-1 expressed inducibly in a Chinese hamster ovary cell line selected for low endogenous Na+-dependent glutamate uptake. J. Neurosci. 18, 9620–8.
Lewerenz, J., Hewett, S.J., Huang, Y., Lambros, M., Gout, P.W., Kalivas, P.W., Massie, A., Smolders, I., Methner, A., Pergande, M., Smith, S.B., Ganapathy, V., Maher, P., 2013. The cystine/glutamate antiporter system x(c)(-) in health and disease: from molecular mechanisms to novel therapeutic opportunities. Antioxid. Redox Signal. 18, 522–55. doi:10.1089/ars.2011.4391
Li, L. Bin, Toan, S.V., Zelenaia, O., Watson, D.J., Wolfe, J.H., Rothstein, J.D., Robinson, M.B., 2006. Regulation of astrocytic glutamate transporter expression by Akt: Evidence for a selective transcriptional effect on the GLT-1/EAAT2 subtype. J. Neurochem. 97, 759–771. doi:10.1111/j.1471-4159.2006.03743.x
Li, D., Hérault, K., Zylbersztejn, K., Lauterbach, M. a., Guillon, M., Oheim, M., Ropert, N., 2015. Astrocyte VAMP3 vesicles undergo Ca^{2+} -independent cycling and modulate glutamate transporter trafficking. J. Physiol. 593, 2807–2832. doi:10.1113/JP270362
Liang, J., Chao, D., Sandhu, H.K., Yu, Y., Zhang, L., Balboni, G., Kim, D.H., Xia, Y., 2014. δ-Opioid receptors up-regulate excitatory amino acid transporters in mouse astrocytes. Br. J. Pharmacol. 171, 5417–5430. doi:10.1111/bph.12857
Liévens, J.C., Bernal, F., Forni, C., Mahy, N., Kerkerian-Le Goff, L., 2000a. Characterization of striatal lesions produced by glutamate uptake alteration: cell death, reactive gliosis, and changes in GLT1 and GADD45 mRNA expression. Glia 29, 222–32.
Liévens, J.C., Salin, P., Had-Aissouni, L., Mahy, N., Kerkerian-Le Goff, L., 2000b. Differential effects of corticostriatal and thalamostriatal deafferentation on expression of the glutamate transporter GLT1 in the rat striatum. J. Neurochem. 74, 909–19.
MacAulay, N., Hamann, S., Zeuthen, T., 2004. Water transport in the brain: Role of cotransporters. Neuroscience 129, 1031–1044. doi:10.1016/j.neuroscience.2004.06.045
MacAulay, N., Zeuthen, T., 2010. Water transport between CNS compartments: Contributions of aquaporins and cotransporters. Neuroscience 168, 941–956. doi:10.1016/j.neuroscience.2009.09.016
Machtens, J., Kortzak, D., Briones, R., Fahlke, C., Machtens, J., Kortzak, D., Lansche, C., Leinenweber, A., Kilian, P., Begemann, B., 2015. Mechanisms of Anion Conduction by Coupled Glutamate Transporters Article Mechanisms of Anion Conduction by Coupled Glutamate Transporters. Cell 160, 542–553. doi:10.1016/j.cell.2014.12.035
Magistretti, P.J., Allaman, I., 2015. A Cellular Perspective on Brain Energy Metabolism and Functional Imaging. Neuron 86, 883–901. doi:10.1016/j.neuron.2015.03.035
Magistretti, P.J., Chatton, J.Y., 2005. Relationship between L-glutamate-regulated intracellular Na+ dynamics and ATP hydrolysis in astrocytes. J. Neural Transm. 112, 77–85. doi:10.1007/s00702-004-0171-6
Marcaggi, P., Attwell, D., 2004. Role of glial amino acid transporters in synaptic transmission and brain energetics. Glia 47, 217–25. doi:10.1002/glia.20027
Marcaggi, P., Billups, D., Attwell, D., 2003. The role of glial glutamate transporters in maintaining the independent operation of juvenile mouse cerebellar parallel fibre synapses. J. Physiol. 552, 89–107. doi:10.1113/jphysiol.2003.044263
Marx, M.-C., Billups, D., Billups, B., 2015. Maintaining the presynaptic glutamate supply for excitatory neurotransmission. J. Neurosci. Res. 96, 1031–1044. doi:10.1002/jnr.23561
Massey, P. V, Johnson, B.E., Moult, P.R., Auberson, Y.P., Brown, M.W., Molnar, E., Collingridge, G.L., Bashir, Z.I., 2004. Differential roles of NR2A and NR2B-containing NMDA receptors in cortical long-term potentiation and long-term depression. J. Neurosci. 24, 7821–8. doi:10.1523/JNEUROSCI.1697-04.2004
Massie, A., Cnops, L., Smolders, I., McCullumsmith, R., Kooijman, R., Kwak, S., Arckens, L.,

Michotte, Y., 2008. High-affinity Na+/K+-dependent glutamate transporter EAAT4 is expressed throughout the rat fore- and midbrain. J. Comp. Neurol. 511, 155–172. doi:10.1002/cne.21823
Mathews, G.C., Diamond, J.S., 2003. Neuronal glutamate uptake Contributes to GABA synthesis and inhibitory synaptic strength. J. Neurosci. 23, 2040–2048. doi:23/6/2040 [pii]
Matos-Ocasio, F., Hernández-López, A., Thompson, K.J., 2014. Ceftriaxone, a GLT-1 transporter activator, disrupts hippocampal learning in rats. Pharmacol. Biochem. Behav. 122, 118–121. doi:10.1016/j.pbb.2014.03.011
Matsugami, T.R., Tanemura, K., Mieda, M., Nakatomi, R., Yamada, K., Kondo, T., Ogawa, M., Obata, K., Watanabe, M., Hashikawa, T., Tanaka, K., 2006. From the Cover: Indispensability of the glutamate transporters GLAST and GLT1 to brain development. Proc. Natl. Acad. Sci. U. S. A. 103, 12161–6. doi:10.1073/pnas.0509144103
Matute, C., Melone, M., Vallejo-Illarramendi, A., Conti, F., 2005. Increased expression of the astrocytic glutamate transporter GLT-1 in the prefrontal cortex of schizophrenics. Glia 49, 451–455. doi:10.1002/glia.20119
McCullumsmith, R.E., O'Donovan, S.M., Drummond, J.B., Benesh, F.S., Simmons, M., Roberts, R., Lauriat, T., Haroutunian, V., Meador-Woodruff, J.H., 2015. Cell-specific abnormalities of glutamate transporters in schizophrenia: sick astrocytes and compensating relay neurons? Mol. Psychiatry 1–8. doi:10.1038/mp.2015.148
McKenna, M.C., 2007. The Glutamate-Glutamine Cycle Is Not Stoichiometric: Fates of Glutamate in Brain. J. Neurosci. Res. 2137, 2126–2137. doi:10.1002/jnr
Medina, A., Burke, S., Thompson, R.C., Bunney, W., Myers, R.M., Schatzberg, A., Akil, H., Watson, S.J., 2013. Glutamate transporters: a key piece in the glutamate puzzle of major depressive disorder. J. Psychiatr. Res. 47, 1150–6. doi:10.1016/j.jpsychires.2013.04.007
Meldrum, B., Garthwaite, J., n.d. EAA pharmacology j amino acid neurotoxicity and neurodegenerative disease I.
Mim, C., Balani, P., Rauen, T., Grewer, C., 2005. The glutamate transporter subtypes EAAT4 and EAATs 1-3 transport glutamate with dramatically different kinetics and voltage dependence but share a common uptake mechanism. J. Gen. Physiol. 126, 571–589. doi:10.1085/jgp.200509365
Min, M., Rusakov, D.A., Kullmann, D.M., 1998. Activation of AMPA, Kainate, and Metabotropic Receptors at Hippocampal Mossy Fiber Synapses: Role of Glutamate Diffusion. Neuron 21, 561–570.
Minelli, A., Barbaresi, P., Reimer, R.J., Edwards, R.H., Conti, F., 2001. The glial glutamate transporter GLT-1 is localized both in the vicinity of and at distance from axon terminals in the rat cerebral cortex. Neuroscience 108, 51–59. doi:10.1016/S0306-4522(01)00375-X
Mineur, Y.S., Picciotto, M.R., Sanacora, G., 2007. Antidepressant-Like Effects of Ceftriaxone in Male C57BL/6J Mice. Biol. Psychiatry 61, 250–252. doi:10.1016/j.biopsych.2006.04.037
Moussawi, K., Riegel, A., Nair, S., Kalivas, P.W., 2011. Extracellular Glutamate: Functional Compartments Operate in Different Concentration Ranges. Front. Syst. Neurosci. doi:10.3389/fnsys.2011.00094
Murphy-Royal, C., Dupuis, J.P., Varela, J. a, Panatier, A., Pinson, B., Baufreton, J., Groc, L., Oliet, S.H.R., 2015. Surface diffusion of astrocytic glutamate transporters shapes synaptic transmission. Nat. Neurosci. 18, 219–226. doi:10.1038/nn.3901
Nie, H., Weng, H.-R., 2009. Glutamate transporters prevent excessive activation of NMDA receptors and extrasynaptic glutamate spillover in the spinal dorsal horn. J. Neurophysiol. 101, 2041–51. doi:10.1152/jn.91138.2008
Nielsen, T.A., DiGregorio, D.A., Silver, R.A., 2004. Modulation of glutamate mobility reveals the mechanism underlying slow-rising AMPAR EPSCs and the diffusion coefficient in the synaptic cleft. Neuron 42, 757–771. doi:10.1016/j.neuron.2004.04.003
Nikkuni, O., Takayasu, Y., Iino, M., Tanaka, K., Ozawa, S., 2007. Facilitated activation of metabotropic glutamate receptors in cerebellar Purkinje cells in glutamate transporter EAAT4-

deficient mice. Neurosci. Res. 59, 296–303. doi:10.1016/j.neures.2007.07.006
Nilsson, P., Hillered, L., Pontén, U., Ungerstedt, U., 1990. Changes in cortical extracellular levels of energy-related metabolites and amino acids following concussive brain injury in rats. J. Cereb. Blood Flow Metab. 10, 631–637. doi:10.1038/jcbfm.1990.115
Oliet, S.H., Piet, R., Poulain, D. a, 2001. Control of glutamate clearance and synaptic efficacy by glial coverage of neurons. Science 292, 923–6. doi:10.1126/science.1059162
Oliveira, J.F., Sardinha, V.M., Guerra-Gomes, S., Araque, A., Sousa, N., 2015. Do stars govern our actions? Astrocyte involvement in rodent behavior. Trends Neurosci. 38, 535–549. doi:10.1016/j.tins.2015.07.006
Omrani, A., Melone, M., Bellesi, M., Safiulina, V., Aida, T., Tanaka, K., Cherubini, E., Conti, F., 2009. Up-regulation of GLT-1 severely impairs LTD at mossy fibre--CA3 synapses. J. Physiol. 587, 4575–88. doi:10.1113/jphysiol.2009.177881
Otis, T.S., Michael P. Kavanaugh, Craig E. Jahr, 1997. Synapse Postsynaptic Glutamate Transport at the Climbing Fiber – Purkinje Cell Synapse. Science (80-.). 1515, 1–5. doi:10.1126/science.277.5331.1515
Otis, T.S., Wu, Y.-C., Trussell, L. 0., 1996. Delayed Clearance of Transmitter and the Role of Glutamate 76, 1634–1644.
Overstreet, L.S., Kinney, G. a, Liu, Y.B., Billups, D., Slater, N.T., 1999. Glutamate transporters contribute to the time course of synaptic transmission in cerebellar granule cells. J. Neurosci. 19, 9663–73.
Owe, S.G., Marcaggi, P., Attwell, D., 2006. The ionic stoichiometry of the GLAST glutamate transporter in salamander retinal glia. J. Physiol. 577, 591–9. doi:10.1113/jphysiol.2006.116830
Palmieri, F., 2013. The mitochondrial transporter family SLC25: Identification, properties and physiopathology. Mol. Aspects Med. 34, 465–484. doi:10.1016/j.mam.2012.05.005
Paoletti, P., Bellone, C., Zhou, Q., 2013. NMDA receptor subunit diversity: impact on receptor properties, synaptic plasticity and disease. Nat. Rev. Neurosci. 14, 383–400. doi:10.1038/nrn3504
Peghini, P., Janzen, J., Stoffel, W., 1997. Glutamate transporter EAAC-1-deficient mice develop dicarboxylic aminoaciduria and behavioral abnormalities but no neurodegeneration. EMBO J. 16, 3822–3832. doi:10.1093/emboj/16.13.3822
Pellerin, L., Magistretti, P.J., 2012. Sweet sixteen for ANLS. J. Cereb. Blood Flow & Metab. 32, 1152–1166. doi:10.1038/jcbfm.2011.149
Petr, G.T., Sun, Y., Frederick, X.N.M., Zhou, Y., Dhamne, S.C., Hameed, X.M.Q., Miranda, X.C., Bedoya, E.A., Fischer, K.D., Armsen, W., Wang, J., Danbolt, N.C., Rotenberg, A., Aoki, X.C.J., Rosenberg, P.A., 2015. Conditional Deletion of the Glutamate Transporter GLT-1 Reveals That Astrocytic GLT-1 Protects against Fatal Epilepsy While Neuronal GLT-1 Contributes Significantly to Glutamate Uptake into Synaptosomes. J. Neurosci. 35, 5187–5201. doi:10.1523/JNEUROSCI.4255-14.2015
Piet, R., Bonhomme, R., Theodosis, D.T., Poulain, D. a., Oliet, S.H.R., 2003. Modulation of GABAergic transmission by endogenous glutamate in the rat supraoptic nucleus. Eur. J. Neurosci. 17, 1777–1785. doi:10.1046/j.1460-9568.2003.02611.x
Pinard, A., Lévesque, S., Vallée, J., Robitaille, R., 2003. Glutamatergic modulation of synaptic plasticity at a PNS vertebrate cholinergic synapse. Eur J Neurosci 18. doi:10.1046/j.1460-9568.2003.03028.x
Pita-Almenar, J.D., Collado, M.S., Colbert, C.M., Eskin, A., 2006. Different mechanisms exist for the plasticity of glutamate reuptake during early long-term potentiation (LTP) and late LTP. J. Neurosci. 26, 10461–71. doi:10.1523/JNEUROSCI.2579-06.2006
Pita-almenar, J.D., Zou, S., Colbert, C.M., Eskin, A., 2005. Relationship between increase in astrocytic GLT-1 glutamate transport and late-LTP. Learn. Mem. 615–626.
Plachez, C., Martin, A., Guiramand, J., Récasens, M., 2004. Astrocytes repress the neuronal expression of GLAST and GLT glutamate transporters in cultured hippocampal neurons from

embryonic rats. Neurochem. Int. 45, 1113–1123. doi:10.1016/j.neuint.2004.03.030
Poitry-Yamate, C.L., Vutskits, L., Rauen, T., 2002. Neuronal-induced and glutamate-dependent activation of glial glutamate transporter function. J. Neurochem. 82, 987–997. doi:10.1046/j.1471-4159.2002.01075.x
Popoli, M., Yan, Z., McEwen, B.S., Sanacora, G., 2012. The stressed synapse: the impact of stress and glucocorticoids on glutamate transmission. Nat. Rev. Neurosci. 13, 22–37. doi:10.1038/nrn3138
Raghupathi, R., 2004. Cell death mechanisms following traumatic brain injury. Brain Pathol. 14, 215–222. doi:10.1111/j.1750-3639.2004.tb00056.x
Raju, K., Doulias, P.-T., Evans, P., Krizman, E.N., Jackson, J.G., Horyn, O., Daikhin, Y., Nissim, I., Yudkoff, M., Nissim, I., Sharp, K.A., Robinson, M.B., Ischiropoulos, H., 2015. Regulation of brain glutamate metabolism by nitric oxide and S-nitrosylation. Sci. Signal. 8, ra68. doi:10.1126/scisignal.aaa4312
Rauen, T., Wießner, M., Sullivan, R., Lee, A., Pow, D. V., 2004. A new GLT1 splice variant: Cloning and immunolocalization of GLT1c in the mammalian retina and brain. Neurochem. Int. 45, 1095–1106. doi:10.1016/j.neuint.2004.04.006
Reagan, L.P., Rosell, D.R., Wood, G.E., Spedding, M., Mun, C., Rothstein, J., Mcewen, B.S., 2004. Chronic restraint stress up-regulates GLT-1 mRNA and protein expression in the rat hippocampus : Reversal by tianeptine. PNAS 101, 2179–2184.
Reichelt, W., Knöpfel, T., 2002. Glutamate uptake controls expression of a slow postsynaptic current mediated by mGluRs in cerebellar Purkinje cells. J. Neurophysiol. 87, 1974–80. doi:10.1152/jn.00704.2001
Reyes, N., Ginter, C., Boudker, O., 2009. Transport mechanism of a bacterial homologue of glutamate transporters. Nature 462, 880–885. doi:10.1038/nature08616
Rimmele, T.S., Rosenberg, P.A., 2016. GLT-1: The elusive presynaptic glutamate transporter. Neurochem. Int. 1–10. doi:10.1016/j.neuint.2016.04.010
Robinson, M.B., Jackson, J.G., 2016. Astroglial glutamate transporters coordinate excitatory signaling and brain energetics. Neurochem. Int. doi:10.1016/j.neuint.2016.03.014
Rosenberg, P. a, Amin, S., Leitner, M., 1992. Glutamate uptake disguises neurotoxic potency of glutamate agonists in cerebral cortex in dissociated cell culture. J. Neurosci. 12, 56–61.
Rossi, D.J., Oshima, T., Attwell, D., 2000. Glutamate release in severe brain ischaemia is mainly by reversed uptake. Nature 403, 316–321. doi:10.1038/35002090
Rothstein, J.D., Levey, A.I., Dykes-hoberg, M., Jin, L., Wu, D., Nash, N., Kuncl, R.W., 1994. localization of Neuronal and Glial Glutamate Transporters. Neuron 13, 713–725.
Rothstein, J.D., Patel, S., Regan, M.R., Haenggeli, C., Huang, Y.H., Bergles, D.E., Jin, L., Dykes Hoberg, M., Vidensky, S., Chung, D.S., Toan, S.V., Bruijn, L.I., Su, Z.-Z., Gupta, P., Fisher, P.B., 2005. Beta-lactam antibiotics offer neuroprotection by increasing glutamate transporter expression. Nature 433, 73–7. doi:10.1038/nature03180
Ryan, R.M., Mindell, J. a, 2007. The uncoupled chloride conductance of a bacterial glutamate transporter homolog. Nat. Struct. Mol. Biol. 14, 365–71. doi:10.1038/nsmb1230
Sadeghi, S.G., Pyott, S.J., Yu, Z., Glowatzki, E., 2014. Glutamatergic Signaling at the Vestibular Hair Cell Calyx Synapse. J. Neurosci. 34, 14536–14550. doi:10.1523/JNEUROSCI.0369-13.2014
Sah, P., Hestrin, R., Nicoll, R.A., 1988. Tonic Activation of NMDA Receptors by Ambient Glutamate Enhances Excitability of Neurons. Science (80-.).
Sanacora, G., Zarate, C. a, Krystal, J.H., Manji, H.K., 2008. Targeting the glutamatergic system to develop novel, improved therapeutics for mood disorders. Nat. Rev. Drug Discov. 7, 426–437. doi:10.1038/nrd2462
Schneider, N., Cordeiro, S., Machtens, J.P., Braams, S., Rauen, T., Fahlke, C., 2014. Functional properties of the retinal glutamate transporters GLT-1c and EAAT5. J. Biol. Chem. 289, 1815–1824. doi:10.1074/jbc.M113.517177
Scimemi, A., Tian, H., Diamond, J.S., 2009. Neuronal transporters regulate glutamate clearance,

NMDA receptor activation, and synaptic plasticity in the hippocampus. J. Neurosci. 29, 14581–95. doi:10.1523/JNEUROSCI.4845-09.2009
Scofield, M.D., Kalivas, P.W., 2014. Astrocytic Dysfunction and Addiction: Consequences of Impaired Glutamate Homeostasis. Neuroscientist 20, 610–622. doi:10.1177/1073858413520347
Seal, R.P., Amara, S.G., 1999. Excitatory amino acid transporters: a family in flux. Annu Rev Pharmacol Toxicol 39, 431–456. doi:10.1146/annurev.pharmtox.39.1.431
Semyanov, a, Kullmann, D.M., 2000. Modulation of GABAergic signaling among interneurons by metabotropic glutamate receptors. Neuron 25, 663–672. doi:10.1016/S0896-6273(00)81068-5
Sepkuty, J.P., Cohen, A.S., Eccles, C., Rafiq, A., Behar, K., Ganel, R., Coulter, D. a, Rothstein, J.D., 2002. A neuronal glutamate transporter contributes to neurotransmitter GABA synthesis and epilepsy. J. Neurosci. 22, 6372–6379. doi:20026650
Shen, Y., Linden, D.J., 2005. Long-term potentiation of neuronal glutamate transporters. Neuron 46, 715–722. doi:10.1016/j.neuron.2005.04.033
Sitcheran, R., Gupta, P., Fisher, P.B., Baldwin, A.S., 2005. Positive and negative regulation of EAAT2 by NF-kappaB: a role for N-myc in TNFalpha-controlled repression. EMBO J. 24, 510–20. doi:10.1038/sj.emboj.7600555
Soni, N., Reddy, B.V.K., Kumar, P., 2014. GLT-1 Transporter: An Effective Pharmacological Target for Various Neurological Disorders. Pharmacol. Biochem. Behav. 1–11. doi:10.1016/j.pbb.2014.10.001
Stobart, J.L., Anderson, C.M., 2013. Multifunctional role of astrocytes as gatekeepers of neuronal energy supply. Front. Cell. Neurosci. 7, 38. doi:10.3389/fncel.2013.00038
Su, Z., Leszczyniecka, M., Kang, D., Sarkar, D., Chao, W., Volsky, D.J., Fisher, P.B., 2003. Insights into glutamate transport regulation in human astrocytes: cloning of the promoter for excitatory amino acid transporter 2 (EAAT2). Proc. Natl. Acad. Sci. U. S. A. 100, 1955–1960. doi:10.1073/pnas.0136555100
Sutherland, M.L., Delaney, T.A., Noebels, J.L., 1996. Glutamate transporter mRNA expression in proliferative zones of the developing and adult murine CNS. J Neurosci 16, 2191–2207.
Szapiro, G., Barbour, B., 2007. Multiple climbing fibers signal to molecular layer interneurons exclusively via glutamate spillover. Nat. Neurosci. 10, 735–742. doi:10.1038/nn1907
Takahashi, K., Foster, J.B., Lin, C.-L.G., 2015. Glutamate transporter EAAT2: regulation, function, and potential as a therapeutic target for neurological and psychiatric disease. Cell. Mol. Life Sci. doi:10.1007/s00018-015-1937-8
Takayasu, Y., 2005. Differential Roles of Glial and Neuronal Glutamate Transporters in Purkinje Cell Synapses. J. Neurosci. 25, 8788–8793. doi:10.1523/JNEUROSCI.1020-05.2005
Takayasu, Y., Iino, M., Shimamoto, K., Tanaka, K., Ozawa, S., 2006. Glial Glutamate Transporters Maintain One-to-One Relationship at the Climbing Fiber-Purkinje Cell Synapse by Preventing Glutamate Spillover. J. Neurosci. 26, 6563–6572. doi:10.1523/JNEUROSCI.5342-05.2006
Takayasu, Y., Iino, M., Takatsuru, Y., Tanaka, K., Ozawa, S., 2009. Functions of glutamate transporters in cerebellar Purkinje cell synapses. Acta Physiol. 197, 1–12. doi:10.1111/j.1748-1716.2009.02019.x
Tanaka, J., Ichikawa, R., Watanabe, M., Tanaka, K., Inoue, Y., 1997. Extra-junctional localization of glutamate transporter EAAT4 at excitatory Purkinje cell synapses. Neuroreport 8, 2461–4.
Tian, G., Lai, L., Guo, H., Lin, Y., Butchbach, M.E.R., Chang, Y., Lin, C.L.G., 2007. Translational control of glial glutamate transporter EAAT2 expression. J. Biol. Chem. 282, 1727–1737. doi:10.1074/jbc.M609822200
Tong, G., Jahr, E., 1994. Block of Glutamate Transporters Potentiates Synaptic Excitation. Neuron 13, 1195–1203.
Trotti, D., Danbolt, N.C., Volterra, A., 1998. Glutamate transporters are oxidant-vulnerable: A molecular link between oxidative and excitotoxic neurodegeneration? Trends Pharmacol. Sci. 19, 328–334. doi:10.1016/S0165-6147(98)01230-9
Trotti, D., Nussberger, S., Volterra, A., Hediger, M.A., 1997. Differential modulation of the uptake

currents by redox interconversion of cysteine residues in the human neuronal glutamate transporter EAAC1. Eur. J. Neurosci. 9, 2207–12. doi:10.1111/j.1460-9568.1997.tb01388.x
Trotti, D., Volterra, A., Lehre, K.P., Rossi, D., Gjesdal, O., Racagni, G., Danbolt, N.C., 1995. Arachidonic acid inhibits a purified and reconstituted glutamate transporter directly from the water phase and not via the phospholipid membrane. J. Biol. Chem. doi:10.1074/jbc.270.17.9890
Tsai, M.-C., Tanaka, K., Overstreet-Wadiche, L., Wadiche, J.I., 2012. Neuronal Glutamate Transporters Regulate Glial Excitatory Transmission. J. Neurosci. 32, 1528–1535. doi:10.1523/JNEUROSCI.5232-11.2012
Tsvetkov, E., Shin, R.M., Bolshakov, V.Y., 2004. Glutamate Uptake Determines Pathway Specificity of Long-Term Potentiation in the Neural Circuitry of Fear Conditioning. Neuron 41, 139–151. doi:10.1016/S0896-6273(03)00800-6
Turecek, R., Trussell, L.O., 2000. Control of Synaptic Depression by Glutamate Transporters. J Neurosci 20, 2054–2063.
Tzingounis, A. V, Wadiche, J.I., 2007. Glutamate transporters : confining runaway excitation by shaping synaptic transmission. Nat Neurosci Rev 8. doi:10.1038/nrn2274
Ullensvang, K., Lehre, K.P., Storm-Mathisen, J., Danbolt, N.C., 1997. Differential developmental expression of the two rat brain glutamate transporter proteins GLAST and GLT. Eur. J. Neurosci. 9, 1646–1655. doi:10.1111/j.1460-9568.1997.tb01522.x
Underhill, S.M., Wheeler, X.D.S., Amara, S.G., 2015. Differential Regulation of Two Isoforms of the Glial Glutamate Transporter EAAT2 by DLG1 and CaMKII. J. Neurosci. 35, 5260–5270. doi:10.1523/JNEUROSCI.4365-14.2015
Vandenberg, R.J., Ryan, R.M., 2013. Mechanisms of glutamate transport. Physiol. Rev. 93, 1621–57. doi:10.1152/physrev.00007.2013
Veruki, M.L., Mørkve, S.H., Hartveit, E., 2006. Activation of a presynaptic glutamate transporter regulates synaptic transmission through electrical signaling. Nat. Neurosci. 9, 1388–96. doi:10.1038/nn1793
Voutsinos-Porche, B., Knott, G., Tanaka, K., Quairiaux, C., Welker, E., Bonvento, G., 2003. Glial glutamate transporters and maturation of the mouse somatosensory cortex. Cereb. Cortex 13, 1110–1121. doi:10.1093/cercor/13.10.1110
Vroman, R., Kamermans, M., 2015. Feedback-induced glutamate spillover enhances negative feedback from horizontal cells to cones. J. Physiol. 13, n/a–n/a. doi:10.1113/JP270158
Wadiche, J.I., Amara, Kavanaugh, 1995a. Ion fluxes associated with excitatory amino acid transport. Neuron 15, 721–728. doi:0896-6273(95)90159-0 [pii]
Wadiche, J.I., Arriza, J.L., Amara, S.G., Kavanaugh, M.P., 1995b. Kinetics of a Human Glutamate Transporter 14, 1019–1027.
Wadiche, J.I., Jahr, C.E., 2005. Patterned expression of Purkinje cell glutamate transporters controls synaptic plasticity. Nat. Neurosci. 8, 1329–34. doi:10.1038/nn1539
Wadiche, J.I., Kavanaugh, M.P., 1998. Macroscopic and microscopic properties of a cloned glutamate transporter/chloride channel. J. Neurosci. 18, 7650–7661.
Wang, Z.-Y., Zhang, Y.-Q., Zhao, Z.-Q., 2006. Inhibition of tetanically sciatic stimulation-induced LTP of spinal neurons and Fos expression by disrupting glutamate transporter GLT-1. Neuropharmacology 51, 764–72. doi:10.1016/j.neuropharm.2006.05.024
Watase, K., Hashimoto, K., Kano, M., Yamada, K., Watanabe, M., Inoue, Y., Okuyama, S., Sakagawa, T., Ogawa, S.I., Kawashima, N., Hori, S., Takimoto, M., Wada, K., Tanaka, K., 1998. Motor discoordination and increased susceptibility to cerebellar injury in GLAST mutant mice. Eur. J. Neurosci. 10, 976–988. doi:10.1046/j.1460-9568.1998.00108.x
Wen, Z.H., Wu, G.J., Chang, Y.C., Wang, J.J., Wong, C.S., 2005. Dexamethasone modulates the development of morphine tolerance and expression of glutamate transporters in rats. Neuroscience 133, 807–817. doi:10.1016/j.neuroscience.2005.03.015
Wersinger, E., Schwab, Y., Sahel, J.-A., Rendon, A., Pow, D. V, Picaud, S., Roux, M.J., 2006. The glutamate transporter EAAT5 works as a presynaptic receptor in mouse rod bipolar cells. J.

Physiol. 577, 221–234. doi:10.1113/jphysiol.2006.118281
Yang, C.-H., Huang, C.-C., Hsu, K.-S., 2005. Behavioral stress enhances hippocampal CA1 long-term depression through the blockade of the glutamate uptake. J. Neurosci. 25, 4288–93. doi:10.1523/JNEUROSCI.0406-05.2005
Zelenaia, O., Schlag, B.D., Gochenauer, G.E., Ganel, R., Song, W., Beesley, J.S., Grinspan, J.B., Rothstein, J.D., Robinson, M.B., 2000. Epidermal growth factor receptor agonists increase expression of glutamate transporter GLT-1 in astrocytes through pathways dependent on phosphatidylinositol 3-kinase and transcription factor NF-kappaB. Mol. Pharmacol. 57, 667–78.
Zerangue, N., Arriza, J.L., Amara, S.G., Kavanaugh, M.P., 1995. Differential Modulation of Human Glutamate Transporter Subtypes by Arachidonic Acid.
Zerangue, N., Kavanaugh, M.P., 1996. Flux coupling in a neuronal glutamate transporter. Nature. doi:10.1038/383634a0
Zheng, K., Scimemi, A., Rusakov, D. a, 2008. Receptor actions of synaptically released glutamate: the role of transporters on the scale from nanometers to microns. Biophys. J. 95, 4584–4596. doi:10.1529/biophysj.108.129874
Zhou, J., 2004. Glutamate Transporter Cluster Formation in Astrocytic Processes Regulates Glutamate Uptake Activity. J. Neurosci. 24, 6301–6306. doi:10.1523/JNEUROSCI.1404-04.2004
Zhou, Y., Danbolt, N.C., 2014. Glutamate as a neurotransmitter in the healthy brain. J. Neural Transm. 121, 799–817. doi:10.1007/s00702-014-1180-8
Zschocke, J., Bayatti, N., Clement, A.M., Witan, H., Figiel, M., Engele, J., Behl, C., 2005. Differential promotion of glutamate transporter expression and function by glucocorticoids in astrocytes from various brain regions. J. Biol. Chem. 280, 34924–34932. doi:10.1074/jbc.M502581200

Part III - STDP

Abbott, L.F., Nelson, S.B., 2000. Synaptic plasticity: taming the beast. Nat. Neurosci. 3 Suppl, 1178–1183. doi:10.1038/81453
Andrade-Talavera, Y., Duque-Feria, P., Paulsen, O., Rodríguez-Moreno, A., 2016. Presynaptic Spike Timing-Dependent Long-Term Depression in the Mouse Hippocampus. Cereb. Cortex bhw172. doi:10.1093/cercor/bhw172
Banerjee, A., González-Rueda, A., Sampaio-Baptista, C., Paulsen, O., Rodríguez-Moreno, A., 2014. Distinct mechanisms of spike timing-dependent LTD at vertical and horizontal inputs onto L2/3 pyramidal neurons in mouse barrel cortex. Physiol. Rep. 2, e00271. doi:10.1002/phy2.271
Bell, C.C., Han, V.Z., Sugawara, Y., Grant, K., 1997. Synaptic plasticity in a cerebellum-like structure depends on temporal order. Nature 387, 278–281. doi:10.1038/387278a0
Bernardinelli, Y., Muller, D., Nikonenko, I., Bernardinelli, Y., Muller, D., Nikonenko, I., 2014. Astrocyte-Synapse Structural Plasticity. Neural Plast. 2014, 1–13. doi:10.1155/2014/232105
Bi, G., Poo, M., 1998. Synaptic Modifications in Cultured Hippocampal Neurons : Dependence on Spike Timing , Synaptic Strength , and Postsynaptic Cell Type 18, 10464–10472.
Bissière, S., Humeau, Y., Lüthi, A., 2003. Dopamine gates LTP induction in lateral amygdala by suppressing feedforward inhibition. Nat. Neurosci. 6, 587–592. doi:10.1038/nn1058
Bliss, T.V.P., Lømo, T., 1973. Long-Lasting Potentiation of Synaptic Transmission in the Dentate Area of the Anaesthetized Rabbit Following Stimulation of the Perforant Path. J. Physiol. 232, 331–356.
Brandalise, F., Gerber, U., 2014. Mossy fiber-evoked subthreshold responses induce timing-dependent plasticity at hippocampal CA3 recurrent synapses. Proc. Natl. Acad. Sci. U. S. A. 111. doi:10.1073/pnas.1317667111

Brzosko, Z., Schultz, W., Paulsen, O., 2015. Retroactive modulation of spike timing-dependent plasticity by dopamine. Elife 4, 1–13. doi:10.7554/eLife.09685
Caporale, N., Dan, Y., 2008. Spike timing-dependent plasticity: a Hebbian learning rule. Annu. Rev. Neurosci. 31, 25–46. doi:10.1146/annurev.neuro.31.060407.125639
Carson, R.G., Kennedy, N.C., 2013. Modulation of human corticospinal excitability by paired associative stimulation. Front. Hum. Neurosci. 7, 823. doi:10.3389/fnhum.2013.00823
Cassenaer, S., Laurent, G., 2012. Corrigendum: Conditional modulation of spike-timing-dependent plasticity for olfactory learning. Nature 487, 128–128. doi:10.1038/nature11261
Cho, J.-H., Bayazitov, I.T., Meloni, E.G., Myers, K.M., Carlezon, W. a, Zakharenko, S.S., Bolshakov, V.Y., 2011. Coactivation of thalamic and cortical pathways induces input timing–dependent plasticity in amygdala. Nat. Neurosci. 15, 113–122. doi:10.1038/nn.2993
Chung, W.-S., Welsh, C.A., Barres, B.A., Stevens, B., 2015. Do glia drive synaptic and cognitive impairment in disease? Nat. Neurosci. 18, 1539–1545. doi:10.1038/nn.4142
Cui, Y., Paillé, V., Xu, H., Genet, S., Delord, B., Fino, E., Berry, H., Venance, L., 2015. Endocannabinoids mediate bidirectional striatal spike-timing-dependent plasticity. J Physiol 593, 2833–2849. doi:10.1113/JP270324
Cui, Y., Prokin, I., Xu, H., Delord, B., Genet, S., Venance, L., Berry, H., 2016. Endocannabinoid dynamics gate spike- timing dependent depression and potentiation. Elife 5, 1–32. doi:10.7554/eLife.13185
D'amour, J.A., Froemke, R.C., 2015. Inhibitory and Excitatory Spike-Timing-Dependent Plasticity in the Auditory Cortex. Neuron 1–15. doi:10.1016/j.neuron.2015.03.014
Dahmen, J.C., Hartley, D.E.H., King, A.J., 2008. Stimulus-Timing-Dependent Plasticity of Cortical Frequency Representation 28, 13629–13639. doi:10.1523/JNEUROSCI.4429-08.2008
Debanne, D., Gahwiler, B.H., Thompson, S.M., 1998. Long-term synaptic plasticity between pairs of individual CA3 pyramidal cells in rat hippocampal slice cultures. J. Physiol. 507, 237–247. doi:10.1111/j.1469-7793.1998.237bu.x
DeCharms, R.C., Zador, A., 2000. NEURAL REPRESENTATION AND THE CORTICAL CODE. Annu. Rev. Neurosci. 24, 1193–1216. doi:10.1146/annurev.neuro.24.1.1193
Dembrow, N.C., Zemelman, B. V., Johnston, D., 2015. Temporal Dynamics of L5 Dendrites in Medial Prefrontal Cortex Regulate Integration Versus Coincidence Detection of Afferent Inputs. J. Neurosci. 35, 4501–4514. doi:10.1523/JNEUROSCI.4673-14.2015
Dudman, J.T., Tsay, D., Siegelbaum, S.A., 2007. A Role for Synaptic Inputs at Distal Dendrites: Instructive Signals for Hippocampal Long-Term Plasticity. Neuron 56, 866–879. doi:10.1016/j.neuron.2007.10.020
Edelmann, E., Cepeda-Prado, E., Franck, M., Lichtenecker, P., Brigadski, T., Leßmann, V., 2015. Theta Burst Firing Recruits BDNF Release and Signaling in Postsynaptic CA1 Neurons in Spike-Timing-Dependent LTP. Neuron 1–14. doi:10.1016/j.neuron.2015.04.007
Edelmann, E., Leßmann, V., Brigadski, T., 2014. Pre- and postsynaptic twists in BDNF secretion and action in synaptic plasticity. Neuropharmacology 76, 610–627. doi:10.1016/j.neuropharm.2013.05.043
Egger, V., Feldmeyer, D., Sakmann, B., 1999. Coincidence detection and changes of synaptic efficacy in spiny stellate neurons in rat barrel cortex. Nat. Neurosci. 2, 1098–105. doi:10.1038/16026
Farries, M. a, Kita, H., Wilson, C.J., 2010. Dynamic spike threshold and zero membrane slope conductance shape the response of subthalamic neurons to cortical input. J. Neurosci. 30, 13180–91. doi:10.1523/JNEUROSCI.1909-10.2010
Feldman, D.E., 2012. The spike-timing dependence of plasticity. Neuron 75, 556–71. doi:10.1016/j.neuron.2012.08.001
Feldman, D.E., 2000. Timing-based LTP and LTD at vertical inputs to layer II/III pyramidal cells in rat barrel cortex. Neuron 27, 45–56. doi:10.1016/S0896-6273(00)00008-8
Fields, R.D., Araque, A., Johansen-Berg, H., Lim, S.-S., Lynch, G., Nave, K.-A., Nedergaard, M., Perez, R., Sejnowski, T., Wake, H., 2014. Glial Biology in Learning and Cognition. Neurosci.

20, 426–431. doi:10.1177/1073858413504465
Fino, E., Deniau, J.-M., Venance, L., 2008. Cell-specific spike-timing-dependent plasticity in GABAergic and cholinergic interneurons in corticostriatal rat brain slices. J. Physiol. 586, 265–282. doi:10.1113/jphysiol.2007.144501
Fino, E., Deniau, J.M., Venance, L., 2009a. Brief subthreshold events can act as Hebbian signals for long-term plasticity. PLoS One 4. doi:10.1371/journal.pone.0006557
Fino, E., Glowinski, J., Venance, L., 2005. Bidirectional activity-dependent plasticity at corticostriatal synapses. J. Neurosci. 25, 11279–11287. doi:10.1523/JNEUROSCI.4476-05.2005
Fino, E., Paillé, V., Cui, Y., Morera-Herreras, T., Deniau, J.-M., Venance, L., 2010. Distinct coincidence detectors govern the corticostriatal spike timing-dependent plasticity. J. Physiol. 588, 3045–62. doi:10.1113/jphysiol.2010.188466
Fino, E., Paillé, V., Deniau, J.-M., Venance, L., 2009b. Asymmetric spike-timing dependent plasticity of striatal nitric oxide-synthase interneurons. Neuroscience 160, 744–754. doi:10.1016/j.neuroscience.2009.03.015
Fino, E., Venance, L., 2011. Spike-timing dependent plasticity in striatal interneurons. Neuropharmacology 60, 780–788. doi:10.1016/j.neuropharm.2011.01.023
Frémaux, N., Gerstner, W., 2016. Neuromodulated Spike-Timing-Dependent Plasticity and Theory of Three-Factor Learning Rules. Front. Neural Circuits 9, 85. doi:10.3389/fncir.2015.00085
Froemke, R.C., Carcea, I., Barker, A.J., Yuan, K., Seybold, B. a, Martins, A.R.O., Zaika, N., Bernstein, H., Wachs, M., Levis, P. a, Polley, D.B., Merzenich, M.M., Schreiner, C.E., 2013. Long-term modification of cortical synapses improves sensory perception. Nat. Neurosci. 16, 79–88. doi:10.1038/nn.3274
Froemke, R.C., Poo, M.-M., Dan, Y., 2005. Spike-timing-dependent synaptic plasticity depends on dendritic location. Nature 434, 221–225. doi:10.1038/nature03366
Fu, Y.-X., Djupsund, K., Gao, H., Hayden, B., Shen, K., Dan, Y., 2002. Temporal specificity in the cortical plasticity of visual space representation. Science 296, 1999–2003. doi:10.1126/science.1070521
Fuenzalida, M., Fernández de Sevilla, D., Couve, A., Buño, W., 2010. Role of AMPA and NMDA receptors and back-propagating action potentials in spike timing-dependent plasticity. J. Neurophysiol. 103, 47–54. doi:10.1152/jn.00416.2009
Groen, M.R., Paulsen, O., Pérez-Garci, E., Nevian, T., Wortel, J., Dekker, M.P., Mansvelder, H.D., van Ooyen, A., Meredith, R.M., 2014. Development of dendritic tonic GABAergic inhibition regulates excitability and plasticity in CA1 pyramidal neurons. J. Neurophysiol. 112, 287–99. doi:10.1152/jn.00066.2014
Han, V.Z., Grant, K., Bell, C.C., 2000. Reversible Associative Depression and Nonassociative Potentiation at a Parallel Fiber Synapse. Neuron 27, 611–622. doi:10.1016/S0896-6273(00)00070-2
Hoffman, D. a, Magee, J.C., Colbert, C.M., Johnston, D., 1997. K+ channel regulation of signal propagation in dendrites of hippocampal pyramidal neurons. Nature 387, 869–875. doi:10.1038/43119
Holbro, N., Grunditz, A., Wiegert, J.S., Oertner, T.G., 2010. AMPA receptors gate spine Ca(2+) transients and spike-timing-dependent potentiation. Proc. Natl. Acad. Sci. U. S. A. 107, 15975–80. doi:10.1073/pnas.1004562107
Huang, S., Huganir, R.L., Kirkwood, A., 2013. Adrenergic gating of Hebbian spike-timing-dependent plasticity in cortical interneurons. J. Neurosci. 33, 13171–8. doi:10.1523/JNEUROSCI.5741-12.2013
Itami, C., Huang, J.-Y., Yamasaki, M., Watanabe, M., Lu, H.-C., Kimura, F., 2016. Developmental Switch in Spike Timing-Dependent Plasticity and Cannabinoid-Dependent Reorganization of the Thalamocortical Projection in the Barrel Cortex. J. Neurosci. 36, 7039–7054. doi:10.1523/JNEUROSCI.4280-15.2016
Itami, C., Kimura, F., 2012. Developmental Switch in Spike Timing-Dependent Plasticity at Layers

4-2/3 in the Rodent Barrel Cortex. J. Neurosci. 32, 15000–15011. doi:10.1523/JNEUROSCI.2506-12.2012
Ito, M., Sakurai, M., Tongroach, P., 1982. Climbing fibre induced depression of both mossy fibre responsiveness and glutamate sensitivity of cerebellar Purkinje cells. J Physiol 324, 113–134.
Jacob, V., Brasier, D.J., Erchova, I., Feldman, D., Shulz, D.E., 2007. Spike Timing-Dependent Synaptic Depression in the In Vivo Barrel Cortex of the Rat. J. Neurosci. 27, 1271–1284. doi:10.1523/JNEUROSCI.4264-06.2007
Kampa, B.M., Clements, J., Jonas, P., Stuart, G.J., 2004. Kinetics of Mg2+ unblock of NMDA receptors: implications for spike-timing dependent synaptic plasticity. J. Physiol. 556, 337–45. doi:10.1113/jphysiol.2003.058842
Karmarkar, U.R., Buonomano, D. V, 2002. A model of spike-timing dependent plasticity: one or two coincidence detectors? J. Neurophysiol. 88, 507–513. doi:10.1152/jn.00909.2001
Kelso, S.R., Ganong, A.H., Brown, T.H., 1986. Hebbian synapses in hippocampus. Proc. Natl. Acad. Sci. U. S. A. 83, 5326–5330. doi:10.1073/pnas.83.14.5326
Koehler, S., Shore, S., 2013a. Stimulus-Timing Dependent Multisensory Plasticity in the Guinea Pig Dorsal Cochlear Nucleus. PLoS One 8. doi:10.1371/journal.pone.0059828
Koehler, S., Shore, S., 2013b. Stimulus Timing-Dependent Plasticity in Dorsal Cochlear Nucleus Is Altered in Tinnitus. J. Neurosci. 33, 19647–19656. doi:10.1523/JNEUROSCI.2788-13.2013
Koester, H.J., Sakmann, B., 1998. Calcium dynamics in single spines during coincident pre- and postsynaptic activity depend on relative timing of back-propagating action potentials and subthreshold excitatory postsynaptic potentials. Proc. Natl. Acad. Sci. U. S. A. 95, 9596–9601. doi:10.1073/pnas.95.16.9596
Larsen, R.S., Smith, I.T., Miriyala, J., Han, J.E., Corlew, R.J., Smith, S.L., Philpot, B.D., 2014. Synapse-Specific Control of Experience-Dependent Plasticity by Presynaptic NMDA Receptors. Neuron 83, 879–893. doi:10.1016/j.neuron.2014.07.039
Letzkus, J.J., Kampa, B.M., Stuart, G.J., 2006. Learning rules for spike timing-dependent plasticity depend on dendritic synapse location. J. Neurosci. 26, 10420–9. doi:10.1523/JNEUROSCI.2650-06.2006
Li, J., Baccei, M.L., 2016. Neonatal Tissue Damage Promotes Spike Timing-Dependent Synaptic Long-Term Potentiation in Adult Spinal Projection Neurons. J. Neurosci. 36, 5405–5416. doi:10.1523/JNEUROSCI.3547-15.2016
Lin, Y.-W., Min, M.-Y., Chiu, T.-H., Yang, H.-W., 2003. Enhancement of associative long-term potentiation by activation of beta-adrenergic receptors at CA1 synapses in rat hippocampal slices. J. Neurosci. 23, 4173–4181.
Lisman, J., 1989. A mechanism for the Hebb and the anti-Hebb processes underlying learning and memory. Proc. Natl. Acad. Sci. U. S. A. 86, 9574–9578. doi:10.1073/pnas.86.23.9574
Litvak, V., Zeller, D., Oostenveld, R., Maris, E., Cohen, A., Schramm, A., Gentner, R., Zaaroor, M., Pratt, H., Classen, J., 2007. LTP-like changes induced by paired associative stimulation of the primary somatosensory cortex in humans: Source analysis and associated changes in behaviour. Eur. J. Neurosci. 25, 2862–2874. doi:10.1111/j.1460-9568.2007.05531.x
Lu, J., Li, C., Zhao, J.-P., Poo, M., Zhang, X., 2007. Spike-timing-dependent plasticity of neocortical excitatory synapses on ibhibitory interneurons depends on target cell type. J. Neurosci. 27, 9711–9720. doi:10.1523/JNEUROSCI.2513-07.2007
Magee, J.C., Johnston, D., 1997. A synaptically controlled, associative signal for Hebbian plasticity in hippocampal neurons. Science 275, 209–213. doi:10.1126/science.275.5297.209
Markram, H., 1997. Regulation of Synaptic Efficacy by Coincidence of Postsynaptic APs and EPSPs. Science (80-.). 275, 213–215. doi:10.1126/science.275.5297.213
Marlin, B.J., Mitre, M., James, a D., Chao, M. V, Froemke, R.C., 2015. Oxytocin enables maternal behaviour by balancing cortical inhibition. Nature. doi:10.1038/nature14402
Martins, A.R.O., Froemke, R.C., 2015. Coordinated forms of noradrenergic plasticity in the locus coeruleus and primary auditory cortex. Nat. Neurosci. 18. doi:10.1038/nn.4090
McMahon, D.B.T., Leopold, D.A., 2012. Stimulus timing-dependent plasticity in high-level vision.

Curr. Biol. 22, 332–337. doi:10.1016/j.cub.2012.01.003
Meliza, C.D., Dan, Y., 2006. Receptive-field modification in rat visual cortex induced by paired visual stimulation and single-cell spiking. Neuron 49, 183–189. doi:10.1016/j.neuron.2005.12.009
Min, R., Nevian, T., 2012. Astrocyte signaling controls spike timing–dependent depression at neocortical synapses. Nat. Neurosci. 15, 746–753. doi:10.1038/nn.3075
Mishra, R.K., Kim, S., Guzman, S.J., Jonas, P., 2016. Symmetric spike timing-dependent plasticity at CA3–CA3 synapses optimizes storage and recall in autoassociative networks. Nat. Commun. 7, 11552. doi:10.1038/ncomms11552
Mitre, M., Marlin, B.J., Schiavo, J.K., Morina, E., Norden, S.E., Hackett, T.A., Aoki, X.C.J., Chao, M. V, Froemke, R.C., 2016. A Distributed Network for Social Cognition Enriched for Oxytocin Receptors. J. Neurosci. 36, 2517–2535. doi:10.1523/JNEUROSCI.2409-15.2016
Nevian, T., Sakmann, B., 2006. Spine Ca2+ signaling in spike-timing-dependent plasticity. J. Neurosci. 26, 11001–11013. doi:10.1523/JNEUROSCI.1749-06.2006
Nishiyama, M., Hong, K., Mikoshiba, K., Poo, M.M., Kato, K., 2000. Calcium stores regulate the polarity and input specificity of synaptic modification. Nature 408, 584–8. doi:10.1038/35046067
Oliveira, J.F., Sardinha, V.M., Guerra-Gomes, S., Araque, A., Sousa, N., 2015. Do stars govern our actions? Astrocyte involvement in rodent behavior. Trends Neurosci. 38, 535–549. doi:10.1016/j.tins.2015.07.006
Paillé, V., Fino, E., Du, K., Morera-Herreras, T., Perez, S., Kotaleski, J.H., Venance, L., 2013. GABAergic circuits control spike-timing-dependent plasticity. J. Neurosci. 33, 9353–63. doi:10.1523/JNEUROSCI.5796-12.2013
Pawlak, V., Kerr, J.N.D., 2008. Dopamine receptor activation is required for corticostriatal spike-timing-dependent plasticity. J. Neurosci. 28, 2435–46. doi:10.1523/JNEUROSCI.4402-07.2008
Ratté, S., Hong, S., DeSchutter, E., Prescott, S. a., 2013. Impact of neuronal properties on network coding: Roles of spike initiation dynamics and robust synchrony transfer. Neuron 78, 758–772. doi:10.1016/j.neuron.2013.05.030
Ruan, H., Saur, T., Yao, W.-D., 2014. Dopamine-enabled anti-Hebbian timing-dependent plasticity in prefrontal circuitry. Front. Neural Circuits 8, 38. doi:10.3389/fncir.2014.00038
Rudolph, M., Destexhe, A., 2003. Tuning Neocortical Pyramidal Neurons between Integrators. J. Comput. Neurosci. 239–251.
Safo, P.K., Regehr, W.G., 2005. Endocannabinoids control the induction of cerebellar LTD. Neuron 48, 647–659. doi:10.1016/j.neuron.2005.09.020
Schiller, J., Schiller, Y., Clapham, D.E., 1998. NMDA receptors amplify calcium influx into dendritic spines during associative pre- and postsynaptic activation. Nat. Neurosci. 1, 114–118. doi:10.1038/363
Schuett, S., Bonhoeffer, T., Hübener, M., 2001. Pairing-induced changes of orientation maps in cat visual cortex. Neuron 32, 325–337. doi:10.1016/S0896-6273(01)00472-X
Schulz, J.M., Redgrave, P., Reynolds, J.N.J., 2010. Cortico-striatal spike-timing dependent plasticity after activation of subcortical pathways. Front. Synaptic Neurosci. 2, 1–13. doi:10.3389/fnsyn.2010.00023
Sejnowski, T.J., 1999. The book of Hebb. Neuron 24, 773–776. doi:10.1016/S0896-6273(00)81025-9
Seol, G.H., Ziburkus, J., Huang, S., Song, L., Kim, I.T., Takamiya, K., Huganir, R.L., Lee, H.K., Kirkwood, A., 2007. Neuromodulators Control the Polarity of Spike-Timing-Dependent Synaptic Plasticity. Neuron 55, 919–929. doi:10.1016/j.neuron.2007.08.013
Shen, W., Flajolet, M., Greengard, P., Surmeier, D.J., 2008. Dichotomous dopaminergic control of striatal synaptic plasticity. Science 321, 848–51. doi:10.1126/science.1160575
Shin, R.M., Tsvetkov, E., Bolshakov, V.Y., 2006. Spatiotemporal Asymmetry of Associative Synaptic Plasticity in Fear Conditioning Pathways. Neuron 52, 883–896.

doi:10.1016/j.neuron.2006.10.010
Shouval, H.Z., Bear, M.F., Cooper, L.N., 2002. A unified model of NMDA receptor dependent bidirectional synaptic plasticity. Proc. Natl. Acad. Sci. USA 99, 10831–10836.
Shulz, D.E., Jacob, V., 2010. Spike-timing-dependent plasticity in the intact brain: Counteracting spurious spike coincidences. Front. Synaptic Neurosci. 2, 1–10. doi:10.3389/fnsyn.2010.00137
Sjöström, P.J., Häusser, M., 2006. A Cooperative Switch Determines the Sign of Synaptic Plasticity in Distal Dendrites of Neocortical Pyramidal Neurons. Neuron 51, 227–238. doi:10.1016/j.neuron.2006.06.017
Sjöström, P.J., Rancz, A., Roth, A., Häusser, M., 2010. Dendritic Excitability and Synaptic Plasticity. Physiol. Rev. 1–28. doi:10.1152/physrev.00016.2007.
Sjöström, P.J., Turrigiano, G.G., Nelson, S.B., 2004. Endocannabinoid-dependent neocortical layer-5 LTD in the absence of postsynaptic spiking. J. Neurophysiol. 92, 3338–3343. doi:10.1152/jn.00376.2004
Sjöström, P.J., Turrigiano, G.G., Nelson, S.B., 2001. Rate, timing, and cooperativity jointly determine cortical synaptic plasticity. Neuron 32, 1149–1164. doi:10.1016/S0896-6273(01)00542-6
Stent, G.S., 1973. A physiological mechanism for Hebb's postulate of learning. Proc. Natl. Acad. Sci. U. S. A. 70, 997–1001. doi:10.1073/pnas.70.4.997
Stuart, G.J., Häusser, M., 2001. Dendritic coincidence detection of EPSPs and action potentials. Nat. Neurosci. 4, 63–71. doi:10.1038/82910
Testa-Silva, G., Verhoog, M.B., Goriounova, N. a., Loebel, A., Hjorth, J.J.J., Baayen, J.C., de Kock, C.P.J., Mansvelder, H.D., 2010. Human synapses show a wide temporal window for spike-timing-dependent plasticity. Front. Synaptic Neurosci. 2, 1–11. doi:10.3389/fnsyn.2010.00012
Tzounopoulos, T., Kim, Y., Oertel, D., Trussell, L.O., 2004. Cell-specific, spike timing-dependent plasticities in the dorsal cochlear nucleus. Nat. Neurosci. 7, 719–725. doi:10.1038/nn1272
Tzounopoulos, T., Rubio, M.E., Keen, J.E., Trussell, L.O., 2007. Coactivation of Pre- and Postsynaptic Signaling Mechanisms Determines Cell-Specific Spike-Timing-Dependent Plasticity. Neuron 54, 291–301. doi:10.1016/j.neuron.2007.03.026
Verhoog, M.B., Goriounova, N. a, Obermayer, J., Stroeder, J., Hjorth, J.J.J., Testa-Silva, G., Baayen, J.C., de Kock, C.P.J., Meredith, R.M., Mansvelder, H.D., 2013. Mechanisms underlying the rules for associative plasticity at adult human neocortical synapses. J. Neurosci. 33, 17197–208. doi:10.1523/JNEUROSCI.3158-13.2013
Vogels, T.P., Froemke, R.C., Doyon, N., Gilson, M., Haas, J.S., Liu, R., Maffei, a, Miller, P., Wierenga, C.J., Woodin, M. a, Zenke, F., Sprekeler, H., 2013. Inhibitory synaptic plasticity: spike timing-dependence and putative network function. Front. Neural Circuits 7, 119. doi:10.3389/fncir.2013.00119
Wang, S.S., Denk, W., Häusser, M., 2000. Coincidence detection in single dendritic spines mediated by calcium release. Nat. Neurosci. 3, 1266–73. doi:10.1038/81792
Wittenberg, G.M., Wang, S.S.-H., 2006. Malleability of spike-timing-dependent plasticity at the CA3-CA1 synapse. J. Neurosci. 26, 6610–7. doi:10.1523/JNEUROSCI.5388-05.2006
Wolters, A., Sandbrink, F., Schlottmann, A., Kunesch, E., Stefan, K., Cohen, L.G., Benecke, R., Classen, J., Grimaldi, G., Argyropoulos, G.P., Bastian, A., Cortes, M., Davis, N.J., Edwards, D.J., Ferrucci, R., Fregni, F., Galea, J.M., Hamada, M., Miall, R.C., Morales-quezada, L., Pope, P.A., Priori, A., Rothwell, J., Tomlinson, P., Celnik, P., Hamada, M., Lazzaro, V. Di, Mazzone, P., Ziemann, U., Rothwell, J.C., Nitsche, M.A., 2003. A Temporally Asymmetric Hebbian Rule Governing Plasticity in the Human Motor Cortex A Temporally Asymmetric Hebbian Rule Governing Plasticity in the Human Motor Cortex. Neurophysiology 89, 2339–2345. doi:10.1152/jn.00900.2002
Wolters, A., Schmidt, A., Schramm, A., Zeller, D., Naumann, M., Kunesch, E., Benecke, R., Reiners, K., Classen, J., 2005. Timing-dependent plasticity in human primary somatosensory cortex. J. Physiol. 565, 1039–1052. doi:jphysiol.2005.084954

[pii]\r10.1113/jphysiol.2005.084954
Wu, C., Martel, D.T., Shore, S.E., 2015. Transcutaneous induction of stimulus-timing-dependent plasticity in dorsal cochlear nucleus. Front. Syst. Neurosci. 9, 116. doi:10.3389/fnsys.2015.00116
Xu, T.X., Yao, W.D., 2010. D1 and D2 dopamine receptors in separate circuits cooperate to drive associative long-term potentiation in the prefrontal cortex. Proc. Natl. Acad. Sci. U. S. A. 107, 16366–16371. doi:10.1073/pnas.1004108107
Yang, K., Dani, J.A., 2014. Dopamine D1 and D5 receptors modulate spike timing-dependent plasticity at medial perforant path to dentate granule cell synapses. J. Neurosci. 34, 15888–97. doi:10.1523/JNEUROSCI.2400-14.2014
Yao, H., Dan, Y., 2001. Stimulus timing-dependent plasticity in cortical processing of orientation. Neuron 32, 315–323. doi:10.1016/S0896-6273(01)00460-3
Yao, H., Shen, Y., Dan, Y., 2004. Plasticity in Visual Cortical Orientation Tuning 101.
Zhao, Y., Tzounopoulos, T., 2011. Physiological activation of cholinergic inputs controls associative synaptic plasticity via modulation of endocannabinoid signaling. J Neurosci 31, 3158–3168. doi:31/9/3158 [pii]\r10.1523/JNEUROSCI.5303-10.2011
Zilberter, M., Holmgren, C., Shemer, I., Silberberg, G., Grillner, S., Harkany, T., Zilberter, Y., 2009. Input specificity and dependence of spike timing-dependent plasticity on preceding postsynaptic activity at unitary connections between neocortical layer 2/3 pyramidal cells. Cereb. Cortex 19, 2308–2320. doi:10.1093/cercor/bhn247

Part III - STDP

Adams, S., Kesner, R.P., Ragozzino, M.E., 2001. Role of the medial and lateral caudate-putamen in mediating an auditory conditional response association. Neurobiol. Learn. Mem. 76, 106–116. doi:10.1006/nlme.2000.3989
Amemori, K.-I., Gibb, L.G., Graybiel, A.M., 2011. Shifting responsibly: the importance of striatal modularity to reinforcement learning in uncertain environments. Front. Hum. Neurosci. 5, 47. doi:10.3389/fnhum.2011.00047
Apicella, P., 2007. Leading tonically active neurons of the striatum from reward detection to context recognition. Trends Neurosci. 30, 299–306. doi:10.1016/j.tins.2007.03.011
Balleine, B.W., Delgado, M.R., Hikosaka, O., 2007. The role of the dorsal striatum in reward and decision-making. J. Neurosci. 27, 8161–8165. doi:10.1523/JNEUROSCI.1554-07.2007
Barnes, T.D., Kubota, Y., Hu, D., Jin, D.Z., Graybiel, A.M., 2005. Activity of striatal neurons reflects dynamic encoding and recoding of procedural memories. Nature 437, 1158–1161. doi:10.1038/nature04053
Barnes, T.D., Mao, J.-B., Hu, D., Kubota, Y., Dreyer, A. a, Stamoulis, C., Brown, E.N., Graybiel, A.M., 2011. Advance cueing produces enhanced action-boundary patterns of spike activity in the sensorimotor striatum. J. Neurophysiol. 105, 1861–1878. doi:10.1152/jn.00871.2010
Bennett, B.D., Callaway, J.C., Wilson, C.J., 2000. Intrinsic membrane properties underlying spontaneous tonic firing in neostriatal cholinergic interneurons. J. Neurosci. 20, 8493–8503. doi:20/22/8493 [pii]
Bergson, C., Mrzljak, L., Smiley, J.F., Pappy, M., Levenson, R., Goldman-Rakic, P.S., 1995. Regional, cellular, and subcellular variations in the distribution of D1 and D5 dopamine receptors in primate brain. J. Neurosci. 15, 7821–7836.
Bevan, M.D., Booth, P. a, Eaton, S. a, Bolam, J.P., 1998. Selective innervation of neostriatal interneurons by a subclass of neuron in the globus pallidus of the rat. J. Neurosci. 18, 9438–52.
Blackwell, K.T., Czubayko, U., Plenz, D., 2003. Quantitative estimate of synaptic inputs to striatal neurons during up and down states in vitro. J. Neurosci. 23, 9123–9132. doi:23/27/9123 [pii]
Burguière, E., Monteiro, P., Mallet, L., Feng, G., Graybiel, A.M., 2015. Striatal circuits, habits, and implications for obsessive-compulsive disorder. Curr. Opin. Neurobiol. 30, 59–65.

doi:10.1016/j.conb.2014.08.008
Calabresi, P., Centonze, D., Gubellini, P., Pisani, A., Bernardi, G., 2000. Acetylcholine-mediated modulation of striatal function. Trends Neurosci. 23, 120–126. doi:10.1016/S0166-2236(99)01501-5
Calabresi, P., Picconi, B., Tozzi, A., Ghiglieri, V., Di Filippo, M., 2014. Direct and indirect pathways of basal ganglia: a critical reappraisal. Nat. Neurosci. 17, 1022–1030. doi:10.1038/nn.3743
Carter, A.G., Sabatini, B.L., 2004. State-dependent calcium signaling in dendritic spines of striatal medium spiny neurons. Neuron 44, 483–93. doi:10.1016/j.neuron.2004.10.013
Centonze, D., Grande, C., Usiello, A., Gubellini, P., Erbs, E., Martin, A.B., Pisani, A., Tognazzi, N., Bernardi, G., Moratalla, R., Borrelli, E., Calabresi, P., 2003. Receptor subtypes involved in the presynaptic and postsynaptic actions of dopamine on striatal interneurons. J. Neurosci. 23, 6245–6254. doi:23/15/6245 [pii]
Charpier, S., Deniau, J.M., 1997. In vivo activity-dependent plasticity at cortico-striatal connections: evidence for physiological long-term potentiation. Proc. Natl. Acad. Sci. U. S. A. 94, 7036–40. doi:10.1073/pnas.94.13.7036
Crittenden, J.R., Graybiel, A.M., 2011. Basal Ganglia disorders associated with imbalances in the striatal striosome and matrix compartments. Front. Neuroanat. 5, 59. doi:10.3389/fnana.2011.00059
Czubayko, U., Plenz, D., 2002. Fast synaptic transmission between striatal spiny projection neurons. Proc. Natl. Acad. Sci. U. S. A. 99, 15764–15769. doi:10.1073/pnas.242428599
Dautan, D., Huerta-Ocampo, I., Witten, I.B., Deisseroth, K., Bolam, J.P., Gerdjikov, T., Mena-Segovia, J., 2014. A Major External Source of Cholinergic Innervation of the Striatum and Nucleus Accumbens Originates in the Brainstem. J. Neurosci. 34, 4509–4518. doi:10.1523/JNEUROSCI.5071-13.2014
Devan, B.D., White, N.M., 1999. Parallel information processing in the dorsal striatum: relation to hippocampal function. J. Neurosci. 19, 2789–2798.
Dias-Ferreira, E., Sousa, J.C., Melo, I., Morgado, P., Mesquita, A.R., Cerqueira, J.J., Costa, R.M., Sousa, N., 2009. Chronic stress causes frontostriatal reorganization and affects decision-making. Science (80-.). 325, 621–625.
Dickinson, A., 1985. Actions and Habits: The Development of Behavioural Autonomy. Philos. Trans. R. Soc. Lond. B. Biol. Sci. doi:10.1098/rstb.1985.0010
Ding, J.B., Guzman, J.N., Peterson, J.D., Goldberg, J.A., Surmeier, D.J., 2010. Thalamic gating of corticostriatal signaling by cholinergic interneurons. Neuron 67, 294–307. doi:10.1016/j.neuron.2010.06.017
Doyon, J., Benali, H., 2005. Reorganization and plasticity in the adult brain during learning of motor skills. Curr. Opin. Neurobiol. 15, 161–167. doi:10.1016/j.conb.2005.03.004
English, D.F., Ibanez-Sandoval, O., Stark, E., Tecuapetla, F., Buzsáki, G., Deisseroth, K., Tepper, J.M., Koos, T., 2012. GABAergic circuits mediate the reinforcement-related signals of striatal cholinergic interneurons. Nat. Neurosci. 15, 123–130. doi:10.1038/nn.2984
Everitt, B.J., Robbins, T.W., 2005. Neural systems of reinforcement for drug addiction: from actions to habits to compulsion. Nat. Neurosci. 8, 1481–9. doi:10.1038/nn1579
Faust, T.W., Assous, M., Shah, F., Tepper, J.M., Ko??s, T., 2015. Novel fast adapting interneurons mediate cholinergic-induced fast GABA<inf>A</inf> inhibitory postsynaptic currents in striatal spiny neurons. Eur. J. Neurosci. 42, 1764–1774. doi:10.1111/ejn.12915
Fino, E., Venance, L., 2011. Spike-timing dependent plasticity in striatal interneurons. Neuropharmacology 60, 780–788. doi:10.1016/j.neuropharm.2011.01.023
Friedman, A., Homma, D., Gibb, L.G., Amemori, K., Rubin, S.J., Hood, A.S., Riad, M.H., Graybiel, A.M., 2015. A Corticostriatal Path Targeting Striosomes Controls Decision-Making under Conflict. Cell 161, 1320–1333. doi:10.1016/j.cell.2015.04.049
Fujiyama, F., Nakano, T., Matsuda, W., Furuta, T., Udagawa, J., Kaneko, T., 2015. A single-neuron tracing study of arkypallidal and prototypic neurons in healthy rats. Brain Struct. Funct. 1–8.

doi:10.1007/s00429-015-1152-2
Fujiyama, F., Sohn, J., Nakano, T., Furuta, T., Nakamura, K.C., Matsuda, W., Kaneko, T., 2011. Exclusive and common targets of neostriatofugal projections of rat striosome neurons: A single neuron-tracing study using a viral vector. Eur. J. Neurosci. 33, 668–677. doi:10.1111/j.1460-9568.2010.07564.x
Gerfen, C.R., 1992. The neostriatal mosaic: multiple levels of compartmental organization. J. Neural Transm. Suppl. 36, 43–59. doi:10.1146/annurev.neuro.15.1.285
Gerfen, C.R., Surmeier, D.J., 2011. Modulation of striatal projection systems by dopamine. Annu. Rev. Neurosci. 34, 441–66. doi:10.1146/annurev-neuro-061010-113641
Gertler, T.S., Chan, C.S., Surmeier, D.J., 2008. Dichotomous Anatomical Properties of Adult Striatal Medium Spiny Neurons. J. Neurosci. 28, 10814–10824. doi:10.1523/JNEUROSCI.2660-08.2008
Gittis, a. H., Berke, J.D., Bevan, M.D., Chan, C.S., Mallet, N., Morrow, M.M., Schmidt, R., 2014. New Roles for the External Globus Pallidus in Basal Ganglia Circuits and Behavior. J. Neurosci. 34, 15178–15183. doi:10.1523/JNEUROSCI.3252-14.2014
Gittis, A.H., Nelson, A.B., Thwin, M.T., Palop, J.J., Kreitzer, A.C., 2010. Distinct roles of GABAergic interneurons in the regulation of striatal output pathways. J. Neurosci. 30, 2223–34. doi:10.1523/JNEUROSCI.4870-09.2010
Gold, P.E., 2004. Coordination of multiple memory systems. Neurobiol. Learn. Mem. 82, 230–242. doi:10.1016/j.nlm.2004.07.003
Gonzales, K.K., Pare, J.F., Wichmann, T., Smith, Y., 2013. GABAergic inputs from direct and indirect striatal projection neurons onto cholinergic interneurons in the primate putamen. J. Comp. Neurol. 521, 2502–2522. doi:10.1002/cne.23295
Graybiel, A.M., 2008. Habits, rituals, and the evaluative brain. Annu. Rev. Neurosci. 31, 359–387. doi:10.1146/annurev.neuro.29.051605.112851
Graybiel, A.M., 2005. The basal ganglia: Learning new tricks and loving it. Curr. Opin. Neurobiol. 15, 638–644. doi:10.1016/j.conb.2005.10.006
Graybiel, A.M., 1998. The basal ganglia and chunking of action repertoires. Neurobiol. Learn. Mem. 70, 119–136. doi:10.1006/nlme.1998.3843
Graybiel, A.M., Grafton, S.T., 2015. The striatum: where skills and habits meet. Cold Spring Harb. Perspect. Biol. 7, a021691. doi:10.1101/cshperspect.a021691
Graybiel, A.M., Ragsdale, C.W., 1978. Histochemically distinct compartments in the striatum of human, monkeys, and cat demonstrated by acetylthiocholinesterase staining. Proc. Natl. Acad. Sci. U. S. A. 75, 5723–6. doi:10.1073/pnas.75.11.5723
Graybiel, A.M., Rauch, S.L., 2000. Toward a Neurobiology 28, 343–347. doi:10.1016/S0896-6273(00)00113-6
Guzmán, J.N., Hernández, A., Galarraga, E., Tapia, D., Laville, A., Vergara, R., Aceves, J., Bargas, J., 2003. Dopaminergic modulation of axon collaterals interconnecting spiny neurons of the rat striatum. J. Neurosci. 23, 8931–8940. doi:23/26/8931 [pii]
Houk, J.C., Wise, S.P., 1995. Distributed modular architectures linking basal ganglia, cerebellum, and cerebral cortex their role in planning and controlling action.pdf 95–110.
Ibáñez-Sandoval, O., Tecuapetla, F., Unal, B., Shah, F., Koós, T., Tepper, J.M., 2011. A novel functionnally distinct subtype of striatal NPY interneuron. J. Neurosci. 31, 16757–16769. doi:10.1523/JNEUROSCI.2628-11.2011
Ibáñez-Sandoval, O., Xenias, H.S., Tepper, J.M., Koós, T., 2015. Dopaminergic and cholinergic modulation of striatal tyrosine hydroxylase interneurons. Neuropharmacology 95, 468–76. doi:10.1016/j.neuropharm.2015.03.036
Isoda, M., Hikosaka, O., 2007. Switching from automatic to controlled action by monkey medial frontal cortex. Nat. Neurosci. 10, 240–248. doi:10.1038/nn1830
Jin, X., Costa, R.M., 2010. Start/stop signals emerge in nigrostriatal circuits during sequence learning. Nature 466, 457–462. doi:10.1038/nature09263
Jog, M.S., Kubota, Y., Connolly, C.I., Hillegaart, V., Graybiel, a M., 1999. Building neural

representations of habits. Science 286, 1745–1749. doi:10.1126/science.286.5445.1745
Johnson, A., van der Meer, M.A., Redish, A.D., 2007. Integrating hippocampus and striatum in decision-making. Curr. Opin. Neurobiol. 17, 692–697. doi:10.1016/j.conb.2008.01.003
Kalivas, P.W., Volkow, N.D., 2005. The neural basis of addiction: A pathology of motivation and choice. Am. J. Psychiatry 162, 1403–1413. doi:10.1176/appi.ajp.162.8.1403
Kawaguchi, Y., 1993. Physiological, morphological, and histochemical characterization of three classes of interneurons in rat neostriatum. J. Neurosci. 13, 4908–4923. doi:10.1016/S0921-8696(05)81133-8
Kawaguchi, Y., Wilson, C.J., Augood, S.J., Emson, P.C., 1995. Striatal interneurones: chemical, physiological and morphological characterization. Trends Neurosci. 18, 527–535. doi:10.1016/0166-2236(95)98374-8
Kerr, J.N.D., 2004. Action Potential Timing Determines Dendritic Calcium during Striatal Up-States. J. Neurosci. 24, 877–885. doi:10.1523/JNEUROSCI.4475-03.2004
Kerr, J.N.D., Plenz, D., 2002. Dendritic calcium encodes striatal neuron output during up-states. J. Neurosci. 22, 1499–1512. doi:22/5/1499 [pii]
Koós, T., Tepper, J., 1999. Inhibitory control of neostriatal projection neurons by GABAergic interneurons. Nat. Neurosci. 19–24. doi:10.1038/8138
Koos, T., Tepper, J.M., 2002. Dual cholinergic control of fast-spiking interneurons in the neostriatum. J. Neurosci. 22, 529–535. doi:22/2/529 [pii]
Koos, T., Tepper, J.M., Wilson, C.J., 2004. Comparison of IPSCs evoked by spiny and fast-spiking neurons in the neostriatum. J. Neurosci. 24, 7916–22. doi:10.1523/JNEUROSCI.2163-04.2004
Kreitzer, A.C., 2009. Physiology and pharmacology of striatal neurons. Annu. Rev. Neurosci. 32, 127–47. doi:10.1146/annurev.neuro.051508.135422
Kubota, Y., Kawaguchi, Y., 2000. Dependence of GABAergic synaptic areas on the interneuron type and target size. J. Neurosci. 20, 375–386.
Lavoie, A.M., Mizumori, S.J.Y., 1994. Spatial, movement- and reward-sensitive discharge by medial ventral striatum neurons of rats. Brain Res. 638, 157–168. doi:10.1016/0006-8993(94)90645-9
Lerchner, A., La Camera, G., Richmond, B., 2007. Knowing without doing. Nat. Neurosci. 10, 15–17. doi:10.1038/nn0107-15
Lévesque, M., Parent, A., 2005. The striatofugal fiber system in primates: a reevaluation of its organization based on single-axon tracing studies. Proc. Natl. Acad. Sci. U. S. A. 102, 11888–93. doi:10.1073/pnas.0502710102
Mahon, S., 2000. Role of a Striatal Slowly Inactivating Potassium Current in Short-Term Facilitation of Corticostriatal Inputs: A Computer Simulation Study. Learn. Mem. 7, 357–362. doi:10.1101/lm.34800
Mahon, S., Deniau, J.-M., Charpier, S., 2001. Relationship between EEG Potentials and Intracellular Activity of Striatal and Cortico-striatal Neurons: an In Vivo Study under Different Anesthetics. Cereb. Cortex 11, 360–373. doi:10.1093/cercor/11.4.360
Mahon, S., Vautrelle, N., Pezard, L., Slaght, S.J., Deniau, J.M., Chouvet, G., Charpier, S., 2006. Distinct patterns of striatal medium spiny neuron activity during the natural sleep-wake cycle. J Neurosci 26, 12587–12595. doi:26/48/12587 [pii]\r10.1523/JNEUROSCI.3987-06.2006
Mallet, N., Micklem, B.R., Henny, P., Brown, M.T., Williams, C., Bolam, J.P., Nakamura, K.C., Magill, P.J., 2012. Dichotomous Organization of the External Globus Pallidus. Neuron 74, 1075–1086. doi:10.1016/j.neuron.2012.04.027
Mallet, N., Moine, C. Le, 2005. Feedforward Inhibition of Projection Neurons by Fast- Spiking GABA Interneurons in the Rat Striatum In Vivo 25, 3857–3869. doi:10.1523/JNEUROSCI.5027-04.2005
Mermelstein, P.G., Song, W.J., Tkatch, T., Yan, Z., Surmeier, D.J., 1998. Inwardly rectifying potassium (IRK) currents are correlated with IRK subunit expression in rat nucleus accumbens medium spiny neurons. J. Neurosci. 18, 6650–6661.
Morris, G., Arkadir, D., Nevet, A., Vaadia, E., Bergman, H., 2004. Coincident but distinct messages

of midbrain dopamine and striatal tonically active neurons. Neuron 43, 133–143. doi:10.1016/j.neuron.2004.06.012
Nisenbaum, E.S., Wilson, C.J., 1995. Potassium currents responsible for inward and outward rectification in rat neostriatal spiny projection neurons. J. Neurosci. 15, 4449–4463.
O'Doherty, J., Dayan, P., Schultz, J., Deichmann, R., Friston, K., Dolan, R.J., 2004. Dissociable roles of ventral and dorsal striatum in instrumental conditioning. Science 304, 452–4. doi:10.1126/science.1094285
Packard, M.G., McGaugh, J.L., 1996. Inactivation of hippocampus or caudate nucleus with lidocaine differentially affects expression of place and response learning. Neurobiol. Learn. Mem. 65, 65–72. doi:10.1006/nlme.1996.0007
Pennartz, C.M. a, Berke, J.D., Graybiel, A.M., Ito, R., Lansink, C.S., van der Meer, M., Redish, a D., Smith, K.S., Voorn, P., 2009. Corticostriatal Interactions during Learning, Memory Processing, and Decision Making. J. Neurosci. 29, 12831–12838. doi:10.1523/JNEUROSCI.3177-09.2009
Perez-Rosello, T., Figueroa, A., Salgado, H., Vilchis, C., Tecuapetla, F., Guzman, J.N., Galarraga, E., Bargas, J., Ga-, E., 2005. Cholinergic Control of Firing Pattern and Neurotransmission in Rat Neostriatal Projection Neurons : Role of Ca V 2 . 1 and Ca V 2 . 2 Ca 2 Channels. J. Neurophysiol. 2507–2519. doi:10.1152/jn.00853.2004.Besides
Pert, C.B., Kuhar, M.J., Snyder, S.H., 1976. Opiate receptor: autoradiographic localization in rat brain. Proc. Natl. Acad. Sci. U. S. A. 73, 3729–33. doi:10.1073/pnas.73.10.3729
Pidoux, M., Mahon, S., Deniau, J.-M., Charpier, S., 2011. Integration and propagation of somatosensory responses in the corticostriatal pathway: an intracellular study in vivo. J. Physiol. 589, 263–81. doi:10.1113/jphysiol.2010.199646
Planert, H., Berger, T.K., Silberberg, G., 2013. Membrane Properties of Striatal Direct and Indirect Pathway Neurons in Mouse and Rat Slices and Their Modulation by Dopamine. PLoS One 8, 1–14. doi:10.1371/journal.pone.0057054
Planert, H., Szydlowski, S.N., Hjorth, J.J.J., Grillner, S., Silberberg, G., 2010. Dynamics of synaptic transmission between fast-spiking interneurons and striatal projection neurons of the direct and indirect pathways. J. Neurosci. 30, 3499–3507. doi:10.1523/JNEUROSCI.5139-09.2010
Plenz, D., 2003. When inhibition goes incognito: Feedback interaction between spiny projection neurons in striatal function. Trends Neurosci. 26, 436–443. doi:10.1016/S0166-2236(03)00196-6
Plenz, D., Kitai, S.T., 1998. Up and down states in striatal medium spiny neurons simultaneously recorded with spontaneous activity in fast-spiking interneurons studied in cortex-striatum-substantia nigra organotypic cultures. J. Neurosci. 18, 266–283.
Plotkin, J.L., Day, M., Surmeier, D.J., 2011. Synaptically driven state transitions in distal dendrites of striatal spiny neurons. Nat. Neurosci. 14, 881–8. doi:10.1038/nn.2848
Poldrack, R.A., Sabb, F.W., Foerde, K., Tom, S.M., Asarnow, R.F., Bookheimer, S.Y., Knowlton, B.J., 2005. The Neural Correlates of Motor Skill Automaticity 25, 5356–5364. doi:10.1523/JNEUROSCI.3880-04.2005
Ragozzino, M.E., Jih, J., Tzavos, A., 2002. Involvement of the dorsomedial striatum in behavioral flexibility: Role of muscarinic cholinergic receptors. Brain Res. 953, 205–214. doi:10.1016/S0006-8993(02)03287-0
Ramanathan, S., Hanley, J.J., Deniau, J.-M., Bolam, J.P., 2002. Synaptic convergence of motor and somatosensory cortical afferents onto GABAergic interneurons in the rat striatum. J. Neurosci. 22, 8158–8169.
Rangel, A., Camerer, C., Montague, P.R., 2008. A framework for studying the neurobiology of value-based decision making. Nat. Rev. Neurosci. 9, 545–556. doi:10.1038/nrn2357
Reig, R., Silberberg, G., 2014. Multisensory Integration in the Mouse Striatum. Neuron 83, 1200–1212. doi:10.1016/j.neuron.2014.07.033
Rymar, V. V., Sasseville, R., Luk, K.C., Sadikot, A.F., 2004. Neurogenesis and Stereological Morphometry of Calretinin-Immunoreactive GABAergic Interneurons of the Neostriatum. J.

Comp. Neurol. 469, 325–339. doi:10.1002/cne.11008
Samejima, K., Doya, K., Ueda, Y., Kimura, M., 2005. Representation of action-specific reward values in the striatum. Science 310, 1337–40. doi:10.1126/science.1115270
Saunders, A., Huang, K.W., Sabatini, B.L., 2016. Globus Pallidus Externus Neurons Expressing parvalbumin Interconnect the Subthalamic Nucleus and Striatal Interneurons. PLoS One 11, 1–20. doi:10.1371/journal.pone.0149798
Schmitzer-Torbert, N., Redish, A.D., 2004. Neuronal activity in the rodent dorsal striatum in sequential navigation: separation of spatial and reward responses on the multiple T task. J. Neurophysiol. 91, 2259–72. doi:10.1152/jn.00687.2003
Smith, K.S., Graybiel, A.M., 2014. Investigating habits: strategies, technologies and models. Front. Behav. Neurosci. 8, 39. doi:10.3389/fnbeh.2014.00039
Soares, J.M., Sampaio, a, Ferreira, L.M., Santos, N.C., Marques, F., Palha, J. a, Cerqueira, J.J., Sousa, N., 2012. Stress-induced changes in human decision-making are reversible. Transl. Psychiatry 2, e131. doi:10.1038/tp.2012.59
Stern, E. a, Jaeger, D., Wilson, C.J., 1998. Membrane potential synchrony of simultaneously recorded striatal spiny neurons in vivo. Nature 394, 475–478. doi:10.1038/28848
Stern, E. a, Kincaid, a E., Wilson, C.J., 1997. Spontaneous subthreshold membrane potential fluctuations and action potential variability of rat corticostriatal and striatal neurons in vivo. J. Neurophysiol. 77, 1697–1715.
Surmeier, D.J., Yan, Z., Song, W.J., 1996. Coordinated Expression of Dopamine Receptors in Neostriatal Medium Spiny Neurons. Adv. Pharmacol. 42, 1020–1023. doi:10.1016/S1054-3589(08)60921-7
Szydlowski, S.N., Pollak Dorocic, I., Planert, H., Carlen, M., Meletis, K., Silberberg, G., 2013. Target Selectivity of Feedforward Inhibition by Striatal Fast-Spiking Interneurons. J. Neurosci. 33, 1678–1683. doi:10.1523/JNEUROSCI.3572-12.2013
Tang, C.C., Root, D.H., Duke, D.C., Zhu, Y., Teixeria, K., Ma, S., Barker, D.J., West, M.O., 2009. Decreased firing of striatal neurons related to licking during acquisition and overtraining of a licking task. J. Neurosci. 29, 13952–61. doi:10.1523/JNEUROSCI.2824-09.2009
Taverna, S., Canciani, B., Pennartz, C.M.A., 2007. Membrane properties and synaptic connectivity of fast-spiking interneurons in rat ventral striatum. Brain Res. 1152, 49–56. doi:10.1016/j.brainres.2007.03.053
Taverna, S., Dongen, Y., Groenewegen, H., Pennartz, C., 2004. Direct Physiological Evidence for Synaptic Connectivity Between Medium-Sized Spiny Neurons in Rat Nucleus Accumbens In Situ. J. Neurophysiol. 91, 1111–1121. doi:10.1152/jn.00892.2003
Tecuapetla, F., Koos, T., Tepper, J.M., Kabbani, N., Yeckel, M.F., 2009. Differential Dopaminergic Modulation of Neostriatal Synaptic Connections of Striatopallidal Axon Collaterals. J. Neurosci. 29, 8977–8990. doi:10.1523/JNEUROSCI.6145-08.2009
Tepper, J.M., Bolam, J.P., 2004. Functional diversity and specificity of neostriatal interneurons. Curr. Opin. Neurobiol. 14, 685–692. doi:10.1016/j.conb.2004.10.003
Tepper, J.M., Ko??s, T., Wilson, C.J., 2004. GABAergic microcircuits in the neostriatum. Trends Neurosci. 27, 662–669. doi:10.1016/j.tins.2004.08.007
Tepper, J.M., Tecuapetla, F., Koós, T., Ibáñez-Sandoval, O., 2010. Heterogeneity and diversity of striatal GABAergic interneurons. Front. Neuroanat. 4, 150. doi:10.3389/fnana.2010.00150
Tepper, J.M., Wilson, C.J., Ko??s, T., 2008. Feedforward and feedback inhibition in neostriatal GABAergic spiny neurons. Brain Res. Rev. 58, 272–281. doi:10.1016/j.brainresrev.2007.10.008
Thorn, C. a., Atallah, H., Howe, M., Graybiel, A.M., 2010. Differential Dynamics of Activity Changes in Dorsolateral and Dorsomedial Striatal Loops during Learning. Neuron 66, 781–795. doi:10.1016/j.neuron.2010.04.036
Tritsch, N.X., Granger, A.J., Sabatini, B.L., 2016. Mechanisms and functions of GABA co‐release. Nat. Publ. Gr. 17, 139–145. doi:10.1038/nrn.2015.21
Tritsch, N.X., Oh, W.J., Gu, C., Sabatini, B.L., 2014. Midbrain dopamine neurons sustain inhibitory

transmission using plasma membrane uptake of GABA, not synthesis. Elife 3, e01936. doi:10.7554/eLife.01936
Tritsch, N.X., Sabatini, B.L., 2012. Dopaminergic Modulation of Synaptic Transmission in Cortex and Striatum. Neuron 76, 33–50. doi:10.1016/j.neuron.2012.09.023
Tunstall, M.J., Oorschot, D.E., Kean, A., Wickens, J.R., 2002. Inhibitory Interactions Between Spiny Projection Neurons in the Rat Striatum. J. Neurophysiol. 88, 1263–9. doi:12205147
Unal, B., Ibáñez-Sandoval, O., Shah, F., Abercrombie, E.D., Tepper, J.M., 2011. Distribution of tyrosine hydroxylase-expressing interneurons with respect to anatomical organization of the neostriatum. Front. Syst. Neurosci. 5, 41. doi:10.3389/fnsys.2011.00041
Valjent, E., Bertran-Gonzalez, J., Hervé, D., Fisone, G., Girault, J.A., 2009. Looking BAC at striatal signaling: cell-specific analysis in new transgenic mice. Trends Neurosci. 32, 538–547. doi:10.1016/j.tins.2009.06.005
Venance, L., Glowinski, J., Giaume, C., 2004. Electrical and chemical transmission between striatal GABAergic output neurones in rat brain slices. J. Physiol. 559, 215–230. doi:10.1113/jphysiol.2004.065672
Voorn, P., Vanderschuren, L.J.M.J., Groenewegen, H.J., Robbins, T.W., Pennartz, C.M.A., 2004. Putting a spin on the dorsal-ventral divide of the striatum. Trends Neurosci. 27, 468–474. doi:10.1016/j.tins.2004.06.006
West, A.R., 2004. The Nitric Oxide-Guanylyl Cyclase Signaling Pathway Modulates Membrane Activity States and Electrophysiological Properties of Striatal Medium Spiny Neurons Recorded In Vivo. J. Neurosci. 24, 1924–1935. doi:10.1523/JNEUROSCI.4470-03.2004
Wickens, J.R., Wilson, C.J., 1998. Regulation of action-potential firing in spiny neurons of the rat neostriatum in vivo. J. Neurophysiol. 79, 2358–2364.
Wilson, C., Kawaguchi, Y., 1996. The Origins of Two-State Spontaneous Membrane Fluctuations of Neostriatal Spiny Neurons 16, 2397–2410.
Wilson, C.J., 2007. GABAergic inhibition in the neostriatum. Prog. Brain Res. 160, 91–110. doi:10.1016/S0079-6123(06)60006-X
Wilson, C.J., Groves, P.M., 1981. Spontaneous firing patterns of identified spiny neurons in the rat neostriatum. Brain Res. 220, 67–80.
Xenias, H.S., Ibanez-Sandoval, O., Koos, T., Tepper, J.M., 2015. Are Striatal Tyrosine Hydroxylase Interneurons Dopaminergic? J. Neurosci. 35, 6584–6599. doi:10.1523/JNEUROSCI.0195-15.2015
Yan, Z., Song, W.-J., Surmeier, D.J., 1997. D2 dopamine receptors reduce N-type Ca2+ currents in rat neostriatal cholinergic interneurons through a membrane-delimited, protein-kinase-C-insensitive pathway. J. Neurophysiol. 77, 1003–1015.
Yan, Z., Surmeier, D.J., 1997. D5 dopamine receptors enhance Zn2+-sensitive GABA(A) currents in striatal cholinergic interneurons through a PKA/PP1 cascade. Neuron 19, 1115–1126. doi:S0896-6273(00)80402-X [pii]
Yin, H.H., Knowlton, B.B.J., 2006. The role of the basal ganglia in habit formation. Nat. Rev. Neurosci. 7, 464–76. doi:10.1038/nrn1919
Yin, H.H., Knowlton, B.J., 2004. Contributions of Striatal Subregions to Place and Response Learning. Learn. Mem. 11, 459–463. doi:10.1101/lm.81004
Yin, H.H., Knowlton, B.J., Balleine, B.W., 2005a. Blockade of NMDA receptors in the dorsomedial striatum prevents action-outcome learning in instrumental conditioning. Eur. J. Neurosci. 22, 505–512. doi:10.1111/j.1460-9568.2005.04219.x
Yin, H.H., Knowlton, B.J., Balleine, B.W., 2004. Lesions of dorsolateral striatum preserve outcome expectancy but disrupt habit formation in instrumental learning. Eur. J. Neurosci. 19, 181–189. doi:10.1111/j.1460-9568.2004.03095.x
Yin, H.H., Ostlund, S.B., Balleine, B.W., 2008. Reward-guided learning beyond dopamine in the nucleus accumbens: The integrative functions of cortico-basal ganglia networks. Eur. J. Neurosci. 28, 1437–1448. doi:10.1111/j.1460-9568.2008.06422.x
Yin, H.H., Ostlund, S.B., Knowlton, B.J., Balleine, B.W., 2005b. The role of the dorsomedial

striatum in instrumental conditioning. Eur. J. Neurosci. 22, 513–523. doi:10.1111/j.1460-9568.2005.04218.x

Methods

Arriza, J.L. et al., 1994. Functional Comparisons of Three Glutamate Cloned from Human Motor Cortex Transporter. , 14(September), pp.5559–5569.

Cui, Y. et al., 2016. Endocannabinoid dynamics gate spike- timing dependent depression and potentiation. *eLife*, 5(FEBRUARY2016), pp.1–32.

Cui, Y. et al., 2015. Endocannabinoids mediate bidirectional striatal spike-timing-dependent plasticity. *J Physiol*, 593(13), pp.2833–2849. Available at: http://www.ncbi.nlm.nih.gov/pubmed/25873197.

Dehorter, N. et al., 2009. Dopamine-deprived striatal GABAergic interneurons burst and generate repetitive gigantic IPSCs in medium spiny neurons. *The Journal of neuroscience : the official journal of the Society for Neuroscience*, 29(24), pp.7776–7787.

Fino, E., Glowinski, J. & Venance, L., 2005. Bidirectional activity-dependent plasticity at corticostriatal synapses. *The Journal of neuroscience : the official journal of the Society for Neuroscience*, 25(49), pp.11279–11287.

Fino, E., Glowinski, J. & Venance, L., 2007. Effects of acute dopamine depletion on the electrophysiological properties of striatal neurons. *Neuroscience Research*, 58(3), pp.305–316.

Fino, E. & Venance, L., 2011. Spike-timing dependent plasticity in striatal interneurons. *Neuropharmacology*, 60(5), pp.780–788. Available at: http://dx.doi.org/10.1016/j.neuropharm.2011.01.023.

Goubard, V., Fino, E. & Venance, L., 2011. Contribution of astrocytic glutamate and GABA uptake to corticostriatal information processing. *The Journal of physiology*, 589(Pt 9), pp.2301–19. Available at: http://www.pubmedcentral.nih.gov/articlerender.fcgi?artid=3098705&tool=pmcentrez&rendertype=abstract [Accessed October 14, 2014].

Lipton, S. a, 2006. Paradigm shift in neuroprotection by NMDA receptor blockade: memantine and beyond. *Nature reviews. Drug discovery*, 5(2), pp.160–70. Available at: http://www.ncbi.nlm.nih.gov/pubmed/16424917 [Accessed July 14, 2014].

Paillé, V. et al., 2013. GABAergic circuits control spike-timing-dependent plasticity. *The Journal of neuroscience : the official journal of the Society for Neuroscience*, 33(22), pp.9353–63. Available at: http://www.ncbi.nlm.nih.gov/pubmed/23719804 [Accessed November 2, 2014].

Xia, P. et al., 2010. Memantine Preferentially Blocks Extrasynaptic over Synaptic NMDA Receptor Currents in Hippocampal Autapses. , 30(33), pp.11246–11250.

General discussion

Aida, T. et al., 2015. Astroglial Glutamate Transporter Deficiency Increases Synaptic Excitability and Leads to Pathological Repetitive Behaviors in Mice. *Neuropsychopharmacology*, 1, pp.1–11. Available at: http://www.nature.com/doifinder/10.1038/npp.2015.26.

Almeida, R.F. et al., 2010. Effects of depressive-like behavior of rats on brain glutamate uptake. *Neurochemical Research*, 35(8), pp.1164–1171. Available at: http://www.ncbi.nlm.nih.gov/pubmed/20405205.

Arriza, J.L. et al., 1994. Functional Comparisons of Three Glutamate Cloned from Human Motor Cortex Transporter. , 14(September), pp.5559–5569.

Bell, C.C. et al., 1997. Synaptic plasticity in a cerebellum-like structure depends on temporal order. *Nature*, 387(6630), pp.278–281.

Bernard, R. et al., 2011. Altered expression of glutamate signaling, growth factor, and glia genes in the locus coeruleus of patients with major depression. *Molecular psychiatry*, 16(6), pp.634–646. Available at: http://dx.doi.org/10.1038/mp.2010.44.

Bernardinelli, Y. et al., 2014. Astrocyte-Synapse Structural Plasticity. *Neural Plasticity*, 2014, pp.1–13. Available at: http://www.hindawi.com/journals/np/2014/232105/.

Boudaba, C. et al., 2003. Increased tonic activation of presynaptic metabotropic glutamate receptors in the rat supraoptic nucleus following chronic dehydration. *The Journal of physiology*, 551(Pt 3), pp.815–23.

Available at: http://www.pubmedcentral.nih.gov/articlerender.fcgi?artid=2343287&tool=pmcentrez&rendertype=abstract.
Chesselet, M.F. et al., 2007. Development of striatal fast-spiking GABAergic interneurons. *Progress in Brain Research*, 160, pp.261–272.
Choudary, P. V et al., 2005. Altered cortical glutamatergic and GABAergic signal transmission with glial involvement in depression. *Proceedings of the National Academy of Sciences of the United States of America*, 102(43), pp.15653–15658.
Clopath, C. et al., 2010. Connectivity reflects coding: a model of voltage-based STDP with homeostasis. *Nature neuroscience*, 13(3), pp.344–52. Available at: http://www.ncbi.nlm.nih.gov/pubmed/20098420 [Accessed March 20, 2014].
Conti, F., Minelli, A. & Melone, M., 2004. GABA transporters in the mammalian cerebral cortex: Localization, development and pathological implications. *Brain Research Reviews*, 45(3), pp.196–212.
Costa, R.P. et al., 2015. Unified pre- and postsynaptic long-term plasticity enables reliable and flexible learning. , (August).
Cui, W. et al., 2014. Glial Dysfunction in the Mouse Habenula Causes Depressive-Like Behaviors and Sleep Disturbance. *Journal of Neuroscience*, 34(49), pp.16273–16285. Available at: http://www.jneurosci.org/cgi/doi/10.1523/JNEUROSCI.1465-14.2014 [Accessed December 3, 2014].
Cui, Y. et al., 2016. Endocannabinoid dynamics gate spike- timing dependent depression and potentiation. *eLife*, 5(FEBRUARY2016), pp.1–32.
Cui, Y. et al., 2015. Endocannabinoids mediate bidirectional striatal spike-timing-dependent plasticity. *J Physiol*, 593(13), pp.2833–2849. Available at: http://www.ncbi.nlm.nih.gov/pubmed/25873197.
Danbolt, N.C., Furness, D.N. & Zhou, Y., 2016. Neuronal vs glial glutamate uptake: Resolving the conundrum. *Neurochemistry International*. Available at: http://linkinghub.elsevier.com/retrieve/pii/S0197018616301085.
Dias-Ferreira, E. et al., 2009. Chronic stress causes frontostriatal reorganization and affects decision-making. *Science*, 325(July), pp.621–625.
Dunlop, J. et al., 2005. Characterization of Novel Aryl-Ether, Biaryl, and Fluorene Aspartic Acid and Diaminopropionic Acid Analogs as Potent Inhibitors of the High-Affinity Glutamate Transporter EAAT2. *Molecular Pharmacology*, 68(4), pp.974–982. Available at: http://molpharm.aspetjournals.org/cgi/doi/10.1124/mol.105.012005.
Feldman, D.E., 2012. The spike-timing dependence of plasticity. *Neuron*, 75(4), pp.556–71. Available at: http://www.pubmedcentral.nih.gov/articlerender.fcgi?artid=3431193&tool=pmcentrez&rendertype=abstract [Accessed July 11, 2014].
Fino, E. et al., 2009. Asymmetric spike-timing dependent plasticity of striatal nitric oxide-synthase interneurons. *Neuroscience*, 160(4), pp.744–754. Available at: http://dx.doi.org/10.1016/j.neuroscience.2009.03.015.
Fino, E. et al., 2010. Distinct coincidence detectors govern the corticostriatal spike timing-dependent plasticity. *The Journal of physiology*, 588(Pt 16), pp.3045–62. Available at: http://www.jphysiol.org/cgi/doi/10.1113/jphysiol.2010.188466\nhttp://www.pubmedcentral.nih.gov/articlerender.fcgi?artid=2956944&tool=pmcentrez&rendertype=abstract.
Fino, E., Deniau, J.-M. & Venance, L., 2008. Cell-specific spike-timing-dependent plasticity in GABAergic and cholinergic interneurons in corticostriatal rat brain slices. *The Journal of physiology*, 586(1), pp.265–282.
Fino, E., Glowinski, J. & Venance, L., 2005. Bidirectional activity-dependent plasticity at corticostriatal synapses. *The Journal of neuroscience : the official journal of the Society for Neuroscience*, 25(49), pp.11279–11287.
Fontana, A.C.K., 2015. Current approaches to enhance glutamate transporter function and expression. *Journal of Neurochemistry*, p.n/a–n/a. Available at: http://doi.wiley.com/10.1111/jnc.13200.
Furness, D.N. et al., 2008. A quantitative assessment of glutamate uptake into hippocampal synaptic terminals and astrocytes: new insights into a neuronal role for excitatory amino acid transporter 2 (EAAT2). *Neuroscience*, 157(1), pp.80–94. Available at: http://www.pubmedcentral.nih.gov/articlerender.fcgi?artid=2775085&tool=pmcentrez&rendertype=abstract [Accessed October 29, 2014].
Furuta, A., Rothstein, J.D. & Martin, L.J., 1997. Glutamate Transporter Protein Subtypes Are Expressed Differentially during Rat CNS Development. , 17(21), pp.8363–8375.
Genoud, C. et al., 2006. Plasticity of astrocytic coverage and glutamate transporter expression in adult mouse

cortex. *PLoS Biology*, 4(11), pp.2057–2064.
Glykys, J. & Mody, I., 2007a. Activation of GABAA Receptors: Views from Outside the Synaptic Cleft. *Neuron*, 56(5), pp.763–770.
Glykys, J. & Mody, I., 2007b. The main source of ambient GABA responsible for tonic inhibition in the mouse hippocampus. *The Journal of Physiology*, 582(Pt 3), pp.1163–1178. Available at: http://www.ncbi.nlm.nih.gov/pmc/articles/PMC2075237/.
Goubard, V., Fino, E. & Venance, L., 2011. Contribution of astrocytic glutamate and GABA uptake to corticostriatal information processing. *The Journal of physiology*, 589(Pt 9), pp.2301–19. Available at: http://www.pubmedcentral.nih.gov/articlerender.fcgi?artid=3098705&tool=pmcentrez&rendertype=abstract [Accessed October 14, 2014].
Groen, M.R. et al., 2014. Development of dendritic tonic GABAergic inhibition regulates excitability and plasticity in CA1 pyramidal neurons. *Journal of neurophysiology*, 112(2), pp.287–99. Available at: http://www.pubmedcentral.nih.gov/articlerender.fcgi?artid=4064406&tool=pmcentrez&rendertype=abstract.
Hanson, E. et al., 2015. Astrocytic glutamate uptake is slow and does not limit neuronal NMDA receptor activation in the neonatal neocortex. *Glia*, p.n/a–n/a. Available at: http://doi.wiley.com/10.1002/glia.22844.
Hashimoto, K., 2009. Emerging role of glutamate in the pathophysiology of major depressive disorder. *Brain Research Reviews*, 61(2), pp.105–123. Available at: http://dx.doi.org/10.1016/j.brainresrev.2009.05.005.
Hill, M.N. et al., 2012. Neurobiology of chronic mild stress: Parallels to major depression. *Neuroscience and Biobehavioral Reviews*, 36(9), pp.2085–2117. Available at: http://dx.doi.org/10.1016/j.neubiorev.2012.07.001.
Hollon, N.G., Burgeno, L.M. & Phillips, P.E.M., 2015. Stress effects on the neural substrates of motivated behavior. *Nature Neuroscience*, 18(10), pp.1405–1412.
Holmseth, S. et al., 2012. The Density of EAAC1 (EAAT3) Glutamate Transporters Expressed by Neurons in the Mammalian CNS. *Journal of Neuroscience*, 32(17), pp.6000–6013.
Itami, C. et al., 2016. Developmental Switch in Spike Timing-Dependent Plasticity and Cannabinoid-Dependent Reorganization of the Thalamocortical Projection in the Barrel Cortex. *Journal of Neuroscience*, 36(26), pp.7039–7054. Available at: http://www.jneurosci.org/cgi/doi/10.1523/JNEUROSCI.4280-15.2016.
Itami, C. & Kimura, F., 2012. Developmental Switch in Spike Timing-Dependent Plasticity at Layers 4-2/3 in the Rodent Barrel Cortex. *Journal of Neuroscience*, 32(43), pp.15000–15011.
John, C.S. et al., 2012. Blockade of astrocytic glutamate uptake in the prefrontal cortex induces anhedonia. *Neuropsychopharmacology*, 37(11), pp.2467–75. Available at: http://www.ncbi.nlm.nih.gov/pubmed/22739467\nhttp://www.pubmedcentral.nih.gov/articlerender.fcgi?artid=PMC3442341.
Katagiri, H., Tanaka, K. & Manabe, T., 2001. Requirement of appropriate glutamate concentrations in the synaptic cleft for hippocampal LTP induction. *Eur J Neurosci*, 14, pp.547–553.
Lee, S. et al., 2010. Channel-Mediated Tonic GABA Release from Glia. *Science*, 330(6005), pp.790–796. Available at: http://www.sciencemag.org/cgi/doi/10.1126/science.1184334.
Lee, Y. et al., 2007. Glia mechanisms in mood regulation: A novel model of mood disorders. *Psychopharmacology*, 191(1), pp.55–65.
Lehre, K.P. & Danbolt, N.C., 1998. The number of glutamate transporter subtype molecules at glutamatergic synapses: chemical and stereological quantification in young adult rat brain. *The Journal of neuroscience : the official journal of the Society for Neuroscience*, 18(21), pp.8751–8757.
Lewerenz, J. et al., 2013. The cystine/glutamate antiporter system x(c)(-) in health and disease: from molecular mechanisms to novel therapeutic opportunities. *Antioxidants & redox signaling*, 18(5), pp.522–55. Available at: http://www.scopus.com/inward/record.url?eid=2-s2.0-84872191631&partnerID=tZOtx3y1.
Li, J. & Baccei, M.L., 2016. Neonatal Tissue Damage Promotes Spike Timing-Dependent Synaptic Long-Term Potentiation in Adult Spinal Projection Neurons. *Journal of Neuroscience*, 36(19), pp.5405–5416. Available at: http://www.jneurosci.org/cgi/doi/10.1523/JNEUROSCI.3547-15.2016.
Massey, P. V et al., 2004. Differential roles of NR2A and NR2B-containing NMDA receptors in cortical long-term potentiation and long-term depression. *The Journal of neuroscience : the official journal of the Society for Neuroscience*, 24(36), pp.7821–8. Available at: http://www.ncbi.nlm.nih.gov/pubmed/15356193 [Accessed April 2, 2014].

Matute, C. et al., 2005. Increased expression of the astrocytic glutamate transporter GLT-1 in the prefrontal cortex of schizophrenics. *Glia*, 49(3), pp.451–455. Available at: http://doi.wiley.com/10.1002/glia.20119.

Mcewen, B.S. et al., 2015. review Mechanisms of stress in the brain. *Nature Neuroscience*, 18(10).

Mineur, Y.S., Picciotto, M.R. & Sanacora, G., 2007. Antidepressant-Like Effects of Ceftriaxone in Male C57BL/6J Mice. *Biological Psychiatry*, 61(2), pp.250–252.

Moussawi, K. et al., 2009. N-Acetylcysteine reverses cocaine-induced metaplasticity. , 12(2), p.2250.

Oliet, S.H., Piet, R. & Poulain, D. a, 2001. Control of glutamate clearance and synaptic efficacy by glial coverage of neurons. *Science (New York, N.Y.)*, 292(5518), pp.923–6. Available at: http://www.ncbi.nlm.nih.gov/pubmed/11340204 [Accessed August 1, 2014].

Olivenza, R. et al., 2000. Chronic Stress Induces the Expression of Inducible Nitric Oxide Synthase in Rat Brain Cortex. *Journal of Neurochemistry*, 74(2), pp.785–791. Available at: http://doi.wiley.com/10.1046/j.1471-4159.2000.740785.x.

Omrani, A. et al., 2009. Up-regulation of GLT-1 severely impairs LTD at mossy fibre--CA3 synapses. *The Journal of physiology*, 587(Pt 19), pp.4575–88. Available at: http://www.pubmedcentral.nih.gov/articlerender.fcgi?artid=2768014&tool=pmcentrez&rendertype=abstract [Accessed May 8, 2014].

Paillé, V. et al., 2013. GABAergic circuits control spike-timing-dependent plasticity. *The Journal of neuroscience : the official journal of the Society for Neuroscience*, 33(22), pp.9353–63. Available at: http://www.ncbi.nlm.nih.gov/pubmed/23719804 [Accessed November 2, 2014].

Pereira, A.C. et al., 2014. Glutamatergic regulation prevents hippocampal-dependent age-related cognitive decline through dendritic spine clustering. *Proceedings of the National Academy of Sciences of the United States of America*, 111(52), pp.18733–18738. Available at: http://www.ncbi.nlm.nih.gov/pubmed/25512503 [Accessed December 18, 2014].

Petr, G.T. et al., 2015. Conditional Deletion of the Glutamate Transporter GLT-1 Reveals That Astrocytic GLT-1 Protects against Fatal Epilepsy While Neuronal GLT-1 Contributes Significantly to Glutamate Uptake into Synaptosomes. *Journal of Neuroscience*, 35(13), pp.5187–5201.

Pinard, A. et al., 2003. Glutamatergic modulation of synaptic plasticity at a PNS vertebrate cholinergic synapse. *Eur J Neurosci*, 18(April).

Popoli, M. et al., 2012. The stressed synapse: the impact of stress and glucocorticoids on glutamate transmission. *Nature reviews. Neuroscience*, 13(1), pp.22–37. Available at: http://www.pubmedcentral.nih.gov/articlerender.fcgi?artid=3645314&tool=pmcentrez&rendertype=abstract [Accessed July 15, 2014].

Potier, B. et al., 2010. Reduction in glutamate uptake is associated with extrasynaptic NMDA and metabotropic glutamate receptor activation at the hippocampal CA1 synapse of aged rat. *Aging Cell*, 33(May), pp.722–735.

Reagan, L.P. et al., 2004. Chronic restraint stress up-regulates GLT-1 mRNA and protein expression in the rat hippocampus : Reversal by tianeptine. *PNAS*, 101(7), pp.2179–2184.

Scimemi, A., Tian, H. & Diamond, J.S., 2009. Neuronal transporters regulate glutamate clearance, NMDA receptor activation, and synaptic plasticity in the hippocampus. *The Journal of neuroscience : the official journal of the Society for Neuroscience*, 29(46), pp.14581–95. Available at: http://www.pubmedcentral.nih.gov/articlerender.fcgi?artid=2853250&tool=pmcentrez&rendertype=abstract [Accessed March 26, 2014].

Scofield, M.D. & Kalivas, P.W., 2014. Astrocytic Dysfunction and Addiction: Consequences of Impaired Glutamate Homeostasis. *The Neuroscientist : a review journal bringing neurobiology, neurology and psychiatry*, 20(6), pp.610–622. Available at: http://www.ncbi.nlm.nih.gov/pubmed/24496610 [Accessed December 27, 2014].

Shin, R.M., Tsvetkov, E. & Bolshakov, V.Y., 2006. Spatiotemporal Asymmetry of Associative Synaptic Plasticity in Fear Conditioning Pathways. *Neuron*, 52(5), pp.883–896.

Soares, J.M. et al., 2012. Stress-induced changes in human decision-making are reversible. *Translational Psychiatry*, 2(7), p.e131. Available at: http://dx.doi.org/10.1038/tp.2012.59.

Soni, N., Reddy, B.V.K. & Kumar, P., 2014. GLT-1 Transporter: An Effective Pharmacological Target for Various Neurological Disorders. *Pharmacology, biochemistry, and behavior*, pp.1–11. Available at: http://www.ncbi.nlm.nih.gov/pubmed/25312503 [Accessed November 9, 2014].

Tanaka, K. et al., 2008. Epilepsy and Exacerbation of Brain Injury in Mice Lacking the Glutamate Transporter GLT-1 Epilepsy and Exacerbation of Brain Injury in Mice Lacking the Glutamate Transporter GLT-1. , 1699(1997), pp.1699–1703.

Tsvetkov, E., Shin, R.M. & Bolshakov, V.Y., 2004. Glutamate Uptake Determines Pathway Specificity of Long-Term Potentiation in the Neural Circuitry of Fear Conditioning. *Neuron*, 41(1), pp.139–151.

Tzingounis, A. V & Wadiche, J.I., 2007. Glutamate transporters : confining runaway excitation by shaping synaptic transmission. *Nat Neurosci Rev*, 8(december).

Tzounopoulos, T. et al., 2004. Cell-specific, spike timing-dependent plasticities in the dorsal cochlear nucleus. *Nature neuroscience*, 7(7), pp.719–725.

Tzounopoulos, T. et al., 2007. Coactivation of Pre- and Postsynaptic Signaling Mechanisms Determines Cell-Specific Spike-Timing-Dependent Plasticity. *Neuron*, 54(2), pp.291–301.

Ullensvang, K. et al., 1997. Differential developmental expression of the two rat brain glutamate transporter proteins GLAST and GLT. *European Journal of Neuroscience*, 9(8), pp.1646–1655.

de Vasconcellos-Bittencourt, A.P.S. et al., 2011. Chronic stress and lithium treatments alter hippocampal glutamate uptake and release in the rat and potentiate necrotic cellular death after oxygen and glucose deprivation. *Neurochemical research*, 36(5), pp.793–800. Available at: http://www.ncbi.nlm.nih.gov/pubmed/21253855.

Wang, Z.-Y., Zhang, Y.-Q. & Zhao, Z.-Q., 2006. Inhibition of tetanically sciatic stimulation-induced LTP of spinal neurons and Fos expression by disrupting glutamate transporter GLT-1. *Neuropharmacology*, 51(4), pp.764–72. Available at: http://www.ncbi.nlm.nih.gov/pubmed/16815482 [Accessed January 10, 2015].

Yang, C.-H., Huang, C.-C. & Hsu, K.-S., 2005. Behavioral stress enhances hippocampal CA1 long-term depression through the blockade of the glutamate uptake. *The Journal of Neuroscience*, 25(17), pp.4288–93. Available at: http://www.ncbi.nlm.nih.gov/pubmed/15858055 [Accessed July 11, 2014].

Zhang, H. & Sulzer, D., 2003. Glutamate spillover in the striatum depresses dopaminergic transmission by activating group I metabotropic glutamate receptors. *The Journal of neuroscience : the official journal of the Society for Neuroscience*, 23(33), pp.10585–92. Available at: http://www.ncbi.nlm.nih.gov/pubmed/14627643.

Zhou, Y. et al., 2014. EAAT2 (GLT-1; slc1a2) Glutamate Transporters Reconstituted in Liposomes Argues against Heteroexchange Being Substantially Faster than Net Uptake. *The Journal of neuroscience : the official journal of the Society for Neuroscience*, 34(40), pp.13472–85. Available at: http://www.ncbi.nlm.nih.gov/pubmed/25274824 [Accessed November 10, 2014].

Zink, M. et al., 2010. Reduced expression of glutamate transporters vGluT1, EAAT2 and EAAT4 in learned helpless rats, an animal model of depression. *Neuropharmacology*, 58(2), pp.465–73. Available at: http://www.ncbi.nlm.nih.gov/pubmed/19747495 [Accessed December 23, 2014].